


Università degli Studi di Cagliari

PHD DEGREE

Civil Engineering and Architecture

Cycle XXXII

TITLE OF THE PHD THESIS

Parametric design and optimization of arched trusses under vertical and horizontal multi-load cases

Scientific Disciplinary Sector(s)

ICAR/09 – Tecnica delle costruzioni (Structural Engineering)

PhD Student:	Eleonora Congiu
Coordinator of the PhD Programme	Ivan Blečić
Supervisor	Luigi Fenu
Co-Supervisor	Giuseppe Carlo Marano

Final exam. Academic Year 2018 – 2019

Thesis defence: January-February 2020 Session

Preface

This dissertation faces the problem of the optimum design of steel truss arches subject to multiple load cases.

Arches are one of the most ancient shape-resistant structures, widely used in both civil engineering and architecture. For instance, arches can be considered as purely compressed structures, provided that their "line of thrust" coincides with the centre line of the arch. The "line of thrust" is the locus of the points of application of the thrusts (internal forces or stress resultants) that must be contained within the cross-section of the arch in such a way that the arch transfers loads to the foundations through axial compressive stresses only. As a matter of fact, the more the "line of thrust" differs from the centre line of the arch, the larger the unfavourable bending moments that arise in the arch. In this regard, the Eddy's theorem for arches states:

"The bending moment at any section of an arch is proportional to the vertical intercept between the linear arch (or theoretical arch) and the centre line of the actual arch"

where the "linear arch" corresponds to the "line of thrust" drawn for a given load.

This is the reason why it is fundamental to pay close attention to the choice of the shape for an arch in order to minimize (or avoid when it is possible) unfavourable bending effects. Several analytical, graphical and physical methods are provided to find the optimal shape of a monolithic (single rib) arch subjected to a certain load case (i.e. the "funicular curve" for that load). However, if multiple load cases must be considered, it is not possible to find a proper optimal shape for an arch with single rib. In this case, the choice of truss arches with at least two chords becomes indispensable.

Indeed, it has been demonstrated that structural optimization of in-plane truss arches with two chords subjected to a single load case leads to optimal solutions in which upper and lower chords tend to coincide with each other and with the "funicular curve" (i.e. the "line of thrust") for that load.

In light of the above, simultaneous shape and size optimization of steel truss arches with two arched chords linked each other through a bracing system (with variable Pratt-type pattern) has been performed for multiple load cases and different structural boundary conditions. Truss arches are effectively used in arch bridges, especially when the arch span exceeds 200 meters (five out of the six steel arch bridges with a span over 500 m are truss arch bridges).

For this purpose, a hybrid optimization routine integrating a parametric definition of the design problem, a metaheuristic optimization algorithm and a code for Finite Element Analysis (FEA) has been developed through a MATLAB program.

Structural optimization aims to find the minimum (or the maximum) value of an objective function that must be defined as a function of several parameters, assumed as design variables of the optimization problem. Therefore, a preliminary parametric definition of the design problem was indispensable to select the design variables among all parameters involved in the problem. The proposed optimization method allows to simultaneously optimize a larger set of design variables, notwithstanding their large number and various nature (topology, shape and size, as well as continuous and discrete variables have been concurrently considered).

In particular, the shape design variables have been chosen among the parameters defining the cubic parametric function of *Rational Bézier Curves* with four control points. *Rational Bézier Curves* are widely used in vector graphics to model smooth curves because they can be easily deformed by changing the position of control points or by varying its corresponding non-negative weight factors (whose values define the attraction level that the "control polygon" exerts on the curve). *Third-degree Rational Bézier Curves* have been chosen to optimize the shape of the arch chords because they can represent a wide family of curves (including conic curves), depending on a small number of parameters, thus allowing to assume a limited number of shape design variables.

In so doing, in-plane truss arches with different span lengths and structural boundary conditions have been optimized for multiple load cases, only considering vertical loads (acting on the same plane as the arch), since in-plane arches are not suited to withstand out-of-plane loads.

On the other hand, spatial arched trusses with two arched chords lying on different planes have been optimally designed for multiple loadings acting in different directions. In particular, a steel arched truss with a lower arched chord variably inclined in the 3D-space and a horizontal upper arched chord linked each other through a bracing system has been designed and optimized for three vertical load cases and a horizontal seismic action parallel to the upper chord plane.

Thus, analysing the obtained results, useful suggestions for steel truss arch design have been deduced and presented in this dissertation.

Prefazione

La presente tesi affronta il tema della progettazione ottimale di archi reticolari in acciaio soggetti a multiple combinazioni di carico.

Gli archi sono tra i più antichi elementi strutturali cosiddetti "resistenti per forma", ampiamente utilizzati tanto nell'Ingegneria Civile quanto nel campo dell'Architettura.

Gli archi possono considerarsi strutture puramente compresse, purché la loro "curva delle pressioni" coincida con la linea d'asse dell'arco. La "curva delle pressioni" è definita come il luogo dei punti di applicazione delle "spinte" (delle azioni interne o delle risultanti degli sforzi) che deve essere contenuta all'interno della sezione trasversale dell'arco affinché l'arco sia in grado di trasferire i carichi esterni alle fondazioni tramite puri sforzi assiali di compressione. Di fatto, tanto più la ""curva delle pressioni" si discosta dalla linea d'asse dell'arco, quanto più si manifestano sfavorevoli momenti flettenti in esso. A tal proposito, il teorema di Eddy per gli archi afferma:

"Il momento flettente agente in ogni sezione di un arco è proporzionale allo scostamento verticale tra "l'arco teorico" e l'asse reale dell'arco"

In cui per "arco teorico" si intende la "curva delle pressioni" disegnata per un dato carico.

Questa è la ragione per la quale è da ritenersi fondamentale prestare grande attenzione alla scelta della forma di un arco al fine di minimizzare (o evitare laddove possibile) sfavorevoli effetti flessionali. Sono svariati i metodi analitici, grafici e fisici disponibili per individuare la forma ottima di un arco monolitico (a singolo corrente) soggetto ad una data condizione di carico (ossia il "poligono funicolare" calcolato per quel dato carico). Tuttavia, se devono essere prese in considerazione differenti combinazioni di carico, non è possibile individuare una forma ottima da assegnare ad un arco con singolo corrente. In questo caso diventa infatti necessario considerare archi reticolari costituiti da almeno due correnti.

È stato infatti dimostrato che l'ottimizzazione strutturale di archi reticolari a due correnti complanari soggetti ad una singola condizione di carico, condurrebbe a soluzioni ottime in cui i correnti inferiore e superiore tendono a coincidere l'uno con l'altro e con il "poligono funicolare" (la "curve delle pressioni") calcolato per il carico considerato.

Alla luce di quanto detto sinora, è stata effettuata la simultanea ottimizzazione di topologia, forma e dimensioni di archi reticolari in acciaio composti da due correnti ad arco interconnessi tramite un sistema di aste (con variabile configurazione di tipo Pratt) soggetti a multiple combinazioni di carico e differenti condizioni di vincolo. Gli archi reticolari sono efficacemente usati nei ponti ad

arco, in particolare nelle condizioni in cui la campata è maggiore di 200 metri (cinque dei sei ponti ad arco in acciaio con campata superiore a 500 metri sono supportati da archi reticolari).

A tal scopo è stato opportunamente sviluppata una ibrida routine di ottimizzazione che incorpora la parametrica definizione del problema di progettazione, un algoritmo di ottimizzazione meta-euristico, unitamente ad un codice per Analisi agli Elementi Finiti (FEA), all'interno di un programma implementato in ambiente MATLAB.

L'Ottimizzazione Strutturale è finalizzata a trovare il minimo (o il massimo) valore di una funzione obiettivo, la quale deve essere definita in funzione di differenti parametri, assunti come variabili di progetto del problema di ottimizzazione. Pertanto, una preliminare definizione parametrica del problema di progettazione è indispensabile al fine di selezionare le variabili di progetto tra tutti i parametri coinvolti nel problema. Il metodo di ottimizzazione qui proposto permette di ottimizzare simultaneamente un unico set di tutte le variabili di progetto, nonostante l'ampio numero e l'eterogenea natura (variabili topologiche, di forma e dimensioni, nonché continue e discrete sono state contemporaneamente prese in considerazione) che le caratterizza.

In particolare, le variabili di progetto di forma sono state scelte tra i parametri che definiscono una funzione parametrica di terzo grado di *Curve Razionali di Bézier* con quattro punti di controllo. Le *Curve Razionali di Bézier* sono ampiamente utilizzate nella grafica vettoriale per modellare curve di forma libera in quanto facilmente deformabili variando la posizione dei relativi punti di controllo o i dei corrispondenti fattori di peso non negativi (i cui valori definiscono il livello di attrazione che il "poligono di controllo" esercita sulla curva). Le *Curve Razionali di Bézier di terzo grado* sono quindi state adottate nell'ottimizzazione della forma dei correnti degli archi considerati in quanto capaci di rappresentare una vasta famiglia di curve (che include anche le coniche) dipendendo da un ridotto numero di parametri, permettendo quindi l'assunzione di un limitato numero di variabili di progetto di forma.

Procedendo come descritto sopra, archi reticolari planari, caratterizzati da campate di differenti luci e da differenti strutturali condizioni al contorno, sono stati ottimizzati per multiple condizioni di carico, considerando soli carichi verticali (agenti nello stesso piano dell'arco), non essendo gli archi planari in grado di resistere a carichi agenti fuori dal piano.

D'altro canto, archi reticolari spaziali aventi due correnti ad arco giacenti su differenti piani, sono stati ottimamente progettati per multiple combinazioni di carico agenti in differenti direzioni. In particolare, una trave reticolare curva avente corrente inferiore ad arco variabilmente inclinato nello spazio 3D e corrente superiore curvo giacente su un piano orizzontale interconnessi tramite un sistema di aste di irrigidimento, è stata opportunamente progettata e ottimizzata per tre combinazioni di carico verticali e un'azione sismica orizzontale parallela al piano del corrente superiore.

Dall’analisi dei risultati ottenuti, sono state quindi tratte utili indicazioni per la progettazione di strutture reticolari ad arco in acciaio, illustrate nel presente lavoro di tesi.

Acknowledgements

I would like to thank my advisor, Prof. Luigi Fenu (affiliated to DICAAR – Department of Environmental Civil Engineering and Architecture of the University of Cagliari (Cagliari, Italy)), and my co-advisor, Prof. Giuseppe Carlo Marano, Ph.D. (Full Professor at DISEG - Department of Structural Engineering, Construction and Soil Mechanics of the Polytechnic University of Turin (Turin, Italy), and Distinguished Professor at the College of Civil Engineering of the Fuzhou University (Fuzhou, China)) for supporting me and guiding my research in the past three years. I am really grateful to them for listening to me, for discussing with me and giving me valuable suggestions in pursuing my research, as well as for helping me to develop different effective optimization strategies.

I further would like to express my sincere gratitude to Prof. Bruno Briseghella, Ph.D. (Distinguished Professor and Dean of the College of Civil Engineering of the Fuzhou University (Fuzhou, China)) for giving me the great opportunity to work in Fuzhou in 2017, 2018 and 2019 for almost one year under his priceless supervision. I am extremely grateful to him for supporting me, inspiring me and guiding my research during the entire course of my doctorate, as well as for allowing me to work more closely with him during the time I spent at the College of Civil Engineering of the Fuzhou University. I am particularly thankful to him to have had the chance to attend his courses concerning bridge design, from which I learned a lot, as well as for giving me the precious opportunity to present my research to his students and several Professors. Among which, I would like to mention and especially thank Prof. Camillo Nuti, Ph.D. (Full Professor at the Department of Architecture of ROMA TRE University (Rome, Italy)), whose constructive criticisms strongly helped me to find weaknesses and strengths of my work, thus motivating me to do always better.

I sincerely hope I will, and I am looking forward to having many more chances to collaborate again in the future with Prof. Fenu, Prof. Marano and Prof. Briseghella, whose guide has been fundamental in pursuing and achieving the overall goals of my research.

Lastly, I want to thank my readers, Prof. Nikos D. Lagaros, Ph.D. (Associate Professor and Dean of the School of Civil Engineering, NTUA - National Technical University Athens (Athens, Greece)) and Prof. Giuseppe Quaranta, Ph.D. (Associate Professor at the Department of Structural and Geotechnical Engineering of Sapienza University of Rome (Rome, Italy)) for scrupulously revising my thesis and giving me useful recommendations, which strongly helped me to improve the quality of my work.

Eleonora Congiu gratefully acknowledges Sardinian Regional Government for the financial support of her PhD scholarship (P.O.R. Sardegna F.S.E. - Operational Programme of the Autonomous Region of Sardinia, European Social Fund 2014-2020 - Axis III Education and training, Thematic goal 10, Investment Priority 10ii), Specific goal 10.5.

Table of Contents

List of figures

Chapter 1

Chapter 2

Chapter 3

Chapter 4

Chapter 5

Chapter 6

List of tables

Chapter 5

Chapter 6

Part I

Introduction

Chapter 1

1. Introduction

1.1 Subject and purposes of the thesis

This dissertation faces the problem of the structural optimization of steel planar and spatial truss arches, for different boundary conditions and multiple load cases. The results of topology, shape and size optimization, simultaneously performed through an optimization macro-algorithm opportunely developed, have been presented and analysed in this work.

The present research aims to demonstrate the importance of concurrently optimizing all design variables whose variation more significantly affects the optimal solutions of a design problem, notwithstanding their various nature (topology, shape and size) and potential large number, in order to guarantee a very high level of optimization in terms of both aesthetic and structural results.

Further intent of this dissertation is also to highlight the pivotal role of parametric design in a structural optimization process, especially in its preliminary phase, to identify the design variables, to properly define their upper and lower bounds, parametrically define the geometry as a function of design variables and then formulate the considered optimization problem as function of them.

The ultimate goal of this study is to deduce (from results obtained applying the proposed optimization strategy) useful suggestions and provide advantageous guidelines for the optimum design of steel arched trusses.

1.2 Parametric design overview

The term *parametric* originates from mathematics, meaning something expressed as function of parameters, constant or variable terms that determine the specific form of a function.

Parametric design (Woodbury 2010) is a complex process that aims to define a design problem as a function of several parameters. For this purpose, the designer must establish the relationships between the parts of the project and define them as function of constant and variable parameters (i.e. as parametric equations). Indeed, parametric design requires a complex act of thinking since

it doesn't lead to a single design solution (as the conventional design) but rather it leads to huge set of possible design solutions. Nowadays, the designers can benefit from advanced computer software and tools that implement standard Computer Aided Design (CAD) systems for *parametric modelling*. However, parametric modelling tools are just viable means for parametric design, as direct modelling techniques (e.g. standard CAD programs) are useful tools for conventional design.

1.2.1 Parametric modelling techniques

Contrary to what is believed, parametric modelling techniques appeared not so recently. Antoni Gaudí, one of the most known Spanish architects, considered as the greatest exponent of Catalan Modernism, started to design architecture by taking advantage of parametric catenary curves and parametric hyperbolic paraboloids at the end of the nineteenth century (Makert and Alves 2016). The upside-down model of church realized (*Figure 1. 1*) in 1898 by the Catalan architect is recognized to be one of the earliest examples of parametric modelling. In his design for the Church of Colònia Güell, he created a model of strings weighted down with birdshot to create complex vaulted ceilings and arches.

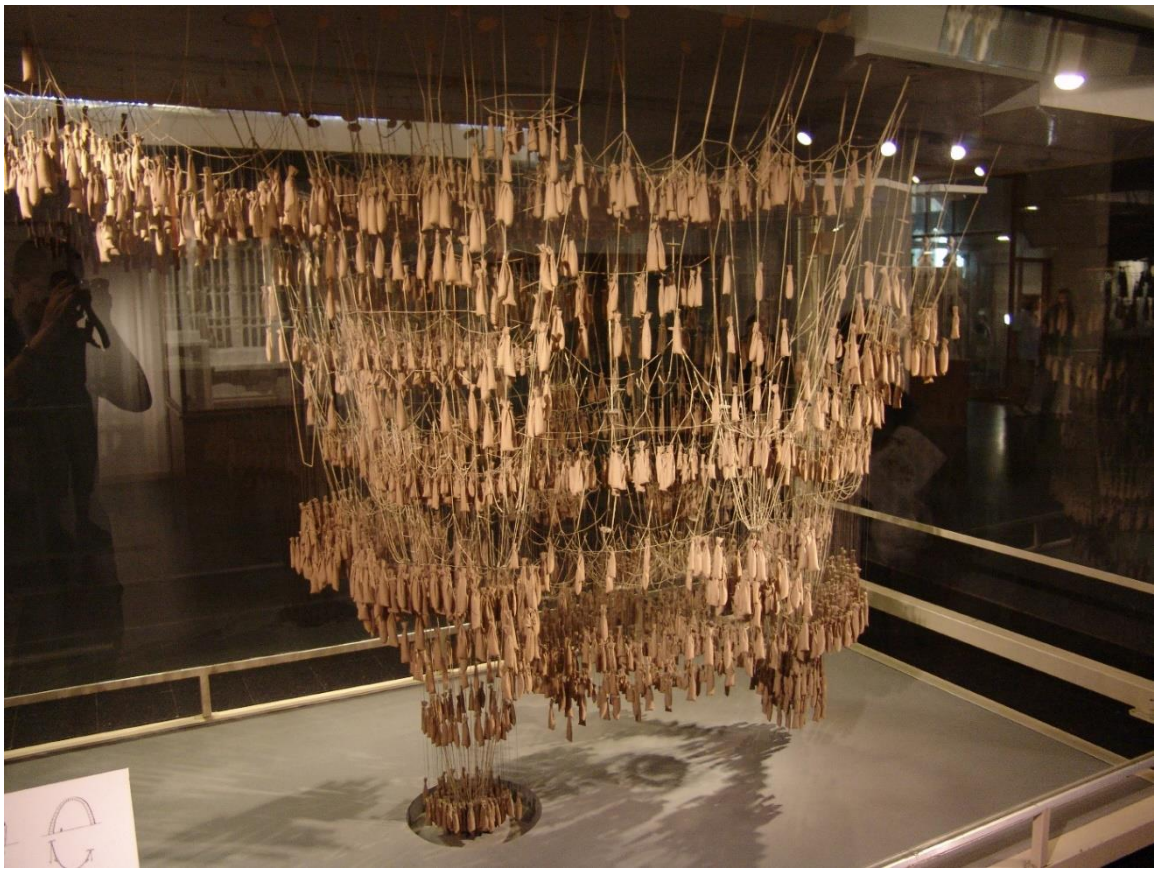

Figure 1. 1 Physical inverted model for the Church of Colònia Güell built up by Antonio Gaudí

By adjusting the position of the weights or the length of the strings he could see in real time how the shape of each arch changed and also how this change affected the shape of other arches

connected to it. As a matter of fact, Antoni Gaudi defined his model as function of several variable parameters as the weights of birdshots, the positions of the weights and the lengths of the strings, in order to easily consider various possible solutions during the (parametric) design process. In so doing, in accordance with Hooke's law, by varying the parameters and inverting his models he could directly obtain different pure compression solutions, without manually solving mathematical parametric equations.

The most important features of parametric modelling are:

- Parametric modelling leads to flexible models;
- In a parametric model, shapes change as soon as a dimension changes and it is possible to automate repetitive changes;
- Attributes are interlinked automatically (by altering only one parameter, the other parameters get adjusted automatically);
- Parametric modelling allows the designer to define entire classes of shapes instead of specific instances;
- Existing data can be easily reused to create new designs.

It is worth noting that, despite the many advantages provided by the parametric modelling, it is not possible to affirm that parametric modelling is better than direct modelling. Most probably, the best Computer Aided Design (CAD) strategy must include both modelling techniques.

Nowadays there are many software choices and tools available in the market for parametric modelling, among which some of the best known are:

- SOLIDWORKS
- CATIA
- CREOPARAMETRIC
- GRASSHOPPER
- AUTODESK REVIT
- AUTODESK DYNAMO.

SOLIDWORKS is used in mechanical design applications and is largely adopted in the plastics industry.

CATIA (Computer Aided three-dimensional Interactive Application) was used by architect Frank Gehry to design some of his award-winning buildings such as the Guggenheim Museum Bilbao.

CREOPARAMETRIC is part of a broader product development system developed by PTC.

GRASSHOPPER is a graphical algorithm editor tightly integrated with Rhinoceros 3-D modelling tool. Grasshopper allows the designer to build a parametric model by means of a "graphical code"

of “components” and “parameters” (whose operation is clearly described in (Tedeschi, Wirz, and Andreani 2014). GRASSHOPPER is considered as a visual programming language. Its integration with Rhinoceros allows a perfect interconnection between parametric and direct modelling.

AUTODESK REVIT is Building Information Modelling (BIM) software developed in response to the need for software that could create three-dimensional parametric models that include both geometry and non-geometric design and construction information.

AUTODESK DYNAMO is also a visual programming tool properly developed for implementing Revit.

1.3 Structural optimization overview

Optimization techniques are effectively applied in scientific, economic and social fields.

The term optimization (Garret N. Vanderplaats 1984) originated from the mathematical technique of finding the minimum or the maximum value of a function, called objective function, depending on several parameters, called design variables. A common optimization problem can be formulated and generalized as follows:

$$\min F(\mathbf{x}) \quad \text{or} \quad \max F(\mathbf{x}) \tag{1}$$

Subject to

$$\mathbf{x}^l \leq \mathbf{x} \leq \mathbf{x}^u \tag{2}$$

in which (in Eq. (1)) $\mathbf{x} = \{\mathbf{x}_1, \dots, \mathbf{x}_j, \dots, \mathbf{x}_n\}$ is the design variable vector (the collection of n system parameters to be identified), $\mathbf{x}^l = \{\mathbf{x}_1^l, \dots, \mathbf{x}_j^l, \dots, \mathbf{x}_n^l\}$ and $\mathbf{x}^u = \{\mathbf{x}_1^u, \dots, \mathbf{x}_j^u, \dots, \mathbf{x}_n^u\}$ are vectors of its lower and upper bounds (Eq. (2)), respectively. Solving an optimization problem means finding the best vector of design variables (i.e. the best solution) that minimizes or maximizes the objective function. Sometimes, the optimization problem is also subjected to some equality (Eq. (3)) and/or inequality (Eq. (4)) constraint functions, depending on design variables, as follows:

$$h_i(\mathbf{x}) = 0, \; i = 1, \dots m \tag{3}$$

$$g_j(\mathbf{x}) \leq 0, \; j = 1, \dots p \tag{4}.$$

Structural optimization is a peculiar branch of design optimization, motivated by the need of optimizing use of materials in mechanical and structural engineering, e.g. minimizing the quantity (its total volume or its weight) of the material needed to withstand loads or minimizing the structural compliance (i.e. maximizing the stiffness) of a system for given boundary conditions.

In the past, the search for more efficient structures was carried out through trial-and-error procedures. The recent advent of advanced structural optimization techniques, starting from innovative optimization algorithms to computer software and tools properly developed for this purpose, allowed to significantly save costs and obtain better results in optimum design process.

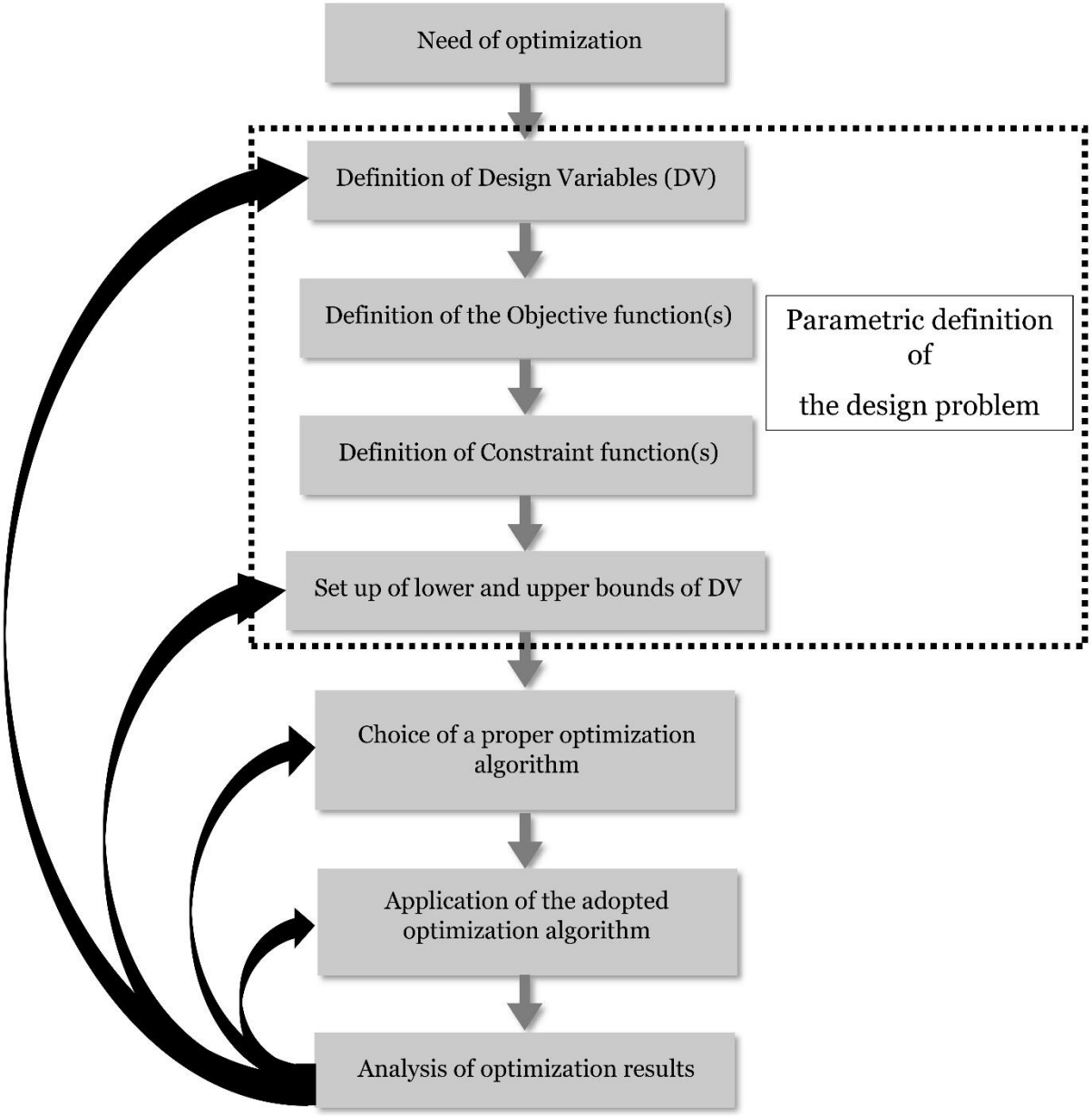

Figure 1. 2 Flowchart of the standard routine of a structural optimization process

In this regard, the flowchart in *Figure 1. 2* schematises a standard optimization routine starting from a need of optimization. A parametric definition of the design problem is then indispensable to select a proper set of design variables and define the objective and constraint function(s) depending on chosen design variables. The choice of a proper optimization algorithm among all provided by the literature plays a crucial role in a structural optimization process (Clune 2013). The algorithm selection must be related to the nature of the optimization problem, depending, in

turn, on the number and nature of design variables (continuous or discrete, size, shape or topology), constraint functions (linear, nonlinear or convex, differentiable or nondifferentiable) and objective (none, single or multiple). Most optimization problems have single objective function. However, there are also cases characterized by none or multiple objective functions. For instance, "feasibility problems" aims to find values for design variables in accordance with several constraints but without any particular objective to optimize ("Types of Optimization Problems | NEOS" n.d.).

Most structural optimization problems are constrained, i.e. subject to constraint functions that for instance limit stresses (strength constraints) or maximum deflections (serviceability constraints) in a structure, in accordance with mechanical properties (e.g. the allowable stress) of materials, as well as with stiffness and stability conditions of the structural system.

Figure 1. 3 represents through very simple examples the most important big categories of structural optimization, whose differentiation is based on the nature of design variables (regardless of being discrete or continuous), as above mentioned:

- Size optimization
- Shape optimization (also known as geometry optimization)
- Topology optimization.

Of which each one will be more in detail described in the following sections *§1.3.1*, *§1.3.2* and *§1.3.3*.

It is worth noting that these formulations of the optimization problem could be integrated in a unique optimization process and performed one after the other (e.g. size optimization commonly follows the other optimization phases) or at the same time, thus formulating the optimization problem considering a unique set of all design variables, independently from their various nature.

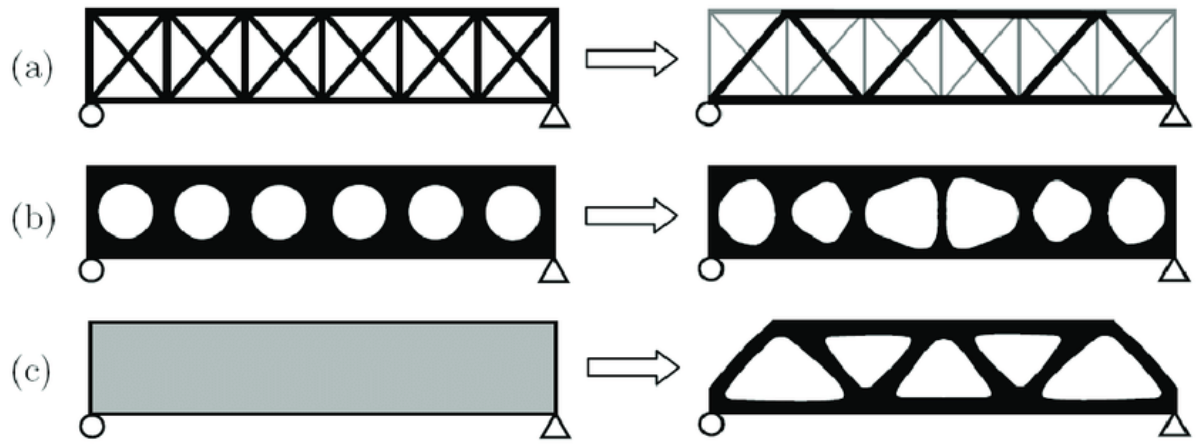

Figure 1. 3 Three categories of structural optimization: (a) Sizing optimization of a truss structure, (b) shape optimization and (c) topology optimization. The initial problems are shown on the left, whereas the optimal solutions are shown on the right (M P Bendsøe and Sigmund 2003)

1.3.1 Size optimization

As before mentioned, in a multidisciplinary structural optimization process, size optimization is commonly performed after shape and topology optimization, since the sizing operation aims to find the optimal values of parameters defining the cross-sections of structural elements.

In particular, in the case of size optimization of plates and shells, their constant or variable thickness can be adopted as design variable (or set of design variables), as shown in *Figure 1. 4*. In this regard, it is a common practice to optimize the variable thickness of thin shell roofs in order to improve their structural behaviour (mainly dependent on their shape) in terms of strength, stiffness and stability, ensuring a distribution of internal stresses as uniform as possible to avoid disadvantageous bending effects (Tomás and Martí 2010).

On the other hand, in the case of size optimization of frame structures, the cross-sectional areas of members are usually assumed as design variables (Tejani et al. 2018; Afshar and Faramarzi 2010; Wang, Zhang, and Jiang 2002). Rarely, single parameters characterizing element cross-sections (e.g. the sides of box cross-sections or the diameters of circular cross-sections, as well as the thicknesses of hollow cross-sections) are assumed as design variables (*Figure 1. 5*), since such an approach would require a significant increase in the number of design variables.

Furthermore, in order to reduce the needed number of size design variables, it is also a common practice to group the elements of frame structures into several groups, on the basis of their various structural functions or some geometrical considerations (as symmetric conditions).

However, in size optimization of discrete structures (e.g. frame structures) it could be convenient to adopt discrete design variables (i.e. characterized by sets of isolated values), whose parameters were taken from a list of commercial structural cross-sections (Pezeshk, Camp, and Chen 2000).

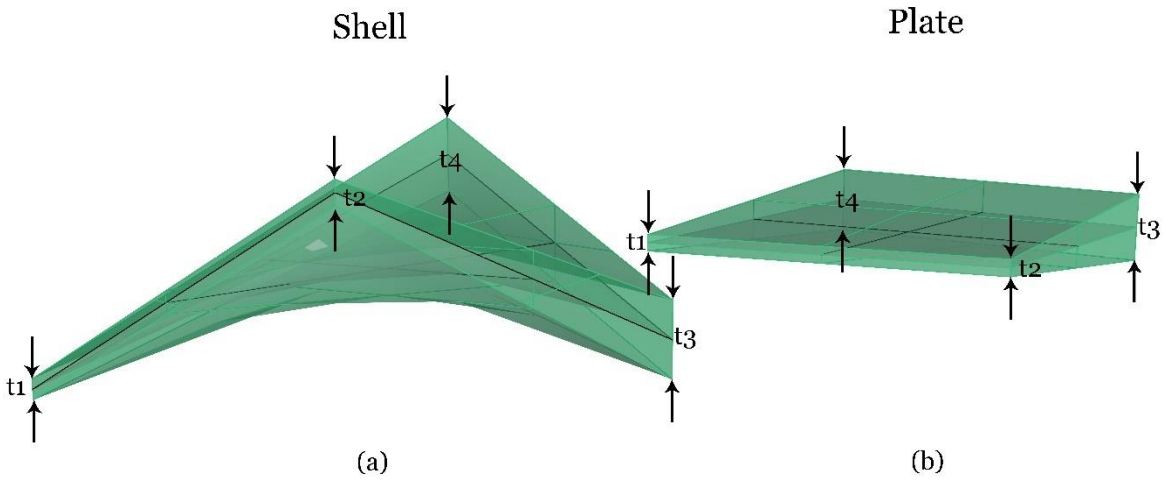

Figure 1. 4 Examples of size design variables of shells (a) and plates (b)

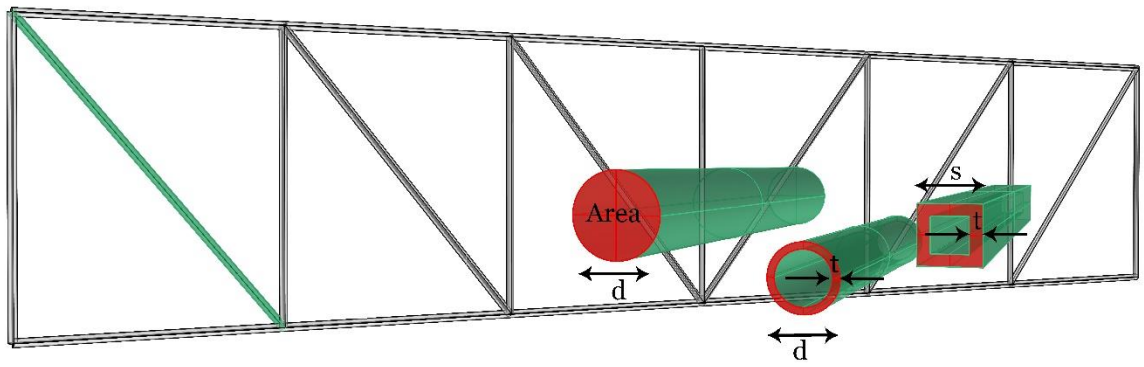

Figure 1. 5 *Examples of size design variables of trusses (i.e. frame structures)*

Since solving an optimization problem with discrete design variables is usually much more difficult than solving similar problems with continuous design variables, design variables can be set as continuous and at a later time, rounded to the closest integer (Haftka and Gürdal 1992) (that could be assumed as index of a list of discrete values).

1.3.2 Shape optimization

Shape (geometry) optimization is a particular section of structural optimization that aims to find the optimal shape of the structure to be optimized for given boundary conditions. In shape optimization problems, the shape is unknown. Nodes coordinates of a discrete or a continuous structure (properly discretized into lines or surface elements) can be directly assumed as shape design variables (as shown in *Figure 1. 6*).

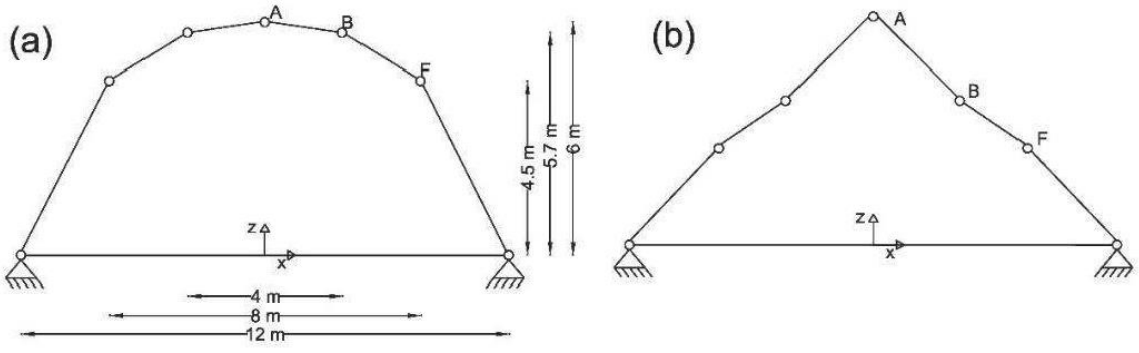

Figure 1. 6 *Shape optimization of a discrete structure: (a) ground structure and (b) optimized structure (Tejani, Savsani, and Bureerat 2018)*

However, the optimization problem of large-scale structures (continuous or discrete) characterized by a large number of nodes would require a high number of design variables. It could be therefore more advantageous to adopt parametric shape functions, depending on a small number of parameters that can be assumed as shape design variables of the optimization problem. The "parametrization" of a shape to be optimized, through appropriate shape functions, makes

easier to modify the shape under consideration by just varying the values of a few parameters (thereby considerably reducing the required number of shape design variables involved).

The process of finding the best shape of a structure for some design requirements (such that compliance with given boundary conditions and loads, material properties, allowable stresses and displacements, a reasonable lifetime and architectural value) is also called "form-finding". Before the advent of advanced computational techniques, engineers and architects in seeking optimal structural shapes employed physical models (e.g. hanging models). The English scientist Robert Hooke (1635-1703) in 1675 discovered and studied the relationship between a hanging chain (which assumes the form of a catenary under its self-weight and can withstand tension forces) and an arch in compression (Block, DeJong, and Ochsendorf 2006). Hooke thus summarized his intuition in a famous Latin anagram "*ut pendet continuum flexile, sic stabit contiguum rigidum inversum*", translated by Heyman as follows: "*as hangs the flexible line, so but inverted will stand the rigid arch*" (Heyman 1998). In a more general sense, the Hooke's principle means that the shape of a string under a set of loads (subject to pure tension forces), if stiffened and inverted, corresponds to a "thrust line" of compressive forces for an arch supporting the same set of loads.

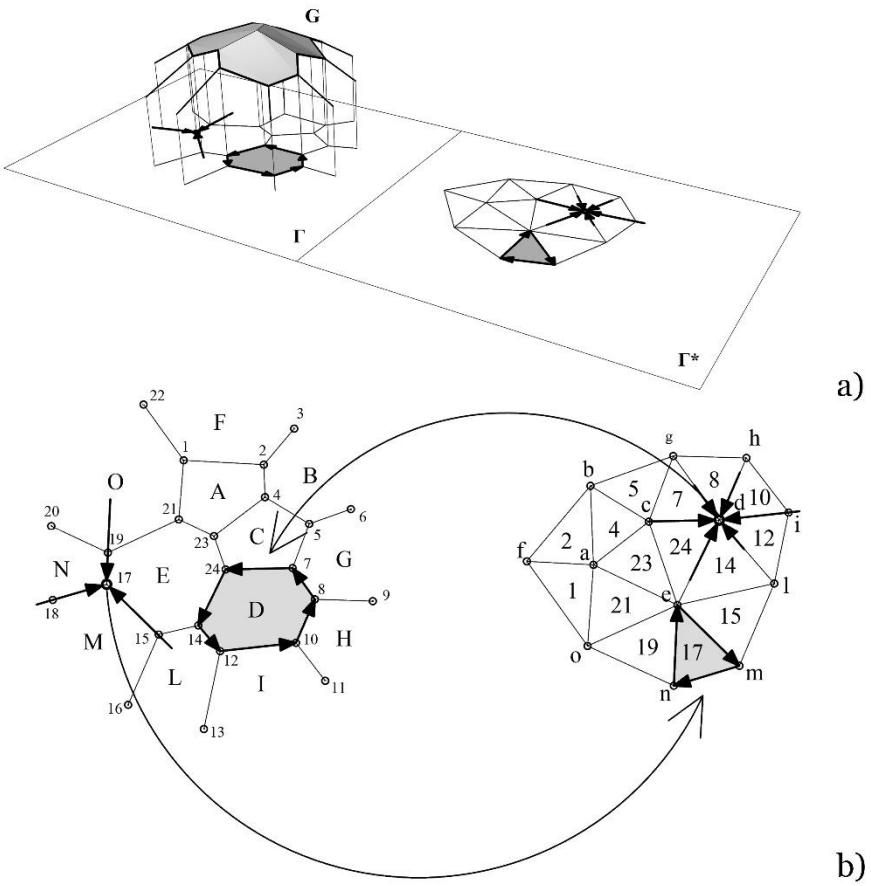

Figure 1. 7 *Form-finding through Thrust Network Analysis (TNA): (a) form diagram (Γ), force diagram (Γ*) and thrust network (G); (b) relation between two reciprocal diagrams*

The so obtained shape of the taut string and the compressed inverted arch define a funicular shape for these loads (Block, DeJong, and Ochsendorf 2006). In 1748, Poleni analysed a real structure using Hooke's idea to assess the safety of the cracked dome of St. Peter's in Rome, showing that the dome was safe by employing the hanging chain principle. The Hooke's principle is also applicable to three-dimensional hanging systems (e.g. hanging membranes or cable networks) to find optimal shapes of discrete or continuous shells for certain load conditions. Antoni Gaudí (1852–1926), Heinz Isler (1926–2009) and Frei Otto (1925-2015) first took advantage of physical, gravity-loaded, inverted hanging models as form-finding tools for designing shell structures, thereby investigating and validating the Hooke's law of inversion.

Even if physical models can always be considered as valid form-finding techniques for both, bidimensional and three-dimensional structures (e.g. arches, vaults and shells), more advanced form-finding techniques have been developed, taking advantage of new computer methods for graphic statics (very intuitive and powerful method for exploring funicular shapes through equilibrium analysis).

These new interactive form-finding techniques can be broadly grouped into three categories (Adriaenssens et al. 2014; Veenendaal and Block 2012):

- Stiffness matrix methods (based on elastic and geometric stiffness matrices) are among the oldest form-finding methods
- Geometric stiffness methods that are material independent. The Force Density Method (FDM) (Schek 1974) and the Thrust Network Analysis (TNA) (i.e. a three-dimensional version of Thrust Line Analysis (Block 2009; Block and Ochsendorf 2007)) are among the most known
- Dynamic equilibrium methods solve problems of dynamic equilibrium by reaching a static equilibrium state. For instance, Dynamic Relaxation (DR) (Adriaenssens et al. 2014) and Particle-Spring (PS) systems (Kilian and Ochsendorf 2005) are among the most known.

Figure 1. 7 illustrates the relationship between the two planar form (Γ) and force (Γ*) diagrams and the three-dimensional spatial network (G) characterizing a form-finding procedure performed through the Thrust Network Analysis (TNA) method, developed by the Block Research Group at the ETH of Zurich (Switzerland) for the form-finding of compressive funicular shells by taking advantage of graphic statics computer techniques.

1.3.3 Topology optimization

Topology optimization can be broadly defined as the optimization of spatial material distribution in a design space. The first paper on topology optimization was published in 1904 by the Australian inventor Michell, who derived optimality criteria for the least weight layout of trusses

(Michell 1904). The work of Michell has set the foundation for research into the optimal layout of trusses, with materials of same or different strength in tension and compression. Michell proved that an optimum truss must follow the orthogonal network of lines of maximum and minimum strain in a constant magnitude strain field. In 1976, Prager and Rozvany (Prager and Rozvany 1977) investigated the Michell's theory and formulated the first general theory of topology optimization, termed "optimal layout theory". Furthermore, Prager and Rozvany introduced the terms "truss-like continua" to define "Michell's trusses" as structures in which, in some regions, members of infinitesimal cross-sectional area have an infinitesimal spacing (Querin, Victoria, and Martí 2010). Besides, Rozvany et al. (Rozvany, Zhou, and Gollub 1993) showed that the optimal topologies for plastic stress design and elastic compliance design are the same, and the volume or weight of the latter is given by the square of the volume of the former (multiplied by a given constant). After that, structural topology optimization of continuum and discrete structures has been extensively explored (Feng 2014).

In structural topology optimization, the distinction between continuum and discrete structures optimization becomes clearer, with respect to other classes of optimization problems.

The goal of topology optimization of continuum structures is to optimise the material distribution, thereby finding the optimal number, position and shape of cavities (Feng 2014), i.e. finding the optimal placement of a given isotropic material within a space (M P Bendsøe and Sigmund 2003). The simplest examples of topology optimization problems for continuum structures are formulated for minimum compliance (maximum global stiffness) as objective function. One may distribute a given amount of material in a certain region, so that the stiffness of the resulting structure is maximized for a given load case (Huang and Xie 2010). In the last decades, several methods for topology optimization of continuum structures have been developed (Tejani, Savsani, and Bureerat 2018):

- Homogenization method, which consists of computing the optimal distribution in space of an anisotropic material that is constructed by introducing an infimum of periodically distributed small holes in a given homogeneous, isotropic material, with the requirement that the resulting structure can carry the given loads as well as satisfy other design requirements. The computation of effective material properties for the anisotropic material is carried out using the method of homogenization (Martin Philip Bendsøe and Kikuchi 1988)
- SIMP (Solid Isotropic Microstructure with Penalization) method, where the design region is meshed into a fixed grid of n finite elements. All elements carry densities assumed as design variables. The objective is to find an optimal material distribution in the design domain to reach quasi-discrete structures, thereby minimizing the compliance of the

structure (objective function) in accordance with some constraints (M P Bendsøe and Sigmund 2003)

- Evolutionary Structural Optimization (ESO)/Bidirectional Evolutionary Structural Optimization Method (BESO), which works on simultaneous removal and addition of material. An application example of ESO method is shown in *Figure 1. 8* (took from (Huang and Xie 2010))
- Level Set Method is based on boundary tracked model. The contours of a parametrized family of level-set functions are here used to generate the boundaries of a structure, and the topology can change with changes in the level-set function. The principal idea of level set method is to remove material in regions of low stress and to add material in regions of high stress (M P Bendsøe and Sigmund 2003).

Discrete topology optimization (also known as Truss Topology Optimization (TTO)) aims to optimize the connectivity between nodes (whose coordinates are known and fixed) of a grid. The problem of topology optimization of trusses can be conveniently formulated by means of the so-called ground structure method (M P Bendsøe and Sigmund 2003).

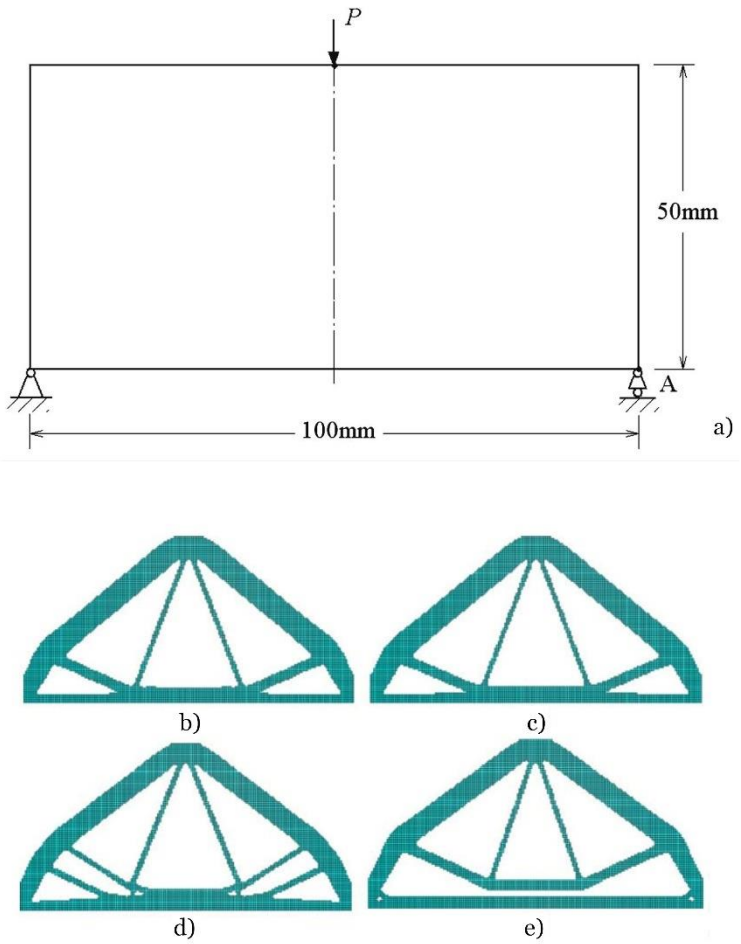

Figure 1. 8 *Evolutionary Structural Optimization(ESO) method for topology optimization of continuum structures: (a) Design domain, boundary and loading conditions, Optimal designs (b) without a*

local displacement constraint, (c) with displacement constraints $u_A^* = 1.4mm$, (d) $u_A^* = 1.2mm$ and (e) $u_A^* = 1.0mm$ (Huang and Xie 2010)

In this approach, the layout of a truss structure is found by allowing a certain set of connections between a fixed grid of nodal points as potential structural or vanishing members. As a matter of fact, truss topology optimization problems based on the "ground structure approach" is commonly formulated as a standard sizing problem, seeing as how it allows for using the continuously varying cross-sectional bar areas as design variables, including the possibility of zero bar areas to be removed. In this regard, the *Figure 1. 9* shows an example of topology and size optimization of a 20-bar truss, which was proposed in (Tejani, Savsani, and Bureerat 2018).

It is worth noting that structural topology optimization is broadly considered like a peculiar category of structural shape (geometry) optimization, even if subjected to strict design bounds (e.g. fixed nodes in cases of TTO).

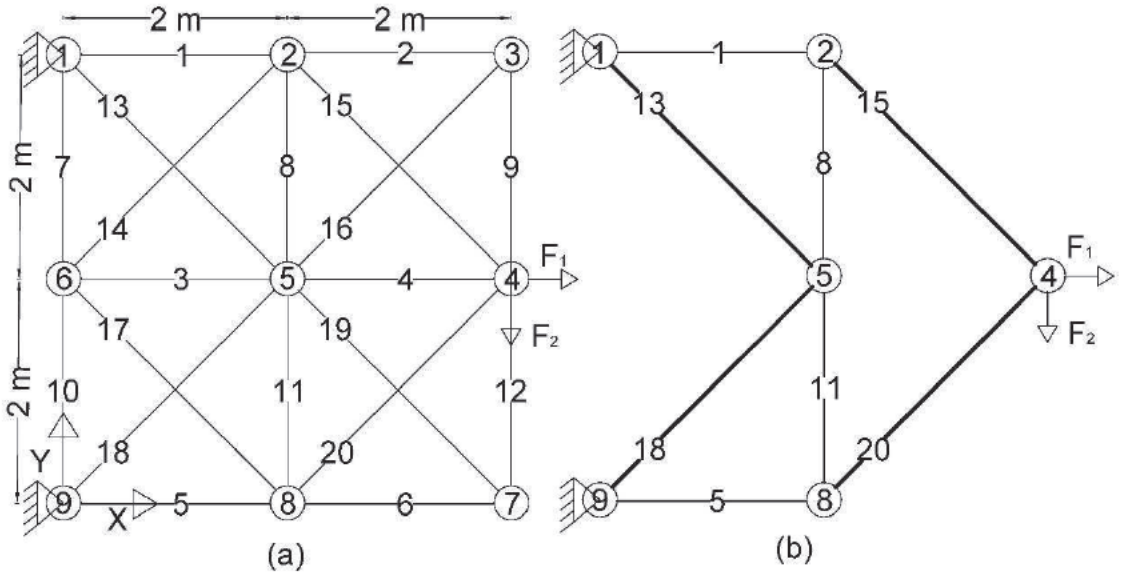

Figure 1. 9 Topology and size optimization of a 20-bar truss: (a) ground structure, (b) optimized solution (Tejani, Savsani, and Bureerat 2018)

1.4 Numerical methods for structural optimization: Overview of optimization algorithms

An optimization algorithm is a sequence of actions (i.e. a procedure) which is executed iteratively by comparing various solutions of an optimization problem until a convergence criterium is satisfied (an optimum or a satisfactory solution is found).

The section §*1.3* provided an introduction to optimization techniques applied to structural design (simply called "structural optimization"). Due to the complexity of most structural optimization

problems, the choice of an appropriate optimization algorithm becomes of utmost importance in structural optimization (Clune 2013). The algorithm selection must be related to the nature of the optimization problem (e.g. constrained or unconstrained), also depending, in turn, on the number and nature of design variables (continuous or discrete, size, shape or topology), constraint functions (linear, nonlinear or convex, differentiable or nondifferentiable) and objective (none, single or multiple).

The strategy used to move from one iteration to the next distinguishes one algorithm from another (Nocedal and Wright 1999). All optimization algorithms can be roughly grouped into the following classes (Cavazzuti 2013):

- Deterministic algorithms
- Optimality Criteria Methods
- Stochastic algorithms

They will be the subjects of the following sections §*1.4.1, §1.4.2* and §*1.4.3,* respectively.

1.4.1 Deterministic algorithms

The term *deterministic* originated from *determinism,* which in physics corresponds to the concept of "cause-and-effect", according to which, every state (or event) within a model is completely *determined* by previous states.

Therefore, *deterministic algorithms* use specific rules for moving one solution to another and for a given set of inputs, they produce the same set of outputs for different runs.

As a matter of fact, *deterministic optimization* algorithms follow a rigorous mathematical approach (they are also known as *mathematical programming techniques*).

The literature provides a large number of *mathematical programming techniques* for both, constrained and unconstrained optimization problems. Some of the most known deterministic are the following:

- Linear Programming (LP) algorithms, which have been properly developed to solve a peculiar class of optimization problems in which the objective and constraint relations are linear functions of design variables. Linear programming involving large number of design variables and constraints are usually solved through the *Simplex Method,* which consists of continuously decreasing the value of the objective function by going from one basic feasible solution to another until the minimum value of the objective function is achieved. *Interior methods* for solving Linear Programming problems (like the *Karmarkar's algorithm*) demonstrated to be much faster than the *Simplex Method*. Special attention deserves the *Integer Linear Programming (ILP) techniques,* developed to solve discrete

programming problems (i.e. optimization problems with discrete design variables). The *Branch-and-Bound algorithm* is a powerful algorithm to solve *Mixed Integer Linear Programming (MILP) problems* (as well as for *Mixed Non-Linear Programming problems*), which are characterized by the coexistence of continuous and discrete design variables. Most structural optimization problems can't be directly formulated as LP without needing a degree of simplification. However, LP algorithms are of interest to designer because most Non-Linear Programming (NLP) problems can be solved as a sequence of repetitive approximate LP problems thereby finding the exact solution of the original NLP problem provided that the procedure is repeated for a certain number of times (Haftka and Gürdal 1992).

- Non-Linear Programming (NLP) algorithms have been developed to solve optimization problems in which the objective and/or the constraints are non-linear functions of the design variables. NLP techniques are subdivided in turn into several categories:
  - ✓ Zeroth Order Methods, (also called "direct methods" or "derivative-free methods"), use only the value of the objective function during the optimization process. The literature provides several methods for minimizing objective functions of a single design variables (e.g. the *bracketing method*, the *Fibonacci and Golden Section Search*, the *Quadratic Interpolation*) as well as for multi-variable optimization problems. Among the latter, the most known is the *Sequential Simplex Method,* which begins with a regular geometric figure called *simplex* (with $n + 1$ vertices in a n-dimensional space) subject to three operations namely "reflection", "contraction" and "expansion" (Haftka and Gürdal 1992)
  - ✓ First Order Methods employ values of the objective function and its first derivatives with respect to the design variables. Among these, the *Bisection Method* was developed to minimize objective functions of only one design variable, operating in a similar manner with respect to the *Bracketing* and the *Golden Section Search* techniques, i.e. progressively reducing the interval where the minimum (the zero of the first derivative) is known to lie. On the other hand, First Order Methods for multidimensional optimization problems use the gradient of the objective function as well as its value in calculating the move direction for the function minimization (the literature provides several *Conjugate Gradient Algorithms* (Haftka and Gürdal 1992))
  - ✓ Second Order Methods use values of the objective function, as well as its first and second derivatives. The oldest second order method for minimizing a nonlinear multivariable function in R^n is the *Newton's Method*, which is known as second order method not only because it uses second order derivatives of the objective function, but also because it has a quadratic rate of convergence. The motivation

behind Newton's is identical to the steepest descent method. (Haftka and Gürdal 1992).

It is worth noting that all methods briefly described so far have been developed to solve *unconstrained optimization problems*. Unfortunately, almost all problems in structural optimization must be formulated as *constrained optimization problems,* in order to obtain optimal solutions that satisfy unavoidable design constraints (e.g. stress, displacement, buckling and frequency constraints). These constraints are usually complex functions of the design variables available only from analysis of a finite element model of the structure (Haftka and Gürdal 1992). In §1.3 a general formulation of a constrained optimization problem was introduced through Eqs. (1), (2), (3) and (4). The constraints divide the design space into two domains, the so-called feasible domain, where all constraints are satisfied, and the infeasible domain where at least one of constraint equalities and/or inequalities is violated.

For this purpose, several methods have been introduced to solve *constraint optimization problems*; among these

- *Lagrange Multiplier techniques*, which is a mathematical method to find minima and maxima of a function subject to equality constraints. In cases of inequalities constraints, they can be easily converted to equivalent equality constraints. The Lagrange multiplier theorem roughly states that at any stationary point of the function that also satisfies the equality constraints, the gradient of the function at that point can be expressed as a linear combination of the gradients of the constraints at that point, with the Lagrange multipliers acting as coefficients (Luenberger 1969). Several methods that use Lagrange multipliers are available. For instance, *Gradient Projection and Reduced Gradient Methods,* which are based on projecting the search direction into the subspace tangent to the active constraints. On the other hand, the *Feasible Direction Method* operates in a opposite manner with respect to the gradient projection method, seeing as instead of following the constraint boundaries, the method try to stay as far away as possible from them (Haftka and Gürdal 1992).
- *Penalty Function methods* allow to replace a constrained optimization problem with an unconstrained one by replacing the constraint functions by penalties depending on the degree of constraint violations. The *Exterior Penalty Functions* (which are applied in the exterior of the feasible domain) associates a penalty with a violation of constraints. It is a common practice to associate a penalty that is proportional to the square of a violation and to choose very high values of penalties in order to ensure that no constraints are violated. With an exterior penalty function, constraints contribute to the penalty terms only when they are violated. When only inequalities constraints are present, it is possible to define an *Interior Penalty Function*, where the penalty term is proportional to the

inverse constraint functions or a logarithmic interior penalty function can be defined. Interior penalty functions ensure feasible designs provided that the optimization process starts from a feasible design. Hence, it may be advantageous to adopt a combination of interior and exterior penalty function, called *Extended Interior Penalty Function* (Haftka and Gürdal 1992).

- *Multiplier Methods* combine the use of *Lagrange multipliers* with *penalty functions*. When only Lagrange multipliers are employed, the minimum is a stationary point rather than a minimum of the Lagrangian function. On the other hand, when only penalty functions are adopted, a minimum is found but the function to be minimized tends to suffer from ill-conditioning (small changes in the independent variables lead to large changes in the dependent ones. For these reasons it may be convenient to adopt multiplier methods (Haftka and Gürdal 1992).
- *Projected Lagrangian Methods (Sequential Quadratic Programming)* pursue the same goal of Multiplier Methods (that is to convert the optimum from a stationary point of the Lagrangian function to a minimum of the *augmented Lagrangian)* but through a different procedure. *Projected Lagrangian Methods* are based on a theorem that states that the optimum is a minimum of the Lagrangian function in the subspace of vectors orthogonal to the gradients of the active constraints (the tangent subspace). These methods apply a quadratic approximation of to the Lagrangian in this subspace. This approach requires the solution of a *Quadratic Programming problem,* which is characterized by a quadratic objective function and linear constraints.

1.4.2 Optimality Criteria Methods

The *Optimality Criteria Methods (OCM)* consist of a combination of a pre-assumed optimality criterion with an algorithm used to resize the structure to be optimized for the purpose of satisfying the optimality criterion. The resizing algorithm can consist of a rigorous mathematical method or it can use a method specifically developed (Haftka and Gürdal 1992).

The so-called *Fully Stressed Design (FSD)* method is probably the most popular among all *Optimality Criteria Methods*.

The *Fully Stressed Design (FSD)* method can be summarized as follow (Haftka and Gürdal 1992):

"For the optimum design each member of the structure that is not at its minimum gage is fully stressed under at least one of the design load conditions".

This optimality criterion implies that some material is removed from members that are not fully stressed, unless prevented by minimum gage constraints.

However, the assumption that adding or removing material to a member primarily affects the stresses in that member is valid only for statically determinate structures. Indeed, in cases of statically indeterminate structures, the minimum weight design may not be fully stressed. Moreover, the *Fully Stressed Design* method may not work well in cases of multiple materials. The method is also complemented by a resizing algorithm based on the assumption that the load distribution in the structure does not depend on member sizes. That is, the stress in each member is calculated and then the member is resized to bring the stresses to their allowable values assuming that the loads remain constant. This assumption is valid only for statically determinate structures. On the other hand, if the structure is statically indeterminate, the resizing routine (called "stress-ratio technique") has to be applied iteratively until convergence to any desired tolerance is achieved (Haftka and Gürdal 1992).

1.4.3 Stochastic Algorithms

Stochastic algorithms use random selection criteria and probabilistic rules for moving from one iteration to another. Stochastic optimization algorithms produce, in different runs, different sets of outputs for a given set of inputs. These techniques are recommended for complex non-linear and discontinuous problems, where classical optimisation techniques might fail. For instance, a common disadvantage of *deterministic algorithms* (*mathematical programming techniques*) is the frequent difficulty in distinguishing local and global minima, especially in solving discrete optimization problems. In fact, a common way to address the discrete optimization problems with multiple minima is to employ random search techniques (Haftka and Gürdal 1992). However, the main drawback of these algorithms is a lack of efficiency and robustness in handling constrained optimization problems. Fortunately, it became a common practice to implement these algorithms with appropriate constraint-handling techniques in order to extend their application to constrained optimization problems.

Stochastic Algorithms can be roughly divided into two groups, *Heuristic* and *Metaheuristic Algorithms* (Yang 2014). *Heuristic* means "to find" or "to discover by trial and error" (self-learning procedure). Quality solutions to a tough optimization problem can be found in a reasonable amount of time, but there is no guarantee that optimal solutions will be reached. However, a drawback of heuristic algorithms is that they are "problem-dependent", since they use rules that have been properly conceived for a specific problem. Further development of heuristic algorithms is the so-called *Metaheuristic Algorithms*. The term *meta* in this context means "beyond" or "higher level". These algorithms overcome the main drawback of simple *heuristic algorithms,* since they are not so sensitive to the nature of the specific problem to be optimized. In addition, another peculiar feature of all *metaheuristic algorithms* is the combination of randomization and local search. Randomization allows to move away from local search to search

on a global scale. For this reason, all *metaheuristic algorithms* are particularly suitable for global optimization (Yang 2014). Metaheuristic algorithms have been grouped in turn into two families:

- Trajectory-based algorithms
- Population-based algorithms.

However, both families of algorithms rely on some naturally observed phenomena, of which they emulate the main rules to find optimal solutions through progressive improvements (Haftka and Gürdal 1992).

1.4.3.1 Trajectory-based algorithms: The Simulated Annealing (SA) algorithm

Trajectory-based algorithms use a single agent that moves through the design space. The steps or moves of the agent trace a trajectory in the search space, with a nonzero probability that this trajectory can reach the global optimum. Among these, the most known trajectory-based algorithm is the *Simulated Annealing (SA) algorithm*, developed in 1983 by Scott Kirkpatrick, C. Daniel Gellat, and Mario P. Vecchi (Kirckpatrick, Gelatt, and Vecchi 1983), inspired by the annealing process of metals (Yang 2014). For instance, during solidification of metals or formation of crystals, a number of solid states with different internal atomic or crystalline structure characterized by different energy levels can be obtained depending on the rate of cooling. If the system is cooled too rapidly, it entails a resulting solid state that would have a small margin of stability because the atoms will assume relative positions in the lattice structure to reach an energy state which is only locally minimal. In order to reach a more stable, globally minimum energy state, the process of annealing is used in which the metal is reheated to a high temperature and cooled slowly, allowing the atoms enough time to find positions that minimize a steady state potential energy. Observing the natural annealing process, it was found that during the time spent at a given temperature, it is possible to have a system jump to a higher temperature temporarily before the steady state is reached. This characteristic of the annealing process makes possible to achieve near global minimum energy states (Haftka and Gürdal 1992). Kirkpatrick et al. (Kirckpatrick, Gelatt, and Vecchi 1983) then developed an optimization algorithm inspired by the above described annealing process of metals. The method requires only function values. A typical *simulated annealing algorithm* starts setting an initial temperature T_0 that will be progressively reduced during the process. The initial value of T_0 must be high enough to increase the probability of finding a global minimum. Once the temperature is set, a large number of moves in the variable space is performed by perturbing the design. A possible convergence criterion could be imposed, for instance allowing the agent to move until the value of the objective function does not change for a specific number of successive iterations. Once convergence is achieved at a

given temperature that should correspond to a thermal equilibrium, the temperature is reduced and the process is repeated. (Haftka and Gürdal 1992).

1.4.3.2 Population-based algorithms: The Evolutionary Algorithms (EAs)

Unlike the trajectory-based algorithms just described in §*1.4.3.1*, population-based algorithms use multiple agents (or particles) that move through the design space (Yang 2014). The name "population-based algorithms" is referred to consider a set of candidate solutions of the problem to be optimized as a "population" of "individuals", that during the optimization process are subjected to operations emulating the main evolution phases of natural species. Algorithms that were inspired by the theory of evolution are known as *Evolutionary Algorithms* (Ashlock 2006; Bäck 1996).

Most biologist accepted the following definition of the term "*evolution*"

"*Evolution is the variation of allele frequencies in populations over time.*"

Where the *allele* is a different variant of a considered *gene* (e.g. different alleles can result in different observable phenotypic traits, such as different pigmentation). *Genes* can be considered as single units of *chromosomes* that are the molecules of DNA (deoxyribonucleic acid).

Three key-concepts are particularly relevant to understand evolutionary computation rules:

- Reproduction
- Variation
- Selection.

At each iteration of an evolutionary algorithm, a "population" of new "individuals" is generated. *Variation* and *Selection* play a crucial role in generating new "offspring" (i.e. a new "generation" of "individuals").

Variation is the process that produces new *alleles* and then, *genes*. *Selection* is the process whereby some *alleles* survive, and others do not. *Variation* produces genetic diversity; *selection* reduces it. *Evolutionary computation* operates on populations of data structures (on sets of design variables). The variation is performed by making random changes in these data structures and by blending parts of different structures (of two parents). These two processes are called *mutation* and *crossover*, and together are referred to as *variation* operators. On the other hand, *selection* is accomplished with any algorithm that favours data structures with a higher fitness score (i.e. best value of the *objective function* of an optimization problem). A general evolutionary computation, in the end, can be condensed into the simple sentence *"Evolution is the result of survival of the fittest"* (Ashlock 2006).

Evolutionary algorithms are suitable to find approximated solutions to all types of problems because they ideally do not require any assumption about the underlying fitness landscape; this generality is shown by successes in fields as diverse as engineering, art, biology, economics, marketing, genetics, operations research, robotics, social sciences, physics, politics and chemistry and so on.

The literature does not provide a universally accepted classification of *evolutionary algorithms*. However, it is possible to mention the most known algorithms of this family

- *Genetic Algorithms,* which are the most popular and oldest evolutionary algorithms. *Genetic algorithm* repeatedly *mutates* a "population" of "individuals" (i.e. candidate solutions). Each candidate solution (i.e. each design variable vector) of a problem is commonly expressed in the form of a string of numbers (traditionally binary, although the best representations are usually those that reflect something about the problem being solved). At each step, a *genetic algorithm* randomly *selects* "individuals" from the current "population" to be "parents" and uses them to produce the children for the next "generation". Over successive "generations", thanks to *mutation*, *crossover* and *selection* operations, the population "evolves" improving the value of the objective function to be maximized or minimized until an optimal solution is obtained.
- *Genetic Programming,* here the solutions are in the form of computer programs (commonly stores in parse trees), and their fitness is determined by their performance in solving a computational problem. For instance, *Genetic Programming* can be applied to search for an optimal formula for encoding and interpolating a data set describing a function (Ashlock 2006).
- *Evolutionary Programming,* these algorithms are similar to genetic programming, but the structure of the program to be optimized is fixed, while its numerical parameters are allowed to evolve.
- *Evolutionary Strategy* algorithms uses floating-point numbers to encode the continuous variables used in the differential equations. They work with vectors of real numbers as representations of solutions, and typically uses self-adaptive mutation rates.
- *Differential Evolution*. The crucial idea behind *Differential Evolution* algorithms is a scheme for generating trial parameter vectors. These algorithms generate new parameter vectors by adding a weighted difference vector between two population members to a third member. If the resulting vector yields a lower objective function value than a predetermined population member, the newly generated vector will replace the vector with which it was compared in the following generation (Storn and Price 1997, 1995).
- *Particle Swarm Optimization* algorithm is a computational method ~~in~~ inspired by swarm intelligence of fish and birds. It is a population-based algorithm where candidate solutions

are dubbed “particles”, whereas the term “swarm” is referred to a “population”. “Particles” move around in the search-space (according to simple mathematical formulae over the particle's position and velocity). In the canonical version of PSO, each particle is moved by two elastic forces, one attracting it with random magnitude to the fittest location so far encountered by the particle (“local best position”), and one attracting it with random magnitude to the best location encountered by any of the particle’s social neighbours in the swarm (“global best position”). If the problem is N-dimensional, each particle’s position and velocity can be represented as a vector with N components. The position of a particle is updated every time step. Eventually, the swarm as a whole is likely to move close to the best location. (Poli 2008; Kennedy and Eberhart 1995).

- *Ant colony optimization* algorithm is a probabilistic technique, inspired by the behaviour of real ant colonies (Monmarché, Guinand, and Siarry 2010) seeking a path between their colony and source of food. This algorithm was developed for solving computational problems that aim to find good paths through graphs. Shortest paths are discovered via pheromone (that is a secreted or excreted chemical factor that triggers a social response in members of the same species) trails. Ants move randomly, depositing some pheromones on the search space. More pheromone on path increases probability of path being followed.
- *Invasive Weed Optimization* algorithm mimics natural behaviour of weeds in colonizing and finding suitable place for growth and reproduction. The IWO algorithm has a simple structure, based on a cooperative co-evolution approach that utilizes a divide-and-conquer (or decomposition) strategy to solve complex optimization problems. (Sang, Duan, and Li 2018)
- *Harmony Search* is a music-inspired algorithm. In HS algorithm, a feasible solution is called “harmony” and each decision variable (design variable) of the solution is corresponding to a “note”. Harmony Search algorithm includes a harmony memory in which a predetermined number of harmonies (N) have been stored. New harmonies are iteratively generated, compared and replaced until the convergence criterion is satisfied (Askarzadeh and Rashedi 2017).
- *Gaussian Adaptation* is an evolutionary algorithm based on information theory. It is a stochastic adaptive process where a number of samples of an n-dimensional vector $\mathbf{x}$ are taken from a multivariate Gaussian distribution, having mean m and moment matrix M. The samples are tested for fail or pass.

1.5 Outline of chapters

This dissertation addressed the problem of the structural optimization of steel arched trusses subjected to multiple load conditions. More specifically, planar truss arches with different spans were optimized considering three different vertical load patterns. On the other hand, a spatial arched truss (with an upper arched chord lying on a horizontal plane and a lower chord, variably inclined in the 3D-space, linked each other through stiffening tubular elements) with a "horizontal span" of 40 meters, was optimized assuming three vertical load cases and a horizontal static seismic action (i.e. parallel to the arched upper chord). Topology, shape and size optimization, were simultaneously performed through an optimization macro-algorithm opportunely developed.

This dissertation is divided into four parts. *Part I* defines the goals of the research, providing an introduction to parametric design and structural optimization in *§Chapter 1*, whereas *§Chapter 2* provides the current state of the art of structural optimization of arches, with a specific emphasis to truss arches.

Part II is divided into two sections:

- *§Chapter 3* illustrates some examples of not-integrated methods combining parametric design and structural optimization techniques, which are applied one after the other in separated phases of a design process
- *§Chapter 4* shows two new integrated methods combining parametric design and structural optimization techniques. In particular, an optimization "macro-algorithm" which combines parametric design and structural optimization techniques in a hybrid environment composed of *MATLAB* and *Grasshopper*, was first proposed. At a later time, a *MATLAB* macro-algorithm containing a parametric definition of the optimum design problem, a code of an optimization algorithm and a parametric definition of a *Finite Element Method (FEM)* model for *SAP2000* was implemented and presented.

Part III shows, through the application of the optimization macro-algorithm (proposed in *§Chapter 4*) fully implemented in a *MATLAB* program, optimal design solutions for steel arched trusses.

More specifically, in *§Chapter 5* the results of simultaneous topology, shape and size optimization of planar truss arches subjected to different constraint conditions and three vertical load cases are discussed. On the other hand, *§Chapter 6* shows an optimal design solution of a steel truss composed by a lower arched chord variably inclined in the 3D-space and a horizontal upper arched chord linked each other through a bracing system, which has been designed and optimized for three vertical load cases and a horizontal seismic action.

Part IV in *§Chapter 7* provides general conclusions, summarizing useful suggestions for the design of steel arched trusses, also anticipating the future developments of the research presented in the present dissertation.

Chapter 2

2. Literature review: Structural optimization of arches

Arched structures are characterized by a wide range of uses in architecture and civil engineering because of their ability to carry large loads and cover larger spans thanks to their shape (they are considered as "shape-resistant structures"). The greater is the span than an arch becomes more convenient than a truss. Arched structures are broadly used in bridges, aqueducts, dams and roofs.

2.1 Structural behaviour of arches

An arch is a vertically curved beam whose main feature is that horizontal reactions (called "*thrusts*"), oriented toward each other, appear even if the structure is subjected to vertical loads only. Thanks to this feature, bending moments and shear forces in "thrusted structures" are considerably smaller than corresponding internal forces in simply supported beams with same span and subjected to same loads. Therefore, the height of the cross section of the arch can be much smaller than the height of a beam to resist the same loading.

Note that a "thrustless" structure with curvilinear axis cannot be considered an arch.

Distribution of internal forces in arches depends on the shape of its central line, which is commonly circular or parabolic.

For instance, the shape of the central line of a circular arch can be defined by the following function

$$y(x) = \sqrt{R^2 - \left(\frac{L}{2} - x\right)^2} - R + f \tag{5}$$

depending on the span (L), the radius of curvature (R) and the rise (f) of the arch.

Similarly, the shape of the central line of a parabolic arch, is characterized by the following function,

$$y(x) = \frac{4fx}{L^2}(L - x) \tag{6}$$

depending on the span (L) and the rise (f) of the arch (Karnovsky and Lebed 2010). Arches can be considered as purely compressed structures, provided that their "line of thrust" coincides with the central line of the arch. The "line of thrust" is the locus of the points of application of the thrusts (internal forces or stress resultants) that must be contained within the cross-section of the arch in such a way that the arch transfers loads to the foundations through axial compressive stresses only. As a matter of fact, the more the "line of thrust" differs from the centre line of the arch, the larger the unfavourable bending moments that arise in the arch. In this regard, the Eddy's theorem for arches states:

"*The bending moment at any section of an arch is proportional to the vertical intercept between the linear arch (or theoretical arch) and the centre line of the actual arch*"

where the "linear arch" corresponds to the "line of thrust" drawn for a given load.

It is well known that a parabolic arch subjected to a load q uniformly distributed along its span (L) will be only subjected to axial compressive forces (i.e. any bending moment will arise in it), since a parabola is the "funicular curve" for a uniform load. However, Timoshenko and Gere (Timoshenko and Gere 2009) showed that by a gradual increase of the load intensity (q), a critical condition in which the arch becomes unstable and buckles similarly to a circular arch can be reached.

Timoshenko and Gere (Timoshenko and Gere 2009) thus provided a formula to calculate the critical value of the load intensity (q) for which a parabolic arch with uniform cross-section becomes unstable (i.e. buckling occurs), which is given by,

$$q_{cr} = \gamma_4 \frac{EI}{L^2} \tag{7}$$

depending on the Young's modulus (E) of the material, the moment of inertia (I) of the cross-section, the arch span (L) and a constant (γ_4) depending in turn on the rise-to-span ratio and the hinges number of the arch. It is worth underlining that the critical load decreases in increasing the number of hinges, whereas it tends to increases in increasing the rise-to-span ratio from 0.1 to 0.4 and to rapidly decrease in gradually increasing the rise-to-span ratio from 0.5 to 1.0 (Timoshenko and Gere 2009).

For what concerns the maximum stresses, it is worth to keep in mind that it is a common practice to assume that cross-sectional dimensions of the rib are small in comparison with the radius of curvature and therefore to use the formulas available for straight bars in the calculation of stresses (Timoshenko and Young 1965).

For straight ribs (or beams) the extreme fibre stresses are given by the following equation,

$$f_{1,2} = \frac{N}{A} \pm \frac{Ma_{1,2}}{I} \quad (8)$$

where N is the axial force acting perpendicular to the cross-section, A is the area of any section of the arch, M is the bending moment about the gravity axis at any section, I is the moment of inertia about the gravity axis of each section, whereas a_1 and a_2 are the distances of the upper and lower fibres from the centre of gravity, respectively.

On the other hand, the exact formula to calculate the extreme fibre stresses in a curved rib with radius of curvature r is given by

$$f_{1,2} = \frac{N}{A} + \frac{M}{Ar} \pm \frac{Mra_{1,2}}{I(r \pm a_{1,2})} \quad (9).$$

However, only if the radius of curvature is small compared to cross-section dimensions Eq. (9) is required to calculate the stresses in ordinary arches, otherwise Eq. (8) is sufficiently accurate (Melan 1915).

The arches are classified as three-hinged, two-hinged and hingeless arches (where the latter have fixed supports), as shown in *Figure 2. 1*.

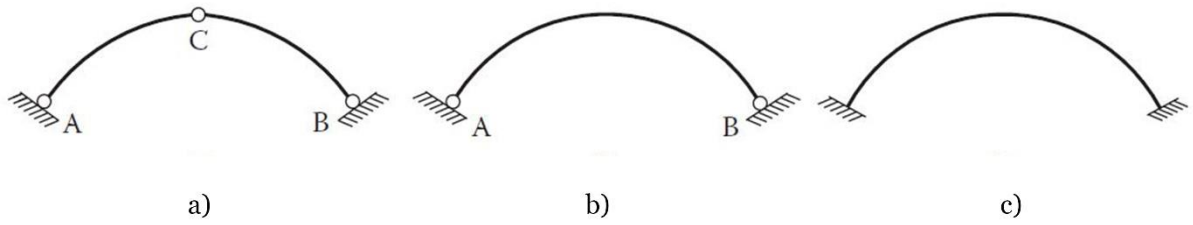

Figure 2. 1 Classification of arches based on articulation: (a) three-hinged arch; (b) two-hinged arch; (c) hingeless arch (Chen and Duan 2014)

2.1.1 Three-hinged arches

A three-hinged arch incorporates a hinge at the crown of the structure in addition to hinges at the supports. Three-hinged arches are statically determinate structures and can be solved through equations developed by the elastic theory; however, hinged arches are less stiff than structures with fixed supports (Sadhwani 2000).

If the arch is subjected to a uniformly distributed load (of intensity q per unit length) on the full span and the crown-hinge is at the mid-point of the span, the horizontal thrust of the arch can be evaluated by the following equation

$$H_1 = H_2 = \frac{1}{8}\frac{qL^2}{f} \quad (10)$$

depending on the full-span load of intensity (q), the span (L) and the rise (f) of the arch.

In the case of a symmetrical arch symmetrically loaded, the vertical reactions have same values as reactions of a simply supported beam with same span, subjected to the same loads; i.e.

$$V_1 = V_2 = \frac{qL}{2} \quad (11).$$

As a matter of fact, the above-mentioned Eq. (6) represents the axis equation of the optimal shape of a momentless symmetrical arch, subject to a symmetrical uniformly distributed load, obtained by equalling to zero the second term of the bending moment equation for a full-span load, which is given by,

$$M(x) = \frac{1}{2}qx(L - x) - \frac{1}{8}\frac{qL^2}{f}y \quad (12).$$

It is worth underlining that Eq. (6) does not depend on the intensity q per unit length of the uniformly distributed load, since it only depends on the arch span (L) and rise (f).

Hence in a three-hinged arch with parabolic shape, uniformly loaded over the entire span, only axial stresses arise; i.e. the pressure is uniformly distributed over each section (Melan 1915).

On the other hand, if the parabolic arch is subjected to an asymmetrical uniform load over one-half of the span, the bending moments in the loaded half will be

$$M'(x) = \frac{1}{8}qx(3L - 4x) - \frac{1}{16}\frac{qL^2}{f}y \quad (13)$$

whereas the bending moments in the unloaded half are

$$M''(x) = \frac{1}{8}qLx - \frac{1}{16}\frac{qL^2}{f}y \quad (14).$$

Note that in Eqs. (13) and (14), the abscissa x is measured from the nearest end of the arch. Furthermore, the maximum bending moments (of intensity $qL^2/64$) occur at the quarter points of the arch while it is zero at its mid-span (Melan 1915), as shown in *Figure 2. 2*.

The horizontal thrusts are opposite and equal to

$$H_1 = H_2 = \frac{1}{16}\frac{qL^2}{f} \quad (15)$$

while the vertical reactions are given by,

$$V_1 = \frac{3}{8}qL \quad (16)$$

for the loaded half, and by,

$$V_2 = \frac{1}{8}qL \quad (17)$$

for the unloaded half of the arch.

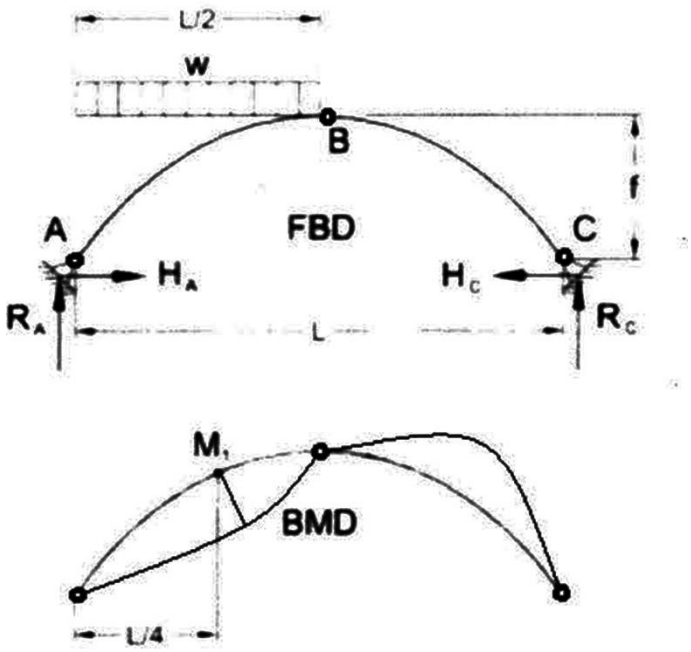

Figure 2. 2 *Bending moment diagram for a three-hinged arch subjected to a uniform load over one half of its span (Momo 2017)*

The ordinates of the lines of thrusts for the two halves of the arch due to the asymmetrical loading, can be readily found by equalling to zero the two corresponding bending moment equations (i.e. Eqs. (13) and (14)).

If the two lines of thrusts, for loading on the loaded and unloaded halves of the arch are considered as the limiting positions of the resistance-line of the arch, their mean curve will give the best shape of the axis of the arch (Melan 1915).

An important advantage of three-hinged arches is that any change of temperature does not induce any additional stress in the arch, since the elongation of the arch-axis is balanced by the unresisted rise or fall of the crown hinge. In the same way, a possible settlement of the abutments does not produce any additional stress in the arch (Melan 1915).

2.1.2 Two-hinged arches

Two-hinged arches have one redundant reaction force, since a vertical load acting on the arch produces vertical and horizontal reactions. Indeed, we have four unknown reactions, for the calculation of which only three equations of statics are available. A fourth equation must be obtained by considering the deformation of the arch (Timoshenko and Young 1965). Assuming that the arch is symmetrical and symmetrically loaded, the two vertical reactions (V_1 and V_2) are equal and can be readily evaluated by Eq. (11). As in the previous case of three-hinged arches, the horizontal reactions (H_1 and H_2) are equal and opposite. In calculating the horizontal reaction,

the deformations of the arch should be considered. However, Eq. (10) provides a good approximate solution.

Assuming that the arch has a parabolic shape, the bending moments and shear forces are zero at any section of the arch since only axial forces arise in it. In this regard, the axial force in three- and two-hinged arches uniformly loaded over the entire span can be evaluated as follow

$$N(x) = \frac{1}{8}\frac{qL^2}{f}\cos\theta + qL\left(\frac{1}{2} - \frac{x}{L}\right)\sin\theta \tag{18}$$

for $x \leq L/2$, and

$$N(x) = \frac{1}{8}\frac{qL^2}{f}\cos\theta + qL\left(\frac{x}{L} - \frac{1}{2}\right)\sin\theta \tag{19}$$

for $x > L/2$; where θ indicates the variable angle formed by the arch and the horizontal reference axis and the quantity $\frac{1}{8}\frac{qL^2}{f}$ corresponds to H, the horizontal reaction (Leontovich 1959).

On the other hand, if the considered two-hinged arch is subjected to an asymmetrical uniform load over one-half of the span, the vertical reactions (V_1 and V_2) are once again given by Eqs. (16) and (17), whereas the opposite horizontal thrusts (H_1 and H_2) can be calculated by Eq. (15).

Accordingly, bending moments at any section of the arch are given by Eq. (13) for the loaded half of the arch and by Eq. (14) for the unloaded half, measuring the abscissa x from the nearest end of the arch (see *Figure 2. 3*). As in the previous case, the maximum bending moments occur at the quarter points of the arch.

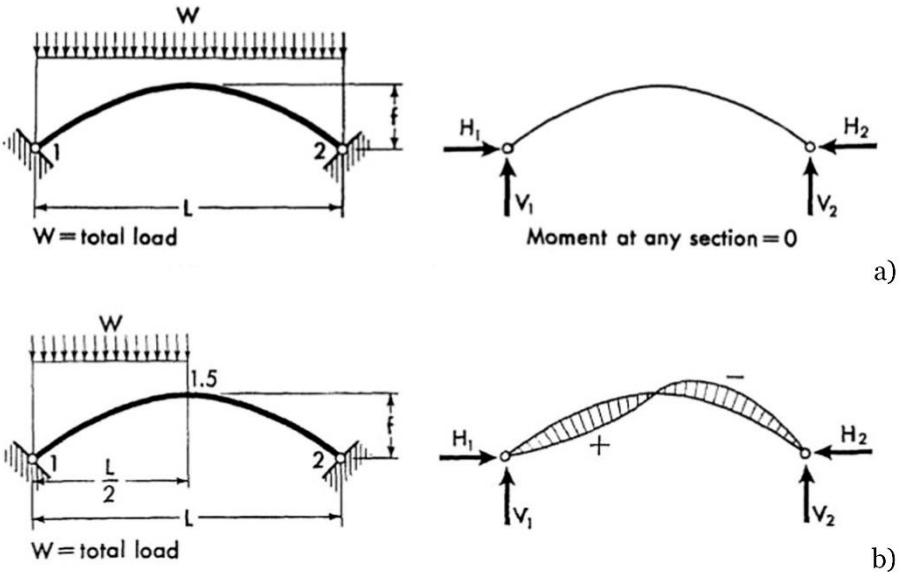

Figure 2. 3 *Bending moment diagrams for parabolic two-hinged arches subjected to a uniform load over the entire arch span (a) and over one half of the arch span (b), shown in (Leontovich 1959)*

Axial forces are predominant in true arched structures compared to other internal forces and they can be evaluated by,

$$N'(x) = \frac{1}{16}\frac{qL^2}{f}\cos\theta + \left(\frac{3L}{8} - x\right) q \sin\theta \tag{20}$$

for the loaded half, and by

$$N''(x) = \frac{1}{16}\frac{qL^2}{f}\cos\theta + \frac{1}{8}qL\sin\theta \tag{21}$$

for the unloaded half of the arch (Leontovich 1959).

Two-hinged arches are stiffer than three-hinged arches; however, they are sensitive to temperature changes and support displacements. In fact, in a hingeless arch or any arch with less than three hinges, a rise of temperature induces an increase, while a fall of temperature a decrease, of the horizontal thrust H. A similar effect is also producible by a support displacement.

It is worth underlining that the maximum stresses due to temperature changes commonly occur at the crown and at the ends of the arch; more specifically, a rise in temperature produces tensile stresses in the extrados and compressive stresses in the intrados at the crown and the reverse at the ends of the arch. A fall in temperature induces opposite effects (Melan 1915).

2.1.3 Hingeless arches

Arches that are rigidly joined to the abutments are commonly known as "hingeless arches" or "fixed arches". Since they have three redundant reactions, the three equations of statics are not enough to calculate the unknown six reaction forces. The three lacking equations necessary to evaluate the redundant reactions, can be derived from conditions governing the deformations of the structure (Melan 1915).

However, Leontovich in (Leontovich 1959), provided useful condensed solutions for parabolic hingeless arches for different load conditions (see *Figure 2. 4*).

For instance, it is shown that for a symmetrical parabolic arch subjected to a symmetrical uniform load over the entire span, the horizontal thrusts (H_1 and H_2) and the vertical reactions (V_1 and V_2) are once again given by Eqs. (10) and (11), respectively. Axial force at any section of the left half of the arch can be determined by Eq. (18), whereas at the right half it can be evaluated by Eq. (19). Accordingly, since the arches under consideration are supposed to be parabolic, symmetrical and symmetrically loaded, bending moments should be zero at any section of the arch.

Conversely, assuming that the parabolic arch is subjected to a uniform load (of intensity q per unit length) over one half of the arch, the horizontal reactions are equal, opposite and given by Eq. (15), whereas the vertical reactions are given by,

$$V_1 = \frac{13}{32} qL \tag{22}$$

at the loaded half of the arch, and by,

$$V_2 = \frac{3}{32} qL \tag{23}$$

at the unloaded half of the arch.

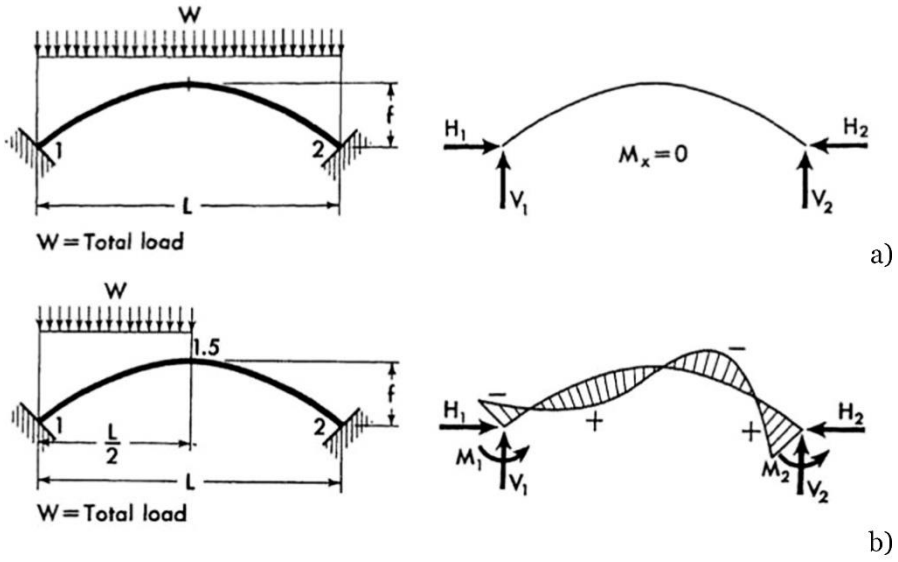

Figure 2. 4 Bending moment diagrams for parabolic hingeless arches subjected to a uniform load over the entire arch span (a) and over one half of the arch span (b), shown in (Leontovich 1959)

Since arches with fixed ends are analysed in the present section, in addition to horizontal and vertical reactions, also moment reactions arise at the arch supports, which are given by,

$$M_1 = -\frac{1}{64} qL^2 \tag{24}$$

and by,

$$M_2 = \frac{1}{64} qL^2 \tag{25}$$

at the loaded and the unloaded halves of the arch, respectively.

Axial force at any section of the loaded half of the arch can be determined as follows

$$N'(x) = \frac{1}{16} \frac{qL^2}{f} \cos\theta + \left(\frac{13}{32} L - x\right) q \sin\theta \tag{26}$$

and by,

$$N''(x) = \frac{1}{16} \frac{qL^2}{f} \cos\theta + \frac{3}{32} qL \sin\theta \tag{27}$$

at the unloaded half.

As already stated, L and f indicate the span and the rise of the arch, respectively, while θ is the angle of inclination of the arch axis at any section.

Bending moments can be determined by,

$$M'(x) = -\frac{1}{64}qL^2 + qx\left(\frac{13}{32}L - \frac{x}{2}\right) - \frac{1}{16}\frac{qL^2}{f}y \tag{28}$$

and by,

$$M''(x) = \frac{1}{64}qL^2 + \frac{3}{32}qL(L-x) - \frac{1}{16}\frac{qL^2}{f}y \tag{29}$$

at the loaded and the unloaded halves of the arch, respectively.

2.2 Structural optimization of monolithic arches: state of the art

As already stated, arches are classified as "shape-resistant" structures since their structural behaviour strongly depends on the shape of their axis. As a matter of fact, an arch will be subjected to only axial compressive forces, provided that the shape of its axis is properly defined as "funicular curve" for a certain load condition.

Several analytical, graphical and physical methods are provided in the literature to find the optimal shape of a monolithic (i.e. with a solid section) arch subjected to a certain load case (i.e. the "funicular curve" for that load).

Moreover, also several examples of topology optimization (which aims to find the optimal material distribution) and size optimization (which aims to find the optimal dimensions of its variable or constant cross-section) of single-rib arches can be found in the literature.

2.2.1 Topology, shape and size optimization of monolithic arches

The present section aims to provide an overview of some significant examples of topology, shape and size optimization of arches with a solid section (i.e. monolithic arches).

For instance, on the basis of the Euler-Bernoulli theory of the nonlinear inextensible plane elasticae, Tadjbakhsh reviewed the concept of "funicular geometry" providing the equations governing the bending stresses that may arise due to live load or partially imposed dead load (Tadjbakhsh 1981). Tadjbakhsh thus determined the buckling load for parabolic arches (subjected to a vertical uniform load) and buried culverts supporting the weight of the soil fill (of variable depth), as well as the shape and the variable cross-sectional area of a funicular (i.e. momentless) arch of constant stress (thus providing a shape and size optimization example of an arch).

Vanderplaats and Han in (G. N. Vanderplaats and Han 1990) provided a method to perform shape and size optimization of two-hinged and fixed arches, approximated by a finite number of straight members and subjected to combined stress constraints. The proposed method, based on an approximate structural analysis using a Taylor series expansion of member and forces, is summarized by the flowchart in *Figure 2. 5*. The optimization algorithm has been applied to minimize the volume of two-hinged and hingeless arches, subjected to a single concentrated force at their mid-span in a first case and to a uniform load over the whole span as a second case. The goodness of numerical results demonstrated the effectiveness and the reliability of the presented method which allowed to simultaneously treat geometric and size design variables of the problem.

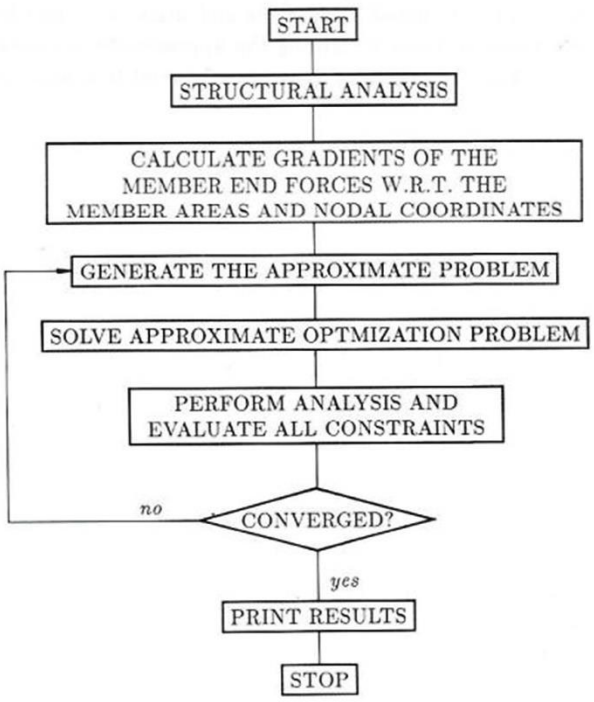

Figure 2. 5 Algorithm proposed by Vanderplaats and Han for shape optimization of arches (G. N. Vanderplaats and Han 1990)

Serra in (Serra 1994) proposed two approximate solutions of optimal uniformly compressed arches under static loads. An analytical solution for arches subjected to a vertical load made up of a uniform part plus a variable linearly depending on the arch shape was first proposed. Serra (Serra 1994) then presented a solution obtained by an iterative numerical method for a generic arch approximated by a polygonal curve, subjected to dead and external (vertical and horizontal) loads applied as concentrate forces on its nodes.

More recently, Marano et al. (Marano, Trentadue, and Petrone 2014) proposed a new analytical method to optimize the shape and the cross-sectional area (variable along the arch) of a statically

determinate arch subjected to its self-weight and to an external distributed load. The work of Marano et al. was aimed to find the optimal shape and cross-sectional area of an arch of equal strength such that all its cross-sections are subjected to a constant stress and the ratio between the self-weight and external load $\int_0^L p(x)dx$ is minimum. It was assumed that the material was homogeneous with constant specific weight. The uniform compression condition for all cross-sections was imposed by equalling to zero the bending moment in each section. Two numerical examples for two different constant loads have been shown, thus demonstrating that for an assigned rise-to-span ratio, only the cross-sectional area depends on the intensity p of the external load, whereas the optimal shape of the central line of the arch was not affected by the value of p.

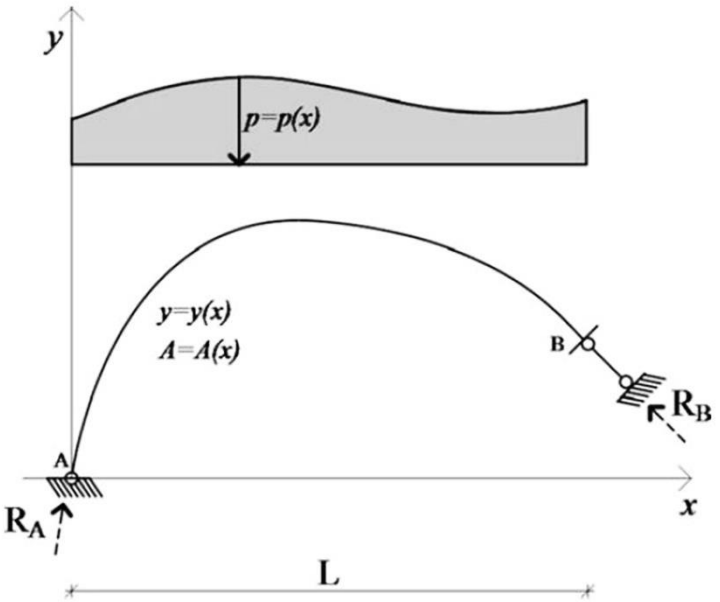

Figure 2. 6 Statically determinate arch with variable cross-sectional area $A(x)$, subjected to a distributed load $p = p(x)$ (Marano, Trentadue, and Petrone 2014)

Furthermore, Marano et al. (Marano et al. 2018) extended the results by (Marano, Trentadue, and Petrone 2014) by integrating the objective function to be minimized by adding the horizontal thrust of the arch to its volume in a linear combination. In particular, the minimization of the horizontal thrust aims to minimize the cost of foundations.

Trentadue et al. (Trentadue et al. 2018) further extended the problem of finding the optimal arch shape and variable cross-sectional area (Marano, Trentadue, and Petrone 2014) to the case of a statically determinate arch subjected to its self-weight and to a concentrated force on its crown section. By imposing that all cross-sections are subjected to uniform compressive stress, the authors analytically found and presented four optimal (i.e. momentless) solutions of different materials (i.e. concrete, steel, wood and masonry). As shown in *Figure 2. 7,* the four optimal arches are characterized by a similar dimensionless rise. However, it is worth noting that while in case of very "efficient" materials (i.e. with a high ratio between their maximum allowable stress

and specific weight) like steel and wood the optimal semi-arches resulted to have an extremely low curvature, in case of less "efficient" materials the curvature of two semi-arches are more emphasised.

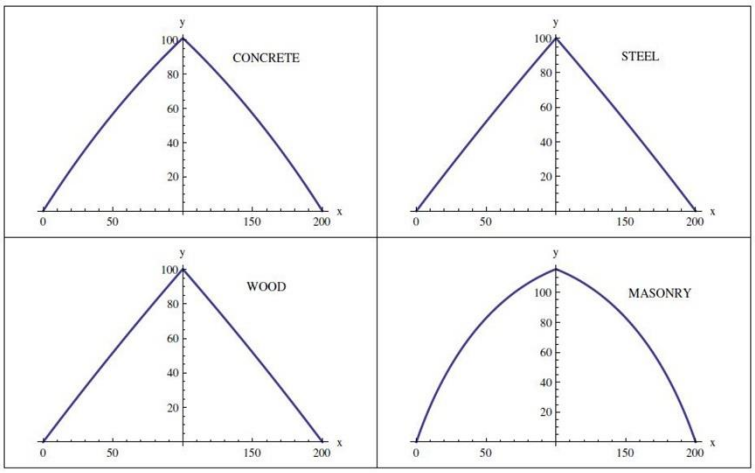

Figure 2. 7 Optimal arch shapes (Trentadue et al. 2018)

Furthermore, it has been shown that in the case of "efficient" materials a not relevant variation of the optimal cross section area between the base section and the key section occurs, while in the other cases this variation is more significant (Trentadue et al. 2018).

Vatulia et al. presented an analytical procedure to find the optimal shape and cross-sectional area of a three-hinged arch subjected to a uniformly distributed load, assumed as constant and variable depending on the arch axis (Vatulia et al. 2020). The authors thus found optimal axis equations and cross-sectional area of a momentless arch for different boundary conditions, by imposing that all cross-sections of the arch were subjected to only axial compressive uniform stress.

Poraminian and Ghaemian (Pouraminian and Ghaemian 2015) proposed an optimum design procedure to find the optimal shape of an open spandrel arch bridge, assuming the Cetina River Bridge (in Croatia) as a case study. A gradient-based Simultaneous Perturbation Stochastic Approximation (SPSA) algorithm was implemented in a MATLAB code. The arch depth at its crown and bases were included in a set of shape design variables even if they also define a dimension of the variable cross-section of the arch. The optimization process aimed to determine the optimal shape and variable depth of the arch minimizing its volume, considering strength (limiting the maximum stress) and serviceability (limiting the maximum displacements) constraints. The optimization of the Centina River Bridge was performed considering three load cases:

- Dead loads
- Live loads defined as traffic uniform and static load

- Wind loads as static actions.

The optimization process leaded to save the 30 % of the total volume of the sub-structure of the arch bridge with respect to its original design (Pouraminian and Ghaemian 2015).

More recently, Pouraminian and Pourbakhshian (Pouraminian and Pourbakhshian 2019) presented a new hybrid optimization algorithm, implemented in a MATLAB code, which allows to call a structural analysis software (ANSYS) in batch mode to perform FEM analysis to evaluate the objective and constraints functions (as shown in *Figure 2. 7*).

The presented method has been implemented to solve a multi-objective optimization problem through a Multi-Objective Particle Swarm Optimization (MOPSO) algorithm. Once again, the Cetina River Bridge was assumed as a case study. The optimization problem was formulated considering eight design variables, two objective functions (conflicting with each other) and several strength and serviceability constraints.

The total volume of the bridge sub-structure (i.e. the concrete arch and piers) was assumed as first objective function whereas the second objective function to be minimized was the first principal stress. The optimization process leaded to a pareto front of 20 optimum designs, among which a best compromise solution saving 25 % of volume with respect to the initial design of Cetina River Bridge.

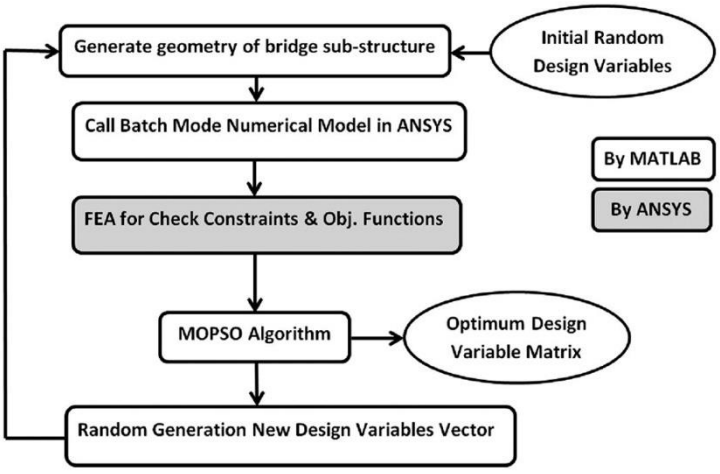

Figure 2. 8 Flowchart of a MATLAB-ANSYS optimization macro-algorithm (Pouraminian and Pourbakhshian 2019)

The literature also provides some examples of application of topology optimization (see section *§1.3.3*) in arch design. For instance, Paul et al. carried out a topology optimization with the help of the MSC Patran /Nastran software to find the optimal shape of an arch bridge with given span and rise, for assigned boundary conditions (Paul et al. 2015). For topology optimisation the arch bridge was modelled as a rectangular structure of height 3.25 m and length 15.0 m, made of

concrete and subjected to a uniformly distributed load, defined as a combination of dead and live loads. The compliance of the structure was assumed as objective function to be minimized, imposing a mass target of 25 % of the initial geometry.

Similarly, Shen et al. provided and compared the results obtained applying different topology optimization methods to find the optimal shape of three kinds of arch bridges (Shen et al. 2018). Several numerical examples have been provided, with different design rectangular domains and different boundary conditions (by changing the position of applied uniform load). Once again, the structural compliance was assumed as objective function to be minimized under volume constraints.

For instance, *Figure 2. 9* shows the design domain, the boundary conditions and the optimal layouts obtained by Parametric Level Set Method (PLSM), by Conventional Level Set Method (CLSM), by Bidirectional Evolutionary Structural Optimization (BESO) method and by Solid Isotropic Material with Penalization (SIMP) method.

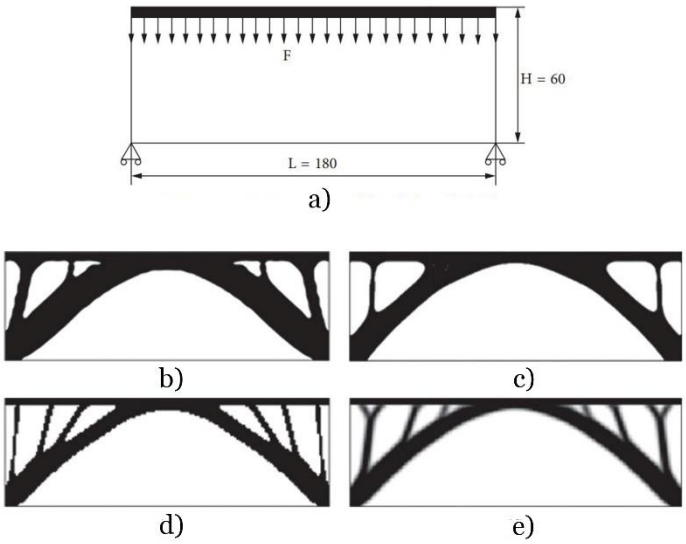

Figure 2. 9 Form-finding of a deck arch bridge through different topology optimization methods (Shen et al. 2018): (a) design domain and boundary conditions; (b) optimal layout by PLSM; (c) optimal layout by CLSM; (d) optimal layout by BESO; (e) optimal layout by SIMP

The problem of finding the optimal shape of arches was widely investigated. However, Tim L. Michiels first proposed a form-finding method for masonry arches under a combination of self-weight and in-plane seismic loading (Michiels 2018; Michiels and Adriaenssens 2018). The authors proposed a form-finding algorithm based on Thrust Line Analysis, which was applied under a combination of gravity and horizontal earth-quake loads. In particular, optimal shapes of arches of different predefined rise-to-span ratios (1/2, 1/4 and 1/8) were obtained for horizontal accelerations of 0.15, 0.3 and 0.45g (where g is the gravity acceleration). The form finding process proposed by Michiels starts by picking an arbitrary arch (for example a catenary arch) with predefined rise and span. After dividing this initial arch into a set of “voussoirs”, a thrust line is

calculated under the combination of gravity and horizontal acceleration. This thrust line usually needs to be adjusted iteratively by changing the location of the pole (thus varying the intensity of horizontal and vertical forces). Subsequently, the thrust line is mirrored along the axis of symmetry of the original arch shape to obtain a second thrust line to account for the other potential direction of the earthquake. The mirrored thrust line can be then horizontally moved to define a proper support thickness and each thrust line is then offset by a distance towards the top and bottom of the initial and mirrored thrust line, leading to four curves (as shown in *Figure 2. 10(a)*). The envelope of these four offset curves defines the new shape of the arch (see *Figure 2. 10(b)*). The obtained shapes require up to 65% less material than circular arches with constant thickness that are designed to withstand the same horizontal acceleration and self-weight, regardless of acceleration magnitude.

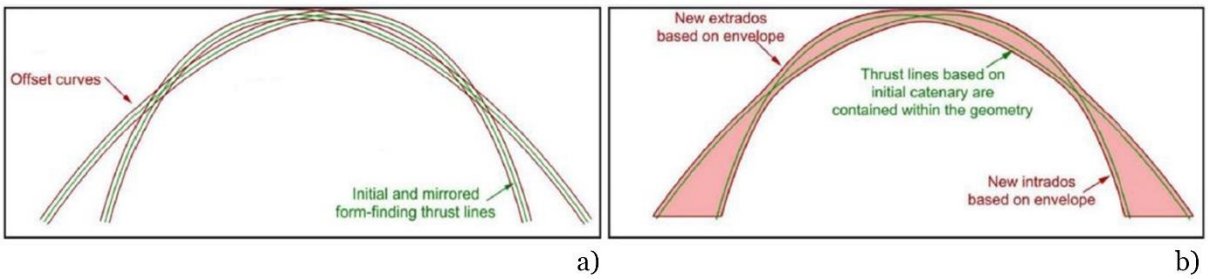

Figure 2. 10 Form-finding of masonry arches under gravity and seismic loading: (a) offset of the initial thrust line; (b) new intrados and extrados after taking the envelope of the curves of the offset curves. (Michiels 2018; Michiels and Adriaenssens 2018)

2.3 Structural optimization of truss arches: state of the art

Arches with multiple ribs, linked each other through two- or three-dimensional bracing-systems, are called *truss arches*. As a matter of fact, truss arches are vertically curved (arched) truss structures. Their structural efficiency is due to the fact that they take advantage of static properties of both truss structures and arches in carrying loading. They are commonly made of steel, that is stronger than masonry and concrete; hence, a steel arch may cover a longer span and be slenderer than a masonry or concrete arch. Furthermore, the innovative use of composite materials that takes advantage of the properties of both steel and concrete became common in arch bridge design. A peculiar example is provided by concrete filled steel tubular (CFST) arch bridges. Indeed, a concrete-filled steel tube (CFST) arch bridge is an outstanding type of steel-reinforced concrete composite bridge, in which the local stability of a steel tube is improved by the concrete filling, while the toughness and strength of the concrete are improved by the external covering of the steel tube. Many CFST arch bridges have been built in China since 1990 (Zheng and Wang 2018). The longest CFST arch bridge in the world, with a main span of 530 m, the First HeJiang Yangtze River Bridge (also known as Bosideng Bridge (*Figure 2. 11(d)*), sited in Rongshan Town, Hejiang, Luzhou City, Sichuan Province, China) is a truss arch bridge (Mou et al. 2015).

Truss arches are effectively used in steel and CFST arch bridges, especially when the arch span exceeds 200 meters (five out of the six steel arch bridges with a span larger than 500 m are truss arch bridges (Chen and Duan 2014)). Truss arch bridges with a span larger than 500 m are the Sydney Harbor Bridge (*Figure 2. 11(a)*), the New York's Bayonne Bridge (*Figure 2. 11(b)*), the New River Gorge Bridge (*Figure 2. 11(c)*), the Bosideng Bridge (*Figure 2. 11(d)*) and the Chaotianmen Bridge (*Figure 2. 11(e)*).

Since a large number of parameters must be considered in the design of truss arch bridges, it is immediate to understand how much beneficial it would be the development of an effective strategy able to optimize truss arches with the purpose of maximizing their structural performance thereby minimizing their cost, in light of their widespread use in long-span arch bridges.

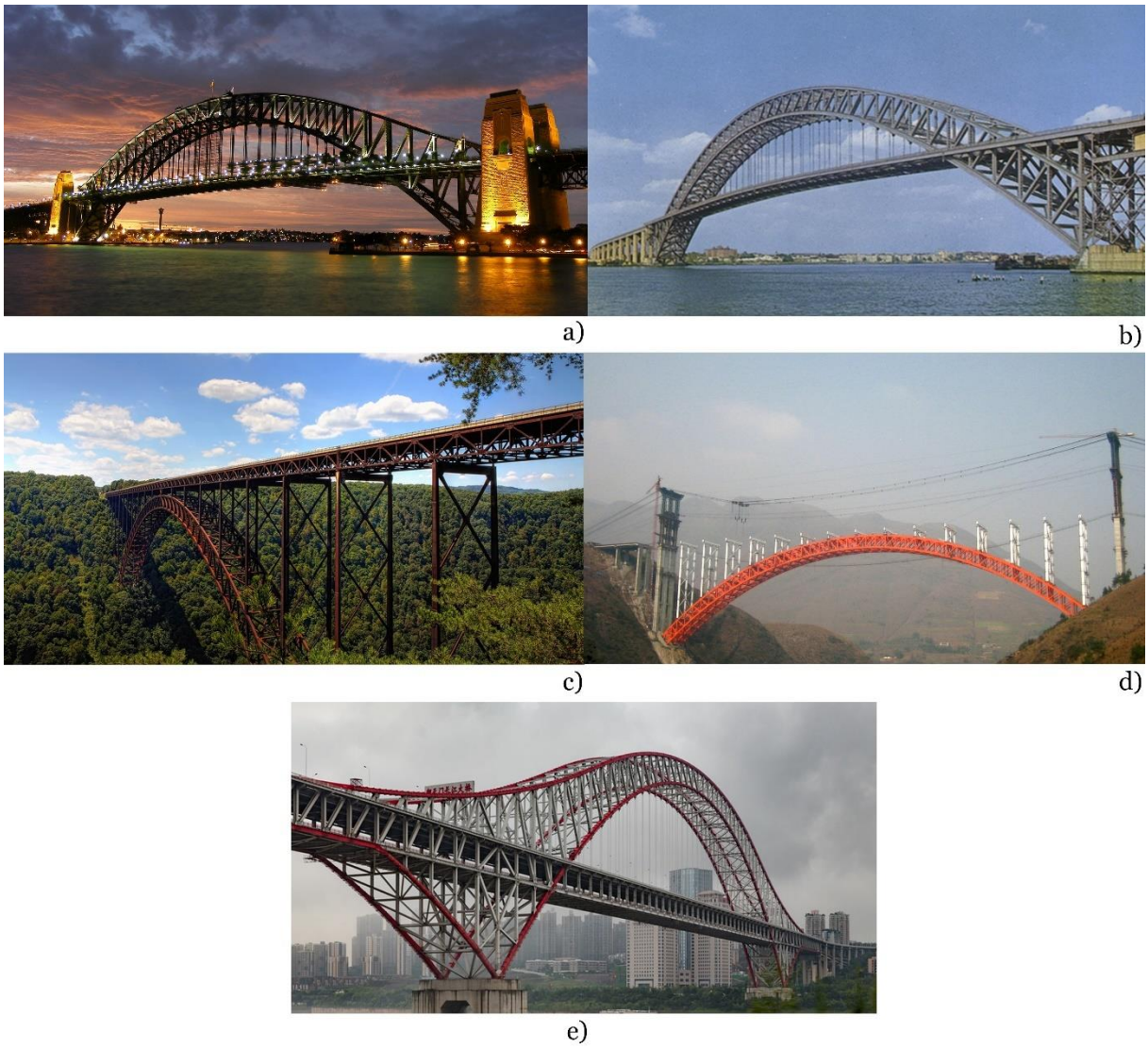

Figure 2. 11 Longest truss arch bridges in the world: (a) Sydney Harbor Bridge, Sydney, Australia, 1932 (503 m); (b) Bayonne Bridge, Staten Island, New York-Bayonne, New Jersey, USA, 1931 (510 m); (c) New River Gorge Bridge, Fayetteville, West Virginia, USA, 1977 (518 m); (d) Bosideng Bridge, Hejiang County, Sichuan, China, 2012 (530 m); (e) Chaotianmen Bridge, Chongqing, China, 2009 (552 m).

2.3.1 Topology, shape and size optimization of truss arches

The literature provides only a few works that faced the problem of structural optimization of truss arches; furthermore, most of them only concern size optimization of member cross-sections.

Jin Cheng in (Cheng 2010) addressed the problem of minimizing the weight of a truss arch bridge, according to strength (stresses) and serviceability (deflections) constraints. The author developed a hybrid optimization algorithm (whose flowchart is illustrated in the *Figure 2. 12*), integrating a Genetic Algorithm (GA) with Finite Element Method (FEM), the latter used to calculate implicit objective and constraint functions.

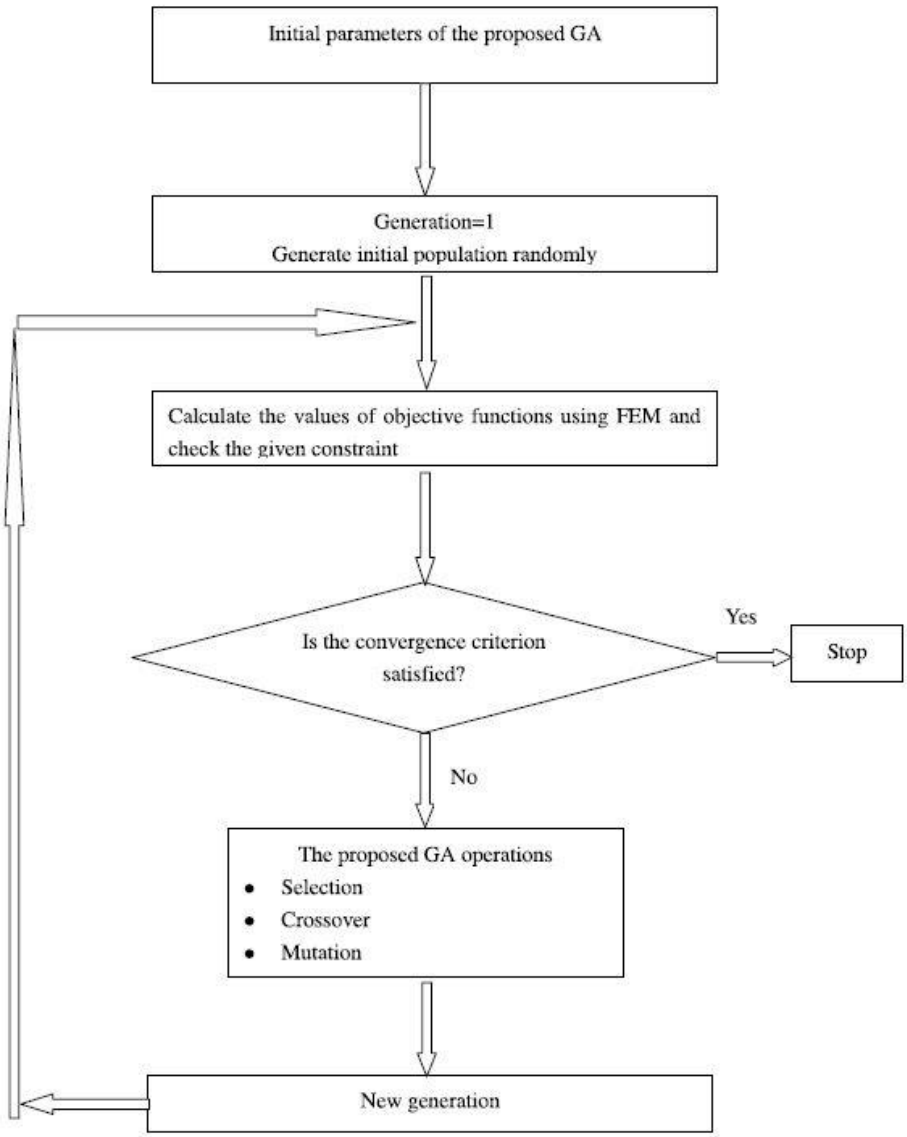

Figure 2. 12 Flowchart of the hybrid genetic algorithm proposed in (Cheng 2010)

The proposed macro-algorithm has been applied to optimize a simplified two-dimensional model of the Chaotianmen Bridge (Chongqing, China, 2009) with a main span of 552 meters (thus resulting the longest steel arch bridge in the World) and a rise to span ratio equal to 1/4.31.

Nonetheless, only size design variables (cross-sectional areas of groups of elements) were involved in the optimization problem. The author applied his hybrid optimization algorithm to different optimization problems, each characterized by a different grouping of elements (as well as by a different number of continuous and discrete size design variables, i.e. assuming 4, 10 and then 41 different cross-sectional areas). In the end, the author compared the results of a traditional design with optimized solutions in order to demonstrate the efficiency of his optimization strategy.

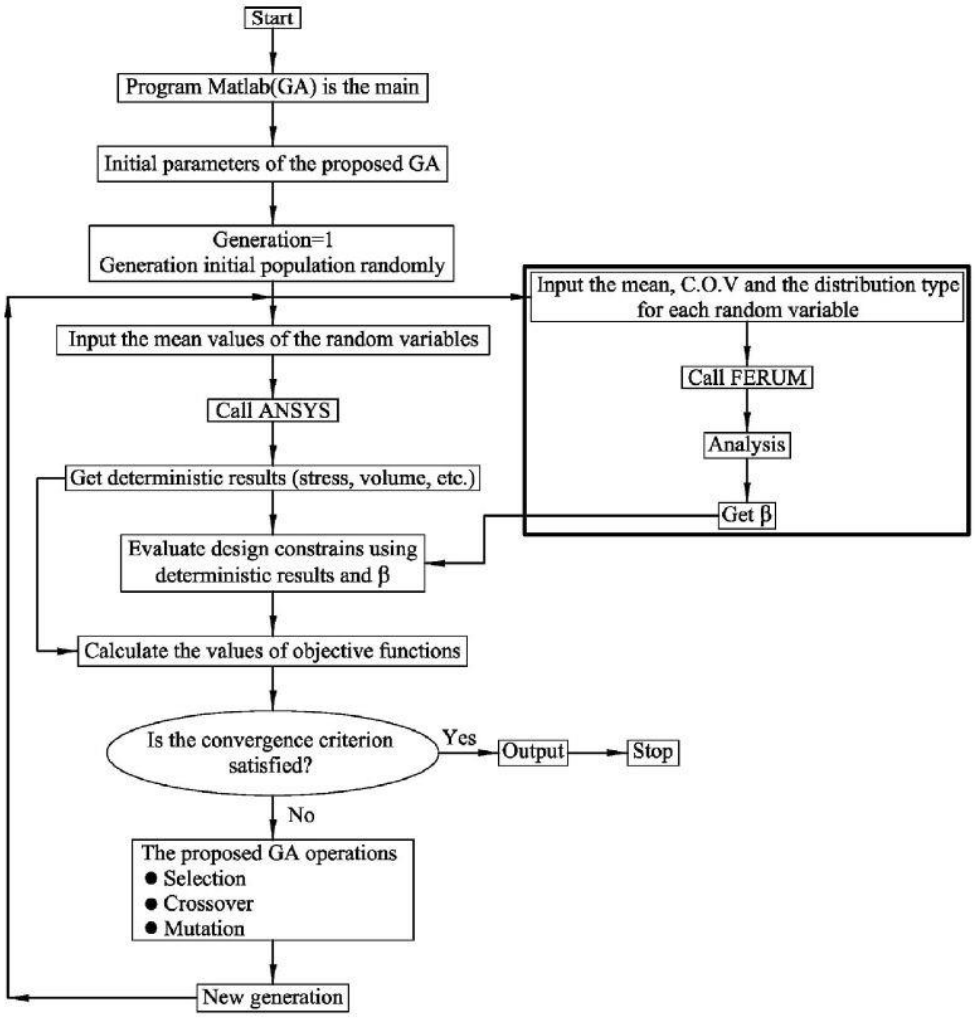

Figure 2. 13 *Flowchart of the hybrid Genetic Algorithm for reliability-based design optimization proposed in (Cheng and Jin 2017)*

More recently, Jin Cheng and Hui Jin in (Cheng and Jin 2017) proposed a reliability-based optimization (RBO) approach applied to minimize the weight of steel truss arch bridges subject to probabilistic (the overall probability failure of the structure) and deterministic (stress and deflection) constraints. The method proposed in this work integrates a Genetic Algorithm (GA), FEM and the first order reliability method (FORM), as shown in *Figure 2. 13*. The finite element method (FEM) and the first order reliability method were used to compute the value of the probabilistic and deterministic constraint functions.

The finite element analysis is performed using the ANSYS program. The reliability problem is solved by using FERUM. For the specific RBO problem considered in (Cheng and Jin 2017), the authors used MATLAB to formulate and solve the design optimization problem, as well as to manage the flow of information from one computer program to another. Once again, a simplified two-dimensional model of the Chaotianmen Bridge has been adopted as numerical study case. Only the cross-sectional areas of four groups of elements (as shown in the *Figure 2. 14*) have been assumed as design variables (continuous and discrete) of the problem; therefore, only size optimization has been performed. Eventually, the authors compared the results of deterministic optimal design and reliability-based optimal design (with reliability constraints), finding that the reliability-based optimal design was about 22% heavier than the deterministic optimal design.

M. H. Makiabadi and other authors (Makiabadi et al. 2013) investigated the effectiveness of a recently developed population-based algorithm, called as *Teaching-Learning-Based Optimization (TLBO)* algorithm in sizing optimization of real truss arch bridges. The *TLBO* algorithm emulates the process of teaching and learning in a classroom. The optimization process involves two stages including teacher phase and learner phase.

The proposed method has been applied to optimize two existing truss arch bridges:

- the Burro Creek Bridge (Arizona, U.S., 1966)
- the West End-North Side Bridge (Pennsylvania, U.S., 1932).

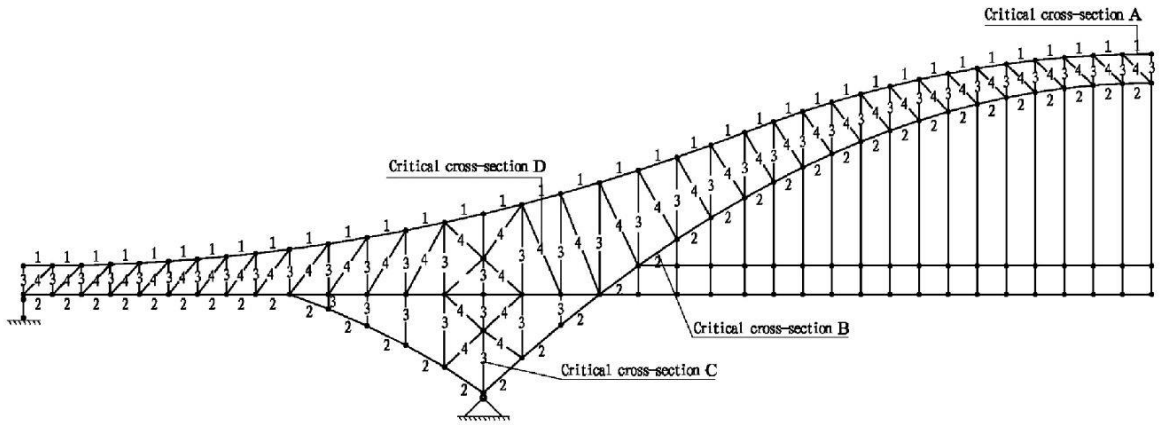

Figure 2. 14 *Element group definitions for the Chaotianmen bridge model (for one half of the bridge, because of its symmetry) from (Cheng and Jin 2017)*

In both cases, the optimization problem has been defined for minimizing the total weight of the structure, in accordance with strength (stresses) and serviceability (deflections) constraints, assuming cross-sectional areas of element groups, as size design variables and a uniform total load (including dead and live loads) applied to the bridge deck.

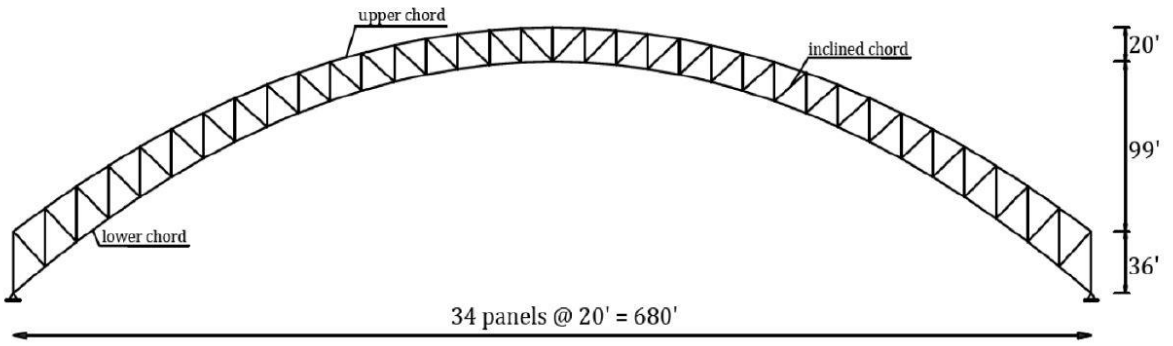

Figure 2. 15 Elevation of Burro Creek Bridge (Makiabadi et al. 2013)

The Burro Creek Bridge (with a span of 207 meters), is a truss arch structure with spandrel columns supporting the roadway deck and plate girder approach spans. Both upper and lower chords shapes are quadratic parabola (see the *Figure 2. 15*).

The sizing optimization problem has been formulated considering three different groups of variables including four, eight and twelve continuous size design variables.

On the other hand, the West End-North Side Bridge (having a span of 240 meters) is a steel bowstring truss arch bridge (whose elevation is illustrated in *Figure 2. 16*).

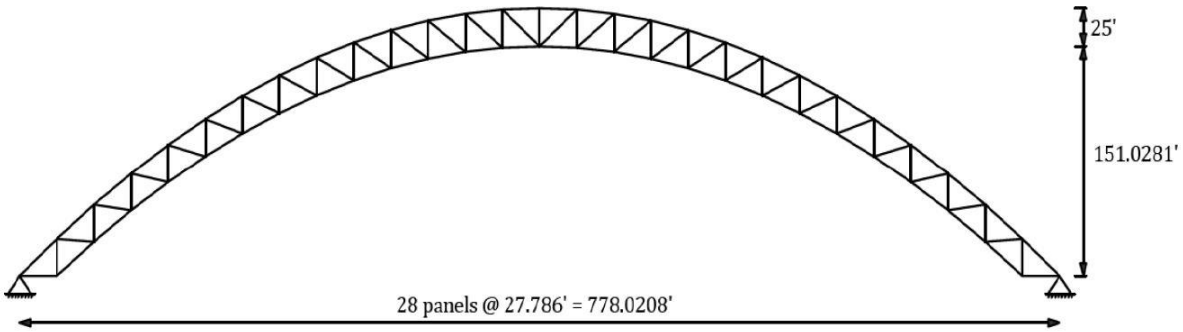

Figure 2. 16 Elevation of West End-North Side Bridge (Makiabadi et al. 2013)

Two different formulations of the optimization problem have been defined, one with four and the other with eight groups of element cross-sections (i.e. four and eight size design variables).

The authors compared the results obtained from different formulations of the optimization problem (each one characterized by a different number of design variables) for both bridges (the Burro Creek Bridge and the West End-North Side Bridge) with the actual weight of the real structures. Furthermore, as expected, they obtained better results (lighter optimal structures) by increasing the number of assumed design variables.

More recently, Malik Mushthofa and other authors (Mushthofa, Aminullah, and Muslikh 2019) showed some applications of shape and size optimization of steel truss arch bridges, assuming

cross-sectional areas of elements groups as size design variables and the rise over span ratio as shape design variable.

In (Mushthofa, Aminullah, and Muslikh 2019) the optimization problem was formulated to minimize the normalized magnitude of differences between maximum and minimum internal forces (axial forces, shear forces and bending moments) in truss arch bridges with different spans and rise-to-span ratios, according to strength and serviceability constraints.

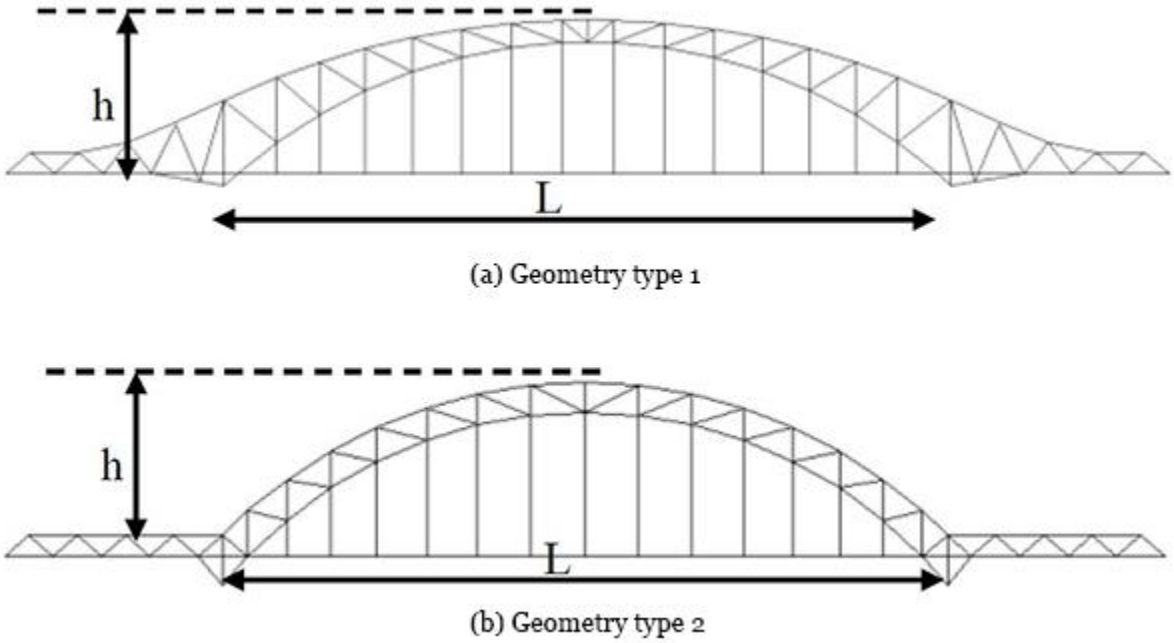

Figure 2. 17 Initial geometries: (a) type 1 and (b) type 2 (Mushthofa, Aminullah, and Muslikh 2019)

The process of geometry optimization is done by using SAP2000 software, by changing rise-to-span ratio parameter.

Bridge modelling is carried out for spans of 150 m, 200 m, 250 m and 300 m, as well as for each of two initial geometries (see Figure 2. 17(a) and (b)). For each span and geometry, a bridge FEM model was realized with a specific rise-to-span ratio, varying from a ratio of 1/2.25 to 1/8.00 with intervals of 1/0.25. The optimization process was then carried out by only comparing internal forces values of 96 FEM models (each characterized by a different rise to span ratio between 1⁄2.25 and 1⁄8.00) for each truss geometric and topological configuration, without applying a proper optimization algorithm.

In the end, Khaoula Msaaf considered the problem of single and multi-objective optimization of steel truss arch bridges in his master's degree dissertation (Khaoula Msaaf 2017). The Gustave Eiffel's Garabit Viaduct (France, 1884) was assumed as case-study (whose frame structure is shown in *Figure 2. 19*).

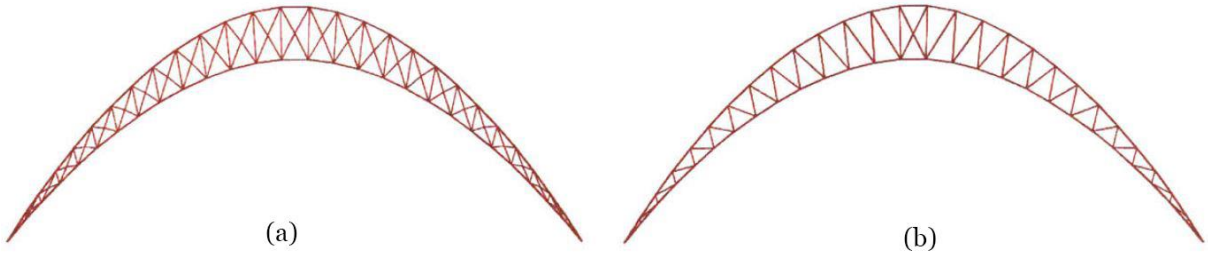

Figure 2. 18 *Two different topologies of the truss arch to be optimized: (a) type 1 and (b) type 2 (Khaoula Msaaf 2017)*

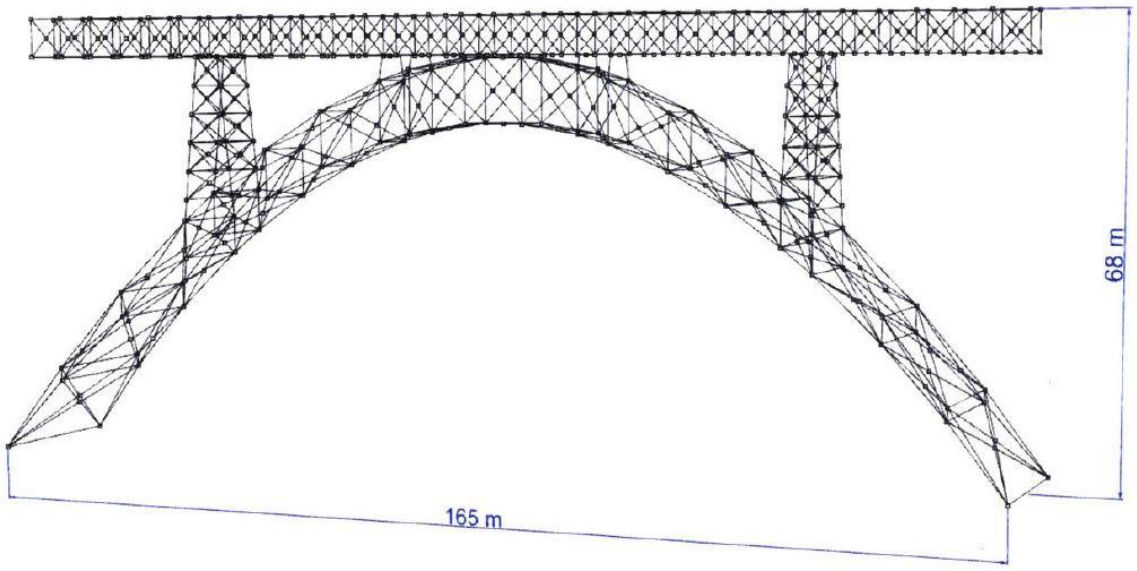

Figure 2. 19 *Three-dimensional frame structure of the Garabit Viaduct designed by Gustave Eiffel (Khaoula Msaaf 2017)*

Two- and three-dimensional parametric models of the truss arch bridge were realized with two different web configurations (see the *Figure 2. 18*), three different spans (100 m, 165 m and 200 m) and optimized uniquely in Grasshopper environment.

Three different combinations of gravity and live loads have been considered in two-dimensions, whereas five load cases have been considered in three-dimensions (since two wind-load combinations have been here considered). For each load case, a FEM analysis was carried out in Grasshopper environment (by means of a proper tool) in order to evaluate the total weight of the structure and its maximum deflection. The author defined a parametrized geometry by different design variables such as the number of piers, the depths at the crown and the base, the number of truss webs, and the height of the deck (shape design variables).

Size design variables (cross-sectional areas of the elements chosen from a list of 40 discrete values) were optimized by means of a specific component of the Grasshopper FEM tool that allows to limit the maximum percentage of the material utilization and maximum deflection, providing the total weight of the structure and its maximum deflection (objective functions of the problem).

Then, single and multi-objective optimization have been carried out by means of proper Grasshopper tools, minimizing the structural weight of the structure and its maximum deflection (resulting from FEM analysis) in separated and simultaneous phases.

It is worth noting that the single-objective optimization tool relies on gradient-free deterministic algorithms. This algorithm was used in two steps: a first run starting from a random point in the design space and using a global algorithm, and a second run starting from the best design chosen by the global algorithm and exploring the small area of the design space surrounding that point using a local algorithm. On the other hand, the Multi-Objective optimization tool was used by adopting an evolutionary algorithm (i.e. a stochastic optimization algorithm).

As expected by the author, deflection-based optimization provided solutions with highest structural weights, whereas weight-based optimization generated solutions with minimum structural weights (saving more than 60% of the weight of the original structure) but greater deflections. Multi-objective optimization runs produced some Pareto optimum solutions, characterized by trade-off between structural weight and maximum deflection optimal values. Furthermore, the author found that the second topology (shown in *Figure 2. 18(b)*) produced best results in most cases and he finally concluded his study pointing out the importance of choosing a proper shape and topology in the design of truss arch bridges.

Part II

Parametric design and structural optimization methods

Chapter 3

3. Not-integrated methods for parametric design and structural optimization

This section briefly illustrates some examples of not-integrated methods combining parametric design and structural optimization techniques, which are applied one after the other in separated phases of a design process.

Despite the disadvantage just mentioned, the effectiveness of these methods has been demonstrated through their application in optimal design of continuous and discrete structures.

3.1 Thrust Network Analysis (TNA) and Finite Element Method (FEM) analysis

Thrust Network Analysis (TNA) is a three-dimensional version of *Thrust-Line Analysis*, as previously anticipated in *§1.3.2* where most known form-finding techniques have been briefly introduced (Adriaenssens et al. 2014; Veenendaal and Block 2012).

Thrust Network Analysis was developed by the Block Research Group at the ETH of Zurich (Switzerland) for the form-finding of compressive funicular shells by taking advantage of graphic statics computer techniques (Block 2009; Block and Ochsendorf 2007). The method belongs to *Geometric Stiffness Methods* for form-finding and it is independent from material properties. It was developed (and is particularly suitable) for designing masonry vaults that should be compressed in any direction due to the low tensile strength of the material.

The *TNA* method is based on the assumption (derived from descriptive geometry) that a three-dimensional network under vertical external loads is in compression when its projection on the horizontal plane is also in compression. The form-finding procedure of a uniformly compressed vault (or shell) by *Thrust Network Analysis* method is performed by the simultaneous manipulation of two reciprocal and planar diagrams:

- the form diagram **Γ**, which is the horizontal projection of a three-dimensional auxiliary network **G**

- the force diagram **Γ***, which is constituted by the horizontal components of the forces that act on each bar of the compressed network.

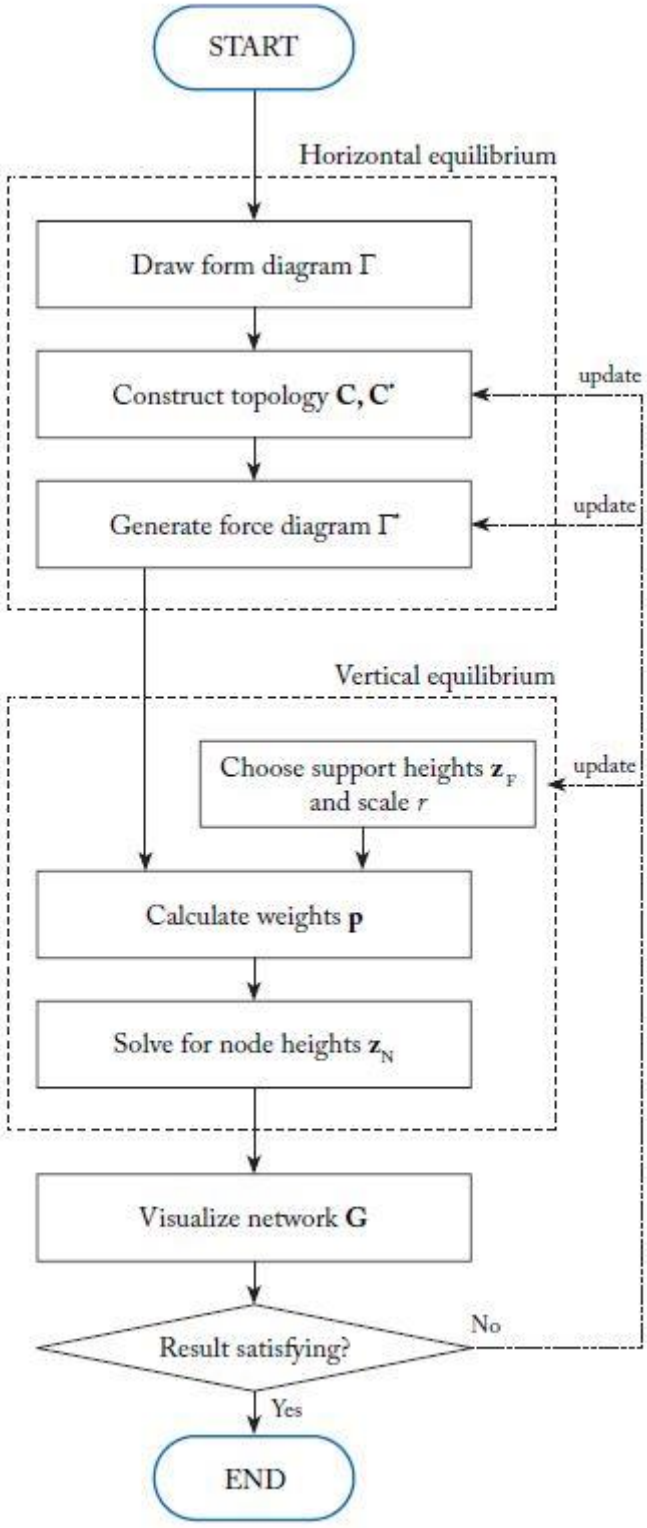

Figure 3. 1 Thrust Network Analysis (TNA) flowchart (Adriaenssens et al. 2014)

The relation between two reciprocal bi-dimensional diagrams and the auxiliary spatial network is clearly illustrated in *Figure 1. 7* in the previous section *§1.3.2*. Form and force diagrams are reciprocally related, i.e. they are *dual parallel graphs*. This means that branches that converge at a certain node in the form diagram **Γ** form an equilibrium force polygon in the force diagram **Γ*** and vice versa. Indeed, each side of all polygons of **Γ** and the corresponding force of the related equilibrium polygon in **Γ*** must be parallel within a certain tolerance angle that is generally included between 5° and 10° ("parallelism condition"). From a statical point of view, the equilibrium of a node in one graph is guaranteed by a closed polygon of force vectors in the other graph, and vice versa. The length of each branch **e*** of the force diagram **Γ***, multiplied by an assigned scale factor ς, provides the magnitude of the axial force that acts in the corresponding branch e of the form diagram **Γ**, as well as the magnitude of the horizontal component of the axial force that acts on the corresponding bar of the three-dimensional thrust network **G**.

The reciprocal relationship between **Γ** and **Γ*** cannot (by itself) guarantee that all network bars are in compression. A further necessary condition so that the funicular network is purely compressed is that vectors of all closed polygons of **Γ** rotate in counterclockwise direction with respect to any point inside the closed polygon. In addition, all polygons of **Γ** and **Γ*** must be convex ("convexity condition") to prevent the formation of tension forces or tensile stresses in any vault regions. Eventually, the auxiliary *thrust network* adopted to find the optimal shape of a masonry vault (or concrete shell) is totally compressed if reciprocity and further just mentioned conditions are satisfied, provided that only vertical loads are considered (Adriaenssens et al. 2014).

Since the equilibrium of horizontal force components can be computed regardless of the external vertical loading, the form-finding procedure through a *Thrust Network Analysis (TNA)* method can be divided into two distinct phases (*Figure 3. 1*):

- the solution of the horizontal equilibrium
- the solution of the vertical equilibrium.

The above described form-finding procedure generates purely compressed networks of nodes and bars that can be easily interpolated through a NURBS surface by means of any CAD (computer-Aided Design) software, by taking advantage of direct and parametric modelling techniques.

In the end, a Finite Element Model (FEM) of the vault or shell, built up by assigning a variable or constant thickness to the medium surface (obtained through a TNA form-finding), as well as real material and boundary conditions, can be analysed to check the quality of results (e.g. by verifying the effectiveness of the method in reducing tensile stress regions). The method cannot be considered integrated since the Finite Element Analysis is not performed at internal steps of the shape optimization (form-finding) procedure. This implies that the whole form-finding procedure

need to be repeated for an undetermined number of times until satisfactory results (in term of both design qualities and structural efficiency) are obtained.

3.1.1 Form-finding (shape optimization) of anticlastic shells for curved footbridges

The effectiveness of the not-integrated optimization method illustrated in *§3.1* was demonstrated by applying it in an unconventional way to find the optimal shape of concrete anticlastic shells, properly designed to support curved footbridges (Luigi Fenu et al. 2019, 2017; Luigi Fenu, Congiu, and Briseghella 2016; Luigi Fenu, Briseghella, and Congiu 2016; L Fenu, Briseghella, and Congiu 2016).

Thrust network Analysis (TNA) method has been applied to find the optimal shape of the medium surface of anticlastic shells. The TNA method was applied in a non-standard manner by drawing form and force diagrams in a vertical plane (*Figure 3. 2*), shaping the shell by applying the boundary conditions (*Figure 3. 2(a)*) and allowing relaxation in the horizontal direction, as the shell was subjected to horizontal forces without gravity.

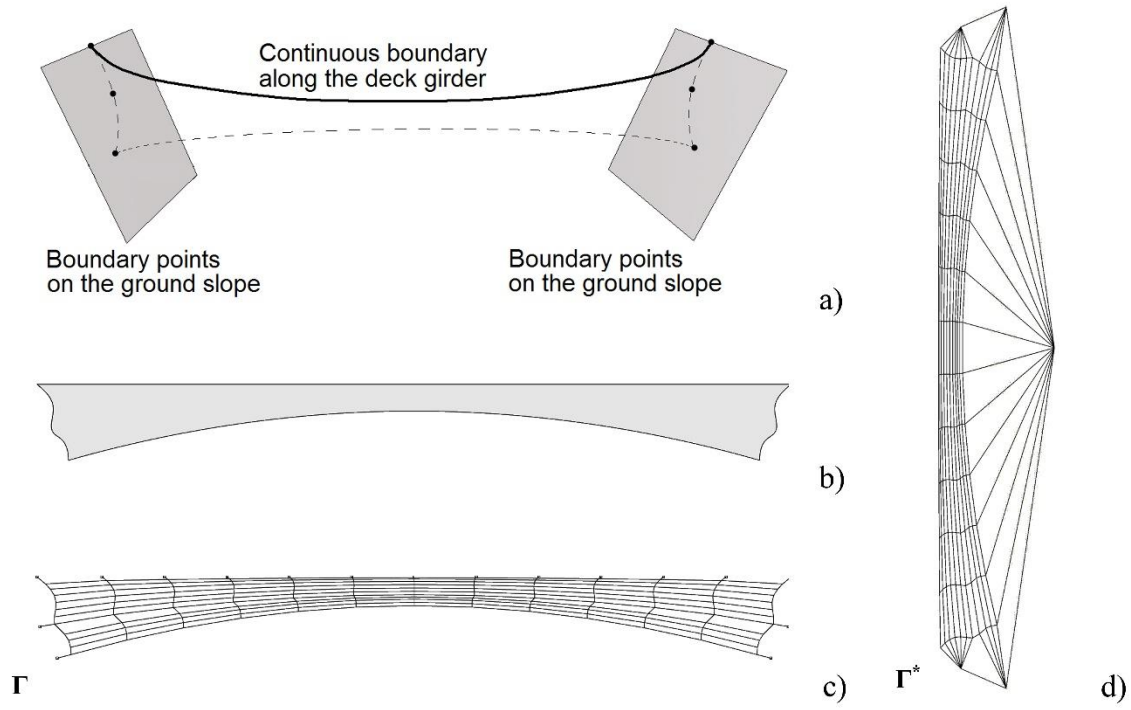

Figure 3. 2 *Thrust Network Analysis (TNA) form-finding: (a) boundary conditions; (b) starting surface; (c) initial form diagram **Γ**; (d) initial force diagram **Γ*** (Luigi Fenu et al. 2019)*

The initial form diagram **Γ** (*Figure 3. 2(c)*) was obtained by discretizing a starting surface (*Figure 3. 2(b)*), whereas the initial force diagram **Γ*** (*Figure 3. 2(d)*) was drawn in accordance with reciprocity conditions (mentioned in the previous section *§3.1*). Indeed, the initial force diagram **Γ*** is reciprocal with respect to the initial configuration of **Γ** but it does not yet represent a diagram

of equilibrium forces. In solving the horizontal equilibrium of the thrust network **G**, form and force diagrams were iteratively and simultaneously deformed until, in addition to "reciprocity condition", even "parallelism" and "convexity conditions" (previously explained in §3.1) were satisfied.

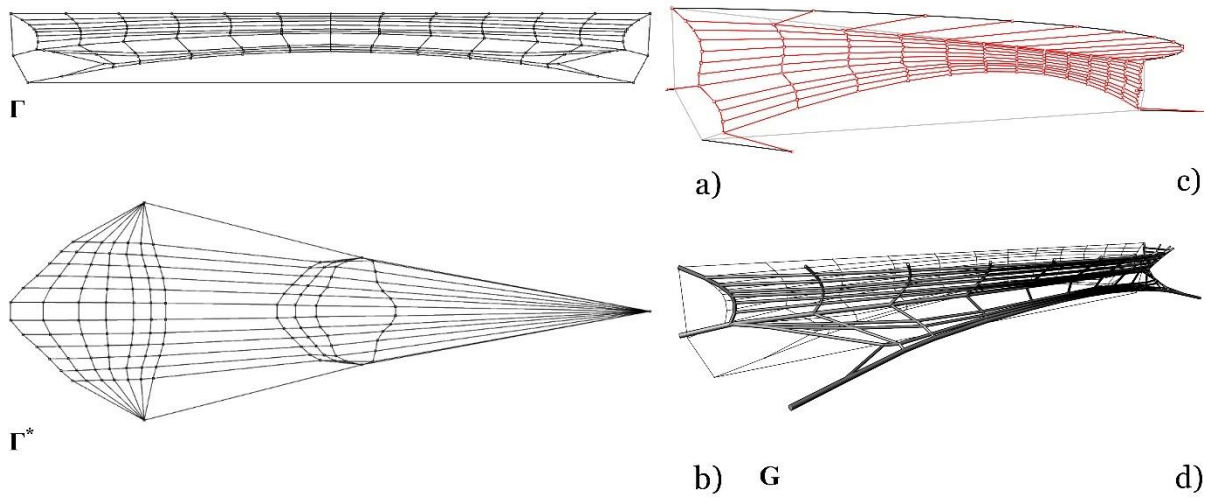

*Figure 3. 3 Thrust network Analysis (TNA) form-finding: (a) final form diagram **Γ**; (b) final force diagram **Γ***; (c) 3D-boundary conditions; (d) optimized thrust network **G** (Luigi Fenu et al. 2019)*

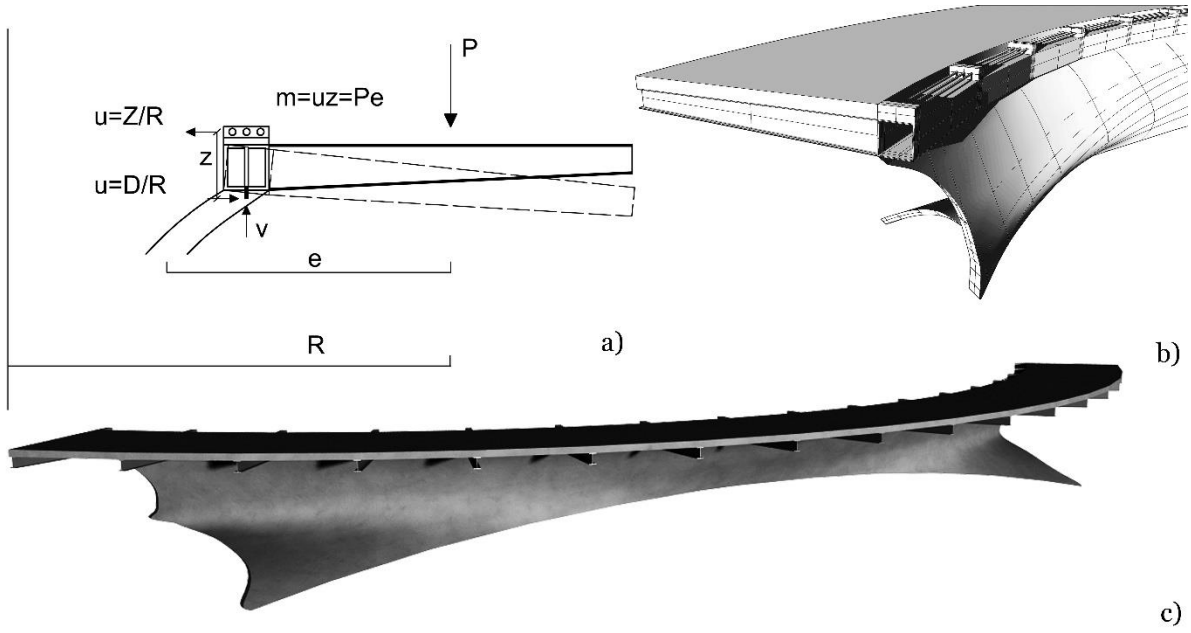

Figure 3. 4 Three-dimensional model of the shell-supported curved footbridge: (a) transversal deck cross-section; (b) perspective detail of the deck arrangement; (c) perspective view of the footbridge (Luigi Fenu et al. 2019)

Once the force diagram really represented the horizontal equilibrium of the network (assuming the configuration of the final force diagram **Γ*** in *Figure 3. 3(b)*), the vertical equilibrium of the network could be solved for given spatial boundary conditions (*Figure 3. 3(c)*) and external loads

that had to be orthogonal to the plane on which form, and force diagrams lie. The so-optimized thrust network **G** was visualized in three-dimensions (*Figure 3. 3(d)*).

For a force diagram representing a horizontal equilibrium configuration, several vertical equilibrium solutions can be found thereby obtaining different thrust networks **G** characterized by different levels of relaxation. Indeed, varying the relaxation level of the thrust network means increase or decrease the load values. Moreover, the more relaxed the network, the lower the internal forces acting in it and vice versa.

As anticipated in the previous section *§3.1,* since the method is not integrated, the quality of results can be only checked once the whole form-finding procedure is concluded. For this reason, the optimal solution was hand-selected by comparing design quality and structural performance of several optimal shells, all obtained by interpolating nodes of different thrust networks generated from a TNA form-finding routine for various boundary conditions (i.e. different loads and support positions).

Each shell was then subjected to a Gaussian curvature analysis (by searching for anticlastic shells with most negative distribution of Gaussian curvature) and structural analysis of a FEM model of the whole bridge structure (shown in *Figure 3. 4*).

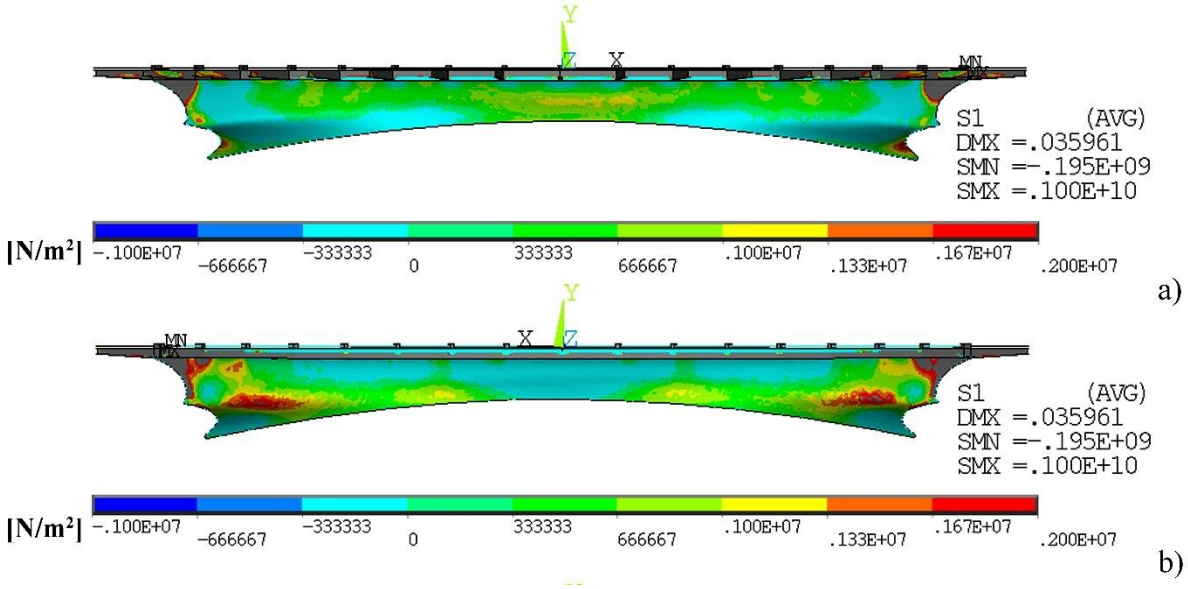

Figure 3. 5 FEM analysis results: (a) tensile stress distribution on the shell front; (b) tensile stress distribution on the shell back (Luigi Fenu et al. 2019)

FEM analysis thus allowed to choose the shell with minimized tensile stress regions (*Figure 3. 5*). Structural analysis indicated that the shell was prevalently in compression with a maximum compressive stress of 18 MPa. The excellent structural behaviour of the shell supported footbridge has been confirmed by the results of the FE analysis, which demonstrated that the non-

conventional form-finding procedure minimised unwished tensile stresses in the concrete anticlastic shell with uniform thickness.

3.1.2 Form-finding and size optimization of concrete free-form vaults

A similar not-integrated method was successfully applied to optimize shape and size (i.e. the thickness) of concrete free-form vaults.

As in the previous case, the medium surface of a free-form vault has been optimized through *Thrust Network Analysis (TNA)* form-finding method (whose resulting final form **Γ** and force **Γ*** diagrams, as well as the optimized thrust network **G** interpolated by a NURBS surface are shown in *Figure 3. 6*).

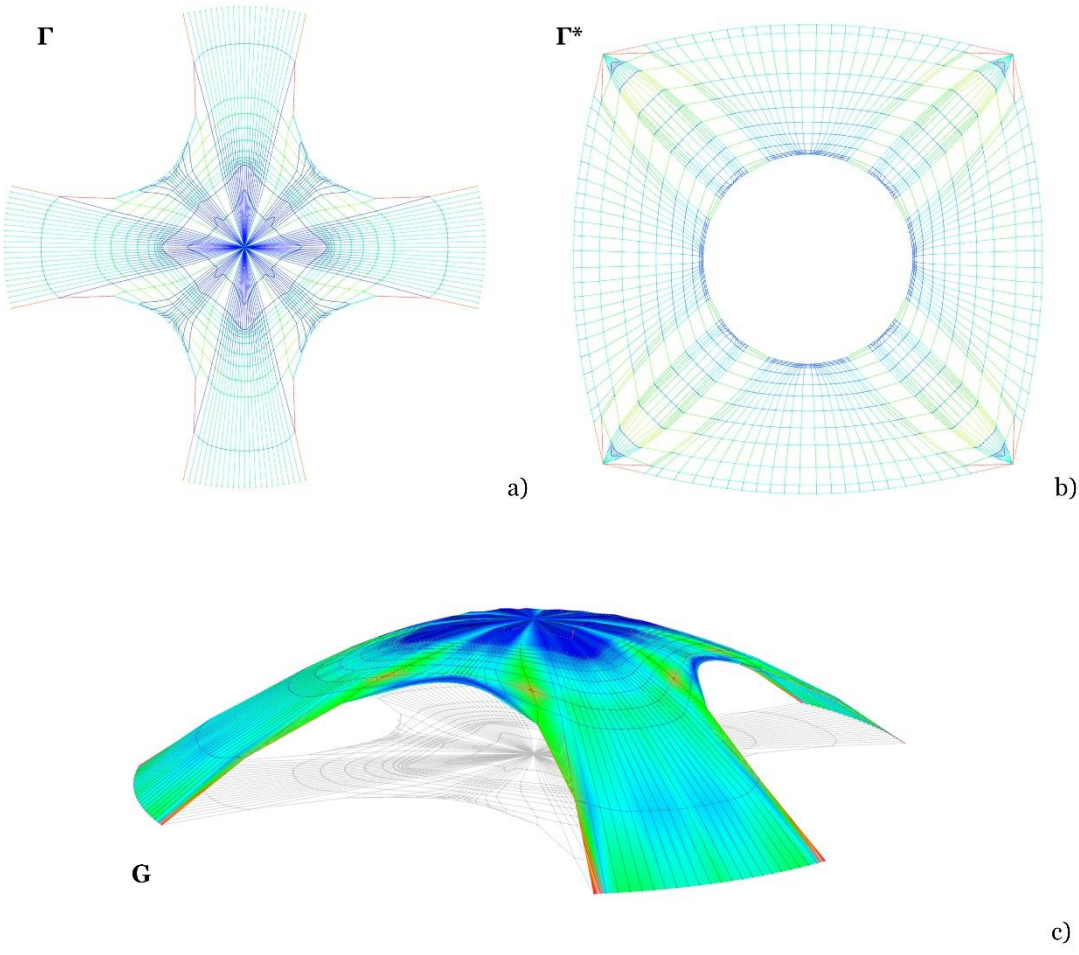

*Figure 3. 6 Vault form-finding through TNA: (a) final form diagram **Γ**; (b) final force diagram **Γ***; (c) optimized thrust network **G** interpolated through a NURBS surface*

Once an optimal medium surface was obtained (i.e. the shape optimization phase was concluded), a parametric FEM model was defined through a proper tool (called *Karamba3D*) for *Grasshopper* (mentioned in *§1.2.1* and described in (Tedeschi, Wirz, and Andreani 2014)). The parametric FEM tool (*Karamba3D*) for *Grasshopper*, allowed to assign a variable thickness to the concrete vault, by optimizing it for given boundary conditions (size optimization phase).

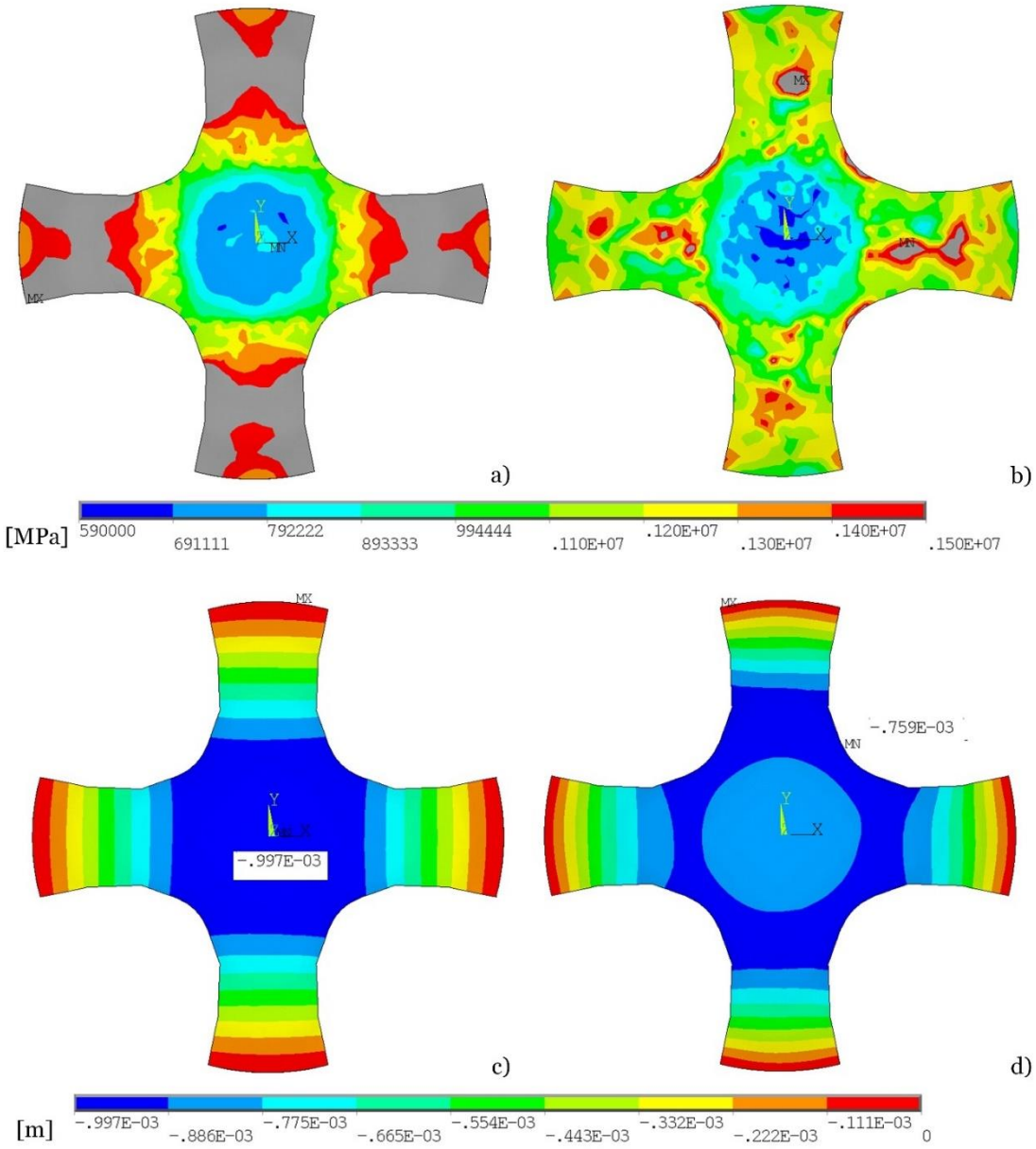

Figure 3. 7 Comparison of FEM analysis results: (a) Von Mises Stress distribution in constant thickness vault; (b) Von Mises Stress distribution in variable thickness vault; (c) maximum vertical deflections (u_z) in constant thickness vault; (d) maximum vertical deflections (u_z) in variable thickness vault

In the end, structural performance (evaluated trough FEM analysis) of a vault with a variable (from 0.015 to 0.12 m) optimized thickness and a constant thickness (of 0.046 m) vault with same optimized medium surface and equivalent volume was compared. It was found that structural behaviour of optimized concrete vault was better than that one of constant thickness vault, in terms of both, stress distribution and maximum deflections (under same loads).

Therefore, the analysis of final results validated the effectiveness of the proposed not-integrated method in optimizing a concrete free-form vaults, besides all phases (shape optimization, parametric FEM analysis and size optimization) were consecutively performed.

3.2 *Particle Spring (PS) System and Finite Element Method (FEM) analysis*

The *Particle-Spring (PS)* method (which is introduced in *§1.3.2*) belongs to *Dynamic Equilibrium* form-finding methods that solve problems of dynamic equilibrium by reaching a static equilibrium state (Adriaenssens et al. 2014). The *Particle-Spring* method aims to find structures in static equilibrium by defining the topology of a particle-spring network with loads on the particles, the masses of the particles, the stiffnesses and rest lengths of the linear elastic springs, and then by attempting to equalize the sum of all forces in this system. For instance, the gravitational pull on a mass causes the displacement of the associated particle and subsequently the elongation of the attached springs. This elongation produces in turn a counter internal force in the springs and stretching continues until the sum of internal forces acting in springs matches the downward force of the mass. Particles motion and springs forces are governed by *Newton's second law of motion* and *Hooke's law of elasticity*, respectively.

A standard *Particle-Spring* form-finding routine is based on the main following assumptions:

- Surfaces are discretized by lines and points. The latter are nodes with mass ("particles") whereas lines represent deformable linear elastic "springs" connecting the "particles" (which can be considered as lumped masses)
- Nodes can be fixed or free to move along each direction (which means that they can have from zero to three degrees of freedom)
- Both external (i.e. gravity and applied loads) and internal (acting in springs) forces act on nodes.

Stretching of "springs" (through applying forces on "particles") leads to iteratively obtain a balance of internal and external forces on each node, as well as an equilibrium optimal shape.

The form-finding flowchart of the *Particle-Spring (PS)* method is illustrated in *Figure 3. 8*. This method is not material-independent, and it can be adopted to perform a stretched cloth or a hanging cloth simulation. In a stretched cloth simulation gravity is usually turned off or set to a very low value and the rest-lengths of all the springs are very low or set to zero.

This type of simulation is commonly used to optimize anticlastic geometries. On the other hand, in a hanging cloth simulation, the particles are allowed to "fall" under the gravity loads and the rest lengths of springs along the boundary edges are set to be equal to their original lengths. Further, additional diagonal springs with differential strengths might be added to ensure that faces do not distort significantly during simulation. This type of simulation is more frequently used to optimize synclastic geometries (Adriaenssens et al. 2014).

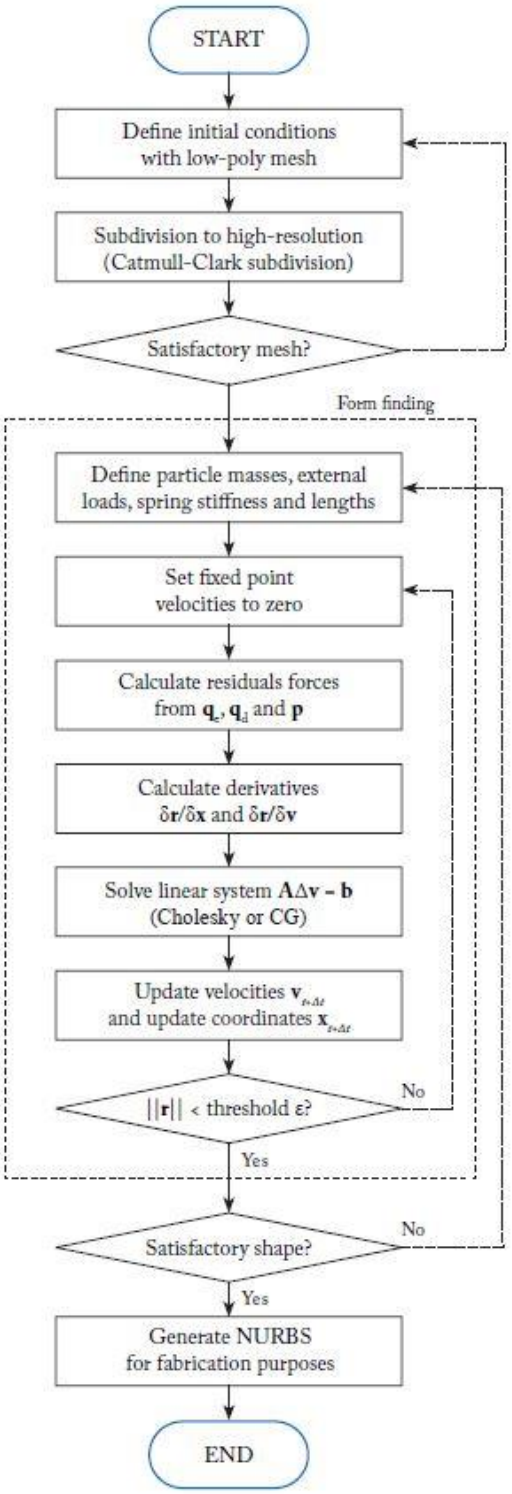

Figure 3. 8 Particle-Spring (PS) form-finding flowchart (Adriaenssens et al. 2014)

The *Particle-Spring (PS)* method can be performed in the parametric *Grasshopper* (Tedeschi, Wirz, and Andreani 2014) environment through a proper tool (called *Kangaroo*) or in the CAD platform *Autodesk Maya* by means of a suitable "dynamic solver" called *Nucleus* (Stam 2009).

However, regardless the adopted tool, once the shape optimization (form-finding) phase is concluded, FEM analysis of the whole model of the vault or shell (with assigned cross-section,

material properties and boundary conditions) need to be carried out in order to evaluate the quality of obtained results. The method cannot be considered integrated since the Finite Element Analysis is not performed at internal steps of the shape optimization (form-finding) procedure. This implies that the whole form-finding procedure need to be repeated for an undetermined number of times until satisfactory results (in term of both design qualities and structural efficiency) are obtained.

3.2.1 Form-finding (shape optimization) of synclastic shells in traditional Lecce's Star Vaults using a Particle-Spring (PS) system

In the region of Puglia in southern Italy, from the late 16th century onward and continuing to today, one finds the architectural tradition of a peculiar type of composite vault called the "Lecce vault" (*volta leccese*). The *Lecce vault*, which derives its name from the eponymous city (i.e. Lecce), is also designated as a "star vault" because, when viewed from below its form resembles a star (Fallacara 2012). As a composite vault, commonly with square or rectangular plan, the *Lecce vaults* combine several features of most traditional vaults as barrel, pavilion and cross vaults. The simplest types of *Lecce vaults* are known as:

- *"a spigoli" star vaults*, which are composed by four cylindrical lunettes (as portions of barrel or cross vaults) and a four-pointed star synclastic shell obtained as a star portion of a peculiar pavilion vault generated by an intersection of two semi-ellipsoids
- *"a squadro" star vaults,* which are also composed by four cylindrical lunettes, an eight-pointed star shell generated by an intersection of a four-pointed star shell (again obtained as a portion of an ellipsoidal pavilion vault) with four slices of a smaller ellipsoidal pavilion vault at its vertices.

The not-integrated optimization method described in *§3.2* was applied to optimize the shape of the star shell of *"a spigoli"* and *"a squadro" Lecce vaults,* by applying a *Particle-Spring (PS)* form-finding system and comparing the structural performance of optimized and not-optimized models in a later phase, in order to afterwards check the goodness of solutions.

The *PS* form-finding method was applied by means of *Kangaroo* dynamic solver in the *Grasshopper* parametric platform. In *Figure 3. 9* the main steps of the form-finding procedure of the four-pointed star shell of a *"a spigoli" Lecce vault* are illustrated. Since hanging cloth simulations are more suitable to find the optimal shape of a synclastic surface (as explained in *§3.2*), PS-method was applied by simulating an inverted hanging cloth, by applying forces upwards directed and assigning to springs a high stiffness coefficient and rest lengths equal to their initial undeformed lengths.

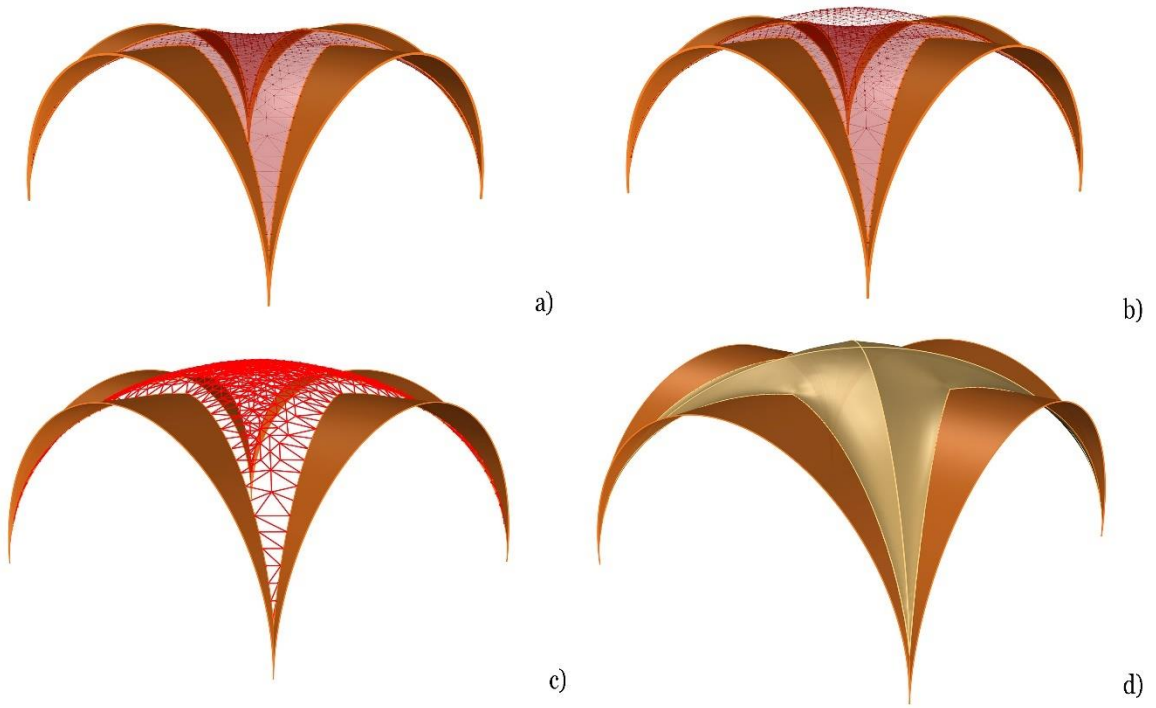

Figure 3. 9 Form-finding through a Particle-Spring (PS) system of a "a spigoli" Lecce vault: (a) initial particle-spring network; (b) particle-spring network deformed by forces acting on particles; (c) static equilibrium configuration of the network; (d) NURBS patch interpolating the optimized network.

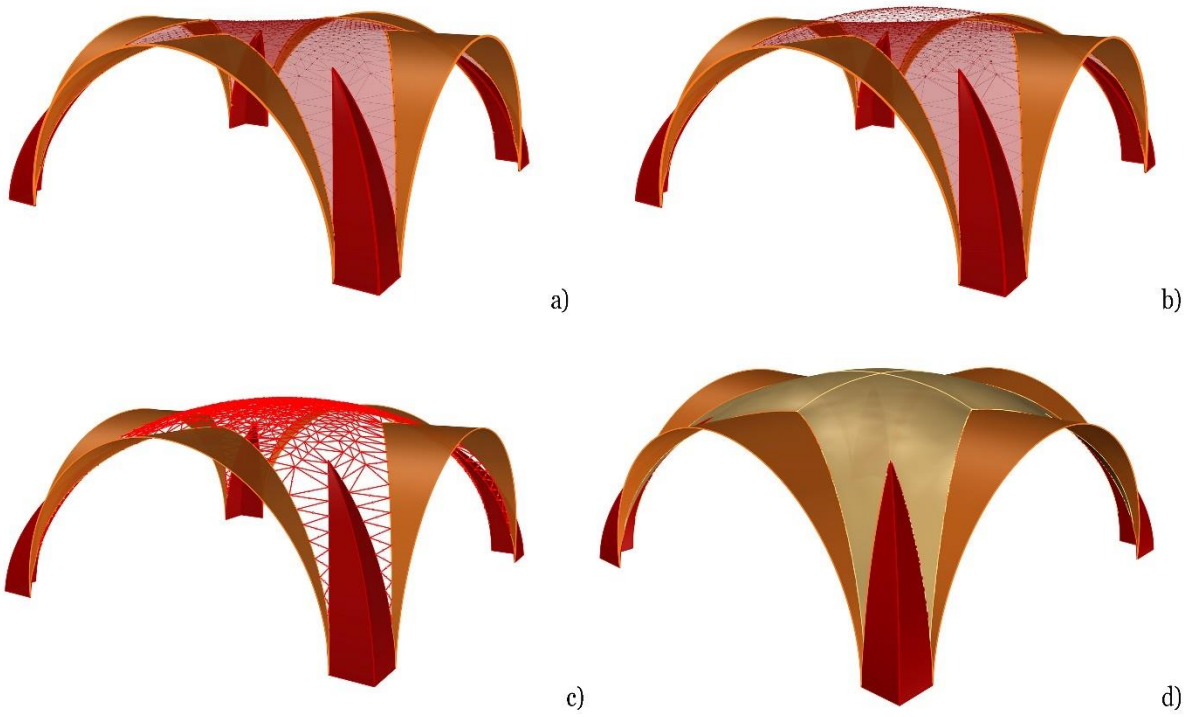

Figure 3. 10 Form-finding through a Particle-Spring (PS) system of a "a squadro" Lecce vault: (a) initial particle-spring network; (b) particle-spring network deformed by forces acting on particles; (c) static equilibrium configuration of the network; (d) NURBS patch interpolating the optimized network.

In the same way, the Particle-Spring form-finding system was applied to optimise the eight-pointed star shell of a *"a squadro" Lecce vault* (as shown in *Figure 3. 10*) by performing an inverted hanging cloth simulation.

Once the form-finding (shape optimization) of the star shells of two types of *Lecce vaults* was concluded, the effectiveness of the method was validated by performing Finite Element Analysis (FEA) of *"a spigoli"* and *"a squadro" Lecce vaults* with optimized (*Figure 3. 9(d)* and *Figure 3. 10(d)*) and not-optimized star shells with same dimensions.

The latter were modelled in accordance with architectural traditions clearly illustrated in (Colaianni 1967), i.e. by modelling the star shells of vaults as star portions of a ellipsoidal pavilion vault.

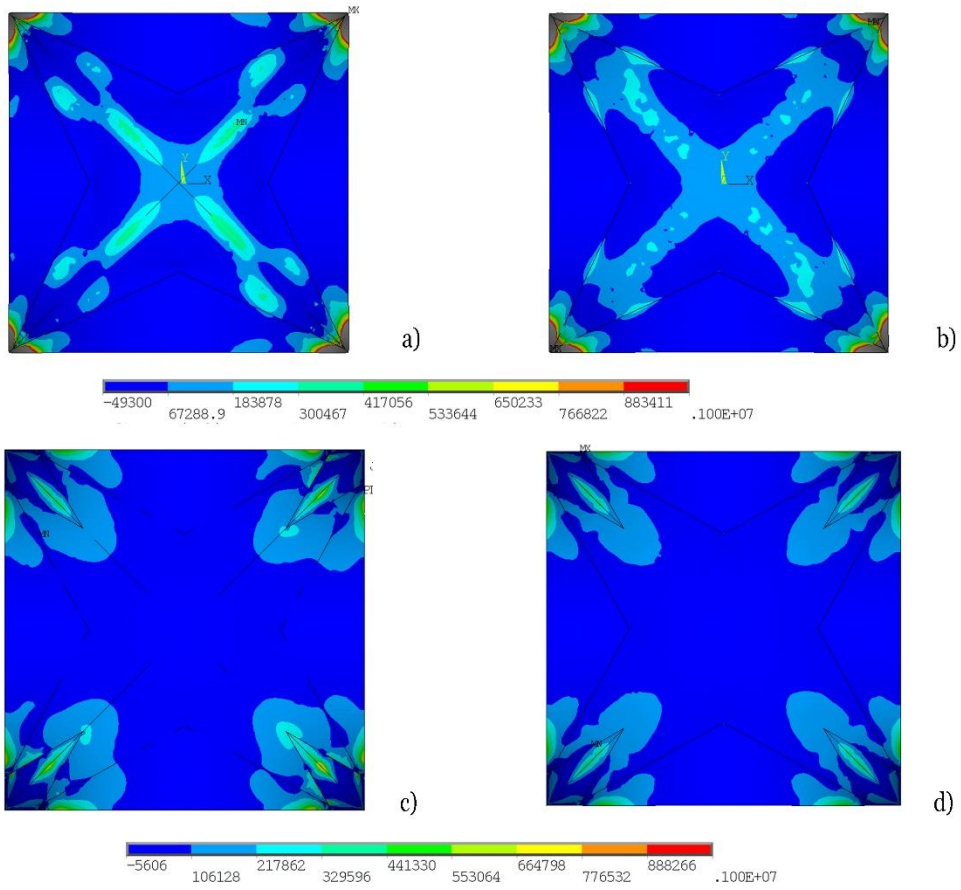

Figure 3. 11 FEM analysis results: (a) first principal stresses on the extrados of a not-optimized "a spigoli" star vault; (b) first principal stresses on the extrados of an optimized "a spigoli" star vault; (c) first principal stresses on the extrados of a not-optimized "a squadro" star vault; (d) first principal stresses on the extrados of an optimized "a squadro" star vault.

In the end, the goodness of optimized solutions came to light from a comparison of FEM analysis results of optimized and not-optimized *Lecce vaults* (only subjected to their self-weight) regarding first principal stress distributions (see *Figure 3. 11*) and maximum deflections.

Since Lecce vaults were traditionally made of stone masonry (whose material properties were brought from (Conte et al. 2011)), the main goal of the optimization procedure was to optimize structural performance of these vaults by minimising tensile stress regions on them. As further proof of that, *Figure 3. 11* shows that first principal stresses (which contain highest tensile stresses) are mainly negative (compressive) and more uniform on the extrados of optimized star vaults.

3.2.2 Form-finding (shape optimization) and size optimization of a footbridge grid-shell

The *Particle-Spring (PS)* method and *Finite Element Analysis (FEA)* have been consecutively applied in a stepwise procedure to perform shape and size optimization of an anticlastic grid-shell supporting a curved footbridge, illustrated in *Figure 3. 12*.

In a first phase, a *Particle-Spring (PS)* method was applied (in the *Autodesk Maya* platform by means of *Nucleus* dynamic solver) by performing a stretched cloth simulation, which is more suitable to obtain an optimal anticlastic surface with minimal area.

Figure 3. 12 Three-dimensional model of the grid-shell footbridge

Once an optimal anticlastic surface was obtained by *PS* form-finding method, the shell was properly discretized by a network lines and nodes, which was suitable to define the central lines of a steel tube grid-shell.

In the next phase, a parametric FEM model of the whole structure of the footbridge (whose deck arrangement was the same adopted in (Luigi Fenu et al. 2019, 2017; Luigi Fenu, Congiu, and Briseghella 2016; Luigi Fenu, Briseghella, and Congiu 2016; L Fenu, Briseghella, and Congiu 2016; Luigi Fenu, Briseghella, and Zordan 2015) shown in *Figure 3. 4*) was defined in the *Grasshopper* environment through the FEM tool *Karamba3D,* in order to assign and optimize steel tube cross-sections (chosen among a list of commercial profiles) of the grid-shell.

More accurate Finite Element Analysis (FEA) were carry out (through A*NSYS Mechanical APDL*) in order to verify the goodness of the optimal solution.

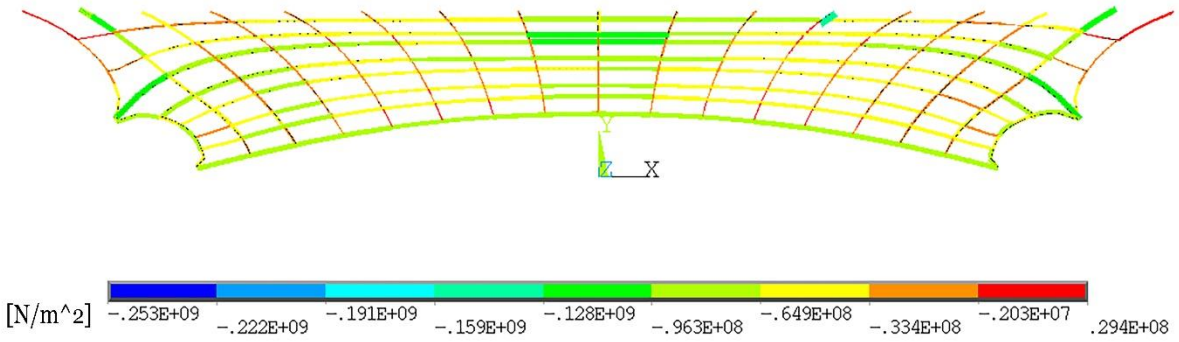

Figure 3. 13 FEM analysis results: Axial stress diagram

Chapter 4

4. Integrated methods for parametric design and structural optimization

All methods presented in the *§Chapter 3* are based on the use of parametric design techniques (e.g. parametric modelling tools like *Grasshopper* platform) and structural optimization methods (e.g. form-finding methods and tools, FEM (Finite Element Method) tools for structural analysis) in a stepwise process. Despite their undeniable effectiveness, since the solution goodness (e.g. through structural Finite Element Analysis) was verified only when the form-finding process was concluded, these not-integrated approaches are extremely time-consuming, and they do not allow to evaluate and compare a large number of candidates in searching for the optimal solution.

In light of the above, new integrated methods combining parametric design and structural optimization techniques have been developed and proposed.

4.1 Macro-algorithm integrating parametric design and structural optimization techniques in a hybrid environment (MATLAB + Grasshopper)

A first attempt to overcome the drawbacks of not-integrated optimization methods previously discussed was made by developing an integrated "macro-algorithm" (i.e. made of several subroutines connected with each other), which combines parametric design and structural optimization techniques in a hybrid environment composed of *MATLAB* and *Grasshopper*.

The flowchart of the whole macro-algorithm under consideration, which is illustrated in *Figure 4. 1*, shows the structure of a common population-based optimization algorithm on the left (e.g. an *Evolutionary Algorithm* like a *Differential Evolution Algorithm*), written in a *MATLAB* program. After setting the values of optimization parameters (depending on the chosen optimization algorithm), the optimization algorithm starts by generating a first Population of Individuals (i.e. a first set of "candidate solution", which are represented as vectors of design variables). It is worth noting that each Individual of the Population corresponds to a vector

containing a set of values for all design variables, regardless their various nature (i.e. topology, shape and size design variables).

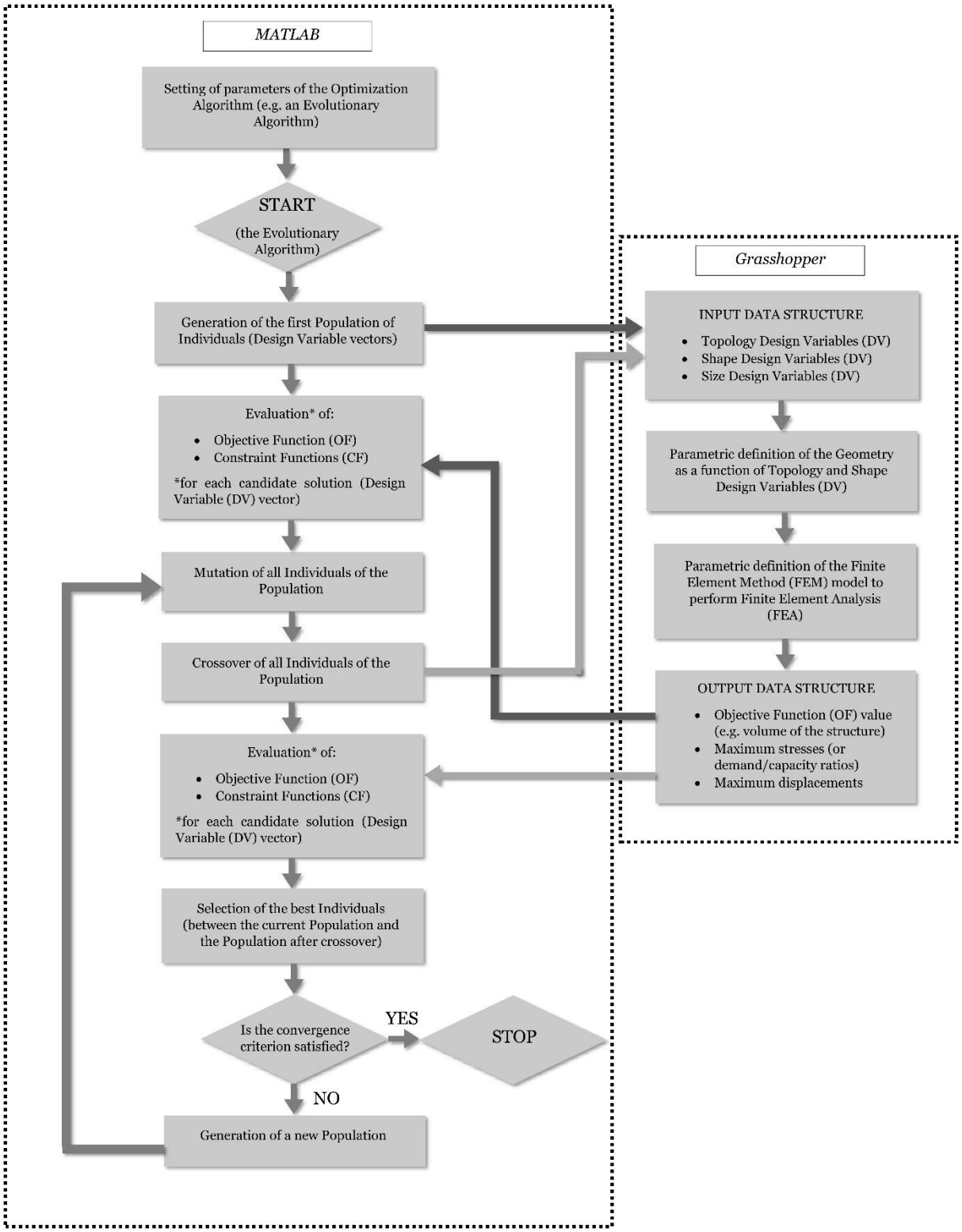

Figure 4. 1 *Flowchart of the macro-algorithm integrating parametric design and structural optimization techniques in a hybrid environment (MATLAB + Grasshopper)*

A parametric model, defined as a function of design variables in the *Grasshopper* environment, is updated for each Individual of the first Population (see *Figure 4. 1*).

The parametric model defined in *Grasshopper* receives from *MATLAB* an "input data structure" (which contains a vector of a certain set of design variables for each Individual of the Population) and, at the end of its sub-routine, sends to *MATLAB* an "output data structure" (containing results from FEM analysis as for instance the total volume of the structure, maximum stresses and maximum deflections). In this regard, this crucial data exchange is allowed by two *Grasshopper* components that were properly programmed by Python language to read and write data on ".csv" files (i.e. comma-separated values files). Therefore, through these two non-standard *Grasshopper* components, at each iteration of the optimization algorithm, the *Grasshopper* parametric model can receive a set of input data from *MATLAB* and send to *MATLAB* a set of output data containing results derived from FE structural analysis of the updated FEM model. The *Grasshopper* file contains a parametric definition of the geometry and a parametric FEM model for structural analysis and the whole model is updated for each Individual (design variable vector) of the Population. As shown in the flow-chart (in the *Figure 4. 1*), at the first iteration, FEM analysis results are used to evaluate the Objective Function and Constraint Function values of candidate solutions of the first Population. At a later time, the Individuals of the initial Population are subjected to some operations typical of Evolutionary Algorithms (e.g. like mutation and crossover briefly described in the section *§1.4.3.2*) which commonly make random changes in original Individuals (mutation operation) and blend parts of different Individuals (crossover operation). The so-varied Individuals provide a new input data structure for the update of the parametric *Grasshopper* model. New FEM results are then produced by analysing all "varied" Individuals (new output data structure for *MATLAB*), for which Objective and Constraint Function values have to be evaluated. The most pivotal phase in population-based optimization algorithms is the selection operation, which compares one by one each Individual of a current Population with its corresponding "varied" Individual of the "after-crossover Population", in order to select the best candidate solutions. In unconstrained optimization problems, the selection of the best candidate solutions is only based on the values of the Objective Function which must be minimized or maximized. On the other hand, in constrained optimization problems the selection must be also based on the feasibility (i.e. a feasible solution satisfies all Constraint Functions) or on the Violation values of Constraints (if violation is allowed) of candidates. Individuals who "survive" to the selection process, will form a new Population (also called "Generation") as long as an optimal solution will be found (which satisfies a default convergence criterion) or a default maximum number of iterations will be reached.

4.1.1 Limitations of the method

The macro-algorithm integrating parametric design and optimization techniques in a *MATLAB-Grasshopper* environment (just illustrated in *§4.1* and summarized by the flow-chart in *Figure 4. 1*) proved to be effective and robust in solving simple structural optimization problems. However, despite the advantage of being able to see in real time the updated geometry and FEM model (for each design variable vector, which is a candidate solution of the optimum design problem) ensured by their parametric definition in the *Grasshopper* environment, the whole process is extremely time-consuming. For this reason, the method is not suitable to solve optimization problems depending on a large number of design variables (as most structural optimization problems are).

Hence, since structural optimization of truss arches, which is the subject of the present dissertation, depends on a very large number of design variables, the optimization strategy proposed in the sub-section *§4.1* cannot be considered appropriate.

4.2 Macro-algorithm integrating parametric design and structural optimization techniques in MATLAB environment

The need to overcome the limitations of methods illustrated so far (in *§Chapter 3* and in previous sections of this Chapter) has made it necessary to develop a new optimization strategy, suitable to manage and solve structural optimization problems with a very large number of design variables in a reasonable time. For this purpose, a *MATLAB* program containing a parametric definition of the optimum design problem, a code of an optimization algorithm and a parametric definition of a *Finite Element Method (FEM)* model for *SAP2000* was implemented. A flowchart of the whole macro-algorithm (i.e. a program integrating several subroutines), which is entirely defined in *MATLAB*, is illustrated in *Figure 4. 2*. It is worth noting that the subroutine of the macro-algorithm containing a *Differential Evolution Algorithm (DEA)* could be easily replaced by another optimization algorithm, whose selection should be based on the nature of the considered optimization problem.

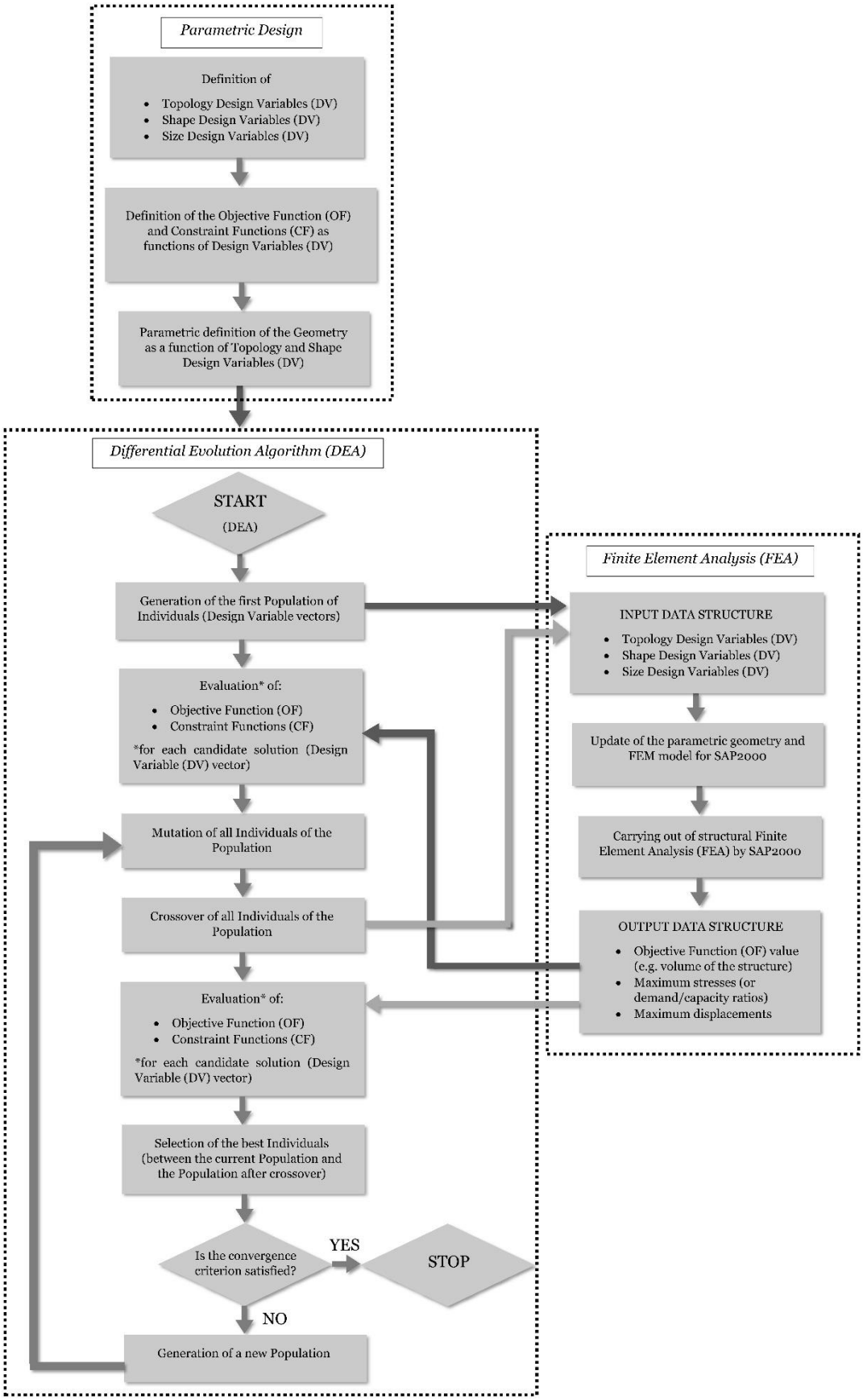

Figure 4. 2 Flowchart of the proposed macro-algorithm integrating parametric design and structural optimization techniques in MATLAB environment

4.2.1 Parametric design and definition of the optimization problem

Parametric design has a pivotal role in the preliminary phase of a structural optimization process, in identifying the design variables (among all parameters that mostly affect the design solutions) and properly defining their upper and lower bounds, as well as in the parametric definition of the geometry as a function of design variables and formulation of the considered optimization problem as function of them (as shown in the flowchart of the proposed macro-algorithm illustrated in *Figure 4. 2*).

More specifically, the parametric definition of an optimum design problem in the method here described, consists of defining a unique set (a vector) of all design variables, regardless their various nature (i.e. topology, shape and size design variables), two vectors of lower and upper bounds of design variables, the objective and constraint functions as functions of design variables, as well as a parametric definition of the geometry depending on topology and shape design variables.

4.2.2 The optimization algorithm: A Differential Evolution Algorithm (DEA) implemented with a Constraint Domination Selection (CDS) criterion

Once the parametric definition of the considered design and optimization problem is concluded, the optimization algorithm can be run. The macro-algorithm here proposed, contains a peculiar version of a *Differential Evolution Algorithm (DEA)*, introduced in (Storn and Price 1997), which is classified as a population-based stochastic algorithm inspired by biological evolution mechanisms, thus belonging to *Evolutionary Algorithms* (which were previously introduced in the section *§1.4.3.2*).

Candidate solutions to the optimization problem play the role of individuals in a population subject to consequent stages (operations) of reproduction, mutation, crossover (also called recombination) and selection. The effectiveness of *Evolutionary Algorithms (EA)* is confirmed by successes in fields as diverse as engineering, art, biology, economics, marketing, genetics, operations research, robotics, social sciences, physics, politics and chemistry.

Notwithstanding, a well-known weak point of *Evolutionary Algorithms (EA)* is lack of efficiency and robustness to handle constraints. Since most structural optimization problems are subjected to several constraint functions (that for instance can limit maximum stresses and deflections in accordance with mechanical properties of materials and technical standards for construction), a dynamic *Constraint Domination Selection-based (CDS) criterion* was adopted to implement the

proposed *Differential Evolution Algorithm (DEA)* in order to extend its applicability to constraint optimization problems.

The *Differential Evolution Algorithm* in its original version (Storn and Price 1997) shares some features with the well-known *Genetic Algorithms*. For instance, both optimizers adopt the same terminology to define the key elements of the algorithm (i.e. a collection of solutions is called "population", each solution is called as "individual" and each iteration is called as "generation") and incorporate operators (like "mutation", "crossover" and "selection") that works in similar manners. Nonetheless, *DEA* is different in handling distance and direction information to move from the population at the current generation toward the next one because it takes into account constructive cooperation between individuals: in this sense, it behaves in a more similar manner to *Particle Swarm Optimization Algorithms (PSOAs)*.

DEA uses the differences between randomly selected individuals as the source of random variations for a third individual referred to as the target vector. Trial solutions are generated by adding weighted difference vectors to the target vector. This process is referred to as the mutation operator: its main goal is to enable diversity in the current population as well as to direct the individuals in such a way a better result is expected. By computing the differences between two individuals randomly chosen from the population, the algorithm estimates the gradient in that zone rather than in a point.

The *Latin Hypercube Sampling (LHS) Technique* is iteratively used to pseudo-randomly generate the best initial population with minimum correlation between samples (Monti, Quaranta, and Marano 2010).

At iteration $k+1$, for each individual ${}^{k}\mathbf{x}_i$, a mutation vector ${}^{(k+1)}\mathbf{v}_i$ is computed by means of one of the following alternatives implemented with a "best" selection based on a *CDS-criterion*:

$${}^{(k+1)}\mathbf{v}_i = {}^{k}\mathbf{x}_{best} + F^1\left({}^{k}\mathbf{x}_{r1} - {}^{k}\mathbf{x}_{r2}\right) \tag{30}$$

$${}^{(k+1)}\mathbf{v}_i = {}^{k}\mathbf{x}_i + F^2\left({}^{k}\mathbf{x}_{best} - {}^{k}\mathbf{x}_i\right) + F^1\left({}^{k}\mathbf{x}_{r1} - {}^{k}\mathbf{x}_{r2}\right) \tag{31}$$

$${}^{(k+1)}\mathbf{v}_i = {}^{k}\mathbf{x}_{best} + F^2\left({}^{k}\mathbf{x}_{r1} - {}^{k}\mathbf{x}_{r2}\right) + F^1\left({}^{k}\mathbf{x}_{r3} - {}^{k}\mathbf{x}_{r4}\right) \tag{32}.$$

In Eqs. (30-32), r_1, r_2, r_3 and r_4 denote integers randomly selected within the set $\{1, \dots, i-1, i+1, \dots, N\}$ and $r_1 \neq r_2 \neq r_3 \neq r_4$. The individual ${}^{k}\mathbf{x}_{best}$ is the best performer in the population (with N individuals) at a k-iteration. The coefficients F^1 and F^2 are the so-called "mutation coefficients" and they are real positive constants (it was assumed that $F^1 = 0.8$ and $F^2 = 0.95$). Any alternative mutation operator leads to different versions of *DEA* (Storn and Price 1997).

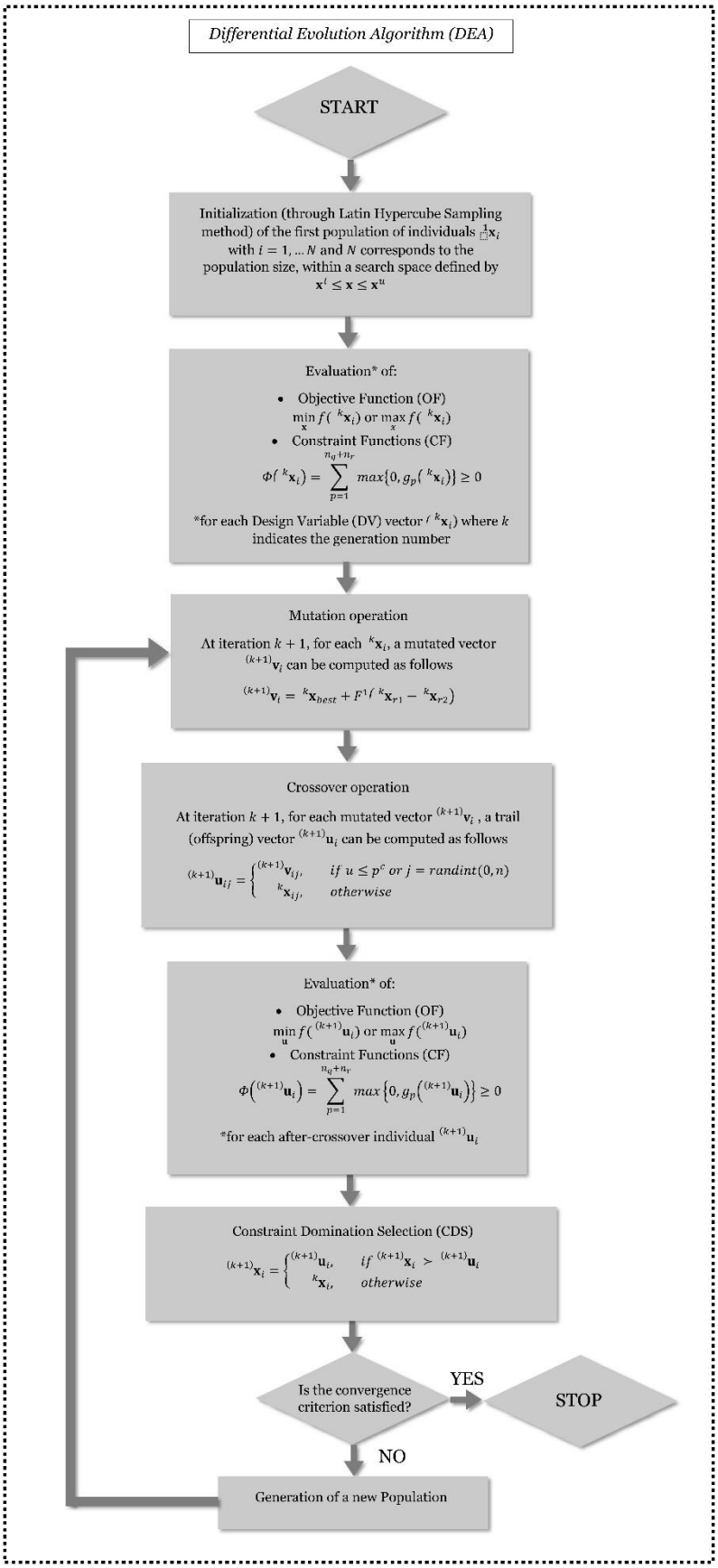

Figure 4. 3 *Flowchart of a Differential Evolution Algorithm (DEA) implemented with a Constraint Domination Selection-based (CDS) criterion*

For each mutated vector ${}^{(k+1)}\mathbf{v}_i$ a trial vector ${}^{(k+1)}\mathbf{u}_i$ (offspring) is generated by using the binomial crossover formalized as follows

$$ {}^{(k+1)}\mathbf{u}_{ij} = \begin{cases} {}^{(k+1)}\mathbf{v}_{ij}, \ if\ u \le p^c\ or\ j = randint(0,n) \\ {}^{k}\mathbf{x}_{ij}, \ otherwise \end{cases} \tag{33}. $$

In Eq. (33), u is a pseudo-random number generated by using the uniform probability density functions in the range [0,1]. On the other hand, p^c is the "probability of crossover" (or "crossover ratio" or "probability of reproduction") and it takes values between 0 and 1. All optimization tests illustrated in the following sections were performed assuming a "probability of crossover" coefficient equal to 0.5. Moreover, $randint(0,n)$ is a pseudo-random integer selected within the set $\{1, \dots, j, \dots, n\}$, where n is the number of design variables of the problem.

After the crossover stage, the selection phase starts. The selection operator in case of unconstrained problems employs a very simple one-to-one competition scheme between ${}^{(k+1)}\mathbf{u}_i$ and ${}^{(k+1)}\mathbf{x}_i$ as follows

$$ {}^{(k+1)}\mathbf{x}_i = \begin{cases} {}^{(k+1)}\mathbf{u}_i, \ if\ f\left({}^{(k+1)}\mathbf{u}_i\right) < f\left({}^{(k+1)}\mathbf{x}_i\right) \\ {}^{k}\mathbf{x}_i, \ otherwise \end{cases} \tag{34}. $$

The output of the selection operator is a new population for the next generation if a stopping criterion has not been satisfied.

For constrained optimization problems, the standard selection criterion formalized in Eq. (34) is replaced by a *CDS* one, also applied to the evaluation of "best" individual over the entire population.

A *Constraint Domination Selection-based (CDS)* criterion is based on the concept of "domination", i.e.

$$ {}^{(k+1)}\mathbf{x}_i = \begin{cases} {}^{(k+1)}\mathbf{u}_i, \ if\ {}^{(k+1)}\mathbf{x}_i \succ {}^{(k+1)}\mathbf{u}_i \\ {}^{k}\mathbf{x}_i, \ otherwise \end{cases} \tag{35} $$

where ${}^{(k+1)}\mathbf{x}_i \succ {}^{(k+1)}\mathbf{u}_i$ denotes that ${}^{(k+1)}\mathbf{u}_i$ is dominated by ${}^{(k+1)}\mathbf{x}_i$. In the same way, a *Constraint Domination Selection-based (CDS)* criterion is also required to compare the best performer of the previous generation (${}^{(k-1)}\mathbf{x}_i^{Pb}$) with each individual (${}^{k}\mathbf{x}_i$) of the current generation in order to find the best solution produced by the whole optimization process.

Furthermore, a violation function for an i_{th} individual can be expressed as follows

$$ \Phi\left({}^{k}\mathbf{x}_i\right) = \sum_{p=1}^{n_q+n_r} max\left\{0, g_p\left({}^{k}\mathbf{x}_i\right)\right\} \ge 0 \tag{36} $$

where n_q and n_r indicate the numbers of the equality and inequality constraints, respectively.

The value of the violation function (expressed by the Eq. (36)) is zero if and only if all constraints are satisfied, otherwise it is a positive scalar number. Note that, if the orders of magnitude of the constraint violations could be largely different, it will be necessary to normalize the magnitude of the violations. Since in all cases addressed in the present dissertation, all constraint violations have the same order of magnitude, it was not indispensable to normalize them.
A static domination-based selection scheme can be formulated for Eq. (9) as follows

$$ {}^{k}\mathbf{x}_i \succ {}^{(k-1)}\mathbf{x}_i^{Pb} \Leftrightarrow \begin{cases} \left(f\left({}^{k}\mathbf{x}_i\right) < f\left({}^{(k-1)}\mathbf{x}_i^{Pb}\right)\right) \wedge \left(\Phi\left({}^{k}\mathbf{x}_i\right) = 0\right) \wedge \left(\Phi\left({}^{(k-1)}\mathbf{x}_i^{Pb}\right) = 0\right) \\ \vee \\ \left(\Phi\left({}^{k}\mathbf{x}_i\right) = 0\right) \wedge \left(\Phi\left({}^{(k-1)}\mathbf{x}_i^{Pb}\right) > 0\right) \\ \vee \\ \Phi\left({}^{k}\mathbf{x}_i\right) < \Phi\left({}^{(k-1)}\mathbf{x}_i^{Pb}\right) \end{cases} \quad (37). $$

A selection scheme (Eq. (35)) based on Eq. (37) is static because the concept of dominance is not dynamically tuned during the evolutionary search.

As a matter of fact, comparing the best performer of the previous generation (${}^{(k-1)}\mathbf{x}_i^{Pb}$) with each individual of the current generation (${}^{k}\mathbf{x}_i$), the selection operator evaluates the following alternatives:

- If both individuals are feasible (which means that $\Phi\left({}^{k}\mathbf{x}_i\right) = 0$ and $\Phi\left({}^{(k-1)}\mathbf{x}_i^{Pb}\right) = 0$) the operator selects the one with minimum value of the objective function;
- If one of them is unfeasible, the selection operator chooses the one that is feasible;
- If both individuals are unfeasible, selection operator chooses the individual characterized by the minimum value of violation function.

4.2.3 Finite Element Analysis (FEA): A MATLAB code for SAP2000

Structural Analysis play an extremely important role in structural optimization process, since it is required to compute the value of the objective function (for instance in cases where the total weight of the structure or maximum deflections nor the compliance of the structure are assumed as objective function to be minimized) and/or the values of parameters which are to be kept within certain ranges (in accordance with mechanical properties of materials and technical standards for construction like maximum stresses or deflections), thus defining constraint functions of the optimization problem.

As shown in the flowchart of the here proposed optimization macro-algorithm (summarized in *Figure 4. 2), Finite Element Analysis (FEA)* need to be performed for all individuals (i.e.

candidate solutions of the considered optimization problem, which are expressed as design variable vectors) of the initial population (i.e. the first generation), as well as for all individuals of the consecutive populations after being subjected to the crossover operation.

Structural analysis is here assumed to be performed by the *FEM* software *SAP2000* to evaluate the objective and constraints functions of the considered optimization problem. However, the *FEM* model for structural analysis is entirely defined and updated (for each design variable vector) in the *MATLAB* environment, by using the so-called *Open Application Programming Interface (OAPI)* functions, in order to minimize the total computational time of the whole process. The *OAPI* functions allow the user to execute *SAP2000* functions (in batch mode) by means of *MATLAB* (or *Visual Basic for Applications (VBA)*, *Visual Basic 2012*, *Visual C# 2012*, *Visual Fortran*, *Microsoft Visual C++ 2012* and *Python* programming languages) strings. Through this powerful tool, parametric *FEM* models have been entirely defined (in terms of element types, material properties, cross-section features, constraint and load conditions) in the *MATLAB* environment through proper codes able to run structural analysis and so obtain needed results.

In the present dissertation, different kind of structural optimization problems of steel arched trussed (planar and spatial) subjected to different boundary conditions have been considered.

In all cases, the total volume of the steel frame structures was assumed as the objective function to be minimized. The value of the total volume was defined as follows

$$V = \frac{W}{\gamma_{steel}} \tag{38}$$

where γ_{steel} is the specific weight of steel ($\gamma_{steel} = 76.97\ kN/m^3$). On the other hand, W is the total weight of the structure to be optimized, evaluated (for each model updated for each design variable vector) by carrying out *Finite Element Analysis (FEA)* and so computing the sum of all vertical reaction forces attributable to the structural masses ($\sum R_{z,Dead}$) as shown in Eq. (39)

$$W = \sum R_{z,Dead} \tag{39}.$$

Moreover, *FEM* analysis need to be performed also to evaluate constraint functions of considered optimization problem. For instance, to keep stress values within allowable ranges according to mechanical properties of materials and technical standards for construction. The maximum "utilization ratio" (i.e. the "demand/capacity ratio") of all truss members, for all applied load cases, was assumed as strength constraint in order to evaluate the combined effect of axial forces and bending moments. In particular, the critical utilization ratio of bars subjected to compression axial forces was calculated by evaluating the combined effect of compression axial forces and bending moments by also checking the flexural and lateral-torsional local buckling by means of

the interaction equations provided by the section EC3-2005 6.3.3(4), here expressed by Eqs. (40) and (41)

$$\frac{N_{Ed}}{\frac{\chi_y N_{Rk}}{\gamma_{M1}}} + k_{yy}\frac{M_{y,Ed}}{\chi_{LT}\frac{M_{y,Rk}}{\gamma_{M1}}} + k_{yz}\frac{M_{z,Ed}}{\chi_{LT}\frac{M_{z,Rk}}{\gamma_{M1}}} \leq 0.99 \tag{40}$$

$$\frac{N_{Ed}}{\frac{\chi_z N_{Rk}}{\gamma_{M1}}} + k_{zy}\frac{M_{y,Ed}}{\chi_{LT}\frac{M_{y,Rk}}{\gamma_{M1}}} + k_{zz}\frac{M_{z,Ed}}{\chi_{LT}\frac{M_{z,Rk}}{\gamma_{M1}}} \leq 0.99 \tag{41}$$

where N_{Ed}, $M_{y,Ed}$ and $M_{z,Ed}$ express the values of the axial force and bending moments acting on the considered member, N_{Rk}, $M_{y,Rk}$ and $M_{z,Rk}$ indicate the characteristic resistance values, k_{yy}, k_{yz}, k_{zy} and k_{zz} are the so-called "interaction factors", χ_y and χ_z are the reduction factors for the local flexural buckling whereas χ_{LT} indicates the reduction factor for the lateral-torsional local buckling. Note that it was assumed to have $\gamma_{M0} = \gamma_{M1} = 1.1$. In this regard, it is important to underline that, since all solutions demonstrated to be very stiff, any global buckling analysis was not performed. However, it could be easily added to the *MATLAB* subroutine for *SAP2000* through specific *OAPI*-functions.

On the other hand, the utilization ratio of members subjected to tensile axial forces is evaluated by checking the combined effect of axial forces and bending moments by means of the interaction equation provided by EC3-2005 6.2.1(7) to evaluate the cross-section resistance, here expressed by the Eq. (42)

$$\frac{N_{Ed}}{N_{Rd}} + \sqrt{\left(\frac{M_{y,Ed}}{M_{y,Rd}}\right)^2 + \left(\frac{M_{z,Ed}}{M_{z,Rd}}\right)^2} \leq 0.99 \tag{42}.$$

For Doubly Symmetric Sections, the previous Eq. (42) is a representation of the code-specified equation (EC3 6.2.9.2(1)) given here

$$\sigma_{x,Ed} \leq \frac{f_y}{\gamma_{M0}} \tag{43}.$$

As a matter of fact, the program (SAP2000) performs the design for resistance of members subjected to tensile axial forces and bending moments whereas it performs the design for local buckling resistance of members subjected to compressive axial forces and bending moments.

Furthermore, in the case of structural optimization of a spatial arched truss subjected to different load cases acting in different directions, it was also necessary to consider serviceability constraints, by limiting maximum deflections in all directions of a three-dimensional space.

For this additional goal, in the particular case of a spatial arched truss, also maximum deflections in all directions of all truss members, for all considered load cases, must be evaluated through

FEM analysis performed by *SAP2000* working in batch-mode by following the instructions provided by the *MATLAB* subroutine (through the *OAPI*-functions).

In conclusion, *FEM* analysis results are indispensable and are used to evaluate the objective and the constraint function values, in order to allow the optimization algorithm (as shown in the *Figure 4. 2* and *Figure 4. 3*) to find an optimal solution among all feasible candidates (i.e. which satisfy all constraint inequality functions).

Part III

Applications and results

Chapter 5

5. Parametric design and structural optimization of planar truss arches

The Part III of the present dissertation aims to show, through the application of the new macro-algorithm (proposed in section *§4.2*) which completely integrates parametric design and structural optimization techniques on *MATLAB*, optimal design solutions for planar and spatial arched trusses, made of steel tubes, subjected to various boundary conditions (e.g. several load cases acting in vertical and/or horizontal directions). The ultimate goal of the Part III is to carefully analyse the obtained results and compare the optimal solutions, in order to deduce useful suggestions for the design of steel arched truss.

The present *Chapter* illustrates the results obtained by optimizing, for different sets of boundary conditions, planar truss arches composed by two arched tubular chords lying on a vertical plane, connected to each other by means of a bracing system with the same configuration of a Pratt truss. In particular, planar truss arches, with different spans and constraints conditions, have been successfully optimized for multiple load cases, all acting on the same plane of the structure, since in-plane structures would not be able to well withstand out-of-plane loads.

5.1 Structural optimization of truss arches under a single load case (demonstrative applications)

In a preliminary phase, for demonstrative purposes, the problem of structural optimization of in-plane truss arches subjected to a single load case (acting on the same plane of the arch) was investigated.

Several analytical, graphical and physical methods are available to find the optimal shape of a monolithic (single rib) arch subjected to a certain load case (i.e. the "funicular curve" for that load). However, only one optimal "funicular curve" can be obtained for a single load case and then assumed as "centre line" of an arched structure so that the arch is mainly subjected to compressive axial forces, thereby minimizing bending moments. In this regard, the optimization examples illustrated in the next sections *§5.1.1* and *§5.1.2* aim to demonstrate that truss arches cannot be optimized for a single load case. For this purpose, optimal solutions obtained by optimizing truss

arches with same span and constraint conditions (one subjected to a single load pattern and the other subjected to multiple load cases) are compared.

5.1.1 Two-hinged truss arches

For demonstrative purposes, the optimization problem of two-hinged planar truss arches, with a fixed span of 40 meters, was formulated in one case considering only one load condition (a symmetric uniform load) whereas, in another case, three different load patterns were assumed, also considering an asymmetric uniform load, which mostly induces unfavourable bending moments.

Both optimization problems were formulated assuming the total volume of the structure as objective function to be minimized and the maximum "utilization ratio" (which has been previously introduced in *§4.2.3*) in all truss members for each load case as constraint function, in order to keep the stress level within allowable values in accordance with Eurocode3-2005. Both problems were solved by applying the integrated method here proposed and described in detail in *§4.2* (summarized by the flowchart in *Figure 4. 2*), assuming the same unique set of design variables (i.e. without any distinction between topology, shape and size variables) for both optimization problems (i.e. single- and multi-load case formulations).

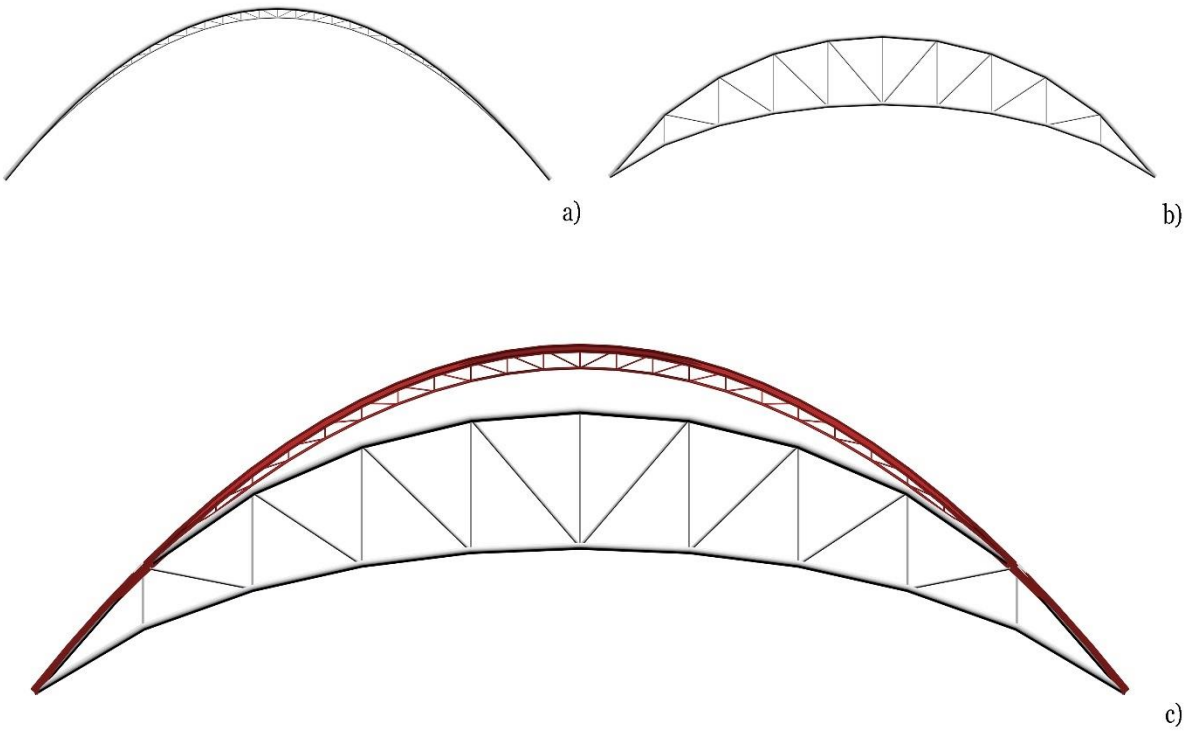

Figure 5. 1 Structural optimization of two-hinged truss arches: (a) optimal solution for a single uniformly distributed load case; (b) optimal solution for multiple load cases; (c) superposition of the two optimal solutions

Since the application here considered has a mere illustrative purpose, a detailed description of the individual phases of the optimization procedure is not provided in the present section.

Figure 5. 1 allows to easily compare the two optimal solutions obtained by solving the same optimum design problem, for one and for three load cases, represented in *Figure 5. 1(a)* and in *Figure 5. 1(b)* and superimposed in *Figure 5. 1(c)*. Topology, shape and size design variables have been simultaneously optimized. The even integer of equal intervals (n_{int}) of subdivisions of the arch span, is assumed as topology design variable (as a continuous value varying between 10 and 70, then rounded to the nearest even integer) since it determines the number of truss members, thereby changing its topology. As shown in *Figure 5. 1* and indicated in *Table 5. 1*, the optimal solution obtained for a single-load pattern is characterized by a number of subdivisions of the span ($n_{int} = 30$) and a resulting total number of elements much higher than the one of the optimal solution obtained for multiple load combinations ($n_{int} = 10$). Further significant differences are represented by geometric parameters like the rise over span ratio, the total height and the crown depth of two compared arches. In this regard, the optimal solution obtained for a single load case is characterized by an almost parabolic shape, with a total height of 12.57 meters, compared to a height of 10.31 meters characterizing the multi-load solution. Moreover, the shape of the multi-load case solution is much lowered than the optimal shape of the single-load case, as demonstrated by the comparison between the two rise over span ratios indicated in *Table 5. 1*.

Table 5. 1 *Comparison of the optimal values of the objective function (i.e. the volume) and design variables mainly characterizing the two compared solutions of two-hinged truss arches*

Compared results	**Single-load case**	**Multi-load case**
volume	0.23 $[m^3]$	0.31 $[m^3]$
n_{int}	30 $[adim.]$	10 $[adim.]$
rise/span	1/1.37 $[adim.]$	1/1.75 $[adim.]$
total height	12.57 $[m]$	10.31 $[m]$
crown depth	0.72 $[m]$	4.98 $[m]$
lower chord diameter	0.103 $[m]$	0.269 $[m]$
upper chord diameter	0.324 $[m]$	0.299 $[m]$
diagonal elements diameter	0.054 $[m]$	0.107 $[m]$
vertical elements diameter	0.057 $[m]$	0.059 $[m]$
lower chord thickness	0.0032 $[m]$	0.0032 $[m]$
upper chord thickness	0.0032 $[m]$	0.0032 $[m]$
diagonal elements thickness	0.0032 $[m]$	0.0032 $[m]$
vertical elements thickness	0.0032 $[m]$	0.0032 $[m]$

On the other hand, the most relevant difference is represented by the “crown depth” of two solutions, since in the single-load solution, the arched chords tend to coincide with each other.

The presented results are justified by the fact that, for a given load pattern, an optimal shape for an arch with a solid and constant cross-section exists (the so-called “line of thrusts”).

For this reason, when only a single-load pattern is considered, the two chords of the truss arch tend to coincide with each other and with the “funicular curve” (also called “line of thrusts”) for that load.

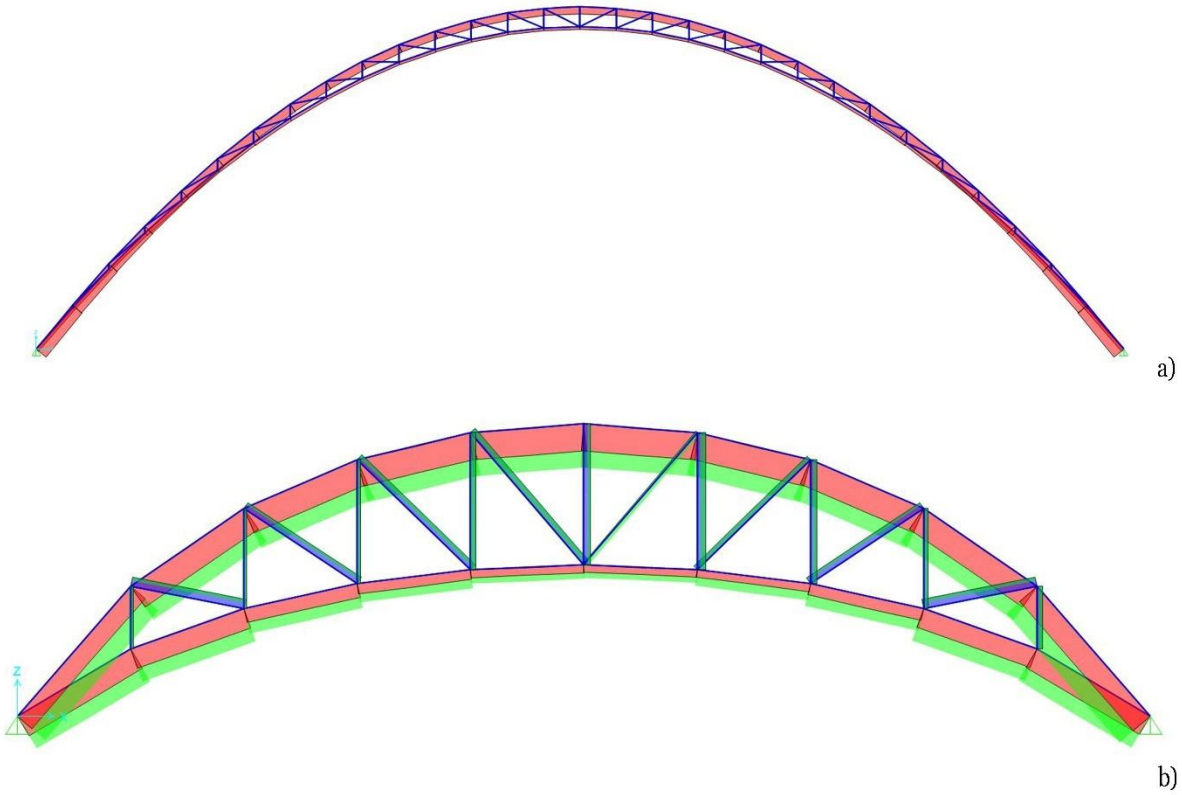

Figure 5. 2 *Structural optimization of two-hinged truss arches: (a) Axial force diagram of the single load case optimal solution; (b) axial force diagram of the multi-load case optimal solution*

As a matter of fact, the optimal truss arch obtained from a single-load case formulation of the optimization problem, behaves like a monolithic arch, as also confirmed by the axial force diagram (illustrated in the *Figure 5. 2(a)*), which shows that the upper chord supports most of the axial force (whose maximum value is about *800 kN* in the upper chord, compared to *195 kN* in the lower one). This remark legitimizes the significantly bigger diameter resulted (from size optimization) for the upper chord with respect to the lower one, as shown in the *Table 5. 1*. All size design variables were assumed as continuous parameters varying between their lower and upper bounds (i.e. $0.054\ [m] \leq diameter \leq 0.508\ [m]$ and $0.0032\ [m] \leq thickness \leq 0.02\ [m]$).

In light of the above, it can be said that two-hinged truss arches are not suitable to be optimized just considering one load condition, since the optimal solution tends to resemble and behave similarly to a single-rib arch. At the same time, it is also possible to affirm that single-rib arches

would not be suitable to withstand and be optimized for multiple-load cases extremely different from each other (as real load cases commonly are and have to be considered in structural design).

5.1.2 Hingeless truss arches

Similarly to the applicative example of two-hinged truss arches (illustrated in the section *§5.1.1*), for the same demonstrative purposes, the optimization problem of planar truss arches constrained by two vertically aligned double-hinges (which prevent rotations in two of three directions), thus behaving like almost hingeless structures, was preliminary investigated. The optimization problem of the "hingeless" truss arches under consideration, with a fixed span of 40 meters, was formulated in one case considering only one load condition (a symmetric uniform load), whereas in another case, three different load patterns were assumed, also considering an asymmetric uniform load, which mostly induces unfavourable bending moments.

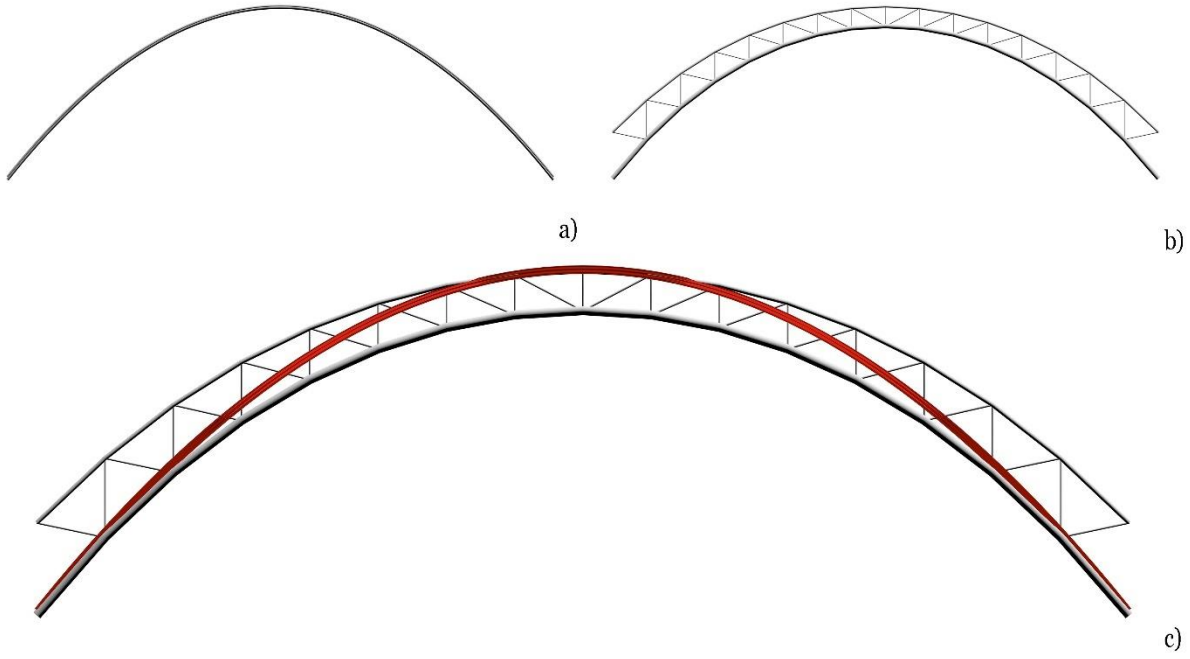

Figure 5. 3 Structural optimization of hingeless truss arches: (a) optimal solution for a single uniformly distributed load case; (b) optimal solution for multiple load cases; (c) superposition of the two optimal solutions

Figure 5. 3 allows to easily compare the two optimal solutions obtained by solving the same optimum design problem, for one and for three load cases, which are illustrated in *Figure 5. 3(a)* and in *Figure 5. 3(b)* respectively while they are superimposed in *Figure 5. 3(c)*. As in the previous case (in *§5.1.1*), the main features that basically distinguish the two optimal solutions clearly come up from a close inspection of *Figure 5. 3,* as well as from the resulting values shown in *Table 5. 2*.

Compared to the previous analysis, it is more evident that the optimal solution obtained for a single-load case looks like a monolithic arch (i.e. a single-rib arch with a constant solid cross-section), as shown in *Figure 5. 3(a)*.

As a matter of fact, it is not possible to distinguish the frame structure of the truss arch because distances between the two chords at the arch bases and crown (whose values are indicated in the *Table 5. 2* as "base depth" and "crown depth", respectively) are smaller than or equal to the sum of cross-section radius of the lower and upper chords. Moreover, the single-load optimal arch is characterized by a much higher number of elements with respect to the multi-load solution, thereby contributing to "fill up" the frame structure of the truss arch. It is worth remembering that the number of arch elements depends on the variable number of equal intervals (represented by the topology design variable n_{int}) in which arch spans are divided. As in the previous case, the parameter n_{int} was defined as a continuous parameter, varying between 10 and 70, then rounded to the closest even integer value. Note that significant differences are also remarkable in size optimization results (contained in *Table 5. 2*) since the multiple load case optimization process produced higher diameters compared to the ones obtained from the single load case optimization. As in the previous case, all size design variables were assumed as continuous parameters varying between their lower and upper bounds (i.e. $0.054\ [m] \leq diameter \leq 0.508\ [m]$ and $0.0032\ [m] \leq thickness \leq 0.02\ [m]$).

Table 5. 2 *Comparison of the optimal values of the objective function (i.e. the volume) and design variables mainly characterizing the two compared solutions of hingeless truss arches*

Compared results	Single-load case	Multi-load case
volume	$0.23\ [m^3]$	$0.28\ [m^3]$
n_{int}	$58\ [adim.]$	$16\ [adim.]$
rise/span	$1/1.32\ [adim.]$	$1/1.36\ [adim.]$
total height	$12.71\ [m]$	$12.59\ [m]$
crown depth	$0.12\ [m]$	$1.44\ [m]$
base depth	$0.20\ [m]$	$3.39\ [m]$
taper ratio	$1/1.67\ [adim.]$	$1/2.35\ [adim.]$
lower chord diameter	$0.206\ [m]$	$0.335\ [m]$
upper chord diameter	$0.181\ [m]$	$0.163\ [m]$
diagonal elements diameter	$0.054\ [m]$	$0.075\ [m]$
vertical elements diameter	$0.054\ [m]$	$0.057\ [m]$
lower chord thickness	$0.0036\ [m]$	$0.0032\ [m]$
upper chord thickness	$0.0033\ [m]$	$0.0032\ [m]$
diagonal elements thickness	$0.0032\ [m]$	$0.0032\ [m]$
vertical elements thickness	$0.0032\ [m]$	$0.0032\ [m]$

A further feature of the two optimal solutions that immediately comes to light by observing the arch shapes, as superimposed each other in *Figure 5. 3(c),* is that the single-load optimal arch is perfectly included in and has same height of the multi-load optimal arch. This is justified by the

fact that the single load pattern considered in the first formulation of the optimization problem also corresponds with one of the three different load conditions adopted in the second formulation of the optimization problem.

It is also worth noting that, since the "base depth" of the solution represented in *Figure 5. 3(a)* is very small, the vertical distance between the two hinges at its base is so small that the arch behaviour should be considered more comparable with a two-hinged arch (instead of a hingeless arch).

On the other hand, the structural behaviour of the truss arch optimized for three different load conditions should be comparable with a "hingeless" arch since the vertical distance between hinges is significant and higher than 3 meters (as indicated in *Table 5. 2*, referred to the value of the "base depth"). A "taper ratio" of two solutions is also compared in the *Table 5. 2* and evaluated as a ratio between the "crown depth" and the "base depth" of the two optimal arches. In this regard, it is easily noted that the optimal truss arch in *Figure 5. 3(b)* is considerably tapered toward its bases, in accordance with the axial force diagram (shown in *Figure 5. 4*). Nevertheless, its peculiar shape is also justified by the fact that it should include all "line of thrusts" derived from all considered load conditions.

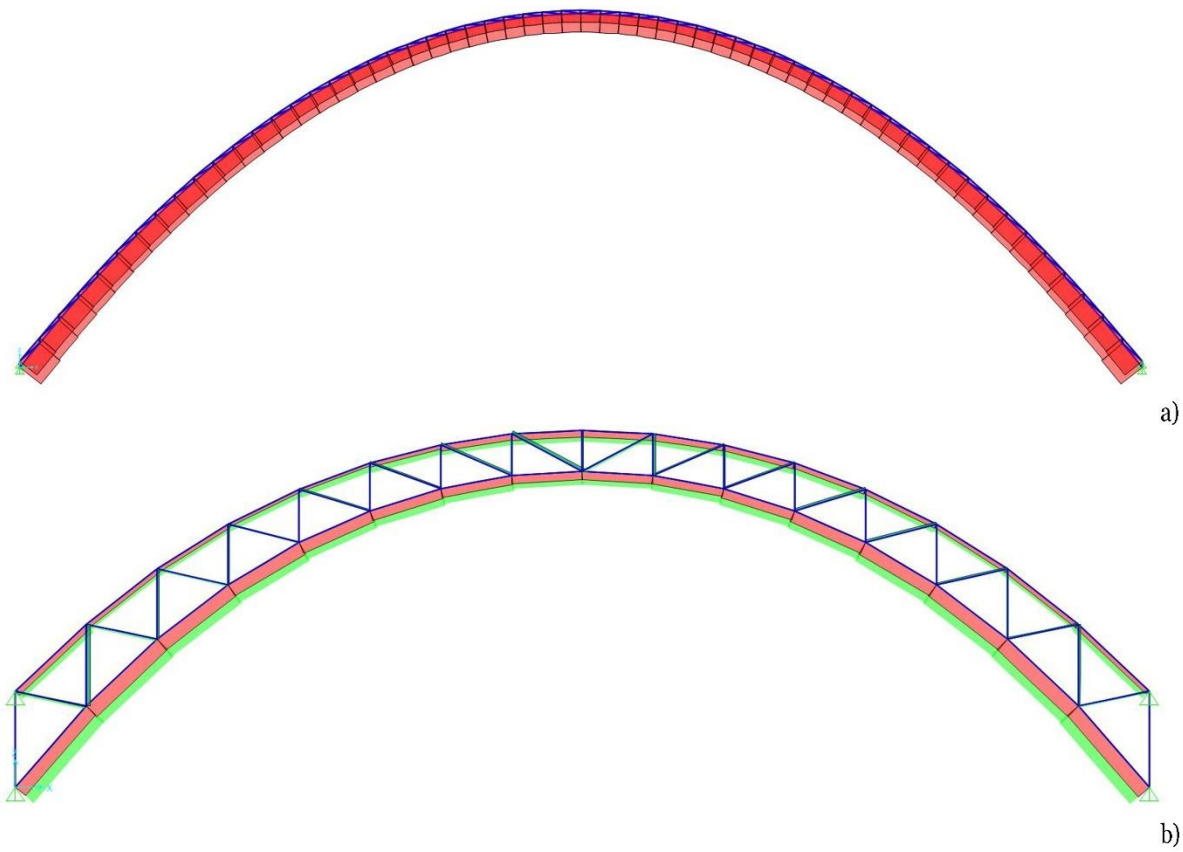

Figure 5. 4 *Structural optimization of hingeless truss arches: (a) Axial force diagram of the single load case optimal solution; (b) axial force diagram of the multi-load case optimal solution*

In the end, this demonstrative application of the optimization macro-algorithm proposed in the present dissertation (described in *§4.2*), once again leads to state that truss arches are not suitable to be optimally designed only considering a single load case, as well as monolithic arches (i.e. single-rib arches) would not be suitable to bear multiple load conditions extremely different from each other.

5.2 Simultaneous topology, shape and size optimization of two-hinged truss arches under multiple load cases

In light of the results obtained from the demonstrative applications previously illustrated in section *§5.1,* the optimization macro-algorithm (proposed in section *§4.2)* was applied to simultaneously perform topology, shape and size optimization of steel arched trusses under multiple load cases.

In particular, the present section will provide a detailed description of the stepwise optimization process of two-hinged truss arches, with different spans (*40*, *80*, *120* and *160 meters*), subjected to multiple different load cases. More specifically, in-plane Pratt trusses, composed by two arched chords connected each other and made of steel tubular members (i.e. with circular hollow cross-sections), were optimally designed for different vertical load patterns (acting in the arch plane). The so obtained results will be illustrated and discussed in subsection *§5.2.4*.

5.2.1 Parametric design

It was earlier underlined the pivotal role that parametric design plays in the preliminary phase of a structural optimization process, in identifying the design variables (among all parameters that mostly affect the design solutions) and properly defining their upper and lower bounds, as well as in the parametric definition of the geometry. This phase is thus indispensable to properly formulate, at a later stage, the considered optimization problem as a function of the design variables (as shown in the flowchart of the proposed macro-algorithm illustrated in *Figure 4. 2*).

Parametric design (Woodbury 2010) has been previously defined (in section *§1.2*) as a complex process aiming to define a design problem as a function of several parameters. As a matter of fact, this phase consists in establishing the relationships between the parts of the project, in order to define them as a function of constant and variable parameters (i.e. as parametric equations). Furthermore, the higher the number of design variables to consider, the more crucial the role of this stage in the whole process becomes.

In this regard, the design problem of truss arches here investigated depends on a large number of parameters, among which a set of design variables needs to be identified and properly defined.

5.2.1.1 Topology design variables

As anticipated in section *§1.3.3*, Truss Topology Optimization (TTO) aims to optimize the connectivity between a set of nodes, by formulating the problem as a size optimization problem thereby allowing zero bar areas (M P Bendsøe and Sigmund 2003).

In the presented case, topology optimization was not considered by the "ground structure" method.

The topology optimization problem of arched Pratt trusses (with spans of *40*, *80*, *120* and *160 meters*) has been here formulated as a function of a variable number of truss elements and joints, thereby assuming, as topology design variable, a parameter indicated as n_{int}, defining the number of equal "intervals" (segments), into which the arch span is subdivided, as follows

$$dL = L/n_{int} \tag{44}$$

Where L represents the length of the arch span, whereas the term dL indicates the length of the equal segments (see *Figure 5. 6*).

The topology design variable n_{int} determines the node number and spacing (their x −coordinates) and the number of the truss bars. In particular, the two-hinged truss arches under consideration are characterized by $2n_{int}$ joint number and $4n_{int} - 3$ number of members.

Furthermore, since a Pratt-type truss has been chosen as bracing system, n_{int} needed to be defined as an even integer, as well as a discrete design variable.

However, the optimization method here proposed (previously illustrated in section *§4.2*) needs to consider a unique set of continuous design variables. For this reason, the value related to the parameter n_{int} needed to be rounded to the nearest even integer.

No other parameter was assumed as topology design variable.

5.2.1.2 Shape design variables: parameters defining Cubic Rational Bézier Curves

As anticipated in the section *§1.3.2*, the shape optimization here means that node coordinates of the structure have to be found. However, the optimization problem of large-scale structures (continuous or discrete) characterized by a large number of nodes would require a high number of design variables. It could be therefore more advantageous to adopt parametric shape functions, depending on a small number of parameters.

For this purpose, *Rational Bézier Curves* have been adopted to parametrize the shape of the top and bottom chords of the planar truss arches under consideration, in order to define it as a function of a limited number of parameters (shape design variables). *Bézier curves* are parametric

curves widely used in vector graphics and animation applications to model smooth curves that can be scaled indefinitely (Farin, Hoschek, and Kim 2002; Piegl and Tiller 1997; Gerald Farin 1988). *Quadratic* and *Cubic Bézier curves* are most commonly adopted because the evaluation of higher degree curves is more computationally demanding. Moreover, Quadratic Rational Bézier curves can exactly represent conic curves (see the *§Appendix A*). However, in this work, the parametric form of *third-degree Rational Bézier curves* (shown in the *Figure 5. 5*) was adopted in order to represent a wider family of curves than conics.

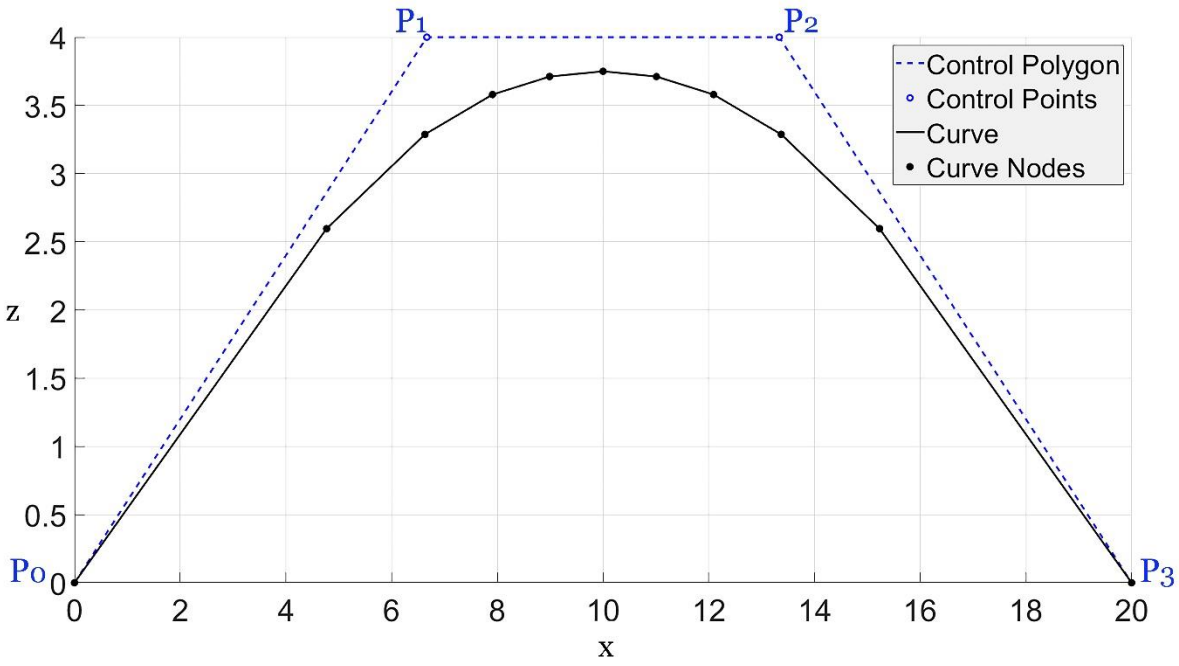

Figure 5. 5 *Third-degree Rational Bézier Curve*

Therefore, the following parametric equation (Eq. 45) was used to determine the z −coordinates of the truss joints

$$C(\mathbf{u}) = \frac{(P_0.w_0.(1-\mathbf{u})^3+P_1.w_1.3\mathbf{u}.(1-\mathbf{u})^2+P_2^2.w_2.3\mathbf{u}^2.(1-\mathbf{u})+P_3.w_3.\mathbf{u}^3)}{(w_0.(1-\mathbf{u})^3+w_1 3\mathbf{u}.(1-\mathbf{u})^2+w_2.3\mathbf{u}^2.(1-\mathbf{u}).w_2+w_3.\mathbf{u}^3)} \quad (45)$$

where P_0, P_1, P_2 and P_3 are called “control points” (they are also the vertices of the so-called “control polygon”), whereas w_0, w_1, w_2 and w_3 are their corresponding so-called “weight factors” (which are non-negative factors, whose values define the attraction level that the control polygon exerts on the curve) and $\mathbf{u}$ is a vector containing a large number of linearly spaced values, included in the interval [0,1]. Both *Rational* and *Non-Rational Bézier Curves* pass through the first and the last control points and are tangent at these points, respectively to the first and the last “control polygon” sides (as shown in the *Figure 5. 5* and in the *Figure 5. 6*).

In this regard, a more detailed description of *Rational Bézier curves* is provided in the *§Appendix A*.

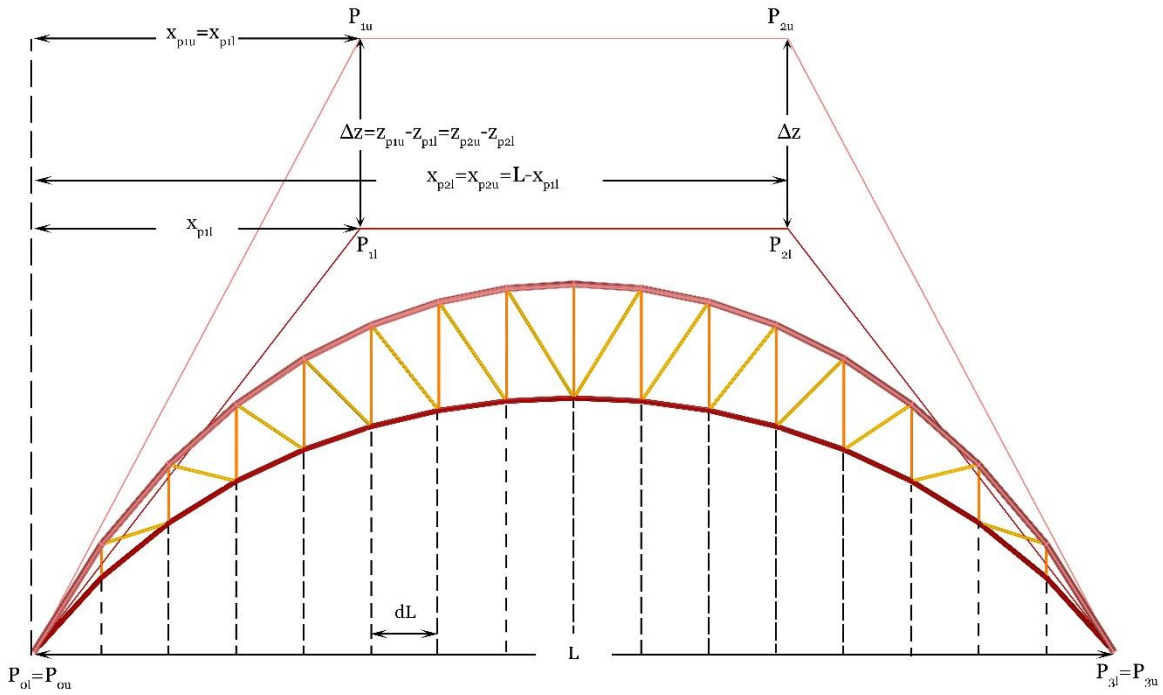

Figure 5. 6 *Parametric definition of the geometry as a function of shape design variables, by taking advantage of Cubic Rational Bézier Curves*

Therefore, based on the Eq. (45), as well as on assumed symmetry conditions (remarked in the *Figure 5. 6*), the following parameters were defined as shape design variables to be optimized

- x_{P1l}, x −coordinate of the second control point (P_{1l}) of the lower chord (shaped as a *Cubic Rational Bézier* arc), assumed as symmetric to the x −coordinate (x_{P2l}) of the third control point (P_{2l}), with respect to a central vertical axis. Furthermore, both x −coordinates of two internal control points (P_{1l} and P_{2l}) of the bottom arched chord were assumed to be equal to the x −coordinates of the internal control points of the upper chord axis (indicated as P_{1u} and P_{2u})
- z_{P1l}, z −coordinate of the second control point (P_{1l}) of the bottom arch rib (shaped as a *Cubic Rational Bézier* arc), which is assumed to be equal to the z −coordinate (z_{P2l}) of the third control point P_{2l}
- w_{P1l}, weight non-negative factor of the second control point (P_{1l}) of the bottom arched chord, which is equal to the weight factors (w_{P2l}, w_{P1u} and w_{P2u}) of other internal control points (P_{2l}, P_{1u} and P_{2u}) of lower and upper arch chords
- Δz, absolute value of the difference between z −coordinates of the internal control points of top and bottom arch chords ($\Delta z = |z_{P1u} - z_{P1l}| = |z_{P2u} - z_{P2l}|$).

It is worth noting that all assumed shape design variables were defined as continuous variable values, each one included in a proper range between a lower and an upper bound limit.

5.2.1.3 Size design variables

Size optimization of discrete structures aims to find the optimal cross-sectional areas of the considered truss members, which could be subdivided into several groups in order to reduce the total number of size design variables.

It is therefore a common practice to assume the cross-sectional areas of elements (or element groups) as continuous or discrete size design variables in a structural optimization process (as already discussed in section *§1.3.1*). In size optimization problems it could be particularly advantageous to assume a set of discrete variables, corresponding to a list of commercial cross-sections.

In this case, the elements of arched trusses were characterized by circular hollow cross-sections. Therefore, the steel tubular elements were grouped as follow

- Bottom chord (lower chord) elements
- Top chord (upper chord) elements
- Diagonals
- Verticals.

Each group of elements is characterized by same diameter, thus assuming

- d_1 as diameter of bottom chord elements
- d_2 as diameter of top chord elements
- d_3 as diameter of diagonals
- d_4 as diameter of verticals.

On the other hand, it was assumed that elements of the same group could have different thicknesses, by just imposing that each couple of elements, which are symmetrical with respect to a central vertical axis (placed in the mid-span and parallel to the reference z −axis), must have same thickness. For this purpose, further n size design variables were considered, thereby assuming n different thicknesses t_i (with $i = 1, \dots n$), for each i_{th} −couple of symmetrical elements.

It is worth noting that the allowable number of different thicknesses (n) depends on n_{int}^{u}, which indicates the considered upper bound of the topological design variable n_{int}, previously described (in section *§5.2.1.1*). More specifically, it was assumed that

$$n = 2 * n_{int}^{u} + 1 \tag{46}$$

which means that the assumed number of different cross-sections must depend on the allowable maximum number of elements, equal to $4n_{int}^{u} - 3$ (see the definition of the topology optimization sub-problem illustrated in *§5.2.1.1*).

5.2.2 Problem formulation

Based on the parametric definition (carry out in *§5.2.1*) of topology and geometry of the two-hinged arched trusses under consideration (see the *Figure 5. 6*), four different optimization problems were formulated for arches with spans of *40*, *80*, *120* and *160 meters*. In particular, the considered optimization problems differ from each other for the allowable minimum and maximum numbers of elements (as shown in the *Table 5. 3*), already defined in the previous section (*§5.2.1.3*), thus evaluated as follows

- for the arch model with a span of $40.0\ [m]$, the even number of equal intervals into which the span is subdivided (n_{int}) can vary from 4 (n_{int}^{l}) to 40 (n_{int}^{u}), the number of elements can then vary from $n_{el}^{MIN} = 4n_{int}^{l} - 3 = 13$ to $n_{el}^{MAX} = 4n_{int}^{u} - 3 = 157$ (CASE 1)
- for the arch model with a span of $80.0\ [m]$, the even number of equal intervals into which the span is subdivided (n_{int}) can vary from 6 (n_{int}^{l}) to 80 (n_{int}^{u}), the number of elements can then vary from $n_{el}^{MIN} = 4n_{int}^{l} - 3 = 21$ to $n_{el}^{MAX} = 4n_{int}^{u} - 3 = 317$ (CASE 2)
- for the arch model with a span of $120.0\ [m]$, the even number of equal intervals into which the span is subdivided (n_{int}) can vary from 8 (n_{int}^{l}) to 120 (n_{int}^{u}), the number of elements can then vary from $n_{el}^{MIN} = 4n_{int}^{l} - 3 = 29$ to $n_{el}^{MAX} = 4n_{int}^{u} - 3 = 477$ (CASE 3)
- for the arch model with a span of $160.0\ [m]$, the even number of equal intervals into which the span is subdivided (n_{int}) can vary from 10 (n_{int}^{l}) to 160 (n_{int}^{u}), the number of elements can then vary from $n_{el}^{MIN} = 4n_{int}^{l} - 3 = 37$ to $n_{el}^{MAX} = 4n_{int}^{u} - 3 = 637$ (CASE 4).

Table 5. 3 summarizes the numbers of design variables, distinguished by type (topology, shape and size), for each optimization problem. As anticipated, the considered problems differ from each other only for the number of size design variables, which was assumed to be proportional to the allowable maximum numbers of elements (defined in proportion to the length of the arch span).

Table 5. 3 Design variable definitions for the four considered optimization problems

Span length	Range of element number	Number of Topology DV	Number of Shape DV	Number of Size DV	Total number of DV
$40.0\ [m]$	$13 \leq n_{el} \leq 157$	1	4	85	90
$80.0\ [m]$	$21 \leq n_{el} \leq 317$	1	4	165	170
$120.0\ [m]$	$29 \leq n_{el} \leq 477$	1	4	245	250
$160.0\ [m]$	$37 \leq n_{el} \leq 637$	1	4	325	330

Table 5. 4 Lower and upper bounds of design variables for the CASE 1 (arch span of 40 meters)

CASE 1				
Design Variable (DV)	**Type of DV**	**Lower bound**	**Upper bound**	**Unit**
n_{int}	*topology*	4	40	$[adim.]$
x_{P1l}	*shape*	0.1	20.0	$[m]$
z_{P1l}	*shape*	0.0	20.0	$[m]$
w_{P1l}	*shape*	0.5	8	$[adim.]$
Δz	*shape*	0.1	20.0	$[m]$
$index_{d1}$	*size*	1	27	$[adim.]$
$index_{d2}$	*size*	1	27	$[adim.]$
$index_{d3}$	*size*	1	27	$[adim.]$
$index_{d4}$	*size*	1	27	$[adim.]$
$index_{t(i)}$ *	*size*	2	20	$[adim.]$

* with $i = 1, \dots n$ (n was defined in the section *§5.2.1.3* by the Eq. (46)).

Table 5. 5 Commercial circular hollow cross-sections

d [m]	t [m]	t [m]	t [m]	t [m]	t [m]	t [m]	t [m]	t [m]	t [m]	t [m]	t [m]	t [m]	t [m]	t [m]	t [m]	t [m]	t [m]	t [m]	t [m]	t [m]
0.054	0.0032	0.0036	0.004	0.0045	0.005															
0.0603	0.0032	0.0036	0.004	0.0045	0.005															
0.07	0.0032	0.0036	0.004	0.0045	0.005															
0.0761	0.0032	0.0036	0.004	0.0045	0.005															
0.0889	0.0032	0.0036	0.004	0.0045	0.005															
0.1016		0.0036	0.004	0.0045	0.005	0.0054	0.0056	0.0059												
0.108		0.0036	0.004	0.0045	0.005	0.0054	0.0056	0.0059												
0.1143		0.0036	0.004	0.0045	0.005	0.0054	0.0056	0.0059	0.0063											
0.127			0.004	0.0045	0.005	0.0054	0.0056	0.0059	0.0063	0.0071										
0.133			0.004	0.0045	0.005	0.0054	0.0056	0.0059	0.0063	0.0071	0.008									
0.1397			0.004	0.0045	0.005	0.0054	0.0056	0.0059	0.0063	0.0071	0.008									
0.1524			0.004	0.0045	0.005	0.0054	0.0056	0.0059	0.0063	0.0071	0.008									
0.159			0.004	0.0045	0.005	0.0054	0.0056	0.0059	0.0063	0.0071	0.008									
0.1683			0.004	0.0045	0.005	0.0054	0.0056	0.0059	0.0063	0.0071	0.008									
0.1937				0.0045	0.005	0.0054	0.0056	0.0059	0.0063	0.0071	0.008									
0.2191					0.005	0.0054	0.0056	0.0059	0.0063	0.0071	0.008	0.0088								
0.2445						0.0054	0.0056	0.0059	0.0063	0.0071	0.008	0.0088	0.01							
0.273							0.0056	0.0059	0.0063	0.0071	0.008	0.0088	0.01	0.011	0.0125					
0.2985								0.0059	0.0063	0.0071	0.008	0.0088	0.01	0.011	0.0125					
0.3239								0.0059	0.0063	0.0071	0.008	0.0088	0.01	0.011	0.0125					
0.3556									0.0063	0.0071	0.008	0.0088	0.01	0.011	0.0125	0.0142				
0.368									0.0063	0.0071	0.008	0.0088	0.01	0.011	0.0125	0.0142				
0.4064									0.0063	0.0071	0.008	0.0088	0.01	0.011	0.0125	0.0142	0.016			
0.419										0.0071	0.008	0.0088	0.01	0.011	0.0125	0.0142	0.016			
0.4572										0.0071	0.008	0.0088	0.01	0.011	0.0125	0.0142	0.016	0.0175		
0.47										0.0071	0.008	0.0088	0.01	0.011	0.0125	0.0142	0.016	0.0175		
0.508										0.0071	0.008	0.0088	0.01	0.011	0.0125	0.0142	0.016	0.0175	0.02	

A further crucial phase of the optimization problem formulation is the definition of proper lower and upper bound values for all design variables. In this regard, the *Table 5. 4* shows the lower and upper bounds of design variables for the CASE 1 (truss arch with a span of 40 meters).

As a matter of fact, size design variables were defined as indexes, which allow to take the values of diameters and thicknesses from a table of parameters of commercial circular hollow cross-sections (see *Table 5. 5*). Size design variables needed to be assumed as discrete. However, since the optimization method here proposed (in *§4.2*) can only generate continuous values, discrete size design variables were obtained by rounding the corresponding continuous values to the nearest integers. It is important to keep in mind that the elements of the truss arches under consideration were subdivided into four groups (previously defined in the section *§5.2.1.3*), each one characterized by same diameter and different thicknesses (by just imposing that couples of symmetrical members have the same thickness).

Furthermore, note that, in all cases, the upper bounds concerning the $x-$ and $z-$coordinates of the internal control point P_{1l} (from which also the $x-$ and $z-$coordinates of the other internal control points P_{1u}, P_{2l} and P_{2u} also depend on), were assumed to be equal to the half-span of the considered arch.

Table 5. 6 shows the lower and upper bounds of design variables for the CASE 2 (truss arch with a span of 80 meters). As in the previous case (as well as in all next cases), the size design variables were defined as indexes identifying rows and columns of *Table 5. 5* (whose first column contains the diameters of a list of 27 commercial steel tubes, whereas the other columns contain all thicknesses available).

Table 5. 6 Lower and upper bounds of design variables for the CASE 2 (arch span of 80 meters)

CASE 2				
Design Variable (DV)	**Type of DV**	**Lower bound**	**Upper bound**	**Unit**
n_{int}	*topology*	6	80	$[adim.]$
x_{P1l}	*shape*	0.1	40.0	$[m]$
z_{P1l}	*shape*	0.0	40.0	$[m]$
w_{P1l}	*shape*	0.5	8	$[adim.]$
Δz	*shape*	0.1	40.0	$[m]$
$index_{d1}$	*size*	1	27	$[adim.]$
$index_{d2}$	*size*	1	27	$[adim.]$
$index_{d3}$	*size*	1	27	$[adim.]$
$index_{d4}$	*size*	1	27	$[adim.]$
$index_{t(i)}$ *	*size*	2	20	$[adim.]$

* with $i = 1, \dots n$ (n was defined in the section *§5.2.1.3* by the Eq. (46)).

Table 5. 7 shows a list of topology, shape and size design variables with their lower and upper bounds defined of for the CASE 3 (i.e. a two-hinged truss arch with a span of 120 meters, made of steel tubular elements). On the other hand, *Table 5. 8* shows the lower and upper bounds of all design variables assumed for the CASE 4 (truss arch with a span of 160 meters).

Table 5. 7 Lower and upper bounds of design variables for the CASE 3 (arch span of 120 meters)

CASE 3				
Design Variable (DV)	**Type of DV**	**Lower bound**	**Upper bound**	**Unit**
n_{int}	*topology*	8	120	$[adim.]$
x_{P1l}	*shape*	0.1	60.0	$[m]$
z_{P1l}	*shape*	0.0	60.0	$[m]$
w_{P1l}	*shape*	0.5	8	$[adim.]$
Δz	*shape*	0.1	60.0	$[m]$
$index_{d1}$	*size*	1	27	$[adim.]$
$index_{d2}$	*size*	1	27	$[adim.]$
$index_{d3}$	*size*	1	27	$[adim.]$
$index_{d4}$	*size*	1	27	$[adim.]$
$index_{t(i)}$ *	*size*	2	20	$[adim.]$

* with $i = 1, \dots n$ (n was defined in the section *§5.2.1.3* by the Eq. (46)).

Table 5. 8 Lower and upper bounds of design variables for the CASE 4 (arch span of 160 meters)

CASE 4				
Design Variable (DV)	**Type of DV**	**Lower bound**	**Upper bound**	**Unit**
n_{int}	*topology*	10	160	$[adim.]$
x_{P1l}	*shape*	0.1	80.0	$[m]$
z_{P1l}	*shape*	0.0	80.0	$[m]$
w_{P1l}	*shape*	0.5	8	$[adim.]$
Δz	*shape*	0.1	80.0	$[m]$
$index_{d1}$	*size*	1	27	$[adim.]$
$index_{d2}$	*size*	1	27	$[adim.]$
$index_{d3}$	*size*	1	27	$[adim.]$
$index_{d4}$	*size*	1	27	$[adim.]$
$index_{t(i)}$ *	*size*	2	20	$[adim.]$

* with $i = 1, \dots n$ (n was defined in the section *§5.2.1.3* by the Eq. (46)).

All different optimization problems (CASE 1, 2, 3 and 4) were formulated with same objective and constraint functions. As described in section *§4.2.3*, the objective and constraint functions needed to be evaluated at each iteration of the proposed optimization macro-algorithm (see the *Figure 4. 2*), by performing *Finite Element Analysis (FEA)* through the software for structural analysis *SAP2000*.

In all considered cases, the total volume of the structure was assumed as objective function to be minimized and calculated by Eqs. (38) and (39) described in the section *§4.2.3*. In order to keep stress values within allowable ranges according to mechanical properties of materials and technical standards for construction, the maximum "utilization ratio" (i.e. the "demand/capacity ratio") of all truss members, for all applied load cases, was assumed as strength constraint in order to evaluate the combined effect of axial forces and bending moments (as anticipated in the section *§4.2.3*). In particular, the critical utilization ratio of bars subjected to compression axial forces was calculated by evaluating the combined effect of compression axial forces and bending moments by also considering flexural and lateral-torsional buckling by means of the interaction equations provided by the section EC3-2005 6.3.3(4), expressed by the Eqs. (40) and (41) in section *§4.2.3*. The utilization ratio of members subjected to tensile axial forces is evaluated by checking the combined effect of axial forces and bending moments by means of the interaction equation (provided by EC3-2005 6.2.1(7)), expressed by Eq. (42) in section *§4.2.3*.

However, the constraint functions can be generalized by the following inequality

$$\max_i Util_i^{LC} \leq 0.99 \tag{47}$$

where $i = 1, \dots n_{frames}$ (i.e. the latter indicating the number of elements of the frame structure), whereas $Util_i^{LC}$ corresponds to the "Utilization ratio" of an i_{th} –truss element evaluated, by means of the aforementioned Eqs. (40), (41) and (42), for each load case (LC). As a matter of fact, the "utilization ratio" is the ratio between real and allowable stresses, whereas the inequality constraint, expressed by the Eq. (47), indicates that the maximum value of the "Utilization ratio" among all truss members must be less than 0.99 for all considered load cases (feasibility condition).

It is important to keep in mind that the values of the objective and constraint functions are indispensable to compare and iteratively select the best candidate solutions of the considered problem during the optimization process, until an optimal solution is achieved.

5.2.3 Boundary conditions

All different optimization problems (CASES 1, 2, 3 and 4) faced in the present section *§5.2*, are characterized by the same boundary conditions.

More specifically, the steel truss arches under consideration, were assumed to be connected to the foundations by two hinges (see the *Figure 5. 7*). Moreover, since all members are connected together through pinned joints, the considered steel arches can be treated as true trusses (i.e. subjected to almost only axial forces).

In planar trusses, the degree of determinacy can be evaluated in the following simplified way

- If $2n_{nodes} > n_{frames} + gdv_{ext}$, the structure is determinate and unstable (which is also called "hypostatic structure")
- If $2n_{nodes} = n_{frames} + gdv_{ext}$, the structure is determinate and stable (which is also called "isostatic structure")
- If $2n_{nodes} < n_{frames} + gdv_{ext}$, the structure is indeterminate (also called "redundant structure"

where n_{nodes} indicates the number of joints, n_{frames} represents the number of elements whereas gdv_{ext} corresponds to the "degree of external constraint", which, in this case, is equal to 4 (since the considered truss arches are characterized by two external hinges).

The structure illustrated in the *Figure 5. 7* is statically redundant or indeterminate, since it is easy to prove that

$$2.n_{nodes} < n_{frames} + gdv_{ext} \tag{48}$$

by substituting the quantities indicating the numbers of nodes (n_{nodes}) and elements (n_{frames}) with their parametric expressions as a function of the parameter n_{int}

$$2.(2.n_{int}) < (4.n_{int} - 3) + 4 \tag{49}$$

which leads to obtain the following simplified inequality

$$4.n_{int} < 4.n_{int} + 1 \tag{50}.$$

Not that the Eq. (50) proves that the considered structure to be optimized is always indeterminate with one degree, regardless the number of its members.

It is clearly shown in *Figure 5. 7* that three different load cases acting in the z −direction (i.e. lying on the same xz −plane as the arch) were applied; which are

- LOAD CASE 1: Non-structural Dead Loads (24.00 kN/m) + Live Loads (15.00 kN/m) applied along the total length of the arch
- LOAD CASE 2: Non-structural Dead Loads (24.00 kN/m) applied along the total length of the arch
- LOAD CASE 3: Non-Structural Dead Loads (24.00 kN/m) applied along the total length of the arch + Live Loads (15.00 kN/m) applied along the right half of the arch.

Note that all load patterns were applied as Point Loads on nodes (of the bottom chord), equivalent to the uniform load conditions just mentioned (and illustrated in *Figure 5. 7*).

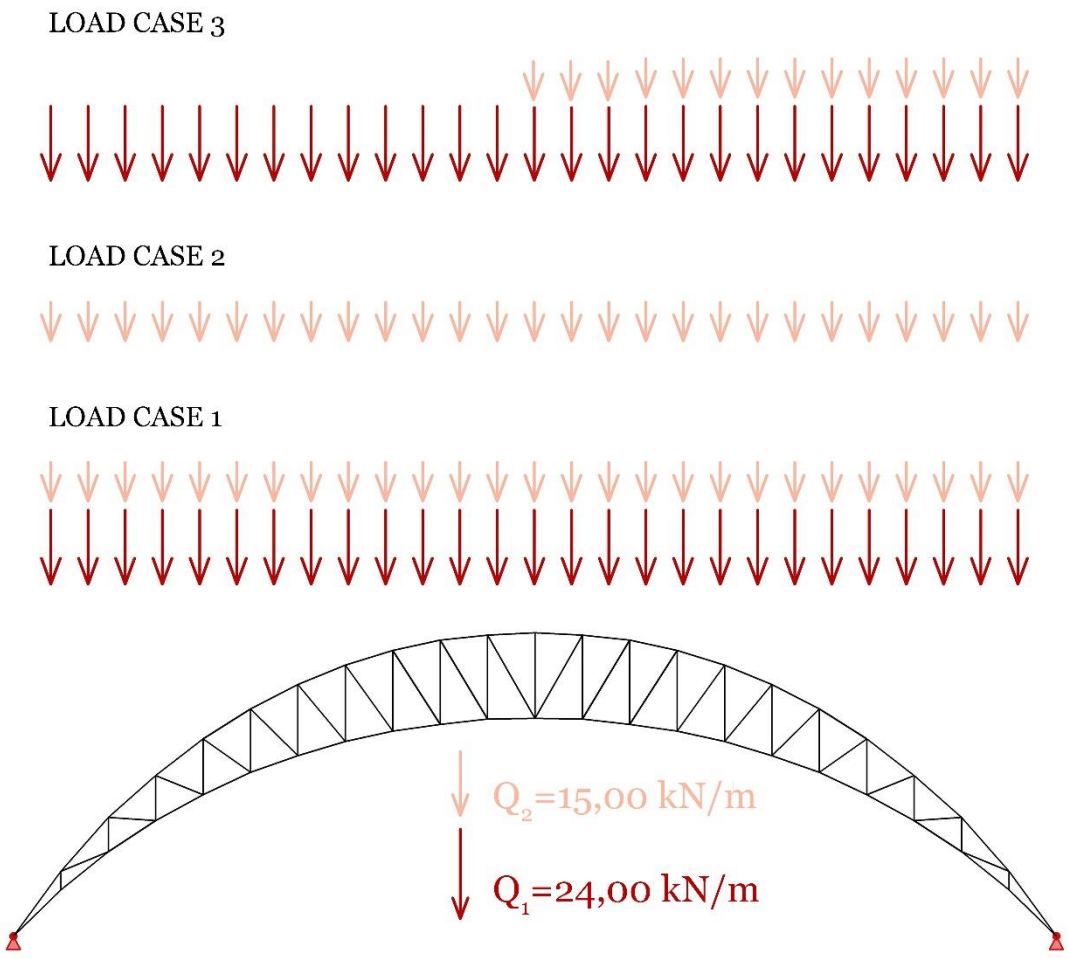

Figure 5. 7 *Boundary conditions (external constraints and multiple load cases) considered in all cases of the optimization problem of two-hinged truss arches*

5.2.4 Results

As discussed in the previous section *§5.2.2*, the problem of the optimum design of two-hinged steel truss arches was faced with four different formulations, each one characterized by a different span (40, 80, 120 and 160 *meters*) and different number of size design variables (which increases as the arch span increases, as shown in *Table 5. 3*). The optimization problems of CASES 1, 2, 3 and 4 were solved by applying the optimization macro-algorithm entirely contained in a MATLAB program (described in the section *§4.2* and summarized in the flowchart in *Figure 4. 2*). The proposed method was applied to find optimal solutions (with minimum weight) of the two-hinged truss arches under consideration, subjected to the above mentioned different load cases (shown in *Figure 5. 7*). The purpose of this section is to illustrate and compare the obtained best solutions of all considered optimization problems (CASES 1, 2, 3 and 4), in order to investigate them and deduce useful suggestions for the design of two-hinged truss arches made of steel tubular elements.

As already mentioned, the proposed macro-algorithm includes a modified version of a *Differential Evolution Algorithm* (in detail described in the section *§4.2.2* and summarized in the *Figure 4. 3*). Since this optimization algorithm belongs to population-based *Evolutionary Algorithms* (introduced in *§1.4.3.2*), in a preliminary phase, following the parametric definition of the considered problem, it was necessary to properly define the "population" size (which corresponds to the number of candidate solutions, called "individuals", of each "generation") and the maximum number of "generations".

Table 5. 9 *Optimization parameters of the Differential Evolution Algorithm (DEA) for the different problem formulations (CASES 1, 2, 3 and 4)*

OPTIMIZATION PARAMETERS					
CASE	**Span length**	**Number of design variables**	**Population size**	**Generations**	**Total number of iterations**
1	40.0 [m]	90	100	300	30000
2	80.0 [m]	170	100	500	50000
3	120.0 [m]	250	100	750	75000
4	160.0 [m]	330	100	1000	100000

In regard, *Table 5. 9* summarizes the main optimization parameters, defined for each case. It is worth noting that all problems were characterized by a large number of design variables, same population size and the maximum number of "generations" is increased according to the number of design variables of the problems in order to ensure a suitable exploration of the search space.

In closing, it is worth highlighting that the proposed optimization method, allowed to simultaneously optimize all design variables despite their various nature (since topology, shape and size, as well as continuous and discrete design variables were considered) and extremely large number leading to satisfactory results.

5.2.4.1 Case 1 optimal solution

As a first case, the problem of the structural optimization of a two-hinged truss arch with a span of 40 meters parametrically defined as shown in the section *§5.2.1* (by taking advantage of *Cubic Rational Bézier curves* to parametrize the geometry, as illustrated in *Figure 5. 6*) and subjected to three vertical load cases (represented in *Figure 5. 7*) was considered and successfully solved. All assumed design variables, with corresponding lower and upper bounds, are indicated in *Table 5. 4*.

In this regard, *Figure 5. 8* shows the optimal shape of the best solution characterized by a minimum volume of 0.339 m^3 (i.e. the minimum value of the objective function), corresponding to a self-weight per unit length of 0.652 kN/m. The so-obtained optimal solution is characterized by a total height of 10.23 m, a rise of 5.83 m and a "crown depth" about 4.40 m (as indicated in *Figure 5. 8*).

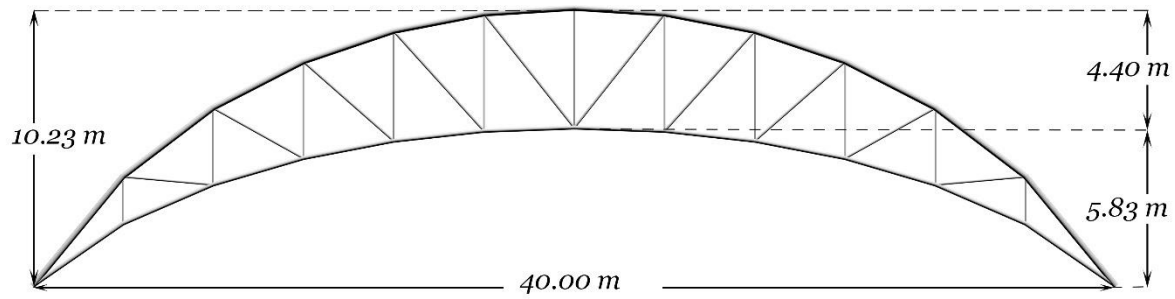

Figure 5. 8 Front view of the optimized truss arch with main dimensions (CASE 1 optimal solution)

As well known, a representative parameter of an arch shape is its "rise-to-span ratio" (commonly included between 1/4 and 1/6), which strongly affects the structural behaviour of the arch. The smaller the rise of an arch, the greater the magnitude of horizontal thrusts (see Eqs. (10) and (15)) that arise at its end. In particular, the optimal arch here considered, has a "rise-to-span ratio" equal to 1/6.86, a "height-to-span ratio" equal to 1/3.91 and a "crown depth-to-span ratio" corresponding 1/9.09. Such a high depth at the arch crown could be justified by the high flexibility of a two-hinged arch, especially under asymmetric load patterns as the one among all load cases considered (represented in *Figure 5. 7*). A further representative parameter of the optimal truss arch under consideration is the total number of elements, which directly depends on the even

integer (n_{int}) of the arch span subdivisions into equal intervals. In this regard, the truss arch represented in the *Figure 5. 8* is characterized by an arch span subdivision number (n_{int}) equal to 12, thereby resulting in a total element number (n_{frames}) equal to 45 (since it was assumed that $n_{frames} = 4n_{int} - 3$) and joint number ($n_{nodes}$) equal to 24 (since $n_{nodes} = 2n_{int}$).

Table 5. 10 *Topology and shape optimization results for the CASE 1: optimal values of topology and shape design variables*

Topology optimization results			
Design Variable (DV)	**Type of DV**	**Best value**	**Unit**
n_{int}	*topology*	12	$[adim.]$
Shape optimization results			
Design Variable (DV)	**Type of DV**	**Best value**	**Unit**
x_{P1l}	*shape*	12.078	$[m]$
z_{P1l}	*shape*	9.310	$[m]$
w_{P1l}	*shape*	0.559	$[adim.]$
Δz	*shape*	7.030	$[m]$

Table 5. 10 contains the optimal values obtained for all topology and shape design variables, which completely define the geometry of the optimal truss arch here analysed. It is worth observing that the obtained arch shape (especially the bottom chord shape) is quite lowered and comparable to that one of a "segmental arch". Note that the obtained arched truss shape must be a trade-off between the optimal shapes for all considered load cases (shown in *Figure 5. 7*), among which the asymmetric load pattern strongly affects the structural response of the structure and the solution of the optimization problem.

Table 5. 11 *Size optimization results for the CASE 1: optimal diameters and thicknesses of circular hollow cross-sections*

Size optimization results					
Element groups	**Type of DV**	**Diameter d_i**	**Min. thickness t_i**	**Max. thickness t_i**	**Unit**
Bottom chord	*size*	0.1524	0.004	0.008	$[m]$
Top chord	*size*	0.2191	0.005	0.005	$[m]$
Diagonals	*size*	0.0889	0.0032	0.005	$[m]$
Verticals	*size*	0.054	0.0032	0.005	$[m]$

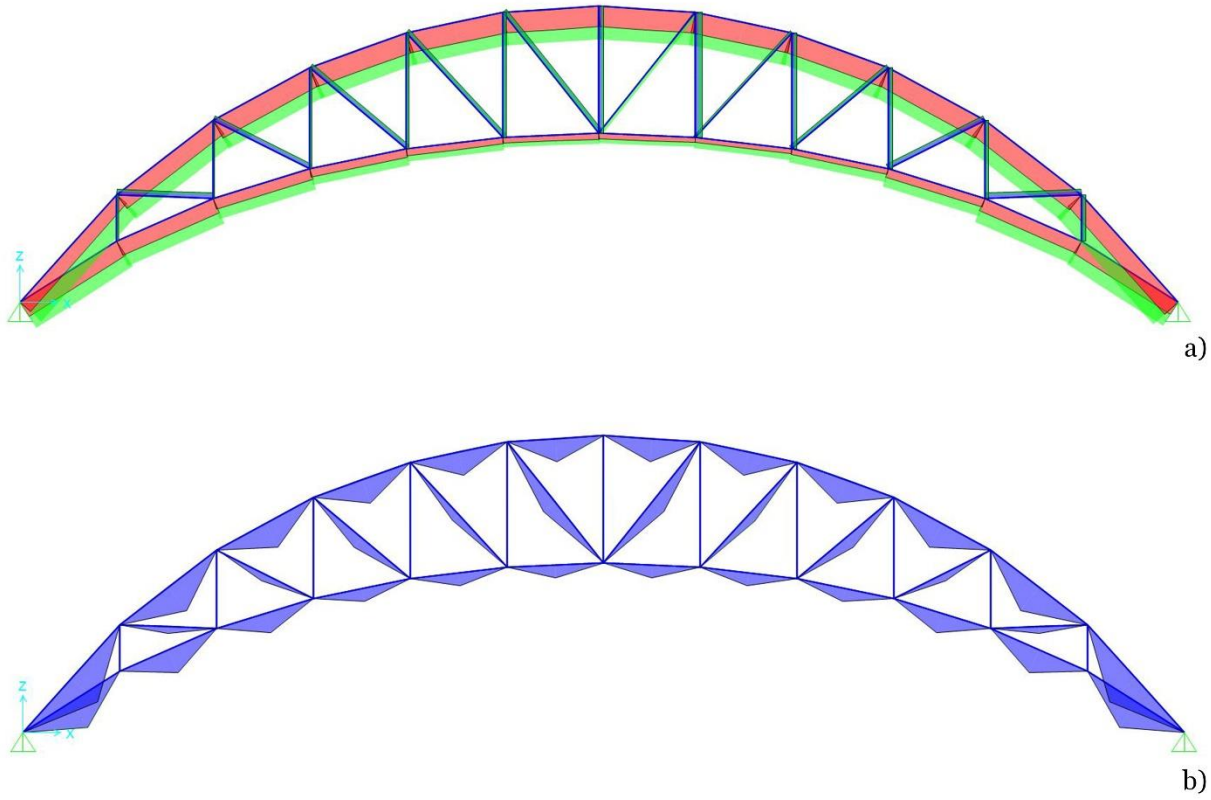

Figure 5. 9 *Finite Element Analysis (FEA) results for the CASE 1: (a) axial force diagram; (b) bending moment diagram*

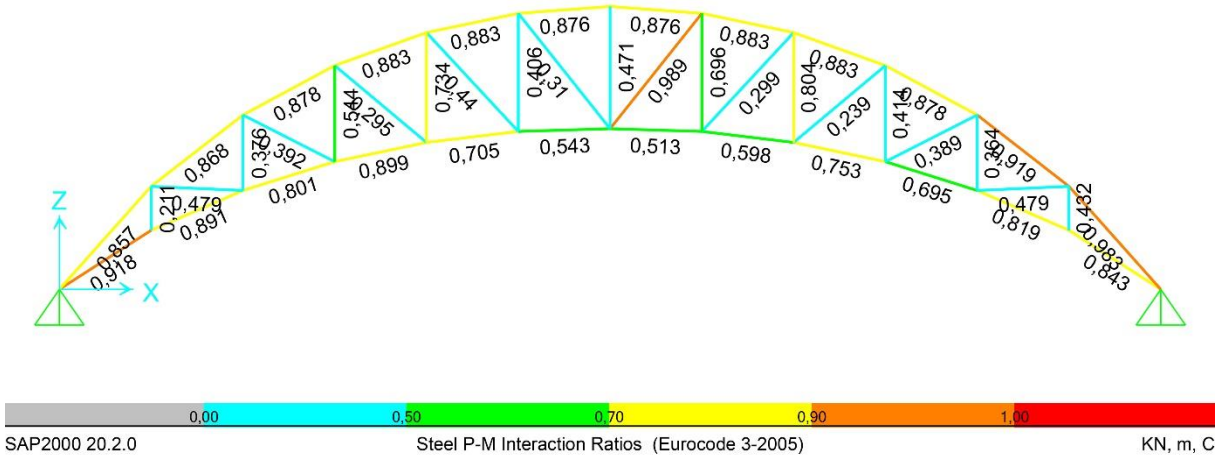

Figure 5. 10 *Finite Element Analysis (FEA) results for the CASE 1: Demand/Capacity ratio (also called "utilization ratio") diagram of the optimal solution for the envelope of all load cases*

However, the optimal shape for an asymmetrical uniform load pattern (like the third load case here considered) should also be asymmetrical but the arch was imposed to be symmetric.

Table 5. 11 shows the optimal values of diameters and thicknesses (taken from *Table 5. 5*) that define the circular hollow cross-sections of the elements. As described in the section *§5.2.1.3*, the

elements were subdivided into four groups (bottom chord elements, top chord elements, diagonals and verticals), each characterized by same diameter and different thicknesses (it was only imposed that couples of symmetrical elements with respect a central vertical axis must have same thickness).

Since the number of size design variables corresponding to the element thicknesses is extremely large, only the minimum and the maximum thicknesses for each element group are indicated in *Table 5. 11*. Note that the tubular elements of the top chord have the largest diameter and constant thickness, because the upper chord is subjected to the maximum axial force (as shown in *Figure 5. 9(a)*). In particular, it was found that the upper chord was subjected to a compressive axial force varying from $578\ kN$ to $674\ kN$ (which could be considered as constant), as well as to bending moments (whose diagram is illustrated in *Figure 5. 9(b)*) varying from $0.36\ kN.m$ to $0.54\ kN.m$.

On the other hand, the bottom chord is subjected to a compressive axial force varying between $193\ kN$ to $553\ kN$, as well as to bending moments varying from $0.20\ kN.m$ to $0.46\ kN.m$. Moreover, diagonal and vertical members are subjected to tensile axial forces, whereas diagonals also withstand bending moment actions varying from $0.1\ kN.m$ to $0.22\ kN.m$.

It is worth highlighting that a structural optimization process of an arch always aims to minimize potential bending effects, since arches were properly conceived to bear and transfer loads by mainly compressive axial stresses. The stress level in the structure to be optimized was kept within an allowable range of values, according to mechanical properties of materials and technical standards for construction, assuming the maximum "utilization ratio" (i.e. the "demand/capacity ratio") of all truss members, for all applied load cases, as strength constraint function (expressed by the Eq. (47)), thus checking the combined effect of axial forces and bending moments with special emphasis to flexural and lateral-torsional buckling in case of combined compressive and bending stresses. *Figure 5. 10* shows a diagram of the optimal truss arch here analysed, indicating the maximum i^{th} −element "utilization ratio" ($Util_i^{LC}$), among all load combinations.

The aforementioned "utilization ratio" diagram shows that more than half of elements is characterized by a critical ratio larger than 0.7. However, a new parameter to express the overall percentage of "utilization" of the whole structure was introduced and evaluated as follows

$$Util_{tot} = \frac{\sum_{i=1}^{n_{frames}} \left(\max_{LC} Util_i^{LC} * W_i \right)}{\sum_{i=1}^{n_{frames}} (W_i)} \tag{51}$$

where the term $\max_{LC} Util_i^{LC}$ indicates the maximum "utilization ratio" characterizing each i^{th} −member among all load cases (LC), whereas W_i indicates the weight of each i^{th} −member.

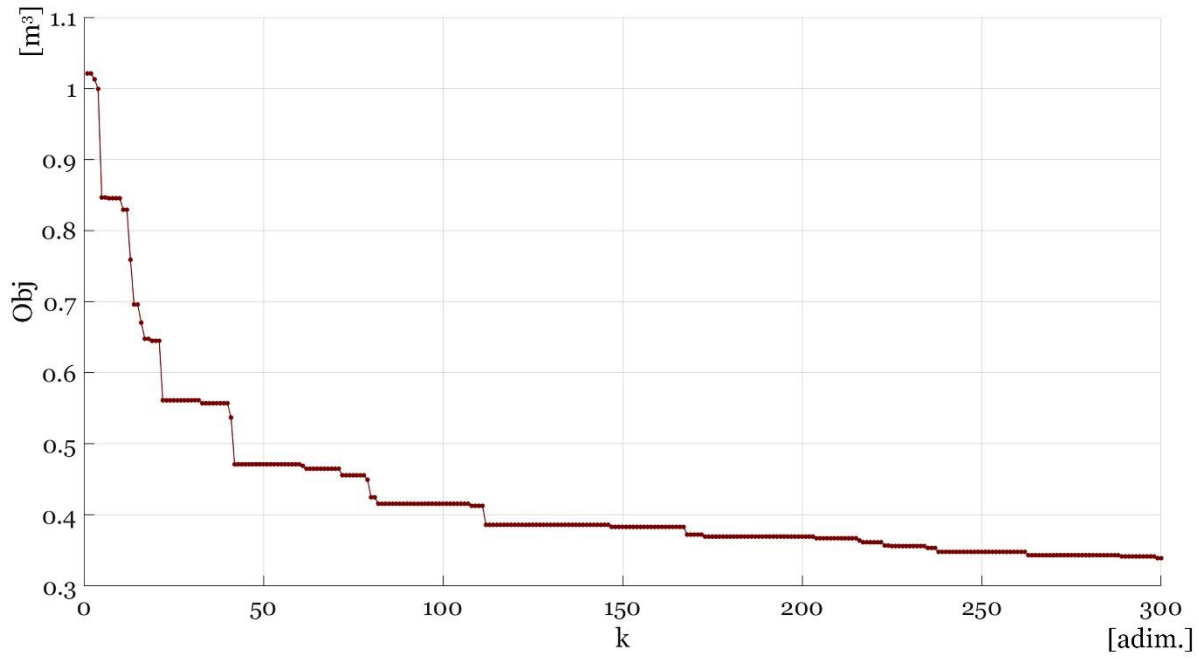

Figure 5. 11 *Convergence curve of the Objective (Obj) function (i.e. the volume of the arch) for all "generations" (for the CASE 1)*

As a matter of fact, the new introduced parameter $Util_{tot}$ was evaluated as a weighted average of Demand/Capacity ratios ($\max_{LC} Util_i^{LC}$) shown in *Figure 5. 10,* with respect to the weight of each member. The "total utilization ratio" ($Util_{tot}$) therefore expresses a quite realistic overall percentage of the material exploitation characterizing the whole structure.

The "total utilization ratio" ($Util_{tot}$) resulting from all values indicated in *Figure 5. 10,* and calculated by the Eq. (51), corresponds to a satisfactory percentage of material exploitation about 76.3 %, which ensures a high level of structural performance of the optimized solution under consideration.

Figure 5. 11 shows the convergence curve of the "objective function" (i.e. the total volume of the structure) to be minimized, in order to validate the goodness of the obtained result, notwithstanding the extremely large number of design variables and their various nature.

For the same purpose, *Figure 5. 12* shows two diagrams, representing the history of two important functions in the optimization process, which are

- The "stagnation function" (whose diagram is shown in *Figure 5. 12(a)*) mathematically represents a particular situation, which could be confused with a premature convergence since it occurs when a population-based optimization algorithm stops proceeding towards the global optimum, although the population has not converged to a local optimum and new individual entered the population

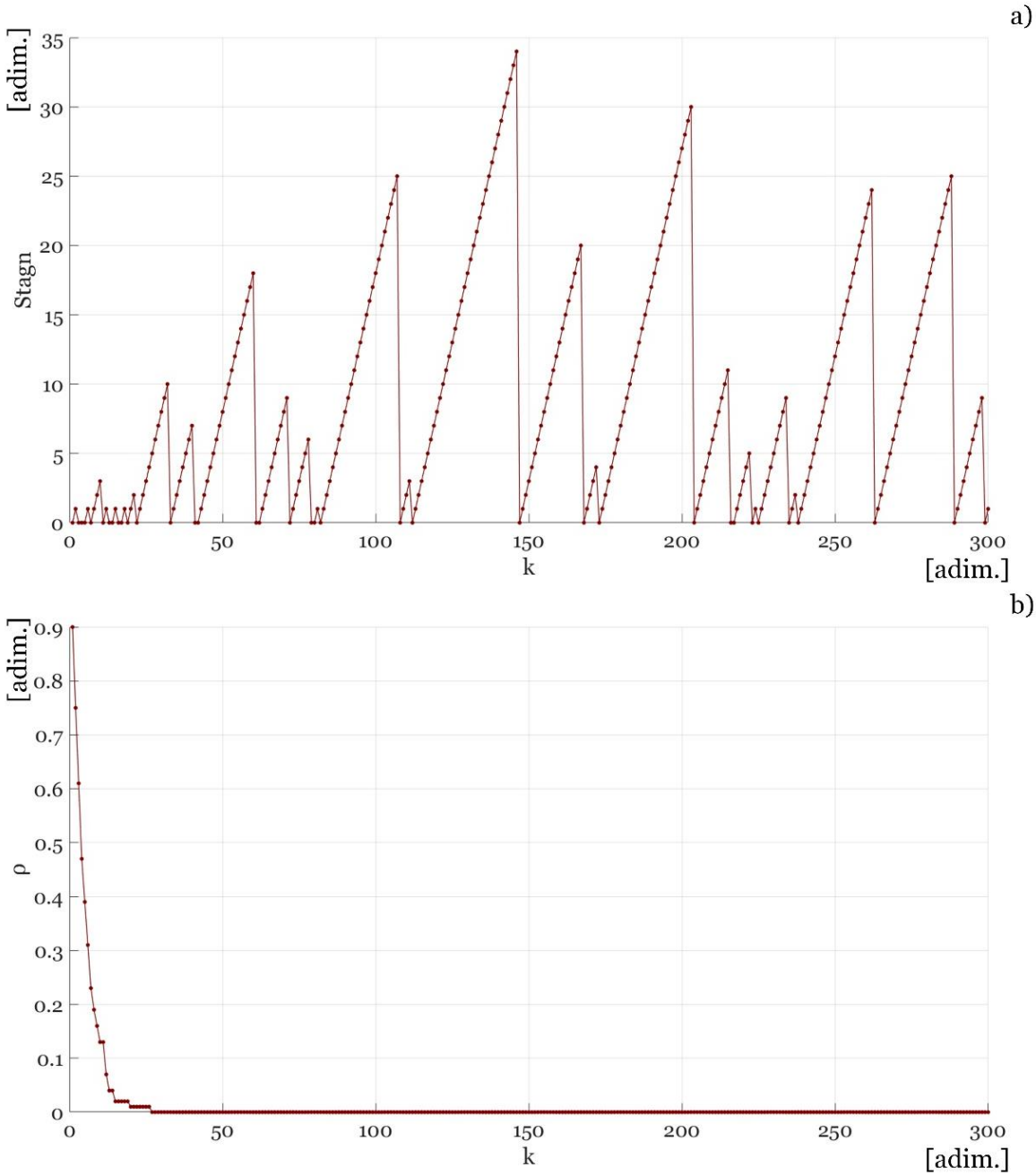

Figure 5. 12 History of optimization functions (for the CASE 1): (a) stagnation function; (b) "unfeasibility function" (ρ)

- The "unfeasibility function" (indicated as ρ in *Figure 5. 12(b)*), evaluates the number of "unfeasible individuals" (i.e. candidate solutions that not satisfy all constraint functions) generated in each generation (k), as follows

  $$\rho^k = \frac{Unf^k}{Pop^k} \quad (52).$$

  More specifically, ρ^k is a value between 0 and 1, calculated as a ratio between "unfeasible individuals" (Unf^k) and all individuals (Pop^k) of a k^{th} –generation.

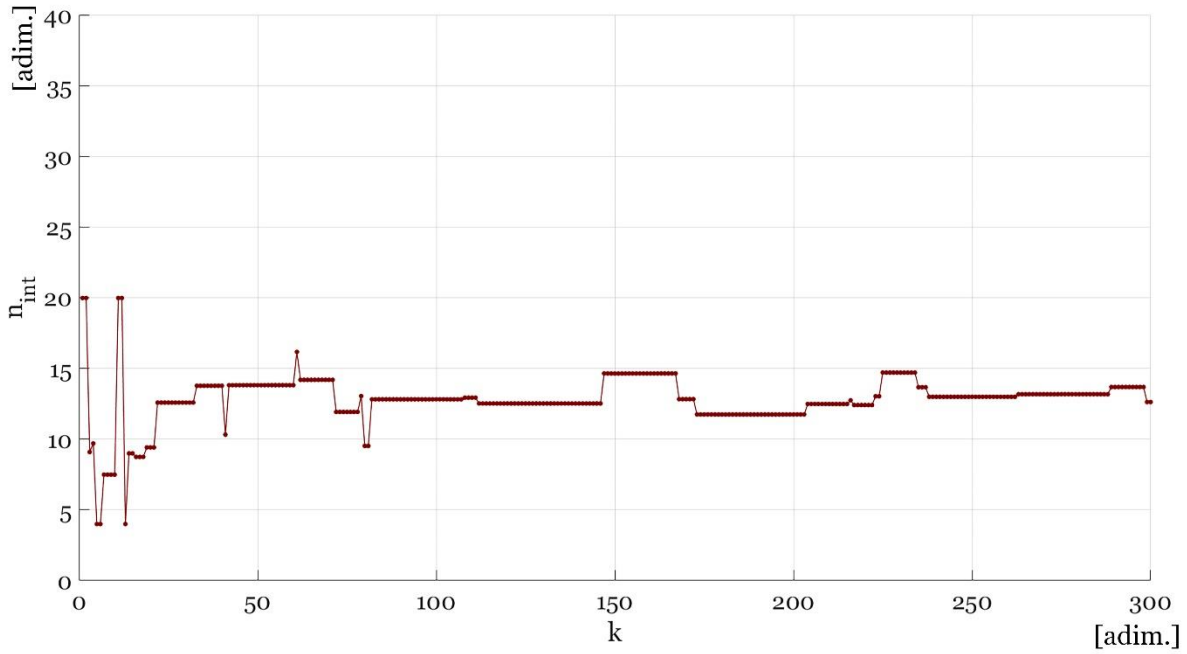

Figure 5. 13 Convergence curve of the topology design variable (n_{int}) for the CASE 1

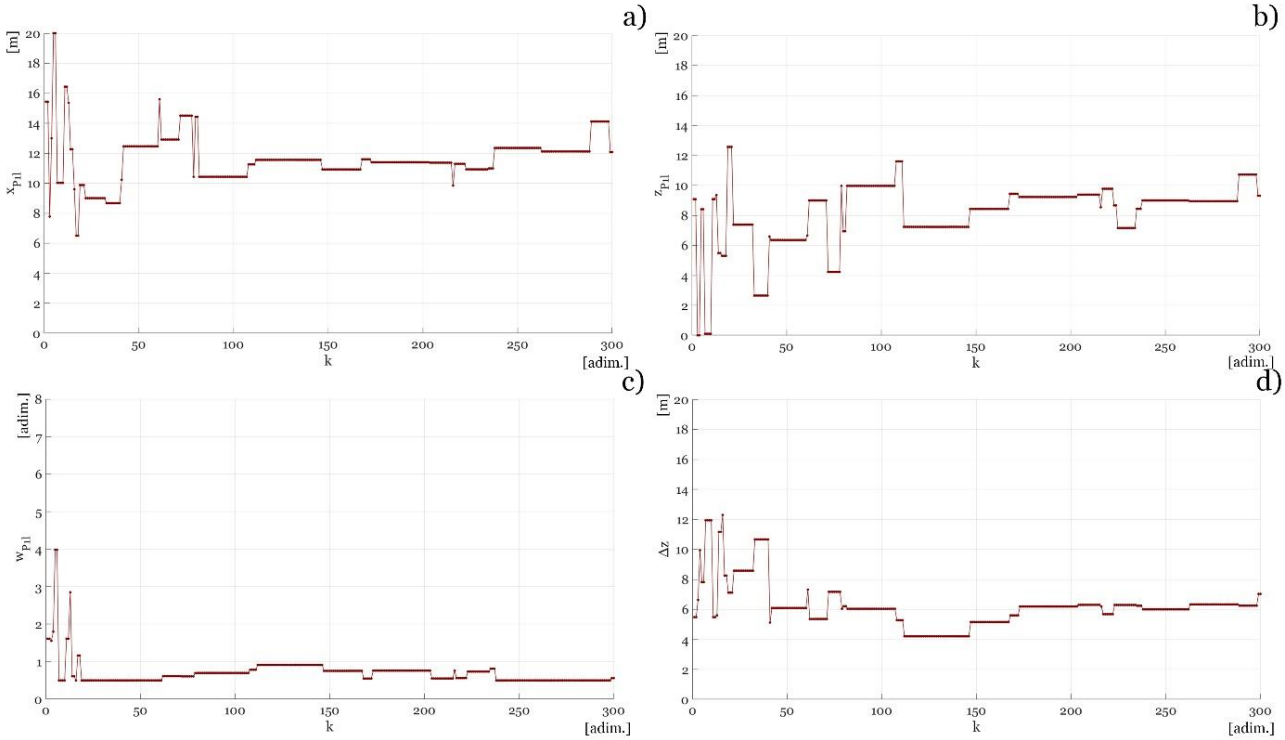

Figure 5. 14 Convergence curves of the shape design variables (variable parameters of third-degree rational Bézier curves) for the CASE 1: (a) x –coordinate of the second control point (x_{P1l}) of the bottom arched chord; (b) z –coordinate of the second control point (z_{P1l}) of the bottom arched chord; (c) weight factor of the second control point (w_{P1l}) of the bottom arched chord; (d) the difference between the z –coordinates (in absolute value) of the top and bottom chord internal control points (Δz)

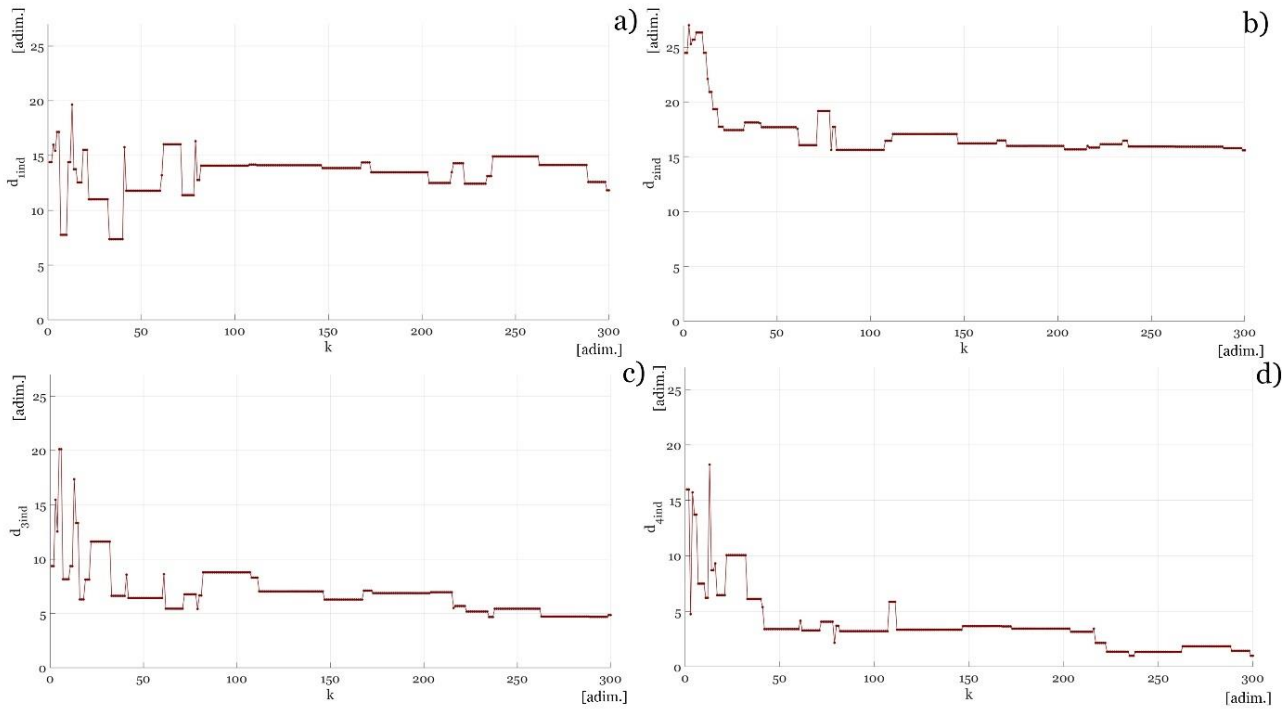

Figure 5. 15 Convergence curves of size design variables (i.e. indexes identifying the element group diameters in a list of commercial circular hollow cross-sections) for the CASE 1: (a) index identifying the bottom chord diameter; (b) index identifying the top chord diameter; (c) index identifying the diameter of diagonals; (d) index identifying the diameter of verticals

The "zigzag" trend of the "stagnation function" (*Figure 5. 12(a)*) occurs because it becomes equal to zero at each generation characterized by an improvement in the objective function compared to the previous generation. On the other hand, the "stagnation function" increases until an improvement in the objective function occurs.

Figure 5. 12(b) shows that the "unfeasibility function" (ρ) becomes and remains zero from the 27^{th} generation to the last one, meaning that the optimization process produces and evaluates only feasible candidate solutions from this point on.

Since the optimization problem here analysed is characterized by an extremely large number of design variables, it is not possible to show all their convergence curves.

In this regard, *Figure 5. 13* represents the convergence diagram of the topology design variable n_{int}, which the total number of the truss arch elements depends on. It is worth recalling that n_{int} was defined as a continuous value between 4 and 40 (to be later rounded to the nearest even integer).

The convergence curve validates the goodness of obtained solution, since from the first 20 generations its value only tends to oscillate between 10 and 14, until an optimal value close to 12 was found (see *Figure 5. 13*).

In *Figure 5. 14* the convergence curves of shape design variables (i.e. the variable parameters defining the shape of the lower and upper arch chords through parametric *Cubic Rational Bézier curves*) are presented to prove the validity of results, despite the large number and the variety of design variables. In the same way, a good convergence trend was also obtained for the size design variables determining the element group diameters (whose curves are shown in *Figure 5. 15*).

The goodness of the obtained results validates the effectiveness of the adopted optimization method (i.e. the *MATLAB* macro-algorithm presented in section *§4.2*) in handling and solving structural optimization problems characterized by an extremely large number of design variables and constraint functions, in a reasonable computational time.

5.2.4.2 Case 2 optimal solution

As a second case, the problem of the structural optimization of a two-hinged truss arch with a span of 80 meters, parametrically defined by taking advantage of parametric *Cubic Rational Bézier curves* (as described in section *§5.2.1* and illustrated in *Figure 5. 6*) and subjected to three vertical load cases (represented in *Figure 5. 7*) was addressed and successfully solved. All assumed design variables, with corresponding lower and upper bounds, are indicated in *Table 5. 6*. *Figure 5. 16* shows the optimal shape of the obtained best solution, characterized by a minimum volume (best objective) equal to 1.508 m^3, corresponding to a self-weight per unit about 1.451 kN/m. The optimal truss arch in *Figure 5. 16*, is 21.47 m high, has a rise of 13.12 m and a "crown depth" about 8.36 m.

Therefore, the optimal arch here considered is characterized by a "rise-to-span ratio" equal to 1/6.10, a "height-to-span ratio" equal to 1/3.72, as well as a "crown depth-to-span ratio" about 1/9.57. As in the previous case (in section *§5.2.4.1*) the "crown depth" of the arch is considerably high, indeed because of the high flexibility of a two-hinged arch system, especially under asymmetric load patterns as the third one among the load cases considered (represented in *Figure 5. 7*).

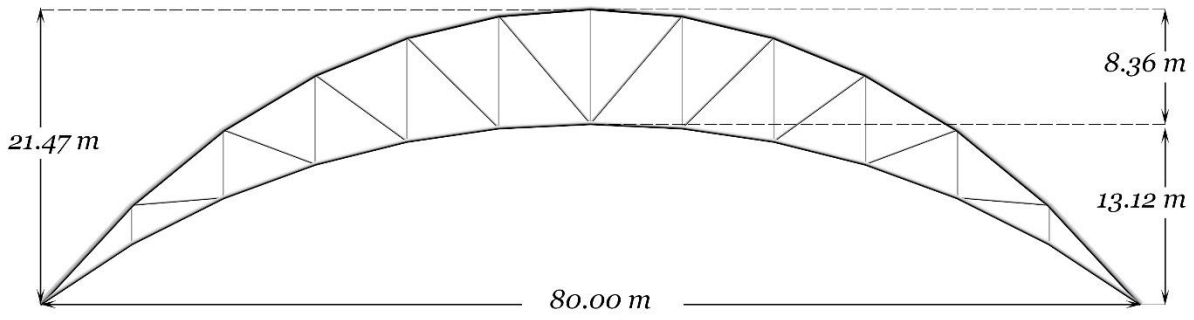

Figure 5. 16 Front view of the optimized truss arch with main dimensions (CASE 2 optimal solution)

Table 5. 12 *Topology and shape optimization results for the CASE 2: optimal values of topology and shape design variables*

Topology optimization results			
Design Variable (DV)	**Type of DV**	**Best value**	**Unit**
n_{int}	*topology*	12	$[adim.]$
Shape optimization results			
Design Variable (DV)	**Type of DV**	**Best value**	**Unit**
x_{P1l}	*shape*	29.224	$[m]$
z_{P1l}	*shape*	21.696	$[m]$
w_{P1l}	*shape*	0.509	$[adim.]$
Δz	*shape*	13.821	$[m]$

Furthermore, the truss arch represented in *Figure 5. 16* is characterized by an arch span subdivision number (n_{int}) equal to 12 as the optimal solution of the CASE 1 thereby resulting in a total element number (n_{frames}) equal to 45 and joint number (n_{nodes}) equal to 24.

Table 5. 12 contains the optimal values of the topology and shape design variables, which defined the optimal shape of the arch under consideration. Note that, as in the previous case, the shape of the arch chords (especially of the lower chord) are quite lowered (even if to a less extent with respect to the optimal arch carried out for the CASE 1), looking like flattened at their crown. It is important to remember that the shape of the truss arch under consideration, has to be optimal for the three considered load conditions, among which an asymmetric load pattern was also assumed (see the *Figure 5. 7*). The asymmetrical uniform load pattern assumed as third load case, as larger effect on the structural behaviour of the symmetric arch to be optimized, since the optimal shape for that load condition should be also asymmetric.

Table 5. 13 *Size optimization results for the CASE 2: optimal diameters and thicknesses of circular hollow cross-sections*

Size optimization results					
Element groups	**Type of DV**	**Diameter d_i**	**Min. thickness t_i**	**Max. thickness t_i**	**Unit**
Bottom chord	*size*	0.2985	0.0059	0.008	$[m]$
Top chord	*size*	0.368	0.007159	0.00904	$[m]$
Diagonals	*size*	0.159	0.004	0.008	$[m]$
Verticals	*size*	0.0761	0.005	0.005	$[m]$

Table 5. 13 shows the optimal values of diameters and thicknesses (taken from *Table 5. 5*) defining the circular hollow cross-sections of the elements. Since the number of size design variables corresponding to the element thicknesses is extremely large, only the diameter, the minimum and the maximum thicknesses for each element group are indicated in *Table 5. 11*. Note that the tubular elements of the top chord have the largest diameter (as occurred in CASE 1), because the upper chord is subjected to the maximum axial force (as shown in *Figure 5. 17(a)*).

In particular, it was found that the upper chord was subjected to a compressive axial force varying from 1118 kN to 1453 kN, as well as to bending moments (whose diagram is illustrated in *Figure 5. 17(b)*) varying from 3.07 $kN.m$ to 5.69 $kN.m$. On the other hand, the bottom chord is subjected to a compressive axial force varying between 544 kN to 1202 kN, as well as to bending moments varying from 2.33 $kN.m$ to 3.74 $kN.m$.

Moreover, diagonal and vertical members are subjected to tensile axial forces, whereas diagonals also withstand bending moment actions varying from 0.89 $kN.m$ to 2.50 $kN.m$. Since the considered loads were applied as point loads on the lower chord nodes, the vertical members are subjected to only tensile axial forces.

A structural optimization process of an arch always aims to minimize potential bending effects. However, since the arch under consideration was imposed to be symmetric, bending moments unavoidably arise, mainly because of the asymmetric load case here assumed.

The combined effect of axial forces and bending moments was evaluated by means of the interaction equation provided by EC3-2005, (expressed by the Eqs. (40), (41) and (42) presented in the section *§4.2.3*), through *Finite Element Analysis (FEA)* to calculate the maximum "utilization ratio" (i.e. the "demand/capacity ratio") of all truss members, for all applied load cases by the Eq. (47), assumed as strength constraint function (as shown in section *§5.2.2*).

The constraint functions allowed to keep the stress level, within an allowable range of values, according to mechanical properties of materials and technical standards for construction.

Figure 5. 18 shows a diagram of the optimal truss arch here analysed, indicating the maximum i^{th} –element "utilization ratio" ($\max_{LC} Util_i^{LC}$) among all load combinations (LC). The so-called "utilization ratio" diagram shows once again that more than half of elements is characterized by a critical ratio larger than 0.7. As in the CASE 1, it was found that the "total utilization ratio" ($Util_{tot}$) resulting from the weighted average of all values indicated in *Figure 5. 18* with respect to their self-weight, calculated by Eq. (51), corresponded to a satisfactory percentage of material exploitation (about 73.9 %), which ensures a high level of structural performance of the optimized solution under consideration.

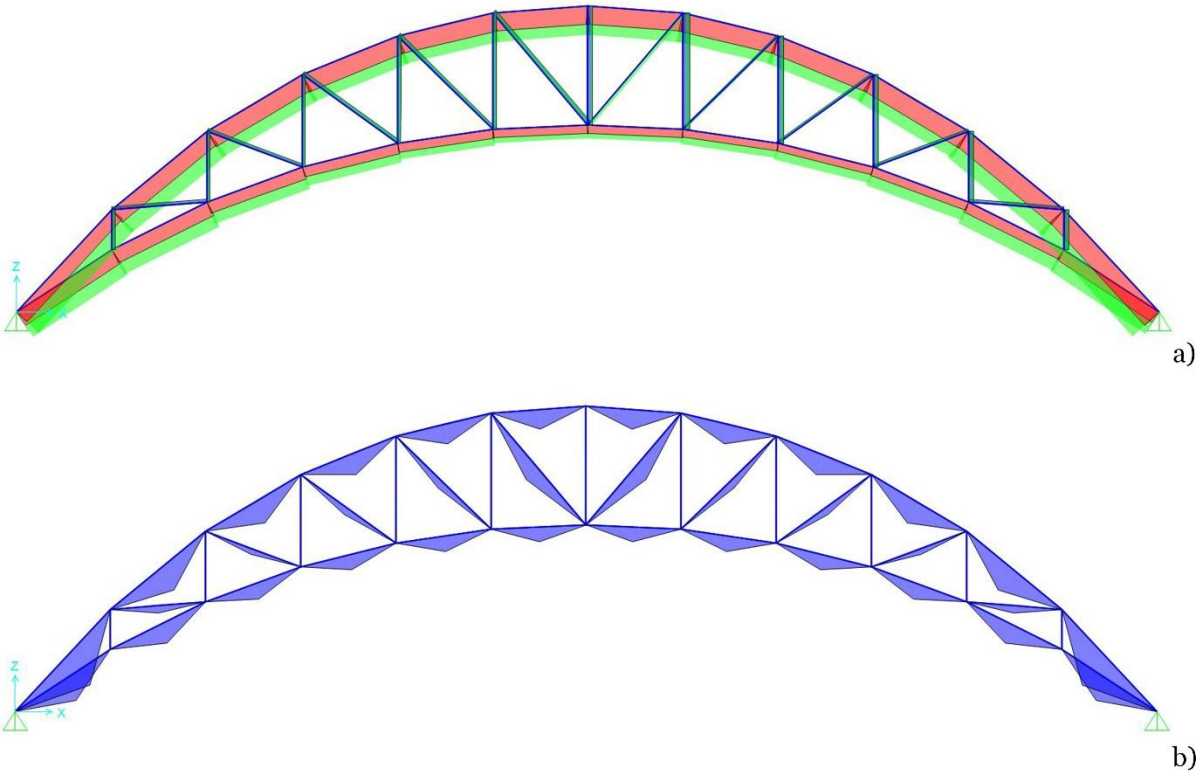

Figure 5. 17 *Finite Element Analysis (FEA) results for the CASE 2: (a) axial force diagram; (b) bending moment diagram*

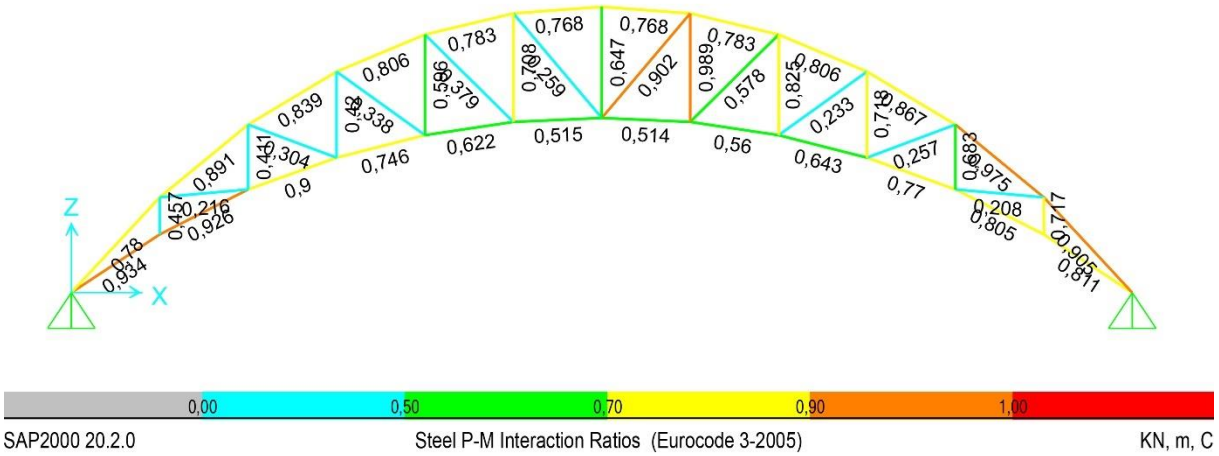

Figure 5. 18 *Finite Element Analysis (FEA) results for the CASE 2: Demand/Capacity ratio (also called "utilization ratio") diagram of the optimal solution for the envelope of all load cases*

The quality of the obtained results is proved by the trend of the convergence curves of the objective function and of most significant design variables.

For instance, *Figure 5. 19* shows the convergence curve of the "objective function" (i.e. the total volume of the structure) to be minimized. The objective function decreases rapidly in the first 100 generations, after which it continues to decrease extremely slowly. This is also confirmed by the "stagnation function" trend (illustrated in *Figure 5. 20(a)*), which for instance, considerably

increases from the 115^{th} to 279^{th} generation because there was not any improvement in the objective function during this interval. This situation could have been confused with a premature convergence. However, after that interval, the objective function starts again to slowly improve until the maximum number of iterations was reached (stop criterion here assumed).

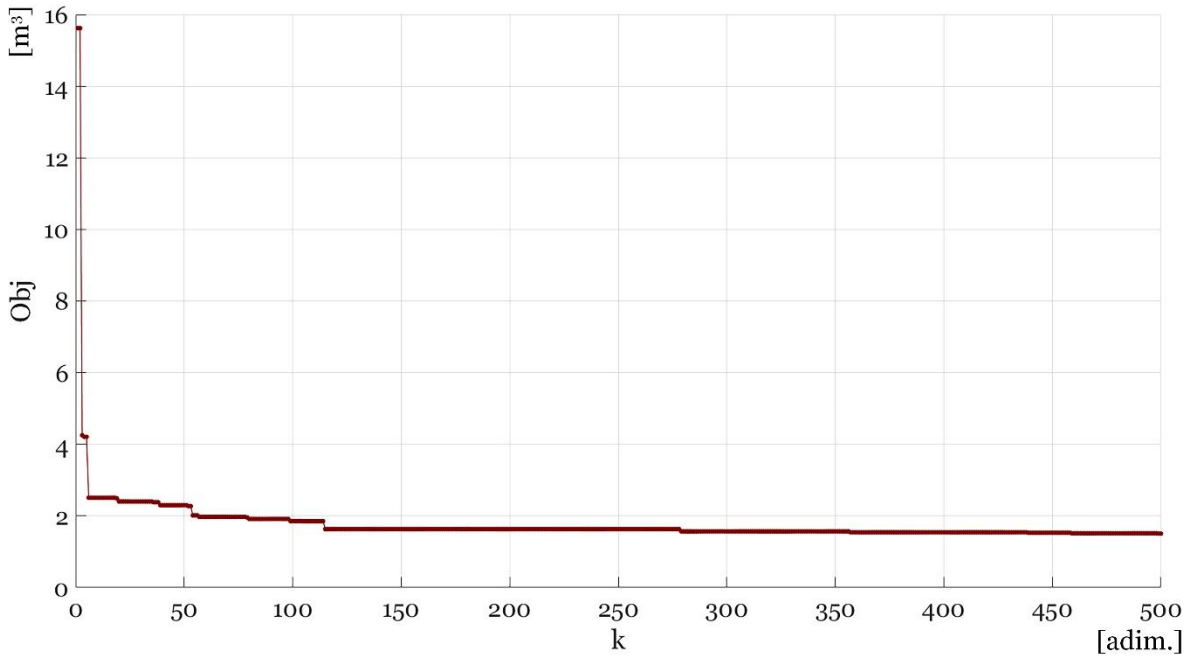

Figure 5. 19 *Convergence curve of the Objective (Obj) function (i.e. the volume of the arch) for all "generations" (for the CASE 2)*

On the other hand, *Figure 5. 20(b)* presents the history of the previously-defined "unfeasibility function" ρ^k (expressed by Eq. (52) introduced in section *§5.2.4.1*), showing that it became and remained 0 from the 61^{th} generation until the last one. This means that the optimization process produced and compared only feasible candidate solutions from the 61^{th} generation onwards.

Figure 5. 21 represents the convergence diagram of the topology design variable n_{int}, which the total number of the truss arch elements depends on. It is worth remembering that n_{int} was defined as a continuous value varying between 6 and 80 (to be rounded to the nearest even integer at a later time), as indicated in *Table 5. 6*. Its history curve shows a good convergence trend, since from the 115^{th} generation its value only tends to oscillate between continuous numbers close to 12 (see *Figure 5. 21*).

In *Figure 5. 22* the convergence curves of shape design variables are presented to prove the validity of results, despite the large number and the variety of design variables.

In the same way, a good convergence trend was also obtained for the size design variables determining the diameters of each element group (see *Figure 5. 23*), thus proving the effectiveness of the *MATLAB* macro-algorithm presented in the section *§4.2*. Once again, the

MATLAB macro-algorithm presented in section *§4.2*, demonstrated to be extremely effective in handling and solve structural optimization problems characterized by an extremely large number of design variables and constraint functions, as all cases analysed in this chapter.

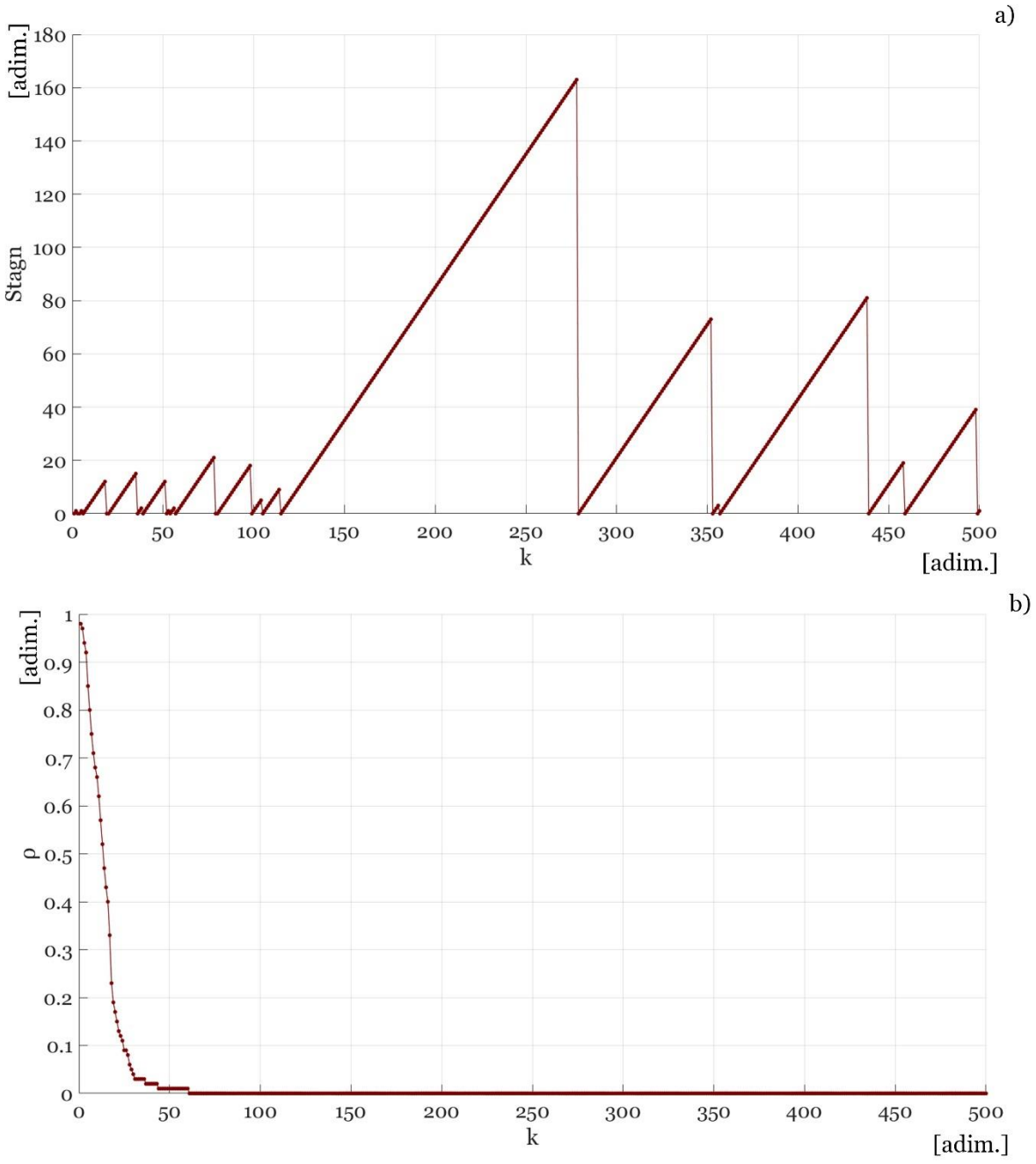

Figure 5. 20 *History of optimization functions for the CASE 2: (a) stagnation function; (b) "unfeasibility function" (ρ)*

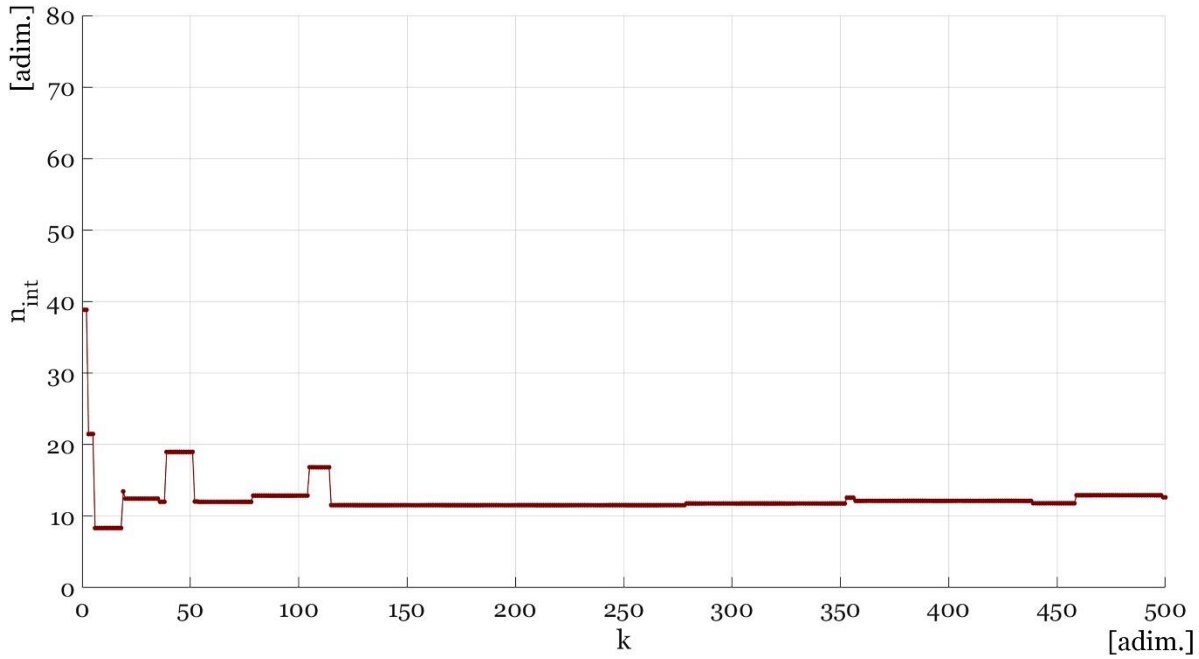

Figure 5. 21 Convergence curve of the topology design variable (n_{int}) for the CASE 2

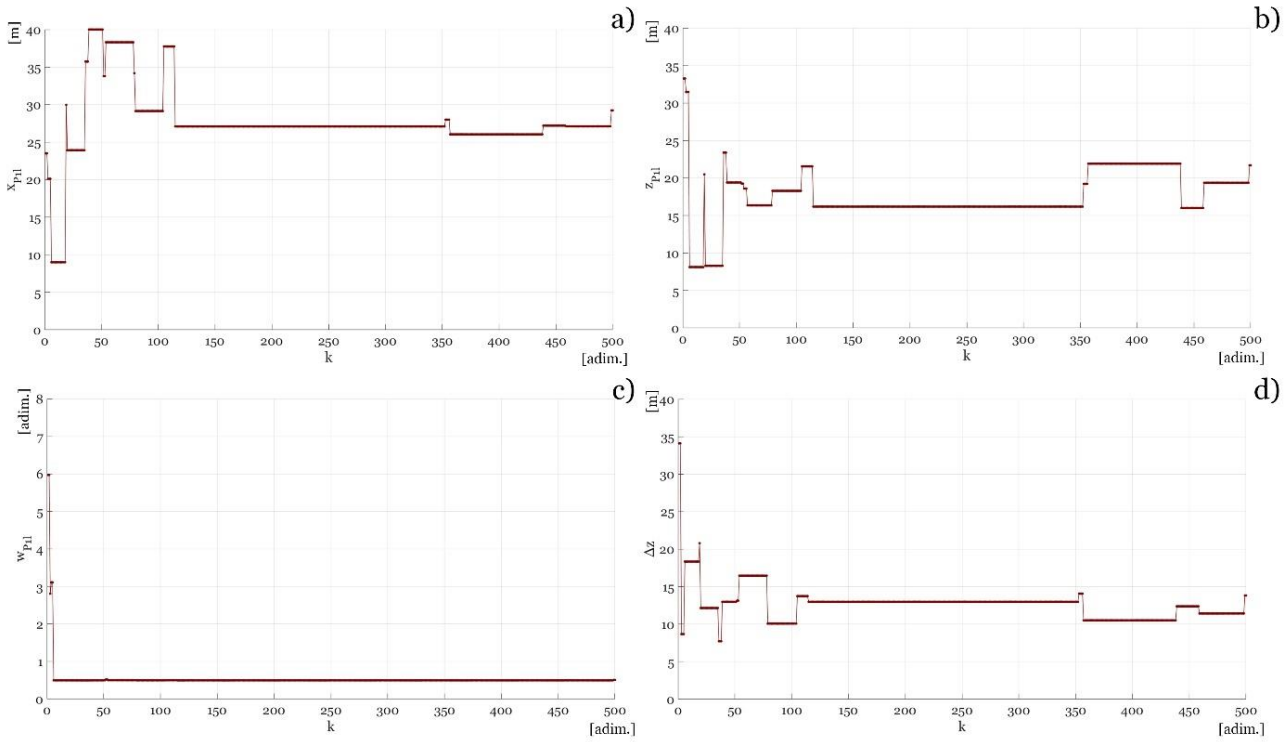

Figure 5. 22 Convergence curves of the shape design variables (variable parameters of third-degree rational Bézier curves) for the CASE 2: (a) x −coordinate of the second control point (x_{P1l}) of the bottom arched chord; (b) z −coordinate of the second control point (z_{P1l}) of the bottom arched chord; (c) weight factor of the second control point (w_{P1l}) of the bottom arched chord; (d) the difference between the z −coordinates (in absolute value) of the top and bottom chord internal control points (Δz)

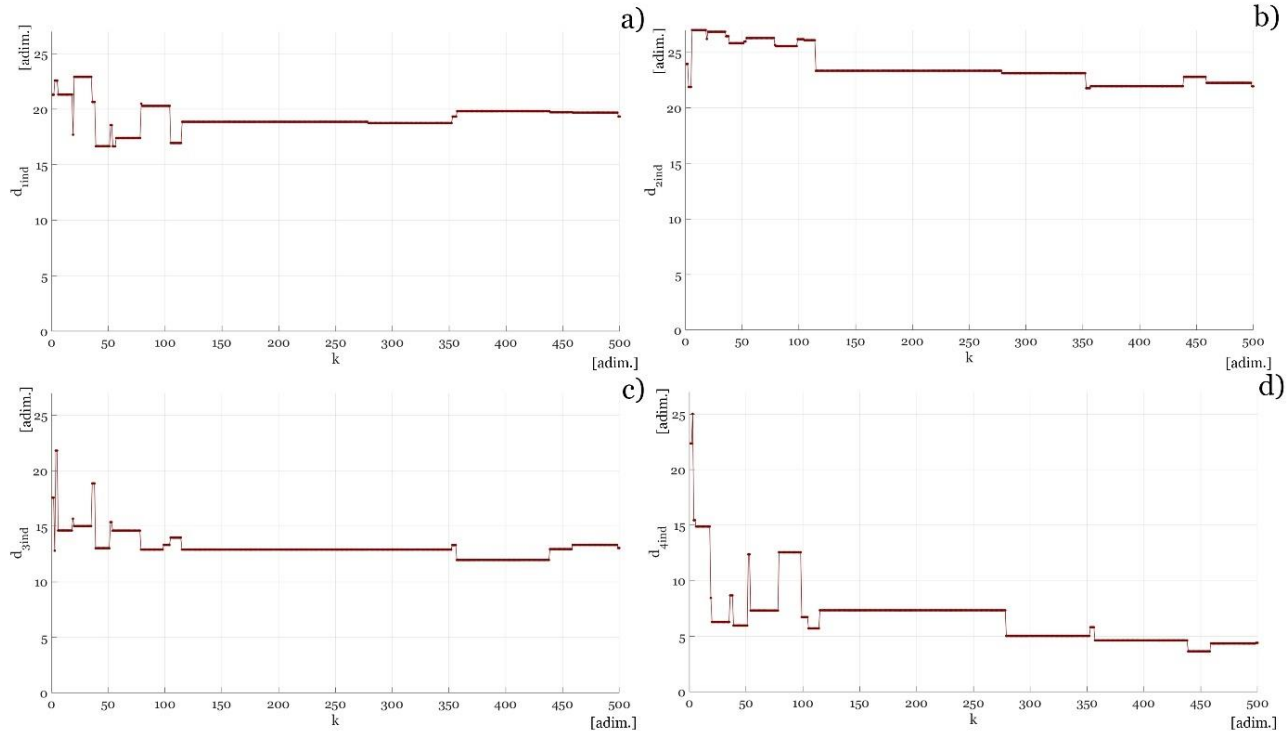

Figure 5. 23 Convergence curves of size design variables (i.e. indexes identifying the element group diameters in a list of commercial circular hollow cross-sections) for the CASE 2: (a) index identifying the bottom chord diameter; (b) index identifying the top chord diameter; (c) index identifying the diameter of diagonals; (d) index identifying the diameter of verticals

5.2.4.3 Case 3 optimal solution

The problem of the structural optimization of a two-hinged truss arch with a span of 120 meters is here treated and discussed. As in the previous cases, the truss arch here considered is subjected to the boundary conditions (constraints and load cases) illustrated in section *§5.2.3*, whereas all assumed design variables, with corresponding lower and upper bounds, are indicated in *Table 5. 7*. The optimal truss arch represented in *Figure 5. 24* has a minimum volume (best objective) equal to 3.572 m^3, corresponding to a self-weight per unit about 2.291 kN/m.

Furthermore, the arch is 31.51 m high, has a rise of 18.65 m and a "crown depth" about 12.86 m, and so characterized by a "rise-to-span ratio" equal to 1/6.43, a "height-to-span ratio" equal to 1/3.81, as well as a "crown depth-to-span" about 1/9.33. With respect to the previous cases 1 and 2 (respectively illustrated in sections *§5.2.4.1* and *§5.2.4.2*) the "crown depth" of the arch is still considerably high, since its corresponding "crown depth-to-span ratio" is always around 1/9. However, the optimal shapes found in the previous cases were comparable to the one typical of "segmental arches", whereas the shape of the arch under consideration is now comparable to a "parabolic arch". Two factors produced this parabolic shape, which are:

- The "weight factor" (w_{P1l}) of the internal control points of *Rational Bézier Curves* (which were introduced in *§5.2.1.2*) equal to 0.501 (as indicated in *Table 5. 14*)

- The value of x_{P1l} indicated in *Table 5. 14*, corresponding to the x −coordinate of the second control point defining the shape of the arch chords (see the definition of the shape design variables in the section *§5.2.1.2*), resulted to be very close to the length of half-span (equal to 60 meters), thus tending to coincide with the third control point (because of imposed symmetry conditions).

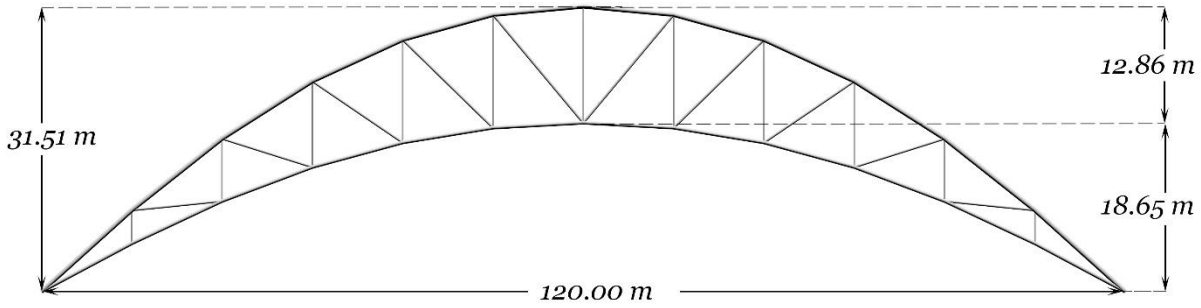

Figure 5. 24 *Front view of the optimized truss arch with main dimensions (CASE 3 optimal solution)*

Note that, the truss arch represented in *Figure 5. 24* is once again characterized by an arch span subdivision number (n_{int}) equal to 12 (as the optimal solutions of the CASES 1 and 2), as well as by a resulting total element number (n_{frames}) equal to 45 and joint number (n_{nodes}) equal to 24.

Table 5. 14 *Topology and shape optimization results for the CASE 3: optimal values of topology and shape design variables*

Topology optimization results			
Design Variable (DV)	**Type of DV**	**Best value**	**Unit**
n_{int}	*topology*	12	$[adim.]$
Shape optimization results			
Design Variable (DV)	**Type of DV**	**Best value**	**Unit**
x_{P1l}	*shape*	56.514	$[m]$
z_{P1l}	*shape*	31.061	$[m]$
w_{P1l}	*shape*	0.501	$[adim.]$
Δz	*shape*	21.428	$[m]$

Table 5. 15 shows the size optimization results, i.e. the optimal values assigned to diameters and thicknesses (taken from *Table 5. 5*) of circular hollow cross-sections of elements. As for the previous cases (1 and 2), only the diameter, the minimum and the maximum thicknesses for each element group are indicated in *Table 5. 15*.

Table 5. 15 *Size optimization results for the CASE 3: optimal diameters and thicknesses of circular hollow cross-sections*

Size optimization results					
Element groups	**Type of DV**	**Diameter d_i**	**Min. thickness t_i**	**Max. thickness t_i**	**Unit**
Bottom chord	*size*	0.4064	0.0063	0.0063	$[m]$
Top chord	*size*	0.508	0.0071	0.011	$[m]$
Diagonals	*size*	0.273	0.0056	0.0056	$[m]$
Verticals	*size*	0.159	0.004	0.0045	$[m]$

The tubular elements of the top chord have the largest diameter (as occurred in the previous CASES 1 and 2), because the upper chord is still subjected to a greater axial force (as shown in *Figure 5. 25(a)*). More specifically, it turned out that the upper chord was subjected to a compressive axial force varying from 1657 kN to 2963 kN, and also to bending moments (whose diagram is illustrated in *Figure 5. 25(b)*) varying from 10.79 $kN.m$ to 22.23 $kN.m$. The same time, the bottom chord resulted to be subjected to an almost constant compressive axial force, varying between 1137 kN to 1325 kN (reason for which the thickness of the bottom chord elements resulted to be constant), as well as to bending moments varying from 7.63 $kN.m$ to 8.63 $kN.m$. Since the external loads were applied as point loads on the lower chord nodes, diagonal and vertical members showed to be subjected to tensile axial forces, whereas diagonals also withstood significant bending actions varying from 4.44 $kN.m$ to 7.05 $kN.m$.

Figure 5. 26 shows a diagram of the optimal truss arch here analysed, where the maximum i^{th} –element "utilization ratio" ($\max_{LC} Util_i^{LC}$), evaluated for the envelope of all load cases (LC), is pointed out on each member, to prove that all constraint functions (generalized by Eq. (47)) are satisfied.

The "utilization ratio" diagram also shows that more than two thirds of the elements are characterized by a critical ratio larger than 0.7.

Furthermore, it was found that the "total utilization ratio" ($Util_{tot}$) resulting from the weighted average of all values indicated in *Figure 5. 26* with respect to their self-weight (calculated by Eq. (51)), corresponded to a very high percentage of material exploitation about 79.2 %, thus guaranteeing a higher level of structural performance of the optimized solution under consideration, compared to the previous solutions of CASES 1 and 2.

The quality of the obtained results is demonstrated by the trend of convergence diagrams of the objective function and design variables. In particular, *Figure 5. 27* shows the convergence curve of the "objective function" (i.e. the total volume of the structure) to be minimized.

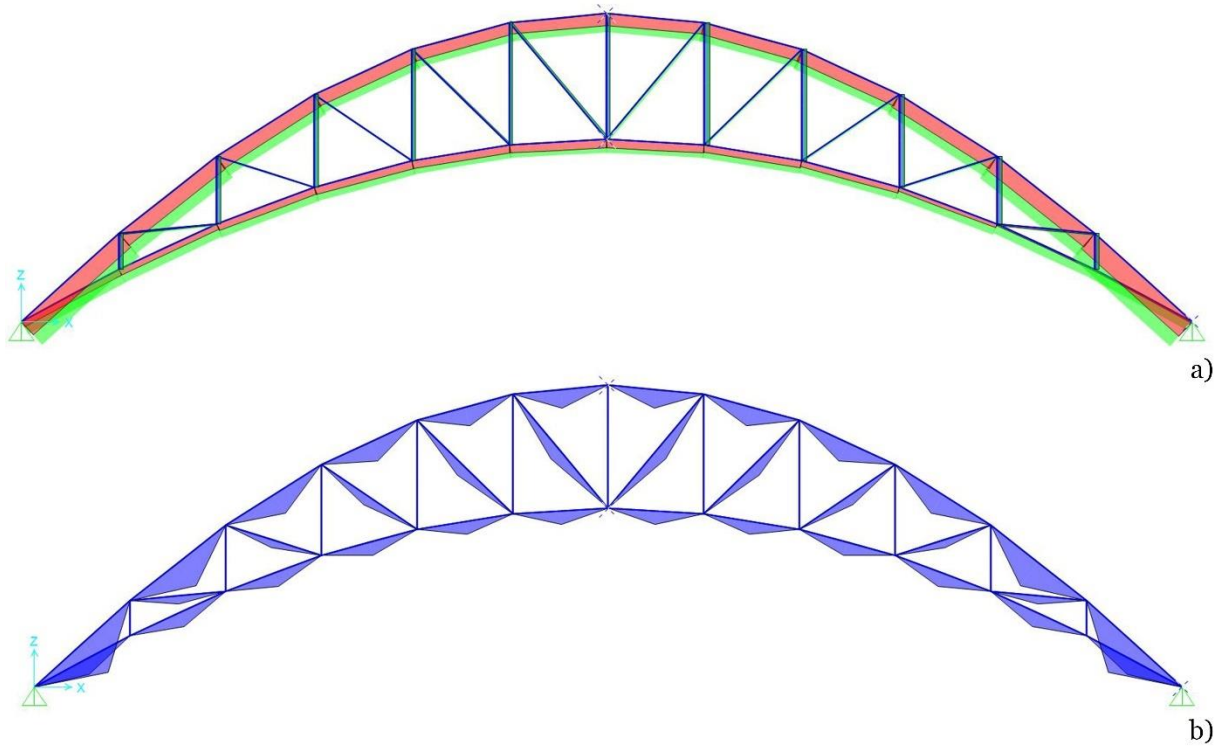

Figure 5. 25 *Finite Element Analysis (FEA) results for the CASE 3: (a) axial force diagram; (b) bending moment diagram*

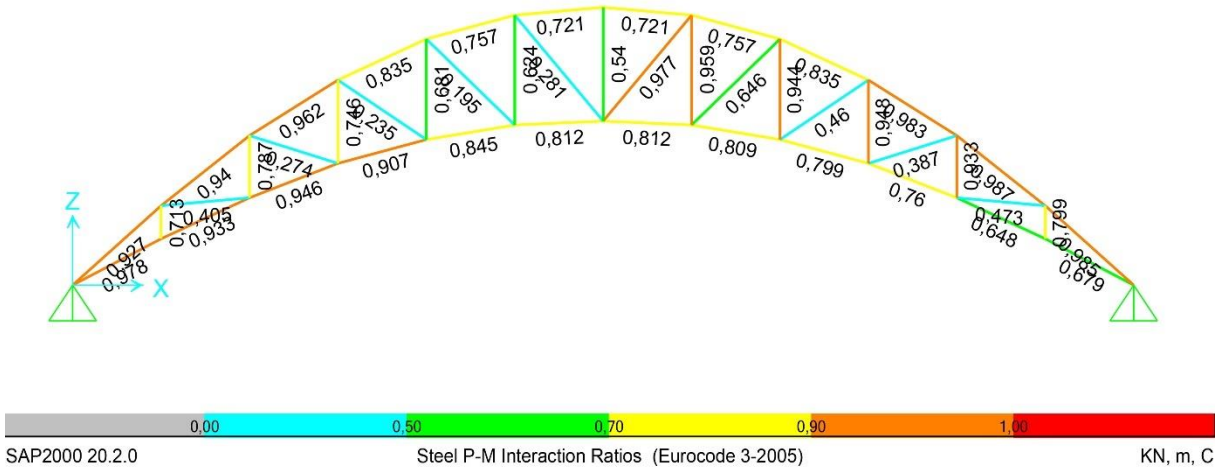

Figure 5. 26 *Finite Element Analysis (FEA) results for the CASE 3: Demand/Capacity ratio (also called "utilization ratio") diagram of the optimal solution for the envelope of all load cases*

The objective function decreases rapidly in the first 300 generations, after which it continues to decrease extremely slowly. Accordingly, the "stagnation function" (illustrated in *Figure 5. 28(a)*), increases more rapidly in two intervals (from the 359^{th} to the 474^{th}, and also from the 499^{th} to 631^{th} generation) due to a lack of improvement in the objective function. However, after that phase, the objective function started again to slowly decrease until the maximum number of iterations was reached.

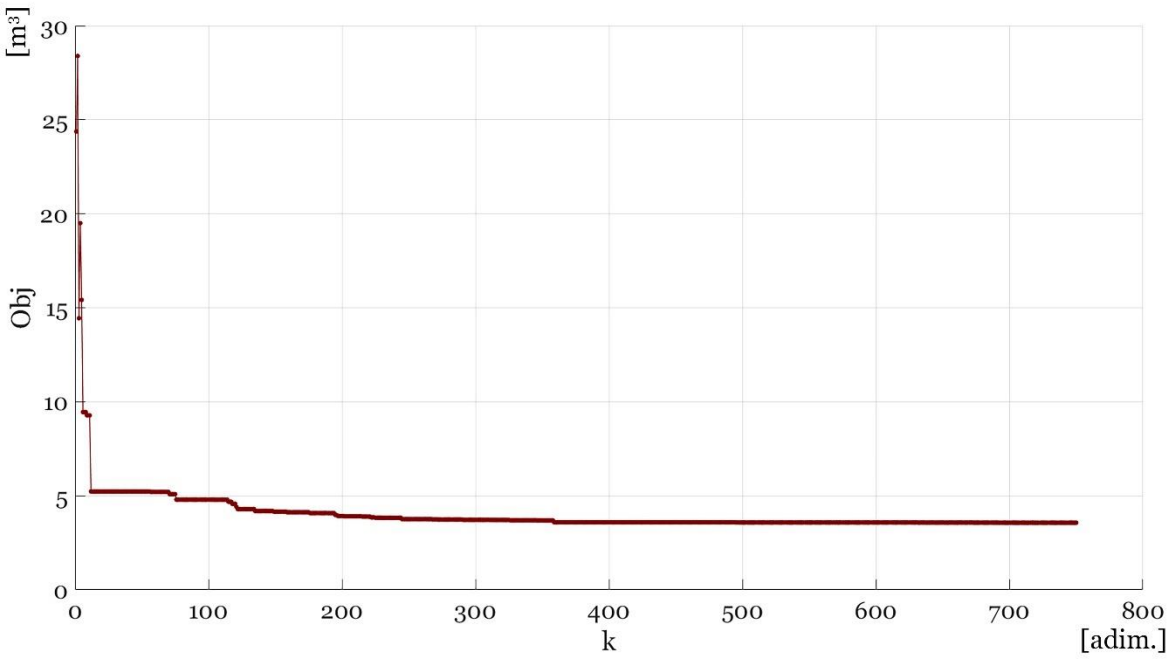

Figure 5. 27 *Convergence curve of the Objective (Obj) function (i.e. the volume of the arch) for all "generations" (for the CASE 3)*

On the other hand, *Figure 5. 28(b)* presents the history of the "unfeasibility function" ρ^k (evaluated by Eq. (52)). That diagram shows that the optimization process generated and compared only feasible candidate solutions from the 113^{th} generation onwards.

For the sake of brevity, it is not possible to show the convergence curves of all design variables of the problem.

However, particular attention is paid to the topology design variable (n_{int}), whose value indirectly defined the total number of the truss arch members. In this regard, *Figure 5. 29* represents the convergence diagram of that parameter.

As indicated in *Table 5. 7*, n_{int} was assumed to vary between 8 and 120. The convergence curve validates the goodness of obtained solution, since from the 115^{th} generation onwards, its value only tends to oscillate between values very close to 12 (see *Figure 5. 29*).

In *Figure 5. 30* the convergence curves of shape design variables (i.e. the variable parameters defining the shape of the lower and upper arch chords through parametric *Cubic Rational Bézier curves*) are also presented to prove the validity of results. In particular, those diagrams show that the optimization process leaded to the optimal values of all shape design variables approximately from the 350^{th} generation.

In the same way, *Figure 5. 31* pointed out that the optimal values of size design variables under consideration were also approximately obtained from the 350^{th} generation.

This is in accordance with the trend of the objective function that showed to decrease extremely slowly from the 300^{th}.

The histories of size design variables corresponding to the indexes defining the thickness elements are not showed for the sake of brevity, but they are also characterized by a satisfactory convergence level, further validating the goodness of results despite the large dimensions of the optimization problem.

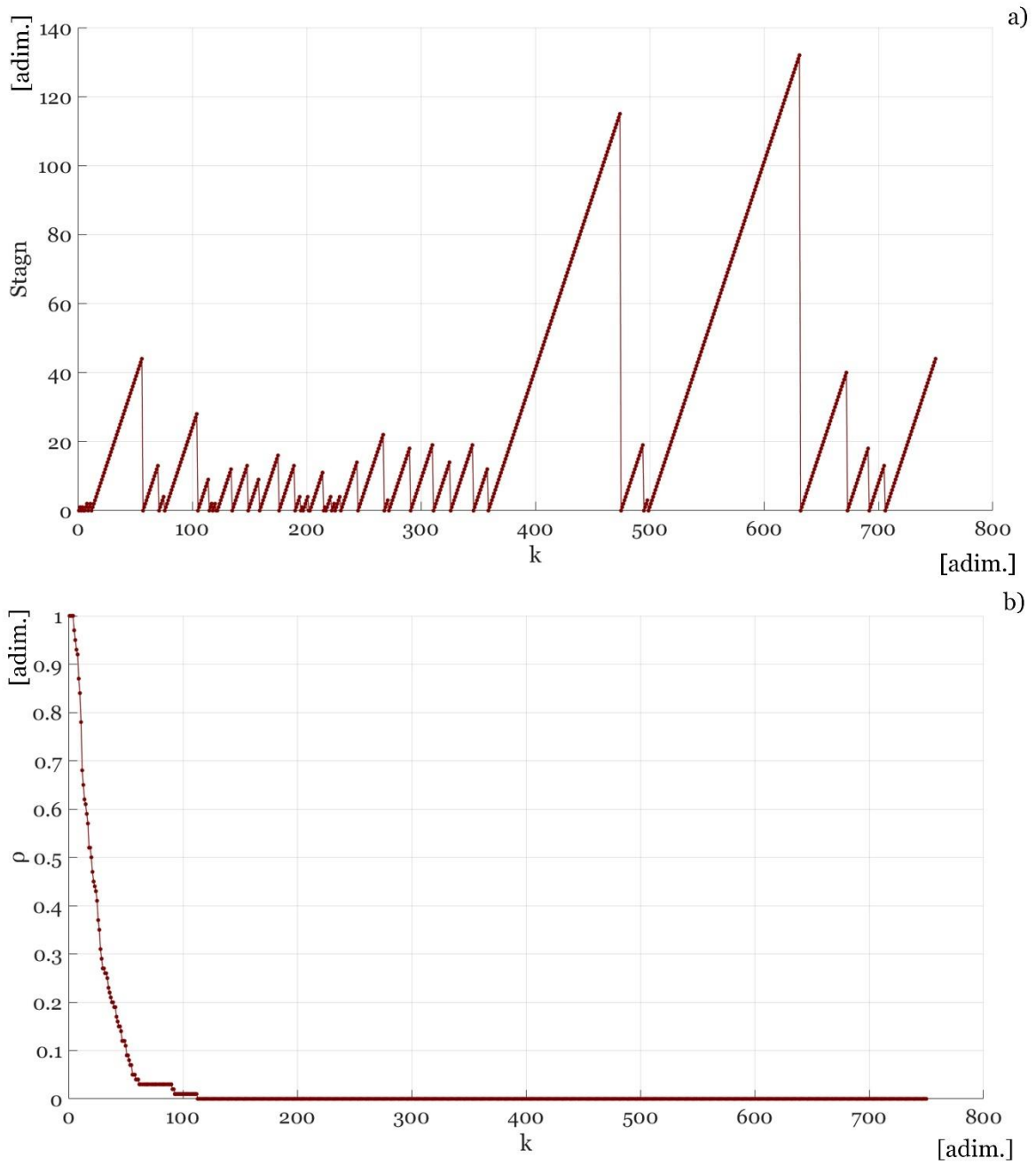

Figure 5. 28 History of optimization functions (for the CASE 3): (a) stagnation function; (b) "unfeasibility function" (ρ)

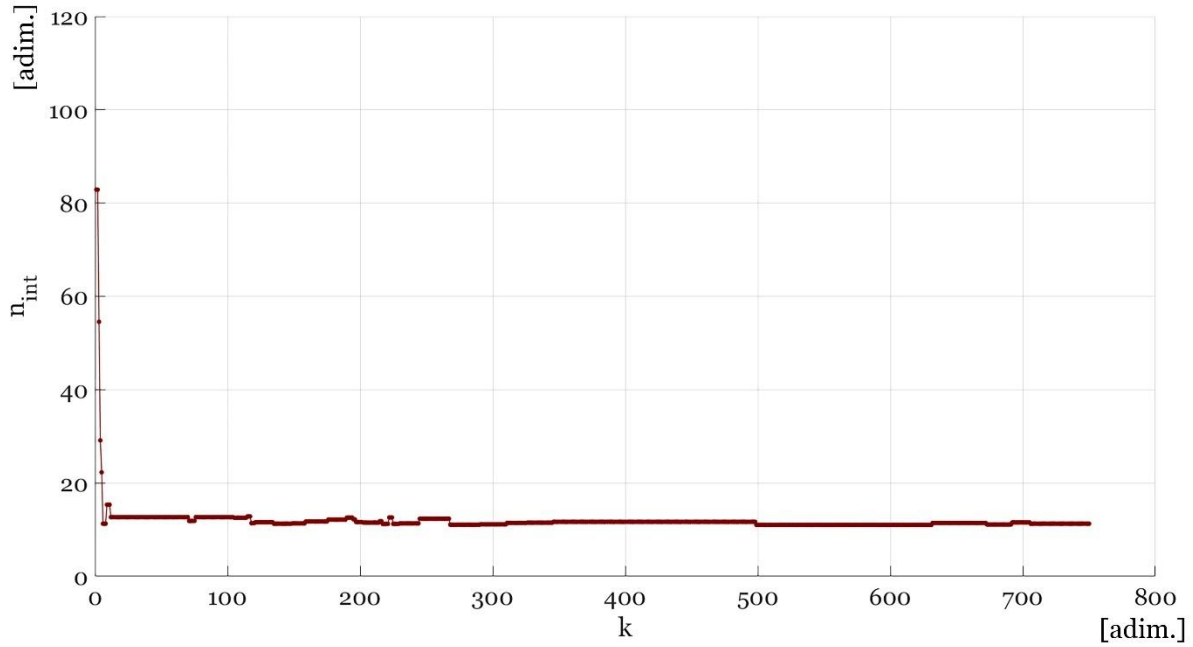

Figure 5. 29 Convergence curve of the topology design variable (n_{int}) (for the CASE 3)

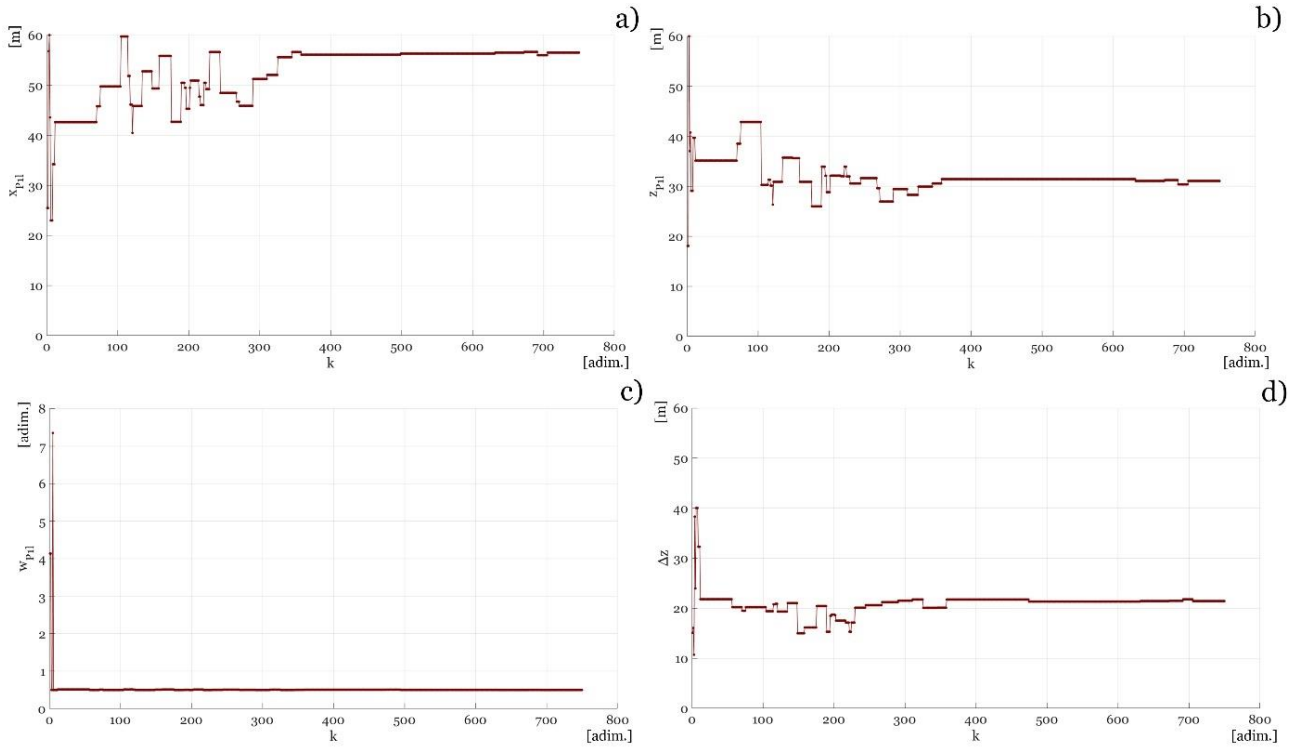

Figure 5. 30 Convergence curves of the shape design variables (variable parameters of third-degree rational Bézier curves) for the CASE 3: (a) x –coordinate of the second control point (x_{P1l}) of the bottom arched chord; (b) z –coordinate of the second control point (z_{P1l}) of the bottom arched chord; (c) weight factor of the second control point (w_{P1l}) of the bottom arched chord; (d) the difference between the z –coordinates (in absolute value) of the top and bottom chord internal control points (Δz)

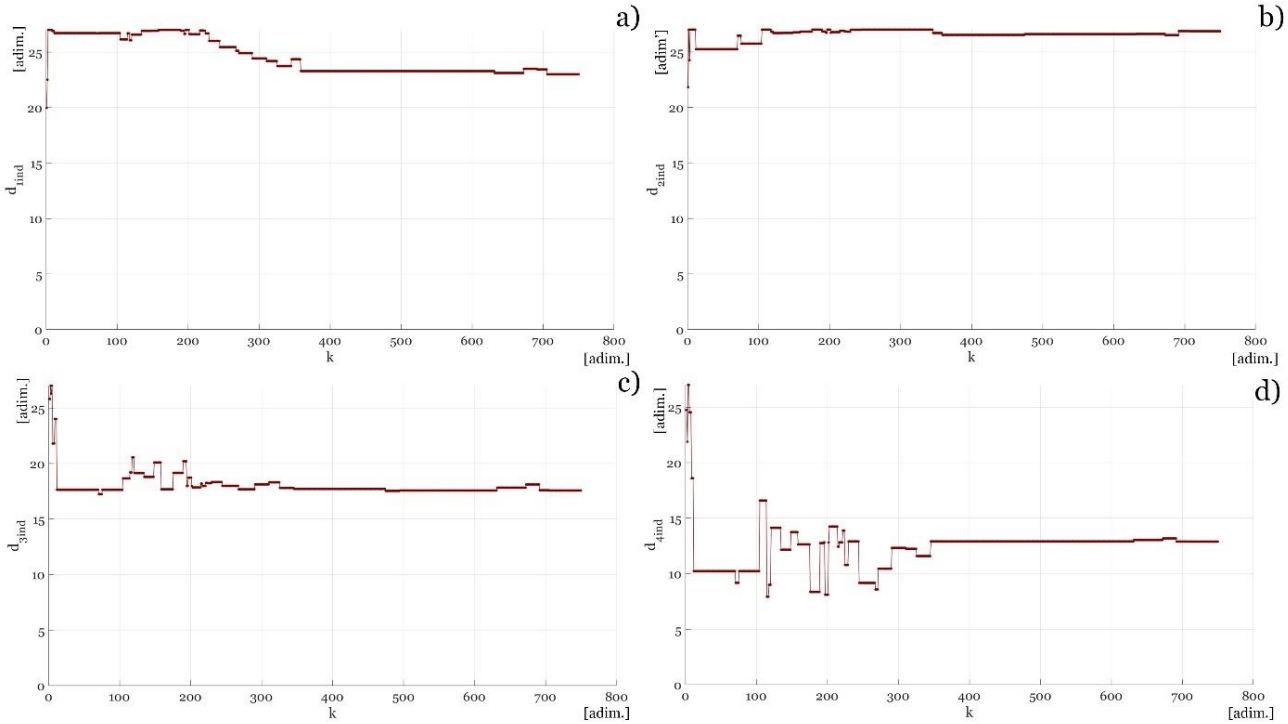

Figure 5. 31 Convergence curves of size design variables (i.e. indexes identifying the element group diameters in a list of commercial circular hollow cross-sections) for the CASE 3: (a) index identifying the bottom chord diameter; (b) index identifying the top chord diameter; (c) index identifying the diameter of diagonals; (d) index identifying the diameter of verticals

5.2.4.4 Case 4 optimal solution

The present section shows the results obtained by applying the *MATLAB* macro-algorithm described in *§4.2* to simultaneously perform topology, shape and size optimization of a two-hinged truss arch with a span of 160 meters, subjected to three different load conditions (shown in *Figure 5. 7*). The optimization problem was parametrically defined as described in sections *§5.2.1* and *§5.2.2*. In particular, as in all previous cases (1, 2 and 3), the arched shape of the top and bottom chords was parametrized by taking advantage of parametric *Cubic Rational Bézier Curves*.

All design variables with corresponding lower and upper bounds are indicated in *Table 5. 8*. Note that the present optimization problem was assumed to depend on 330 different design variables, thus requiring a very large number of iterations (100000) to ensure a good convergence in finding a reliable optimal solution.

Figure 5. 32 shows the optimal solution thus obtained, characterized by a minimum volume (best objective) equal to 6.005 m^3, corresponding to a self-weight per unit about 2.889 kN/m. The arch under consideration is 46.53 m high and characterized by a "rise-to-span ratio" about 1/4.79, a "height-to-span ratio" equal to 1/3.44 and a "crown depth-to-span ratio" about 1/12.15. Note that the "rise-to-span" and the "crown depth-to-span" ratios are significantly different from the ones characterizing the previous solutions.

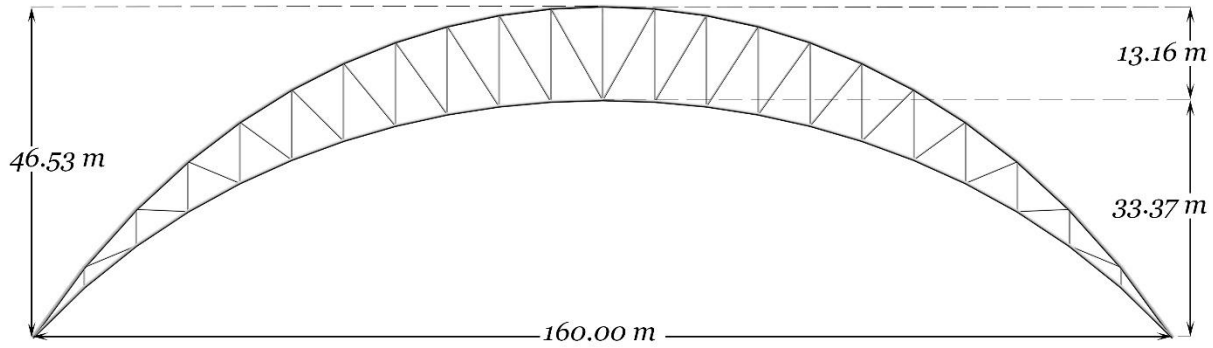

Figure 5. 32 Front view of the optimized truss arch with main dimensions (CASE 4 optimal solution)

Table 5. 16 contains the obtained optimal values of the topology and shape design variables. Among these, the topology design variable n_{int} plays a crucial role, since it defines the total number of elements of the structure. In fact, since it was found an optimal value of n_{int} equal to 22, the optimal truss arch in *Figure 5. 32* is composed by 85 tubular members and 44 joints.

As in the previous cases, the size optimization results, summarized in *Table 5. 17,* shows that the tubular elements of the top chord have the largest diameter because most of its elements is subjected to a larger axial force (as shown in *Figure 5. 33(a)*). In particular, the upper chord resulted to be subjected to a compressive axial force varying from 913 kN to 2405 kN (see *Figure 5. 33(a)*), and to bending moments (whose diagram is illustrated in *Figure 5. 33(b)*) varying from 5.69 $kN.m$ to 9.61 $kN.m$.

Table 5. 16 Topology and shape optimization results for the CASE 4: optimal values of topology and shape design variables

Topology optimization results			
Design Variable (DV)	**Type of DV**	**Best value**	**Unit**
n_{int}	*topology*	22	$[adim.]$
Shape optimization results			
Design Variable (DV)	**Type of DV**	**Best value**	**Unit**
x_{P1l}	*shape*	51.393	$[m]$
z_{P1l}	*shape*	55.610	$[m]$
w_{P1l}	*shape*	0.500	$[adim.]$
Δz	*shape*	21.941	$[m]$

Table 5. 17 *Size optimization results for the CASE 4: optimal diameters and thicknesses of circular hollow cross-sections*

Size optimization results					
Element groups	**Type of DV**	**Diameter d_i**	**Min. thickness t_i**	**Max. thickness t_i**	**Unit**
Bottom chord	*size*	0.4572	0.0071	0.0142	$[m]$
Top chord	*size*	0.508	0.0071	0.0071	$[m]$
Diagonals	*size*	0.2445	0.0054	0.01	$[m]$
Verticals	*size*	0.2191	0.005	0.005	$[m]$

On the other hand, the bottom chord is subjected to a compressive axial force, varying between 672 kN to 3882 kN, as well as to bending moments varying from 5.11 $kN.m$ to 14.06 $kN.m$.

Note that in the present case, the end elements of the bottom chord resulted to be subjected to the absolute maximum values of axial force and bending moments. However, most of the elements of the top chord elements resulted to be more axially and flexibly stressed with respect to the bottom chord members. Diagonal and vertical members are stretched (i.e. under tension) whereas diagonals also withstand significant bending actions, varying from 2.23 $kN.m$ to 6.14 $kN.m$.

Finite Element Analysis (FEA) were also carried out to calculate the maximum "utilization ratio" (i.e. the "demand/capacity ratio") of all truss members, for all applied load cases, which has been assumed as strength constraint function (expressed by Eq. (47)).

In order to prove the feasibility of the obtained solution under consideration, a diagram of the optimal truss arch pointing out the maximum i^{th} –element "utilization ratio" ($\max_{LC} Util_i^{LC}$), among all load combinations (LC) is presented in *Figure 5. 34*. Indeed, the "utilization ratio" diagram shows that all elements are characterized by a critical ratio lower than 0.99 (thus satisfying the constraint functions generalized by Eq. (47)) and also larger than 0.7 for most of them. Furthermore, the "total utilization ratio" ($Util_{tot}$) resulting from the weighted average of all values indicated in *Figure 5. 34* with respect to element self-weights, (calculated by Eq. (51)), showed to be equal to 71.5 %, thus ensuring a high level of material exploitation.

The reliability of the obtained results is primarily demonstrated by the convergence curve of the objective function to be minimized (the total volume of the structure) represented in *Figure 5. 35*. Indeed, the objective function tends to decrease rapidly until the 400^{th} generation, after which it continues to progress more slowly towards the obtained minimum.

Accordingly, the "stagnation function" trend (represented in *Figure 5. 36(a)*) also confirms that from the 850^{th} generation the objective function stops to decrease for two significant intervals.

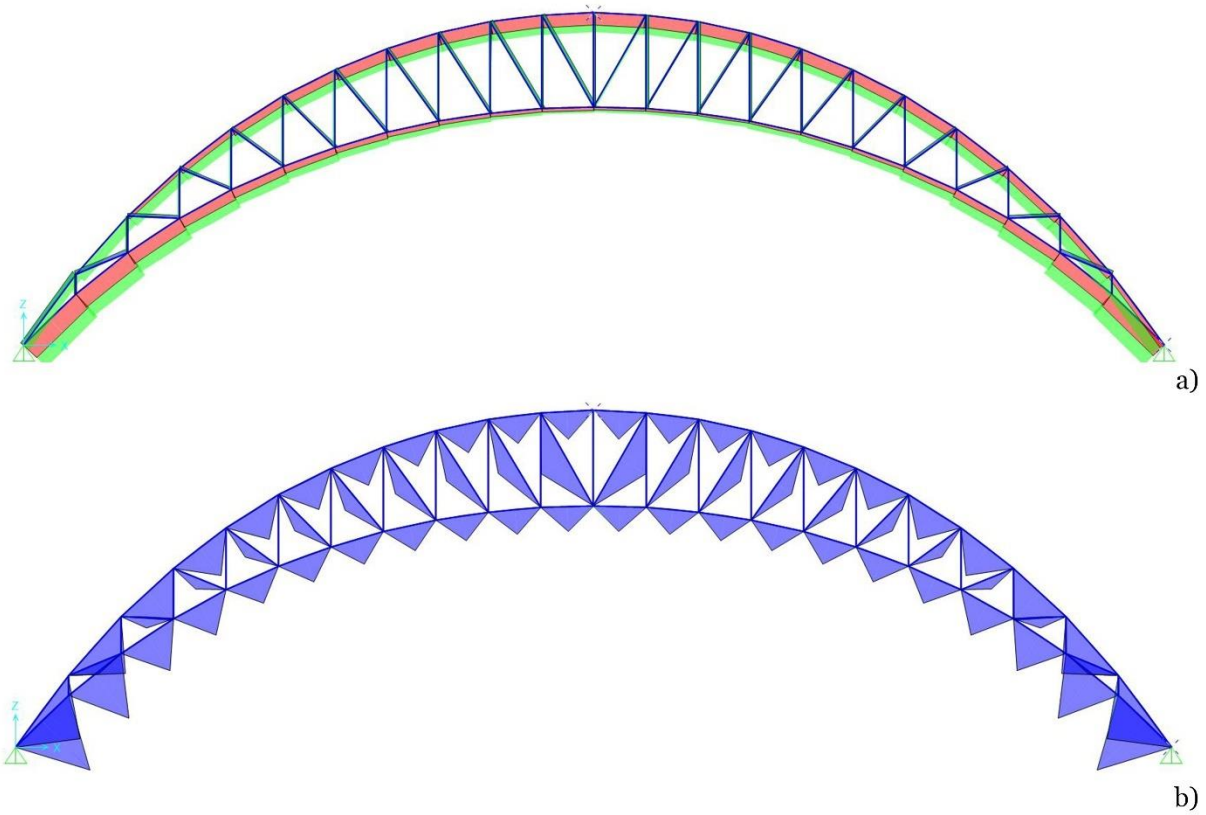

Figure 5. 33 Finite Element Analysis (FEA) results for the CASE 4: (a) axial force diagram; (b) bending moment diagram

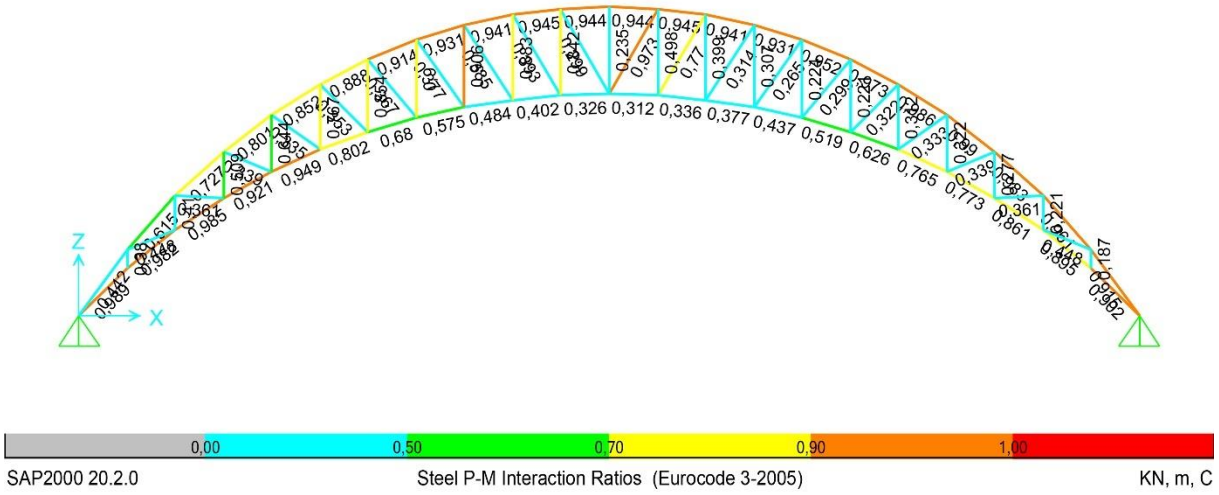

Figure 5. 34 Finite Element Analysis (FEA) results for the CASE 4: Demand/Capacity ratio (also called "utilization ratio") diagram of the optimal solution for the envelope of all load cases

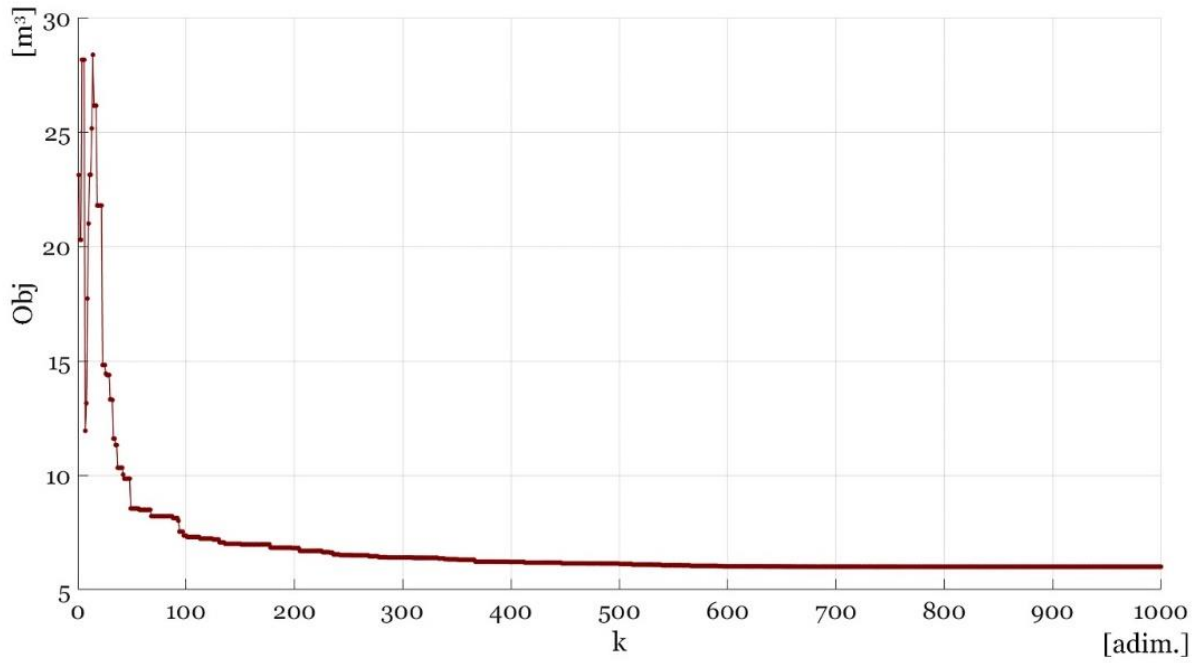

Figure 5. 35 *Convergence curve of the Objective (Obj) function (i.e. the volume of the arch) for all "generations" (for the CASE 4)*

On the other hand, the history of the previously-defined "unfeasibility function" ρ^k (expressed by Eq. (52)) is shown in *Figure 5. 36(b)*. That diagram shows that the optimization process produced and evaluated only feasible candidate solutions from the 76^{th} to the 1000^{th} generation.

For the sake of brevity, only the convergence curves of design variables that more affect the results are presented and analysed.

For instance, particular attention is paid to the topology design variable (n_{int}), whose value indirectly defines the total number of the truss arch members.

In this regard, *Figure 5. 37* represents its convergence diagram. As indicated in *Table 5. 8*, n_{int} was defined as a continuous value between 10 and 160 (to be rounded to the nearest even integer at a later time). Its convergence curve shows that its value only tends to oscillate between values extremely close to 22 from the 200^{th} generation onwards (see *Figure 5. 37*).

In *Figure 5. 38* the convergence curves of shape design variables (i.e. the variable parameters defining the shape of the lower and upper arch chords through parametric *Cubic Rational Bézier curves*) are presented to prove the validity of results, despite the large number and the variety of design variables. In particular, those diagrams show that the optimization process leaded to values very close to the optimal ones of all shape design variables approximately from the 250^{th} generation.

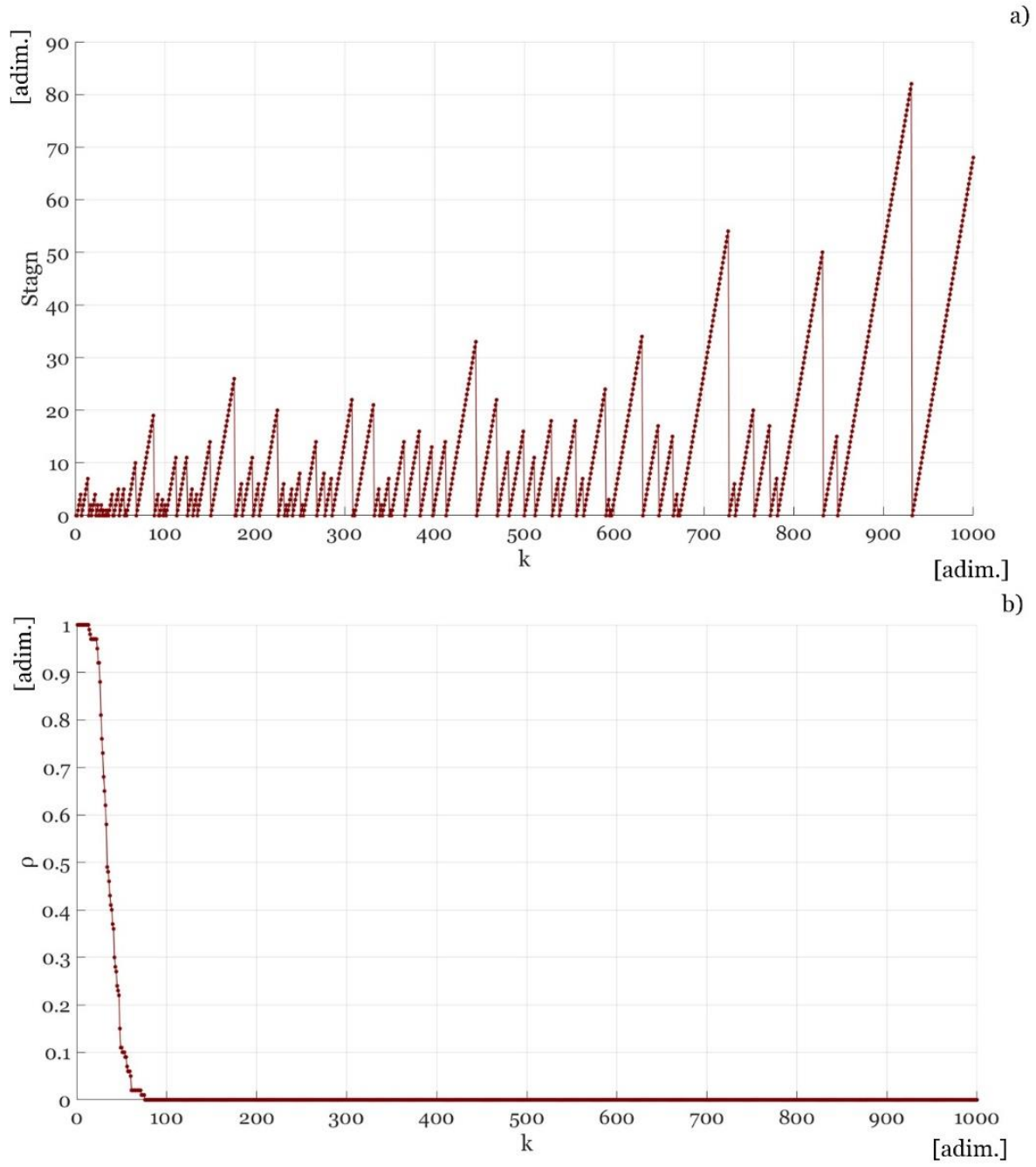

Figure 5. 36 *History of optimization functions for the CASE 4: (a) stagnation function; (b) "unfeasibility function" (ρ)*

In the same way, a good convergence trend was also obtained for the size design variables determining the element group diameters (whose curves are shown in *Figure 5. 39*).

It is worth highlighting that the goodness of the presented results, obtained for all different formulations of the optimization problem, prove the effectiveness and robustness of the optimization macro-algorithm proposed in section *§4.2* in solving problems with a very large number of design variables of different nature.

Nevertheless, the present dissertation mainly aims to deduce precious suggestions for the optimum design of steel truss arches from the analysis and comparison of these results (see section *§5.2.4.5*).

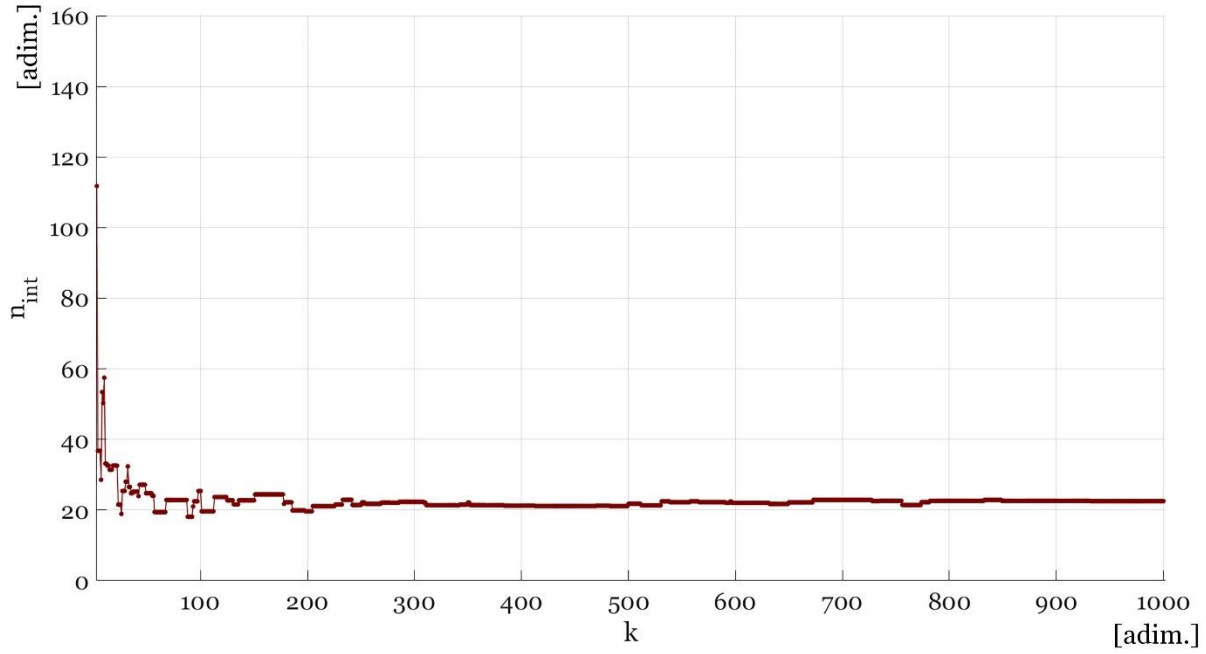

Figure 5. 37 Convergence curve of the topology design variable (n_{int}) for the CASE 4

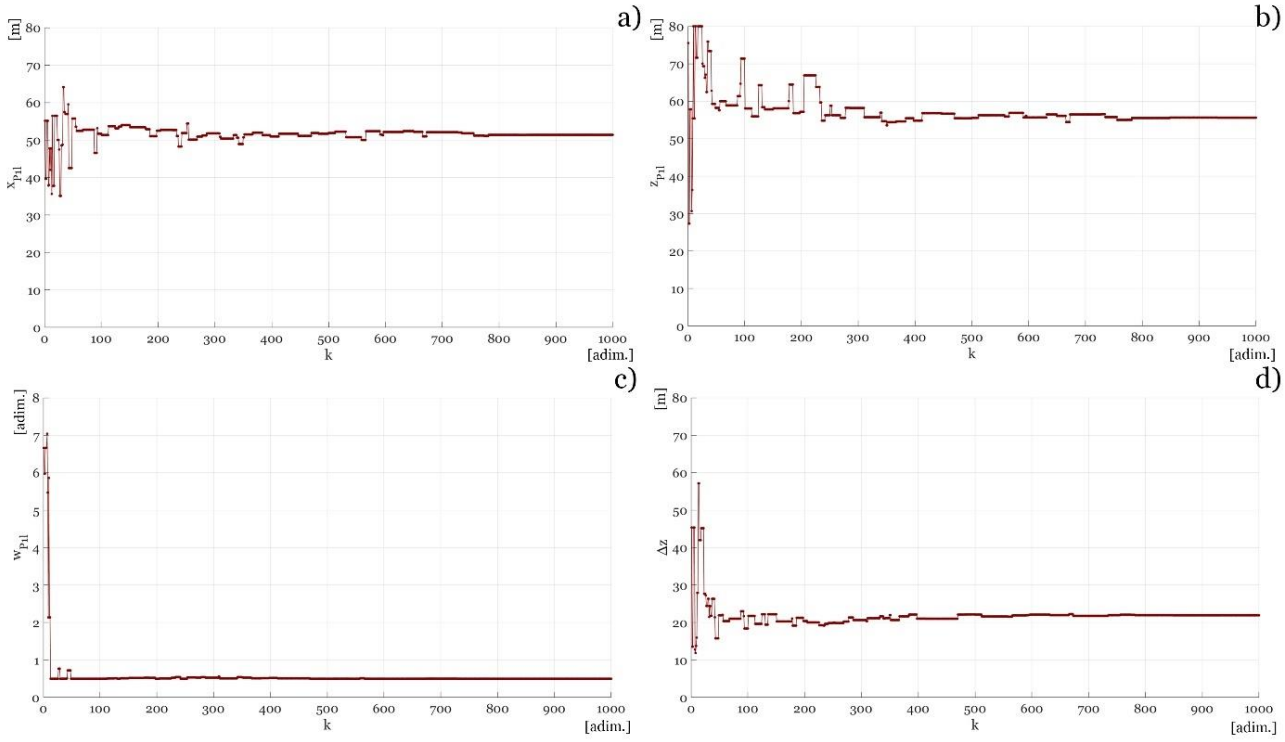

Figure 5. 38 Convergence curves of the shape design variables (variable parameters of third-degree rational Bézier curves) for the CASE 4: (a) x −coordinate of the second control point (x_{P1l}) of the bottom arched chord; (b) z −coordinate of the second control point (z_{P1l}) of the bottom arched chord; (c) weight factor of the second control point (w_{P1l}) of the bottom arched chord; (d) the difference between the z −coordinates (in absolute value) of the top and bottom chord internal control points (Δz)

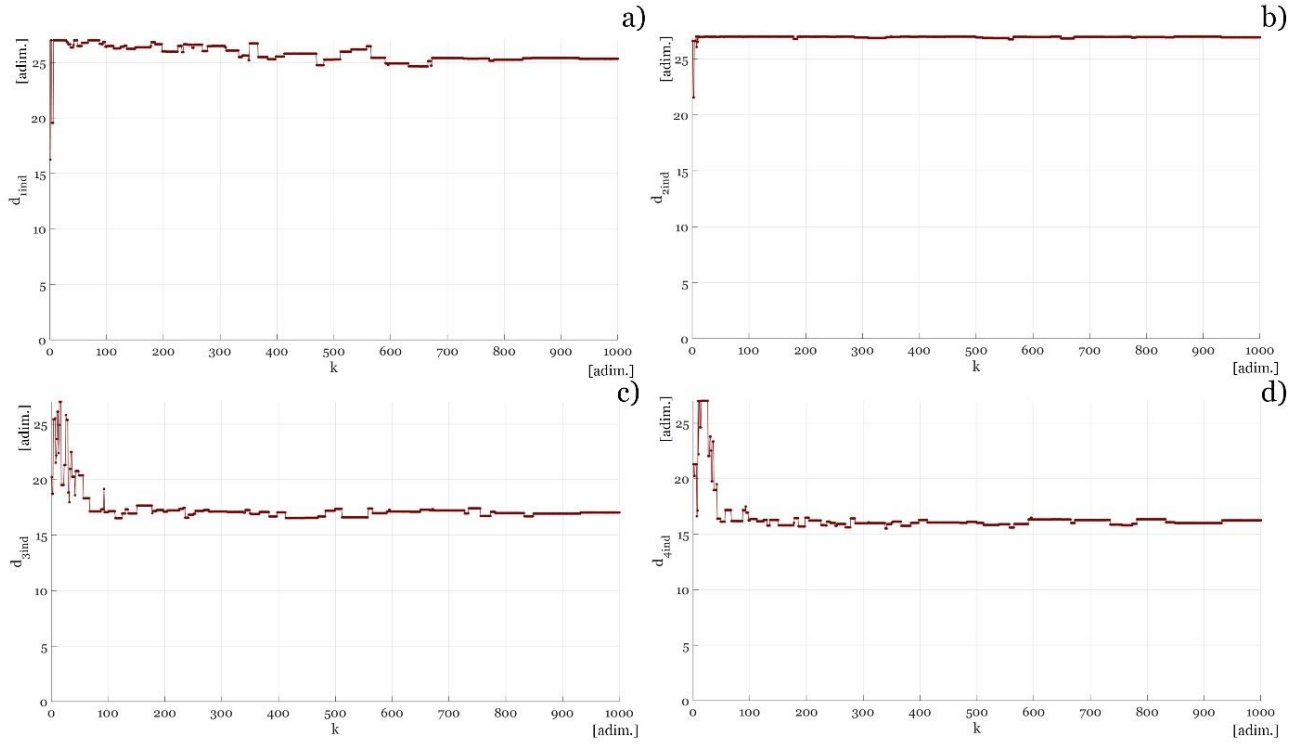

Figure 5. 39 Convergence curves of size design variables (i.e. indexes identifying the element group diameters in a list of commercial circular hollow cross-sections) for the CASE 4: (a) index identifying the bottom chord diameter; (b) index identifying the top chord diameter; (c) index identifying the diameter of diagonals; (d) index identifying the diameter of verticals

5.2.4.5 Comparison of optimal solutions

In the present section, the optimal solutions obtained for all different formulations (i.e. the CASES 1, 2, 3 and 4) of the optimization problem considered in section *§5.2*, are investigated and compared by an aesthetical and structural points of view.

First of all, in *Figure 5. 40* the optimal layouts of the obtained solutions are superimposed, in order to clearly show how the optimal shape and topology of the considered truss arch change as the arch span increases. The main features characterizing the optimal solutions are summarized in *Table 5. 18*.

Primarily, the self-weight of the optimal solutions tends to grow very rapidly (from 0.652 to 2.889 kN/m) as the span uniformly increases. Consequently, this implies that the ratio between variable (equal to 15.00 kN/m) and permanent loads (the latter obtained by adding the self-weight of the considered arch to the external permanent load assumed to be equal to 24.00 kN/m) rapidly decreases from 1/1.64 to 1/1.79, as pointed out in *Figure 5. 41* (where the objective function values, the self-weights and the variable-to-permanent loads ratios of all CASES are compared).

In particular, the trend of variable-to-permanent loads ratios (in *Figure 5. 41(c))* must be strongly considered in analysing and comparing all results, since its reduction implies a lower effect of the asymmetric combination of variable loads on the optimization process.

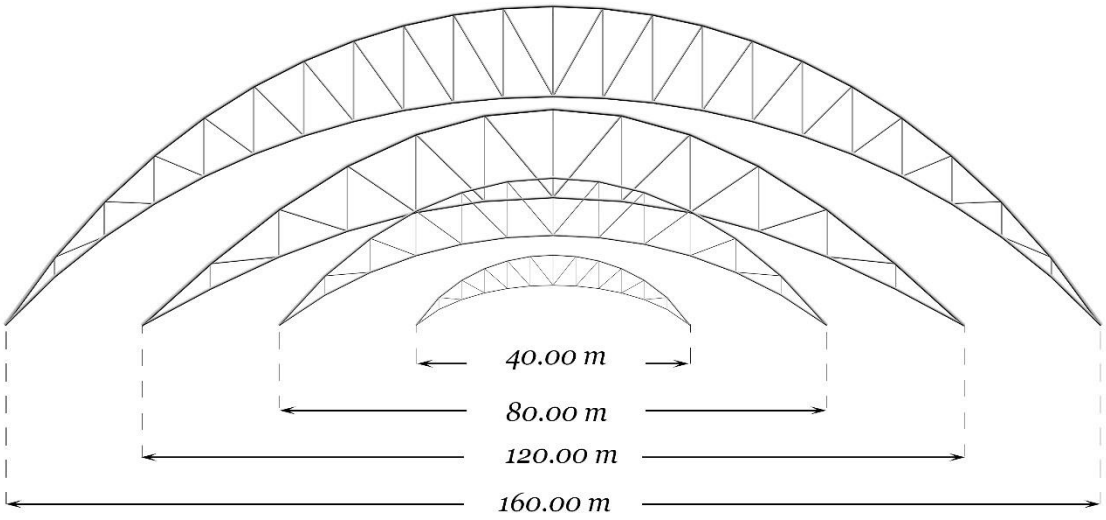

Figure 5. 40 Shape comparison of the optimal solutions for the CASES 1, 2, 3 and 4

As previously highlighted, the topology design variable n_{int} (defined in section *§5.2.1.1*) plays a fundamental role from a constructive point of view since it indirectly defines the total element number and joints. In this regard, *Figure 5. 42* shows that it was found a value of arch span subdivisions (n_{int}) equal to 12 for CASES 1, 2 and 3, whereas it resulted to be equal to 22 for the truss arch of CASE 4.

Consequently, truss arches with spans of 40, 80 and 120 meters showed to have 45 elements, whereas the optimal solution with a span of 160 meters resulted to be characterized by 85 tubular elements (as indicated in *Table 5. 18*).

It is worth noting that the optimal solution with a span of 160 meters also significantly differs from the others on its shape. In this regard, in *Figure 5. 43* the "height-to-span ratios" (a), the "rise-to-span ratios" (b) and the "crown depth-to span ratios" which characterize all optimal truss arches are compared. It can be easily noted that the "height-to-span ratio" varies from 1/3.8 to 1/3.9 in optimal solutions with spans from 40 to 120 meters, while for the arch with a span of 160 meters it was found a higher value, equal to 1/3.44 (as pointed out in *Figure 5. 43(a)).*

Table 5. 18 Comparison of main parameters characterizing the optimal solutions

CASE	Span length $[m]$	Min. volume $[m^3]$	Self-weight $[kN/m]$	Elem. number $[adim.]$	Height/span $[adim.]$	Rise/span $[adim.]$	Crown-Depth/span $[adim.]$
1	40	*0.339*	*0.652*	*45*	*1/3.91*	1/6.86	1/9.09
2	80	*1.508*	*1.451*	*45*	1/3.72	1/6.10	1/9.57
3	120	*3.572*	*2.291*	*45*	1/3.81	1/6.43	1/9.33
4	160	*6.005*	*2.889*	*85*	1/3.44	*1/4.79*	1/12.15

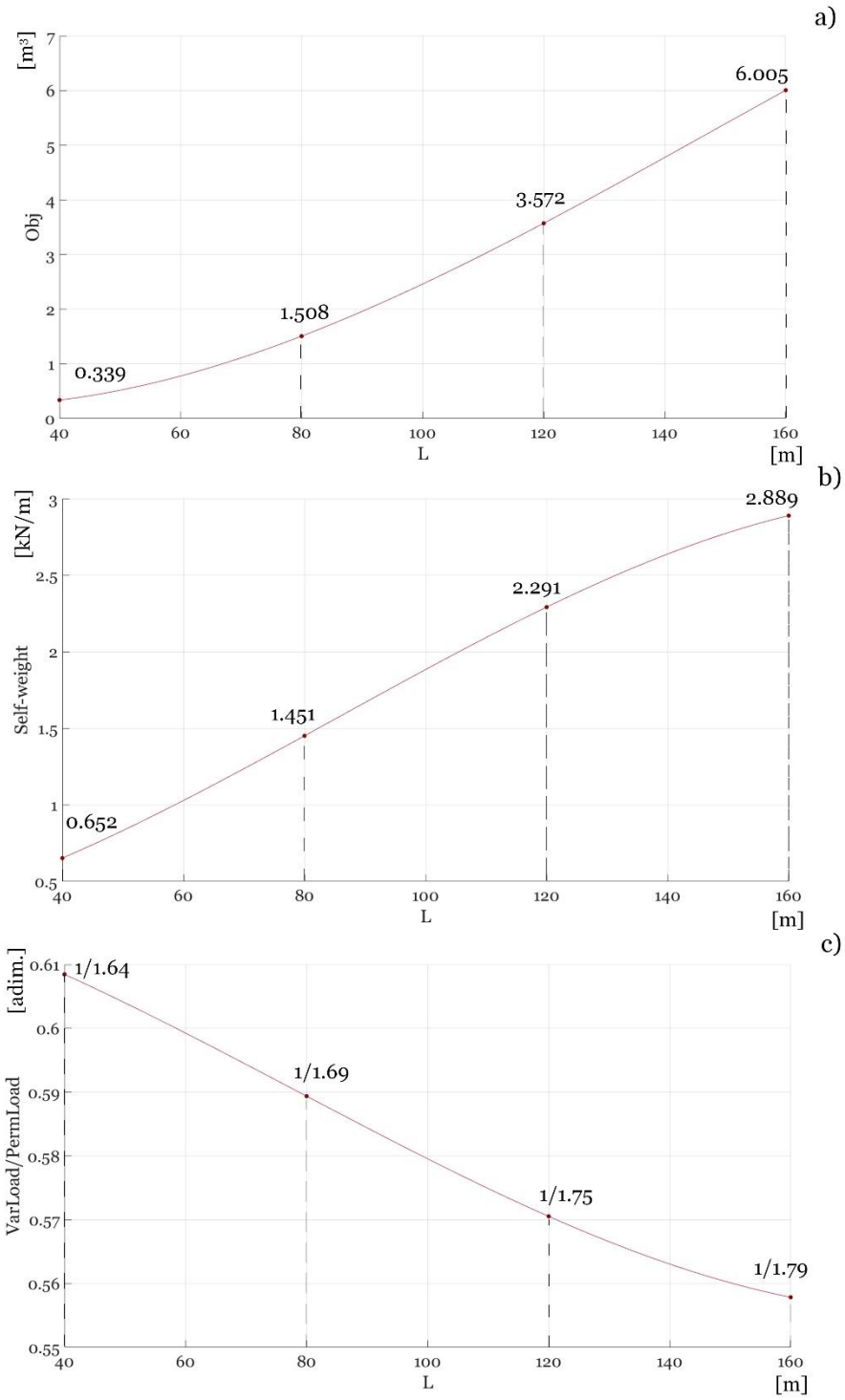

Figure 5. 41 *Comparison of the results of the optimal solutions: (a) best objective values; (b) arch self-weights per unit; (c) variable-to-permanent load ratios*

Table 5. 19 Comparison of optimal values of shape design variables

CASE	Span length $[m]$	x_{P1l} $[m]$	z_{P1l} $[m]$	w_{P1l} $[adim.]$	Δz $[m]$	x_{P1l} /span $[adim.]$	z_{P1l} /span $[adim.]$
1	40	*12.078*	*9.310*	*0.559*	*7.030*	*1/3.31*	1/4.30
2	80	*29.224*	*21.696*	*0.509*	*13.821*	1/2.74	1/3.69
3	120	*56.514*	*31.061*	*0.501*	*21.428*	1/2.12	1/3.86
4	160	*51.393*	*55.610*	*0.500*	*21.941*	1/3.11	*1/2.88*

On the other hand, *Figure 5. 43(b)* compares the "rise-to-span ratios", which proved to be always close to 1/6 for CASES 1, 2 and 3 (varying from 1/6.86 and 1/6.10), whereas the optimal solution of the CASE 4 showed to be characterized by a "rise-to-span ratio" equal to 1/4.79. It is therefore possible to state that as the arch span increases, its optimal shape becomes less lowered and less flattened at its crown. This should be related to the progressive reduction of the effect of the asymmetric load combination of variable loads as the arch self-weight grows with its span. In particular, the "x_{P1l}-to-span ratio" tends to rapidly increase from 1/3.31 to 1/2.12 from 40 to 120 meters of span while a value of 1/3.11 was obtained for the CASE 4. It is important to remark that small values of this dimensionless parameter make the arch shape flattened at its crown. Similarly, the "z_{P1l}-to-span ratio" tends to slowly increase (oscillating between 1/4.30 and 1/3.69) till the arch span reaches 120 meters, whereas it rapidly reaches a value about 1/2.88 in the CASE 4, thus determining its higher "height-to-span" and "rise-to-span ratios" with respect to the other solutions.

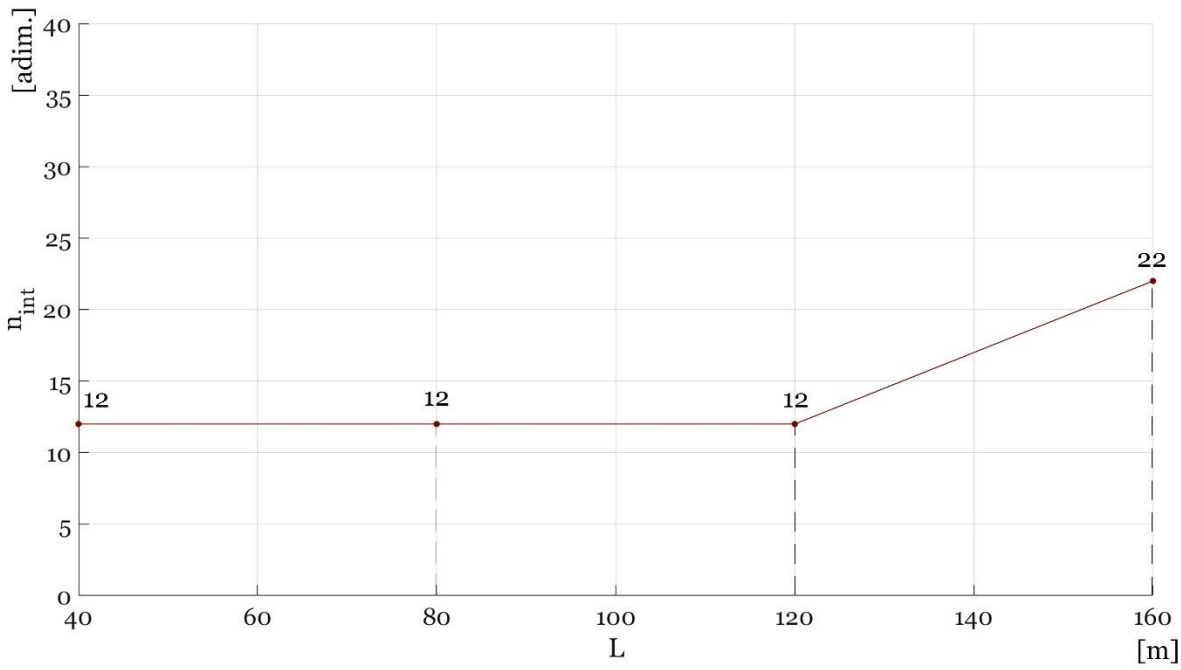

Figure 5. 42 Optimal values of the topology design variable (n_{int}), which defines the number of the truss arch element

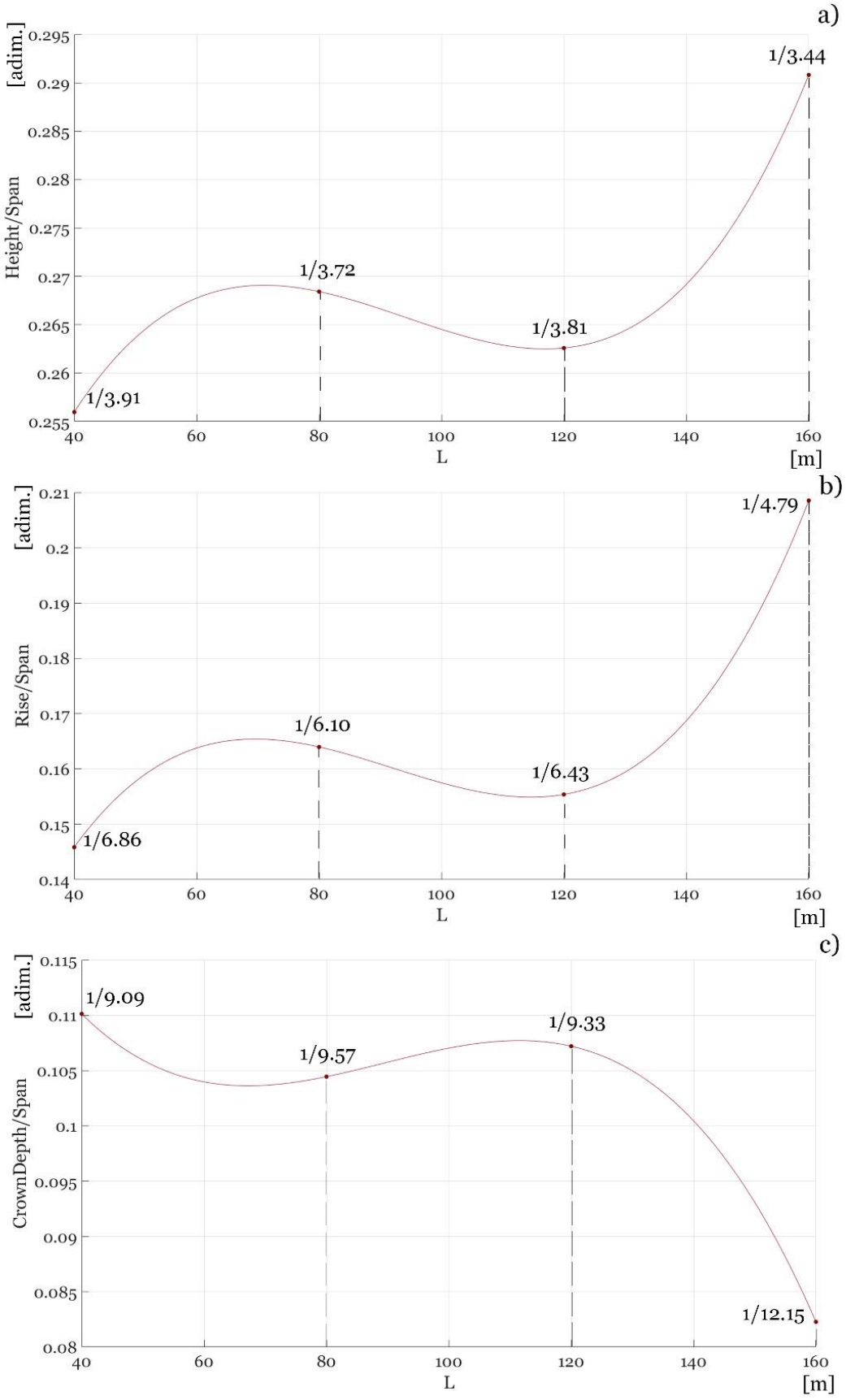

Figure 5. 43 *Comparison of the results of the optimal solutions: (a) height-to-span ratios; (b) rise-to-span ratios; (c) crown depth-to-span ratios*

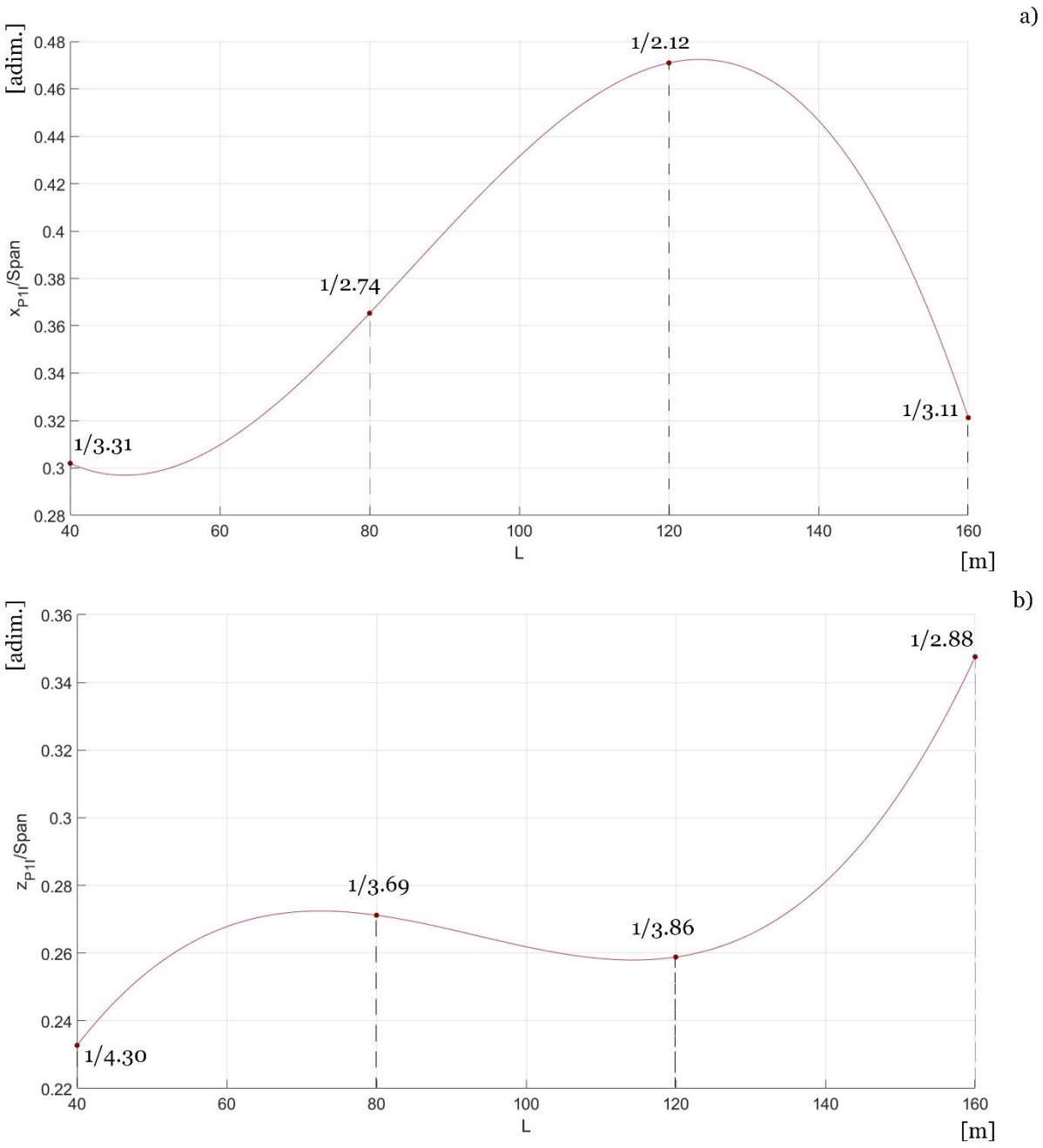

Figure 5. 44 *Comparison of the results of the optimal solutions: (a) x_{P1l}-to-span ratios; (b) z_{P1l}-to-span ratios*

As anticipated in section *§5.2.4.1*, a new parameter was introduced by Eq. (26) (i.e. the "total utilization ratio"($Util_{tot}$)) to provide an approximate overall percentage of material exploitation. In this regard, *Figure 5. 45* shows that a "total utilization ratio" greater than 70% was obtained for all cases, reaching a peak of 79.2 % for the truss arch with a span of 120 meters. This meaning that the structural optimization process here discussed leaded to satisfactory results in terms of structural performances.

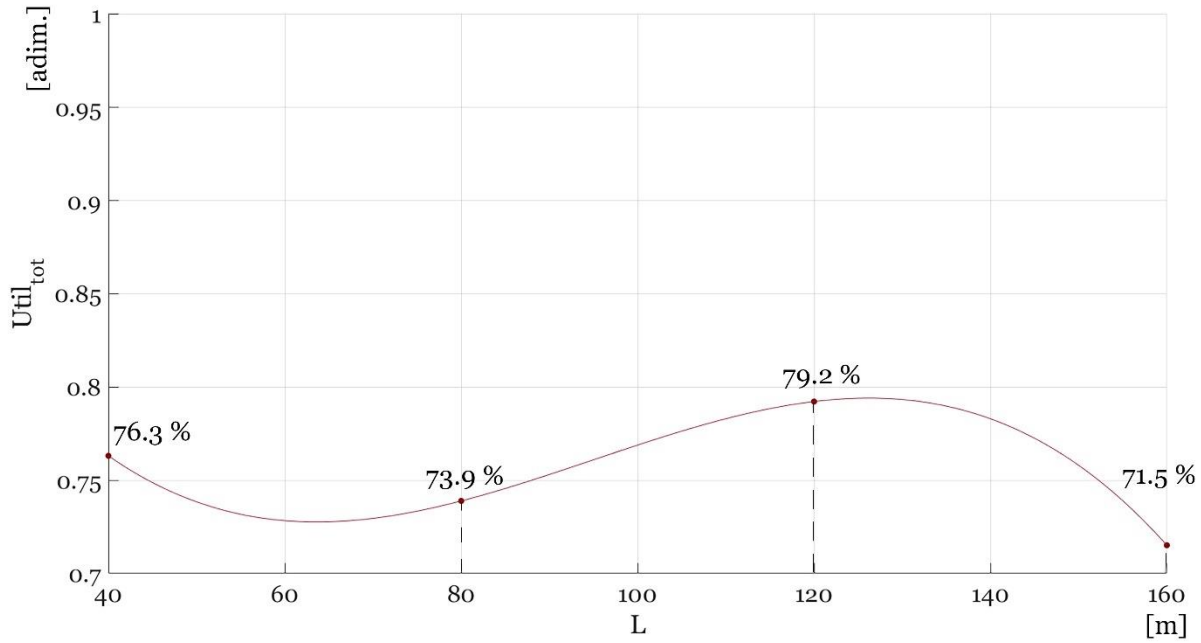

Figure 5. 45 *Resulting values of the "total utilization ratio" ($Util_{tot}$), evaluated through the Eq. (26), providing an overall percentage of the material exploitation*

5.3 Simultaneous topology, shape and size optimization of hingeless truss arches under multiple load cases

The present section will provide a detailed description of the stepwise process carried out, by the optimization macro-algorithm presented in section *§4.2,* to simultaneously perform topology, shape and size optimization of "hingeless" truss arches, with different spans (*40*, *80*, *120* and *160 meters*), subjected to multiple different load cases. More specifically, in-plane Pratt trusses, composed by two arched chords with hinged ends and made of steel tubular members (i.e. with circular hollow cross-sections), were optimally designed for different vertical load patterns (acting in the arch plane). As a matter of fact, the truss-arches under consideration are comparable to "fixed" arches (i.e. to a "hingeless" arch) since the two double-hinges, vertically aligned, prevent rotations in the arch plane.

The so obtained results will be illustrated and discussed in subsection *§5.3.4*.

5.3.1 Parametric design

The pivotal role that parametric design plays in the preliminary phase of a structural optimization process has been already underlined in sub-section *§4.2.1*. This phase is indispensable to properly define all design variables within a range of lower and upper bounds and then formulate the considered optimization problem as a function of the assumed design variables (as shown in the flowchart of the proposed macro-algorithm illustrated in *Figure 4. 2*).

The higher the number of design variables to consider, the more crucial the role of this stage in the whole process becomes.

In this regard, the design problem of truss arches here investigated depends on a large number of parameters, among which several design variables have been identified and different sets of them have been properly defined for different formulations of the problem.

5.3.1.1 Topology design variables

As in cases of two-hinged truss arches treated in the previous section *§5.2*, the topology optimization problem of "hingeless" arched trusses under consideration (with spans of *40*, *80*, *120* and *160 meters*) has been formulated as a function of a variable number of truss elements and joints, thereby assuming, as topology design variable, a parameter indicated as n_{int}, defining the number of equal "intervals" (dL), into which the arch span is subdivided (as expressed by Eq. (44) and indicated in *Figure 5. 46*).

The topology design variable n_{int} affects the node number and spacing (their x −coordinates), as well as the number of the truss bars. In particular, the "hingeless" truss arches under consideration are characterized by $2n_{int} + 2$ joint number and $4n_{int} + 1$ number of members.

Furthermore, since a Pratt-type truss has been chosen as bracing system, n_{int} is required to be defined as an even integer, as well as a discrete design variable.

However, the optimization method here adopted (previously illustrated in section *§4.2*) requires a unique set of continuous design variables. For this reason, the value related to the parameter n_{int} is rounded to the nearest even integer during the optimization process.

5.3.1.2 Shape design variables: parameters defining Cubic Rational Bézier Curves

In shape optimization of continuous and discrete structures, the nodes coordinates are commonly assumed as design variables. However, as anticipated in the section *§1.3.2,* the optimization problem of large-scale structures (characterized by a large number of members and joints) would require a high number of design variables. For this reason, it has become a common practice to adopt parametric shape functions to significantly reduce the number of shape design variables.

For this purpose, the parametric form of *third-degree Rational Bézier curves* (represented in *Figure 5. 5* and expressed by Eq. (45)) was adopted to define shape design variable in order to represent a very wide family of curves.

Therefore, on the basis of Eq. (45) and several symmetry conditions (pointed out in *Figure 5. 46*), the following parameters have been assumed as shape design variables to be optimized

- x_{P1l}, x –coordinate of the second control point (P_{1l}) of the lower chord (shaped as a *Cubic Rational Bézier* arc). As shown in *Figure 5. 46,* the third control point (P_{2l}) of the bottom rib has been assumed as symmetric to P_{1l} with respect to a central vertical axis, by imposing that $x_{P2l} = L - x_{P1l}$. Furthermore, x –coordinates of two internal control points (P_{1l} and P_{2l}) of the bottom arched chord also define x –coordinates of the corresponding control points (P_{1u} and P_{2u}) of the upper control polygon
- z_{P1l}, z –coordinate of the second control point (P_{1l}) of the bottom arch rib (shaped as a *Cubic Rational Bézier* arc), which is assumed to be equal to the z –coordinate (z_{P2l}) of the third control point P_{2l}
- w_{P1l}, weight non-negative factor of the second control point (P_{1l}) of the bottom arched chord, which is equal to the weight factors (w_{P2l}, w_{P1u} and w_{P2u}) of other internal control points (P_{2l}, P_{1u} and P_{2u}) of lower and upper arch chords
- z_{P0u}, z –coordinate of the first control point (P_{0u}) of the upper arched rib (shaped as a *Cubic Rational Bézier* arc), which defines the arch depth at its ends
- Δz, absolute value of the difference between z –coordinates of the internal control points of top and bottom arch chords ($\Delta z = |z_{P1u} - z_{P1l}| = |z_{P2u} - z_{P2l}|$).

It is worth remarking that all shape design variables have been defined as continuous variables within proper ranges of lower and upper limits.

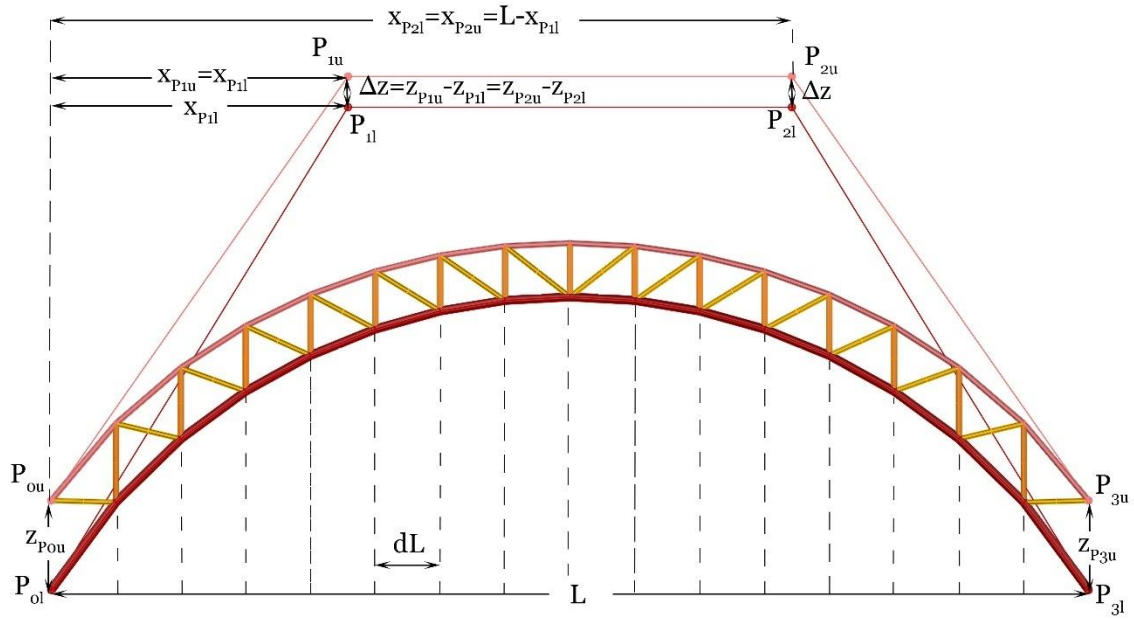

Figure 5. 46 Parametric definition of the geometry as a function of shape design variables, by taking advantage of Cubic Rational Bézier Curves

5.3.1.3 Size design variables

The cross-sectional areas of members are commonly assumed as design variables in size optimization of discrete structures. The elements of frame structures are often split into several groups (each one characterized by same cross-section features) in order to reduce the total number of size design variables.

Analogously to the case of two-hinged truss arches (treated in section *§5.2*), the arched trusses under consideration are assumed to be composed by elements with circular hollow cross-sections, grouped as follow

- Bottom chord (lower chord) elements
- Top chord (upper chord) elements
- Diagonals
- Verticals.

Each group of elements is characterized by same diameter, thus assuming

- d_1 as diameter of bottom chord elements
- d_2 as diameter of top chord elements
- d_3 as diameter of diagonals
- d_4 as diameter of verticals.

On the other hand, it was assumed that couples of elements that are symmetrical with respect to a central vertical axis (i.e. placed in the mid-span and parallel to the reference z −axis), must have same thickness. Therefore, four diameters and n different thicknesses t_i (with $i = 1, \dots n$) were assumed as size design variables, for each i_{th} −couple of symmetrical elements.

Since the element number is variable and depending on the topology design variable n_{int}, the number n of different thicknesses t_i (with $i = 1, \dots n$) has been defined as a function of n_{int}^u (i.e. upper limit of n_{int}) as follows

$$n = 2 * n_{int}^u + 1 \tag{53}$$

As a matter of fact, the number of different cross-sections expressed by Eq. (53) showed to depend on the allowable maximum number of elements, equal to $4n_{int}^u + 1$.

To be more precise, as previously stated in section §5.2.2, size design variables were defined as indexes, which allow to extract the values of diameters and thicknesses from a table of parameters of commercial circular hollow cross-sections (see *Table 5. 5*). Therefore, size design variables needed should be discrete. However, since the optimization method here proposed (in *§4.2*) can

only generate continuous values, discrete size design variables were obtained by rounding the corresponding continuous values to the nearest integers.

5.3.2 Problem formulation

Analogously to what has been done for two-hinged truss arches, four different optimization problems were formulated for "hingeless" arches with spans of *40*, *80*, *120* and *160 meters*. The considered optimization problems once again differ from each other for the allowable range of numbers of elements (as shown in the *Table 5. 20*), defined as follows

- for the arch model with a span of 40.0 $[m]$, the even number of equal intervals into which the span is subdivided (n_{int}) can vary from 10 (n_{int}^{l}) to 40 (n_{int}^{u}), the number of elements can then vary from $n_{el}^{MIN} = 4n_{int}^{l} + 1 = 41$ to $n_{el}^{MAX} = 4n_{int}^{u} + 1 = 161$ (CASE 1)
- for the arch model with a span of 80.0 $[m]$, the even number of equal intervals into which the span is subdivided (n_{int}) can vary from 10 (n_{int}^{l}) to 80 (n_{int}^{u}), the number of elements can then vary from $n_{el}^{MIN} = 4n_{int}^{l} + 1 = 41$ to $n_{el}^{MAX} = 4n_{int}^{u} + 1 = 321$ (CASE 2)
- for the arch model with a span of 120.0 $[m]$, the even number of equal intervals into which the span is subdivided (n_{int}) can vary from 10 (n_{int}^{l}) to 120 (n_{int}^{u}), the number of elements can then vary from $n_{el}^{MIN} = 4n_{int}^{l} + 1 = 41$ to $n_{el}^{MAX} = 4n_{int}^{u} + 1 = 481$ (CASE 3)
- for the arch model with a span of 160.0 $[m]$, the even number of equal intervals into which the span is subdivided (n_{int}) can vary from 10 (n_{int}^{l}) to 160 (n_{int}^{u}), the number of elements can then vary from $n_{el}^{MIN} = 4n_{int}^{l} + 1 = 41$ to $n_{el}^{MAX} = 4n_{int}^{u} + 1 = 641$ (CASE 4).

Table 5. 20 Design variable definitions for the four considered optimization problems

Span length	Range of element number	Number of Topology DV	Number of Shape DV	Number of Size DV	Total number of DV
40.0 $[m]$	$41 \leq n_{el} \leq 161$	1	5	85	91
80.0 $[m]$	$41 \leq n_{el} \leq 321$	1	5	165	171
120.0 $[m]$	$41 \leq n_{el} \leq 481$	1	5	245	251
160.0 $[m]$	$41 \leq n_{el} \leq 641$	1	5	325	331

In *Table 5. 20* the ranges of element numbers and the numbers of design variables, distinguished by type (topology, shape and size), are indicated for each optimization problem. The different formulations of the problem differ from each other for the number of size design variables, which was assumed to be proportional to the allowable maximum numbers of elements (defined in proportion to the length of the arch span).

Table 5. 21 shows the lower and upper bounds of design variables for the CASE 1 (truss arch with a span of 40 meters). It is worth noting that the upper limits of the $x-$ and $z-$coordinates correspond to the half span of the arch. Furthermore, also note that the arch depth at its crown

and bases can vary between 0.10 and 12.00 meters in all formulations of the optimization problem.

Table 5. 21 Lower and upper bounds of design variables for the CASE 1 (arch span of 40 meters)

CASE 1				
Design Variable (DV)	**Type of DV**	**Lower bound**	**Upper bound**	**Unit**
n_{int}	*topology*	10	40	$[adim.]$
x_{P1l}	*shape*	0.1	20.0	$[m]$
z_{P1l}	*shape*	6.0	20.0	$[m]$
w_{P1l}	*shape*	0.5	8	$[adim.]$
z_{P1u}	*shape*	0.1	12.0	$[m]$
Δz	*shape*	0.1	12.0	$[m]$
$index_{d1}$	*size*	1	27	$[adim.]$
$index_{d2}$	*size*	1	27	$[adim.]$
$index_{d3}$	*size*	1	27	$[adim.]$
$index_{d4}$	*size*	1	27	$[adim.]$
$index_{t(i)}$ *	*size*	2	20	$[adim.]$

* with $i = 1, \dots n$ (n was defined in the section *§5.3.1.3* by the Eq. (21))

Table 5. 22 Lower and upper bounds of design variables for the CASE 2 (arch span of 80 meters)

CASE 2				
Design Variable (DV)	**Type of DV**	**Lower bound**	**Upper bound**	**Unit**
n_{int}	*topology*	10	80	$[adim.]$
x_{P1l}	*shape*	0.1	40.0	$[m]$
z_{P1l}	*shape*	6.0	40.0	$[m]$
w_{P1l}	*shape*	0.5	8	$[adim.]$
z_{P1u}	*shape*	0.1	12.0	$[m]$
Δz	*shape*	0.1	12.0	$[m]$
$index_{d1}$	*size*	1	27	$[adim.]$
$index_{d2}$	*size*	1	27	$[adim.]$
$index_{d3}$	*size*	1	27	$[adim.]$
$index_{d4}$	*size*	1	27	$[adim.]$
$index_{t(i)}$ *	*size*	2	20	$[adim.]$

* with $i = 1, \dots n$ (n was defined in the section *§5.3.1.3* by the Eq. (21))

Table 5. 22, *Table 5. 23* and *Table 5. 24* contain the sets of topology, shape and size design variables with relative lower and upper bounds defined for CASES 2, 3 and 4, respectively.

Table 5. 23 Lower and upper bounds of design variables for the CASE 3 (arch span of 120 meters)

CASE 3				
Design Variable (DV)	**Type of DV**	**Lower bound**	**Upper bound**	**Unit**
n_{int}	*topology*	10	120	$[adim.]$
x_{P1l}	*shape*	0.1	60.0	$[m]$
z_{P1l}	*shape*	6.0	60.0	$[m]$
w_{P1l}	*shape*	0.5	8	$[adim.]$
z_{P1u}	*shape*	0.1	12.0	$[m]$
Δz	*shape*	0.1	12.0	$[m]$
$index_{d1}$	*size*	1	27	$[adim.]$
$index_{d2}$	*size*	1	27	$[adim.]$
$index_{d3}$	*size*	1	27	$[adim.]$
$index_{d4}$	*size*	1	27	$[adim.]$
$index_{t(i)}$ *	*size*	2	20	$[adim.]$

* with $i = 1, \dots n$ (n was defined in the section *§5.3.1.3* by the Eq. (21))

Table 5. 24 Lower and upper bounds of design variables for the CASE 4 (arch span of 160 meters)

CASE 4				
Design Variable (DV)	**Type of DV**	**Lower bound**	**Upper bound**	**Unit**
n_{int}	*topology*	10	160	$[adim.]$
x_{P1l}	*shape*	0.1	80.0	$[m]$
z_{P1l}	*shape*	6.0	80.0	$[m]$
w_{P1l}	*shape*	0.5	8	$[adim.]$
z_{P1u}	*shape*	0.1	12.0	$[m]$
Δz	*shape*	0.1	12.0	$[m]$
$index_{d1}$	*size*	1	27	$[adim.]$
$index_{d2}$	*size*	1	27	$[adim.]$
$index_{d3}$	*size*	1	27	$[adim.]$
$index_{d4}$	*size*	1	27	$[adim.]$
$index_{t(i)}$ *	*size*	2	20	$[adim.]$

* with $i = 1, \dots n$ (n was defined in the section *§5.3.1.3* by the Eq. (21))

All different optimization problems (CASE 1, 2, 3 and 4) were formulated with same objective and constraint functions. As described in section *§4.2.3*, the objective and constraint functions are evaluated at each iteration of the adopted optimization process (see *Figure 4. 2*), by performing *Finite Element Analysis (FEA)* through the software for structural analysis *SAP2000*.

In all considered cases, the total volume of the structure was assumed as objective function to be minimized and calculated by Eqs. (38) and (39) described in the section *§4.2.3*.

Analogously to what has been done for the two-hinged truss arches, strength constraints (expressed by Eq. (47)) have been imposed in order to keep stress values within allowable ranges according to mechanical properties of materials and technical standards for construction. More specifically, the inequality constraint function, expressed by the Eq. (47), indicates that the maximum value of the afore-mentioned "Utilization ratio" (also called "Demand/Capacity ratio", since it corresponds to the ratio between real and allowable stresses acting in a section) among all truss members must be less than (or equal to) 0.99 for all considered load cases (feasibility condition). In particular, the critical "Utilization ratio" of bars subjected to compression axial forces was calculated by evaluating the combined effect of compression axial forces and bending moments by also considering flexural and lateral-torsional buckling of cross-sections by means of the interaction equations provided by the section EC3-2005 6.3.3(4), expressed by the Eqs. (40) and (41) in section *§4.2.3*. On the other hand, the "utilization ratio" of members subjected to tensile axial forces is evaluated by checking the combined effect of axial forces and bending moments by means of the interaction equation (provided by EC3-2005 6.2.1(7)), expressed by Eq. (42) in section *§4.2.3*.

As already underlined, the values of the objective and constraint functions are determined and compared to iteratively select the best candidate solutions during the optimization process, until an optimal solution is achieved.

5.3.3 Boundary conditions

All different formulations (the CASES 1, 2, 3 and 4) of the optimization problem just described in §5.3.2, are characterized by the same boundary conditions.

More specifically, the steel truss arches under consideration were assumed to be connected to the foundations by two double hinges, vertically aligned (see *Figure 5. 47*). Moreover, since all members are connected to each other by pinned joints and external loads are applied as concentrated forces on nodes, the considered arched trusses can be treated as "true trusses" (i.e. subjected to almost only axial forces).

The structure illustrated in *Figure 5. 47* is statically redundant or indeterminate, since by substituting in Eq. (48) the quantities indicating the numbers of nodes (n_{nodes}) and elements

(n_{frames}) with their parametric expressions as a function of the parameter n_{int}, and a value of gdv_{ext} (i.e. the "degree of external constraint") equal to 8 (since the considered truss arches are connected to the soil by four external hinges), you find that,

$$2.(2.n_{int}+2) < (4.n_{int}+1)+8 \quad (54)$$

Thus, leading to,

$$4.n_{int}+4 < 4.n_{int}+9 \quad (55).$$

In addition, *Figure 5. 47* shows that the "hingeless" truss arches under consideration are subjected to the same combinations of vertical load patterns applied in optimizing the two-hinged arches (see section *§5.2.3*). Furthermore, the external loads have been analogously applied as concentrated forces on nodes (of the lower chord), equivalent to non-structural Dead Loads ($24.00\ kN/m$) and Live Loads ($15.00\ kN/m$), uniformly distributed along the arch span.

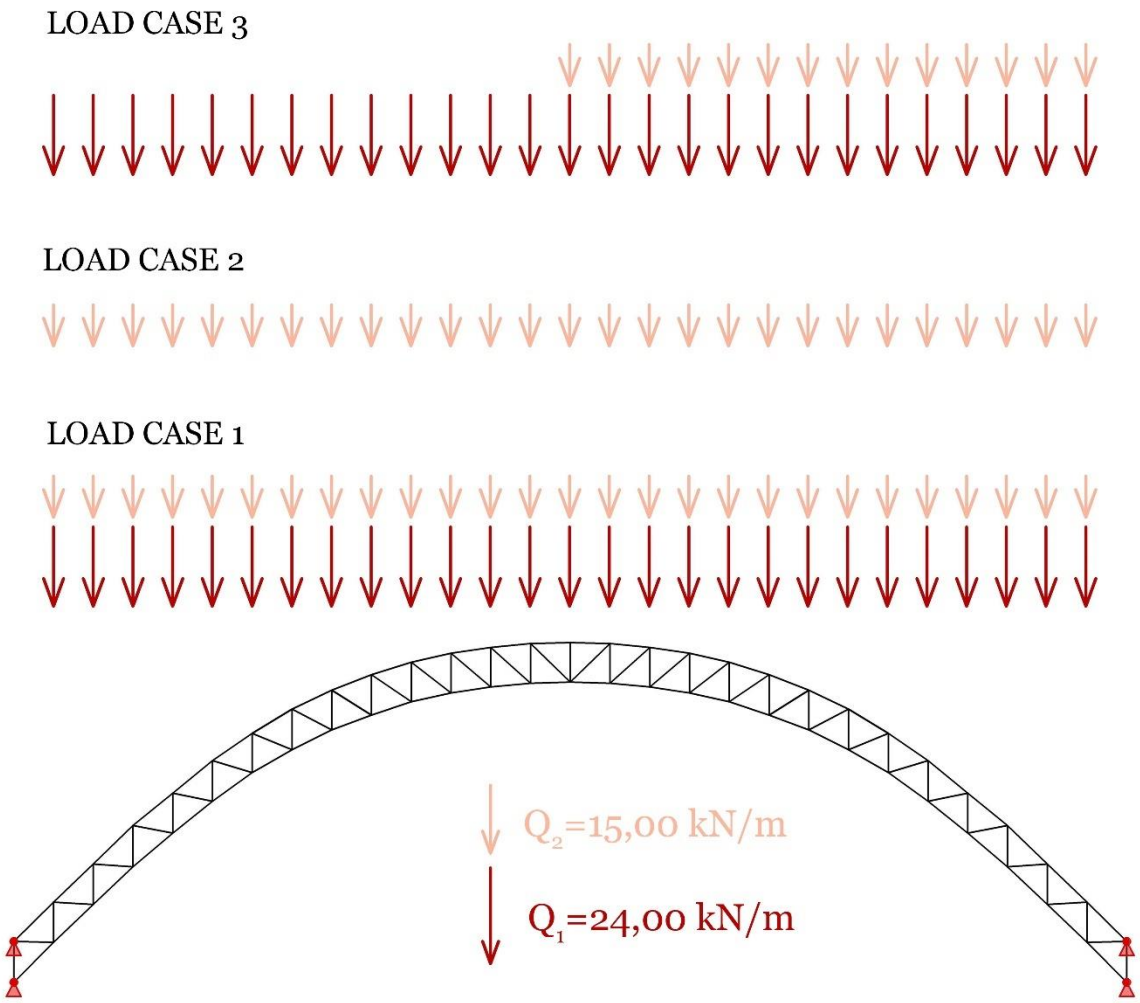

Figure 5. 47 *Boundary conditions (external constraints and multiple load cases) considered in all cases of the optimization problem of hingeless truss arches*

5.3.4 Results

The optimization macro-algorithm proposed and described in section *§4.2* has been applied to solve the problem of the optimum design of "hingeless" truss arches defined by four different formulations (just described in the previous section *§5.3.2*) each one characterized by a different span (40, 80, 120 and 160 *meters*), different sets of design variables and relative lower and upper bounds.

In this regard, the purpose of this section is to illustrate and compare the obtained best solutions of all considered optimization problems (CASES 1, 2, 3 and 4), in order to investigate them and deduce useful suggestions for the design of two-hinged truss arches made of steel tubular elements.

As already stated, the macro-algorithm here proposed includes a modified version of a *Differential Evolution Algorithm* (in detail described in section *§4.2.2* and summarized in the flowchart in *Figure 4. 3*). The chosen optimization algorithm belongs to population-based *Evolutionary Algorithms* (introduced in *§1.4.3.2*) that requires an appropriate definition of the "population" size (i.e. the number of candidate solutions, called "individuals", of each "generation") and maximum number of "generations" for all formulations of the optimization problem under consideration.

Table 5. 25 Optimization parameters of the Differential Evolution Algorithm (DEA) for the different problem formulations (CASES 1, 2, 3 and 4)

OPTIMIZATION PARAMETERS					
CASE	**Span length**	**Number of design variables**	**Population size**	**Generations**	**Total number of iterations**
1	40.0 [m]	91	100	300	30000
2	80.0 [m]	171	100	500	50000
3	120.0 [m]	251	100	750	75000
4	160.0 [m]	331	100	1000	100000

In this regard, *Table 5. 25* shows that all considered problems were characterized by an extremely large number of design variables, same population size (equal to 100 "individuals") and a maximum number of "generations" properly increased, according to the number of design variables of the optimization problems in order to ensure a suitable exploration of the search space.

The optimization method here adopted showed to be robust and effective in performing topology, shape and size optimization of the considered truss arches at the same time. However, the analysis

of the obtained results mainly aims to identify the most peculiar features of the best solutions and then deduce precious design recommendations.

5.3.4.1 Case 1 optimal solution

The solution of the optimization problem of a "hingeless" truss arch with a span of 40 meters (parametrically defined by taking advantage of *Cubic Rational Bézier curves*, as illustrated in *Figure 5. 46*) and subjected to three vertical load cases (represented in *Figure 5. 47*) is here presented. All assumed design variables, with corresponding lower and upper bounds, are indicated in *Table 5. 21*.

In this regard, *Figure 5. 48* shows the shape of the optimized arch under consideration, characterized by a minimum volume of $0.293\ m^3$ (i.e. the minimum value of the objective function), corresponding to a self-weight per unit length of $0.563\ kN/m$. Furthermore, the optimal arch has a total height of $11.92\ m$ and a rise of $10.92\ m$ (as indicated in *Figure 5. 48*).

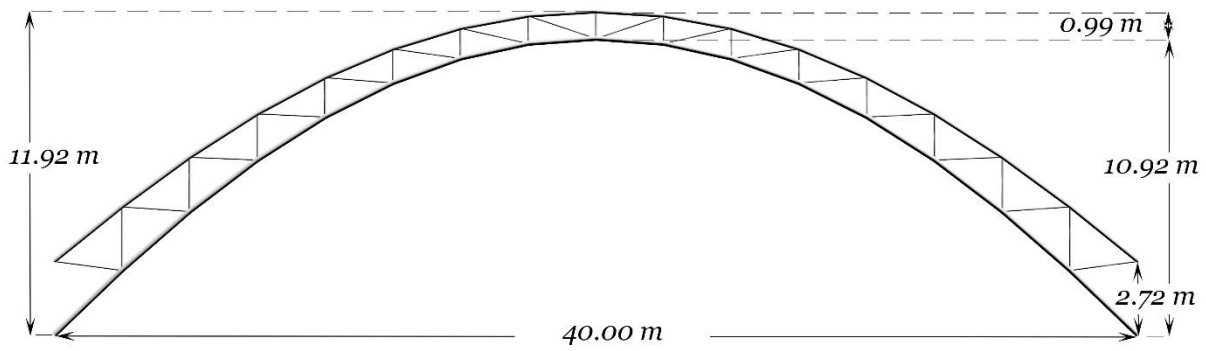

Figure 5. 48 Front view of the optimized truss arch with main dimensions (CASE 1 optimal solution)

As well known, the rise-to-span ratio of an arch (commonly included between 1/4 and 1/6) is one of most peculiar shape parameters that more affect the structural behaviour of the arch. In fact, the smaller the rise of an arch, the greater the magnitude of horizontal thrusts that arise at its ends (as demonstrated by Eqs. (10) and (15) in *§2.1*). In particular, the optimal arch here considered, showed to have a "rise-to-span ratio" equal to 1/3.66 and a "height-to-span ratio" equal to 1/3.36. Moreover, it can be also easily seen that the arch in *Figure 5. 48* is characterized by an extremely small "crown depth", about $0.99\ m$, and a much higher "base depth" of $2.72\ m$, thus leading to a "crown depth-to-span ratio" corresponding to 1/40.20 and a "base depth-to span ratio" about 1/14.71. In addition, a further parameter, called "taper ratio" was evaluated and considered in analysing the optimal shape of the arch under consideration. This parameter expresses how much the arch depth tends to vary from its crown to its ends, since it was defined as a ratio of the "crown-depth" over the "base-depth" of the arch. In the current case, a "taper ratio" of 1/2.73, confirming that the optimized truss arch here considered is significantly tapered.

Table 5. 26 *Topology and shape optimization results for the CASE 1: optimal values of topology and shape design variables*

Topology optimization results			
Design Variable (DV)	**Type of DV**	**Best value**	**Unit**
n_{int}	*topology*	16	$[adim.]$
Shape optimization results			
Design Variable (DV)	**Type of DV**	**Best value**	**Unit**
x_{P1l}	*shape*	16.7584	$[m]$
z_{P1l}	*shape*	16.5854	$[m]$
w_{P1l}	*shape*	0.643	$[adim.]$
z_{P0u}	*shape*	2.719	$[m]$
Δz	*shape*	0.100	$[m]$

The depth of an arch commonly needs to be increased from its crown to its bases proportionally to axial force variation in it, also ensuring greater stability.

A further representative parameter of the optimal truss arch under consideration, extremely important by a constructive point of view, is the total number of its elements, depending on the even integer (n_{int}) of the arch span subdivisions into equal intervals (i.e. the topological design variable). In this regard, the truss arch represented in *Figure 5. 48* is characterized by an arch span subdivision number (n_{int}) equal to 16, thereby resulting in a total element number (n_{frames}) equal to 65 (since it was assumed that $n_{frames} = 4.n_{int} + 1$) and joint number ($n_{nodes}$) equal to 34 (since $n_{nodes} = 2n_{int} + 2$).

Table 5. 27 *Size optimization results for the CASE 1: optimal diameters and thicknesses of circular hollow cross-sections*

Size optimization results					
Element groups	**Type of DV**	**Diameter d_i**	**Min. thickness t_i**	**Max. thickness t_i**	**Unit**
Bottom chord	*size*	0.1937	0.0045	0.008	$[m]$
Top chord	*size*	0.159	0.004	0.004	$[m]$
Diagonals	*size*	0.07	0.0032	0.005	$[m]$
Verticals	*size*	0.07	0.004	0.005	$[m]$

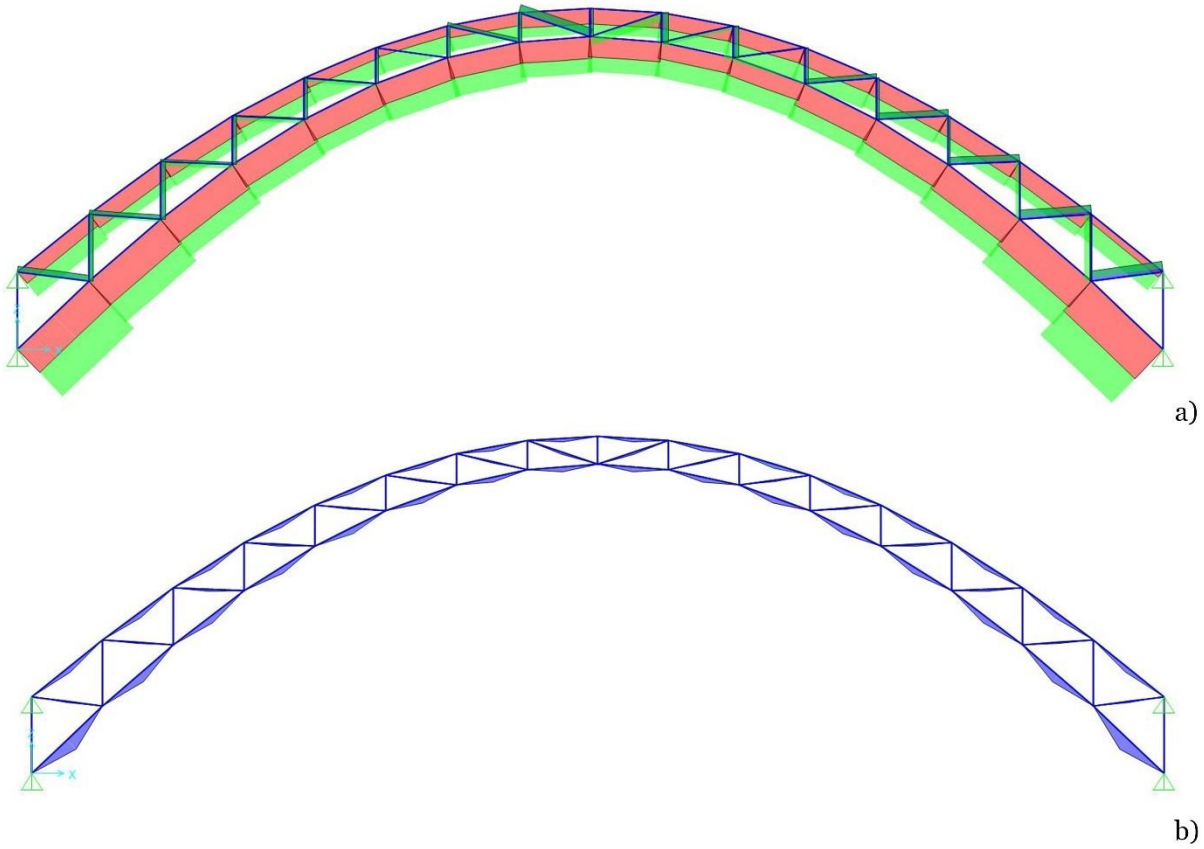

Figure 5. 49 Finite Element Analysis (FEA) results for the CASE 1: (a) axial force diagram; (b) bending moment diagram

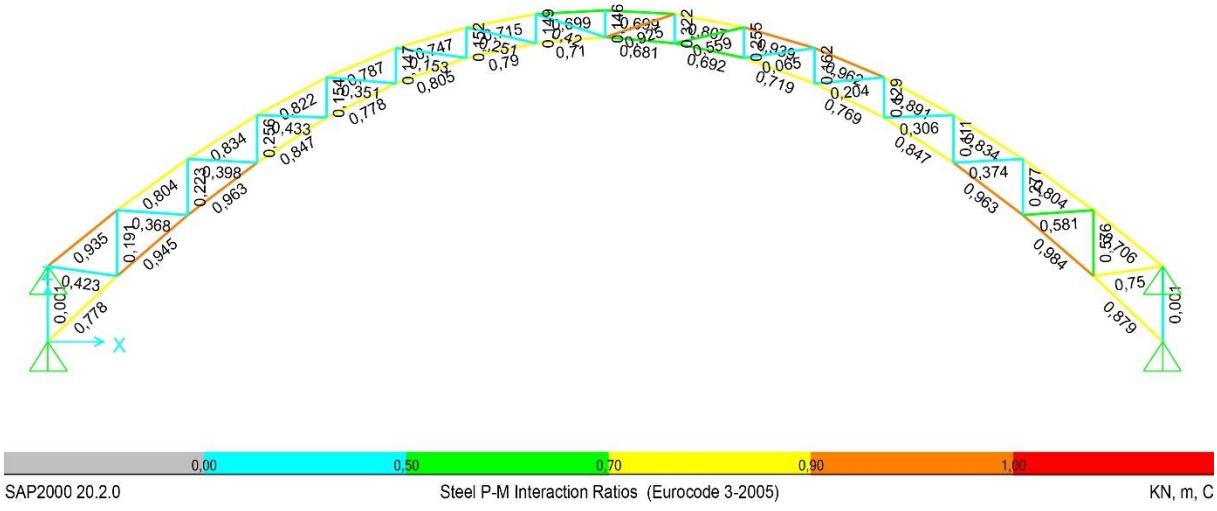

Figure 5. 50 Finite Element Analysis (FEA) results for the CASE 1: Demand/Capacity ratio (also called "utilization ratio") diagram of the optimal solution for the envelope of all load cases

Table 5. 26 contains the optimal values obtained for all topology and shape design variables, which completely define the geometry of the optimal truss arch here analysed. Note that the optimal shape of the considered arched truss must be a trade-off between the optimal shapes for all considered load cases (shown in Figure 5. 47), among which the asymmetric load pattern strongly affects the structural response of the structure and the solution of the optimization problem.

On the other hand, in *Table 5. 27* size optimization results are summarized. Since the number of size design variables corresponding to the element thicknesses is extremely large, in addition to the diameters, only the minimum and the maximum thicknesses for each element group are indicated in *Table 5. 27*.

Unlike the case of two-hinged truss arches previously treated in *§5.2,* the bottom chord elements required a greater diameter compared to other elements, because they are subjected to greater axial forces and bending moments (as shown in *Figure 5. 49*). In particular, it was found that the lower chord was subjected to a compressive axial force varying from 426 kN to 901 kN (see *Figure 5. 49(a))* as well as to bending moments (whose diagram is illustrated in *Figure 5. 49(b)*) varying from 0.15 $kN.m$ to 0.37 $kN.m$.

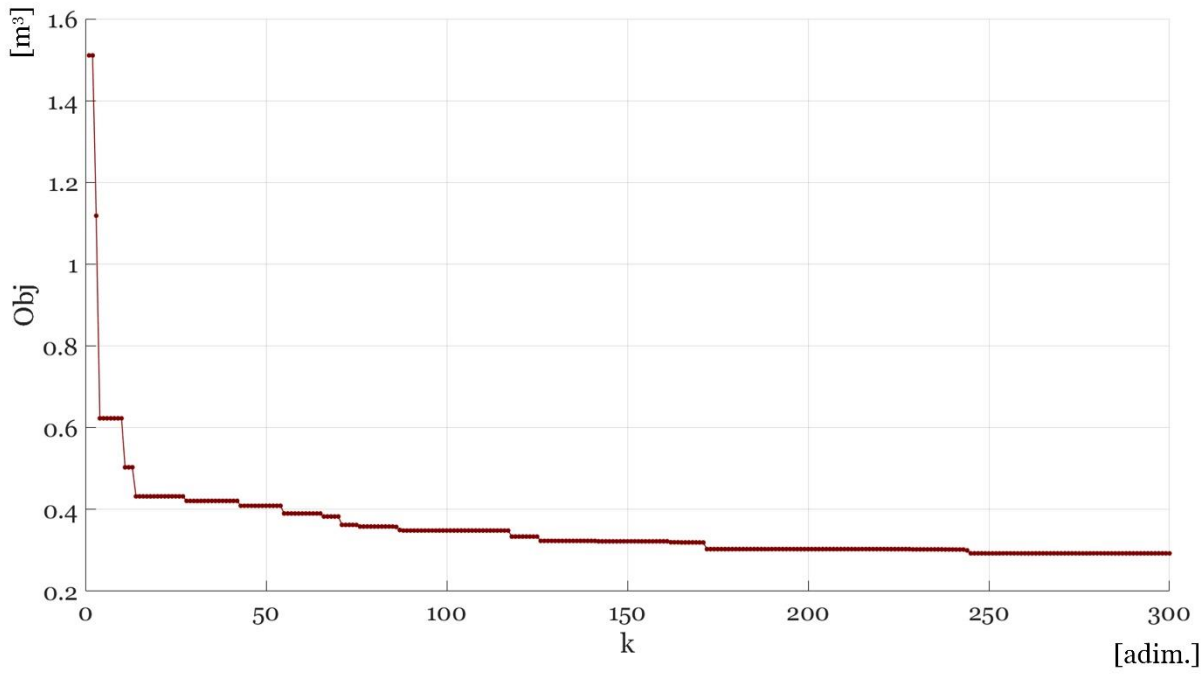

Figure 5. 51 *Convergence curve of the Objective (Obj) function (i.e. the volume of the arch) for all "generations" (for the CASE1)*

On the other hand, the upper chord showed to be subjected to a compressive axial force varying between 291 kN to 387 kN, as well as to bending moments varying from 0.11 $kN.m$ to 0.15 $kN.m$. Since axial forces and bending moments showed to be approximately uniform, a constant value

of 0.004 m has been obtained for the thickness of all upper chord elements (as indicated in *Table 5. 27)*. Moreover, diagonal and vertical members are subjected to tensile axial forces (varying from 1 kN to 123 kN in diagonal, and from 6 kN to 82 kN in vertical bars), whereas diagonal tubes also withstand bending moment actions varying from 0.03 $kN.m$ to 0.06 $kN.m$.

Analogously to what has been done for two-hinged truss arches, the stress level in the structure to be optimized was kept within an allowable range of values, according to mechanical properties of materials and technical standards for construction, imposing that the maximum "utilization ratio" (i.e. the "demand/capacity ratio" evaluated by Eqs. (40-42)) of all truss members, for all applied load cases, was less or equal to 0.99 (see Eq. (47) assumed as strength constraint function). Eqs. (40-42) allowed to check the combined effect of axial forces and bending moments by also considering flexural and lateral-torsional buckling of cross-sections subjected to combined axial compressive and bending stresses.

Figure 5. 50 shows a diagram of the optimal truss arch here analysed, indicating the maximum i^{th} –element "utilization ratio" ($\max_{LC} Util_i^{LC}$), for the envelope of all considered load combinations. That diagram shows that more than half of elements is characterized by a critical ratio larger than 0.7. Furthermore, a "total utilization ratio" ($Util_{tot}$) expressing a quite realistic overall percentage of the material exploitation of the whole structure was evaluated as a weighted average of Demand/Capacity ratios ($\max_{LC} Util_i^{LC}$) shown in *Figure 5. 50,* with respect to the weight of each member (Eq. (51)). A satisfactory percentage of material exploitation about 71.6 % has been obtained, thus ensuring a high level of structural performance of the optimized steel truss arch under consideration.

Figure 5. 51 shows the convergence curve of the "objective function" (i.e. the total volume of the structure) to be minimized, in order to validate the goodness of the obtained result, notwithstanding the extremely large number of design variables and their various nature. It can be easily seen that the objective function tends to become almost flat from the 172^{th} generation, meaning that from this point it starts do decrease extremely slowly.

The "objective function" tendency is further confirmed by the history of the "stagnation function" (introduced in section *§5.2.4.1*), whose "zig-zag" trend occurs because it becomes zero at each generation characterized by an improvement in the objective function compared to the previous generation, otherwise it linearly increases (see *Figure 5. 52(a)*). In this specific case, the "stagnation function" showed to have the greatest peaks from the 172^{th} to the 228^{th} generation and from 245^{th} generation to the maximum iteration.

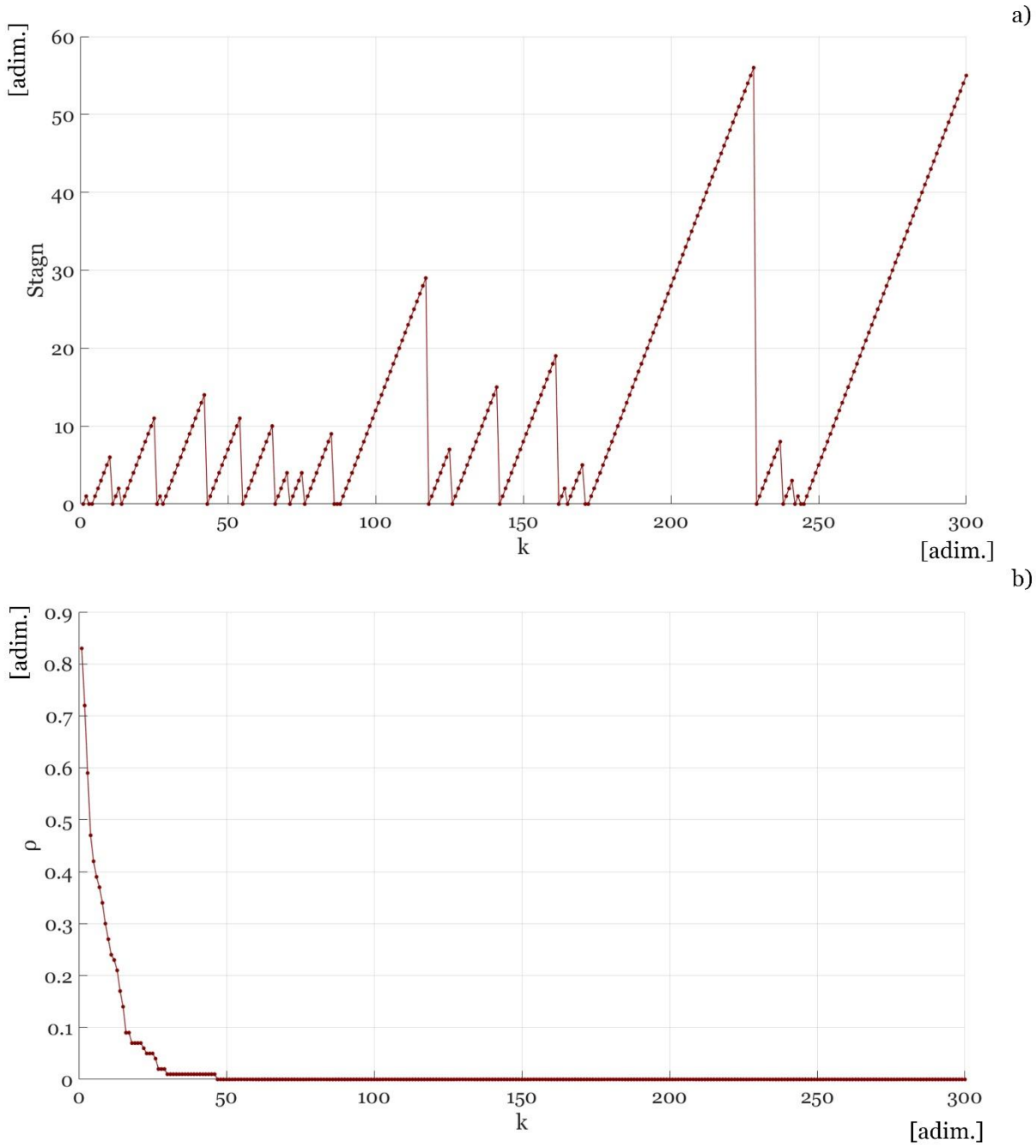

Figure 5. 52 History of optimization functions (for the CASE 1): (a) stagnation function; (b) "unfeasibility function" (ρ)

Figure 5. 52(b) shows the history of the "unfeasibility function" (ρ^k), which was introduced in section *§5.2.4.1* and defined by Eq. (52), as a ratio between "unfeasible individuals" (Unf^k) and all individuals (Pop^k) of a k^{th} –generation. The "unfeasibility function" (ρ^k) therefore produces values between 0 (i.e. all "individuals" are feasible, since all constraints are satisfied) and 1 (all "individuals" are unfeasible, since at least one constraint is violated). In this specific case, it has been found that ρ becomes and remains zero from the 47^{th} generation to the last one, meaning

that the optimization process produces and evaluates only feasible candidate solutions from this point on (as shown in *Figure 5. 52(b)*).

The quality of results produced by an optimization process should be also validated by the convergence curves of design variables. However, since the optimization problem here discussed is characterized by an extremely large number of design variables, it is not possible to present all their convergence curves.

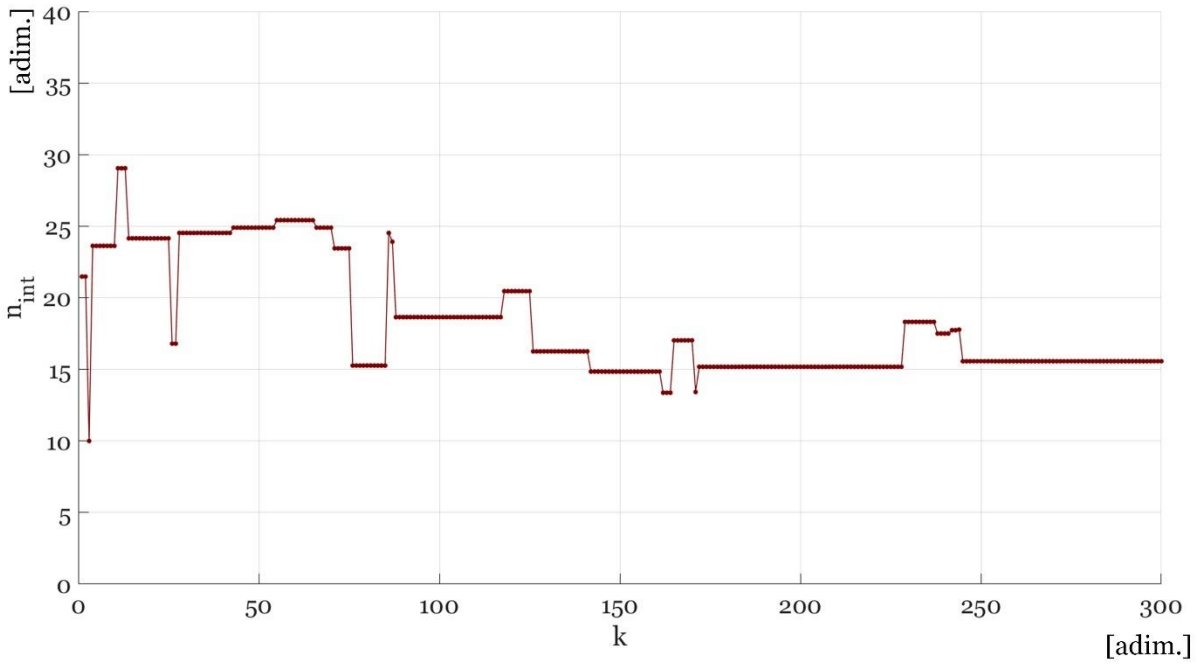

Figure 5. 53 Convergence curve of the topology design variable (n_{int}) for the CASE 1

In this regard, *Figure 5. 53* shows the history of the topology design variable n_{int}, which the total number of the truss arch elements depends on. Seeing as how the number of bars and joints strongly affects the cost of a truss structure, its value has a great importance by a constructive point of view. It is worth recalling that n_{int} was defined as a continuous value between 10 and 40 (to be later rounded to the nearest even integer). The convergence curve validates the goodness of obtained solution, since from the first 172^{th} generation its value only tends to oscillate between 15 and 18, until an optimal value (to which 16 was the nearest even integer) was found (see *Figure 5. 53*). In *Figure 5. 54* the convergence curves of shape design variables (i.e. the variable parameters defining the shape of lower and upper arch chords by parametric *Cubic Rational Bézier curves*) are presented to prove the validity of results, despite the large number and the variety of design variables. In the same way, a good convergence trend was also obtained for the size design variables determining the element group diameters (whose curves are shown in *Figure 5. 55*). It can be easily noted that the optimal values (summarized in *Table 5. 26* and in *Table 5. 27*) have been achieved at the 245^{th} generation.

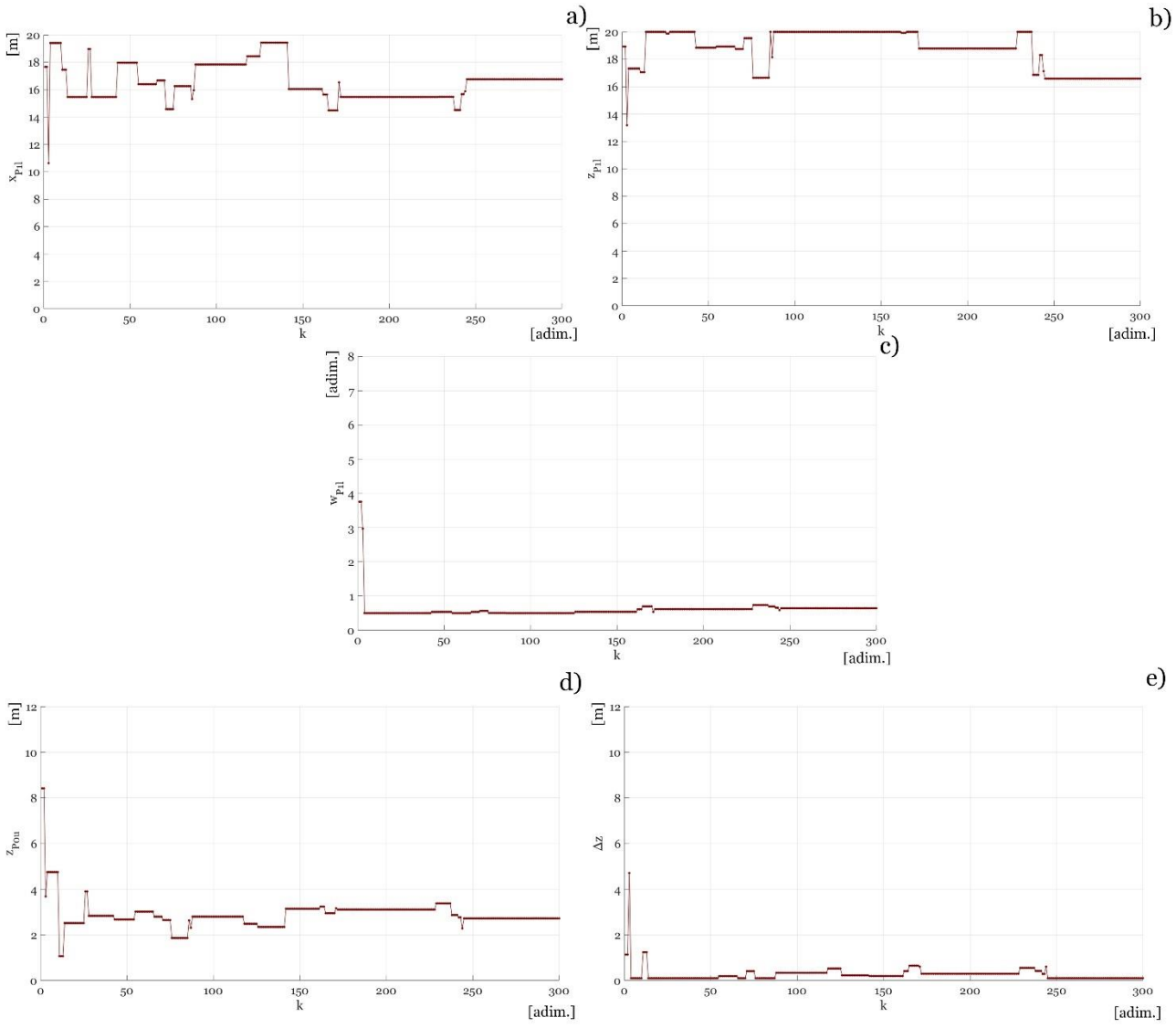

Figure 5. 54 Convergence curves of the shape design variables (variable parameters of third-degree rational Bézier curves) for the CASE 1: (a) x −coordinate of the second control point (x_{P1l}) of the bottom arched chord; (b) z −coordinate of the second control point (z_{P1l}) of the bottom arched chord; (c) weight factor of the second control point (w_{P1l}) of the bottom arched chord; (d) z −coordinate of the first control point (z_{P0u}) of the top arched chord;(e) the difference between the z −coordinates (in absolute value) of the top and bottom chord internal control points (Δz)

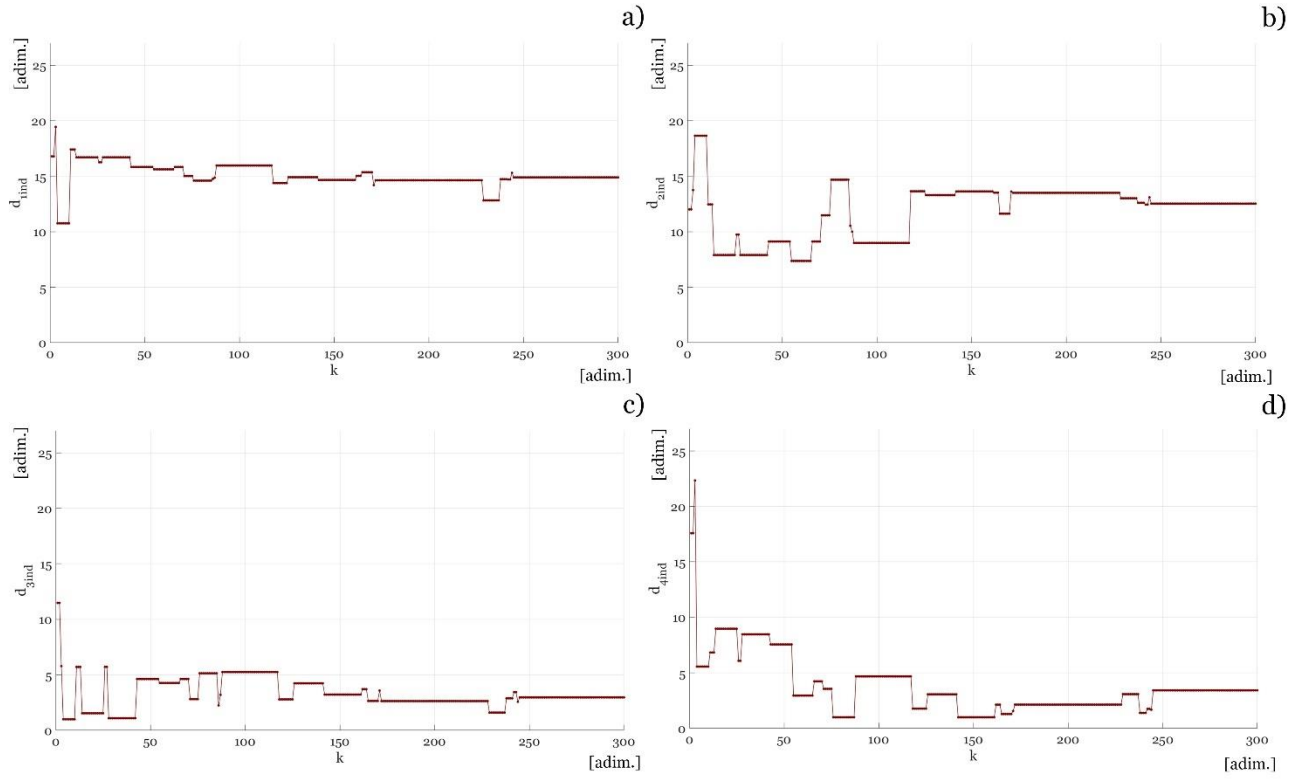

Figure 5. 55 Convergence curves of size design variables (i.e. indexes identifying the element group diameters in a list of commercial circular hollow cross-sections) for the CASE 1: (a) index identifying the bottom chord diameter; (b) index identifying the top chord diameter; (c) index identifying the diameter of diagonals; (d) index identifying the diameter of verticals

5.3.4.2 Case 2 optimal solution

As a second case, the optimization problem of a "hingeless" truss arch with a span of 80 meters (parametrically defined by taking advantage of *Cubic Rational Bézier curves*, as illustrated in *Figure 5. 46*) and subjected to three vertical load cases (in *Figure 5. 47*) was addressed and solved. All assumed design variables, with corresponding lower and upper bounds, are indicated in *Table 5. 22*.

In this regard, *Figure 5. 56* shows the shape of the optimized arch under consideration, characterized by a minimum volume of 1.194 m^3 (i.e. the objective function), corresponding to a self-weight per unit length of 1.149 kN/m. Furthermore, the optimal arch has a total height of 25.70 m and a rise of 23.15 m (as indicated in *Figure 5. 56*).

Therefore, the optimal arch here considered, has a resulting "rise-to-span ratio" equal to 1/3.46 and a "height-to-span ratio" equal to 1/3.11. Moreover, similarly to the CASE 1, the arch in *Figure 5. 56* is still characterized by a small "crown depth", about 2.55 m, and a much higher "base depth" of 4.48 m, but leading to a greater "crown depth-to-span ratio", equal to 1/31.36 and a smaller "base depth-to span ratio" about 1/17.86. Consequently, the arch under consideration showed to be less tapered from its crown to its ends compared to the previous case (discussed in *§5.3.4.1*),

since its "taper ratio" (i.e. the "crown-depth" divided by the "base-depth" of the arch) has grown to 1/1.76.

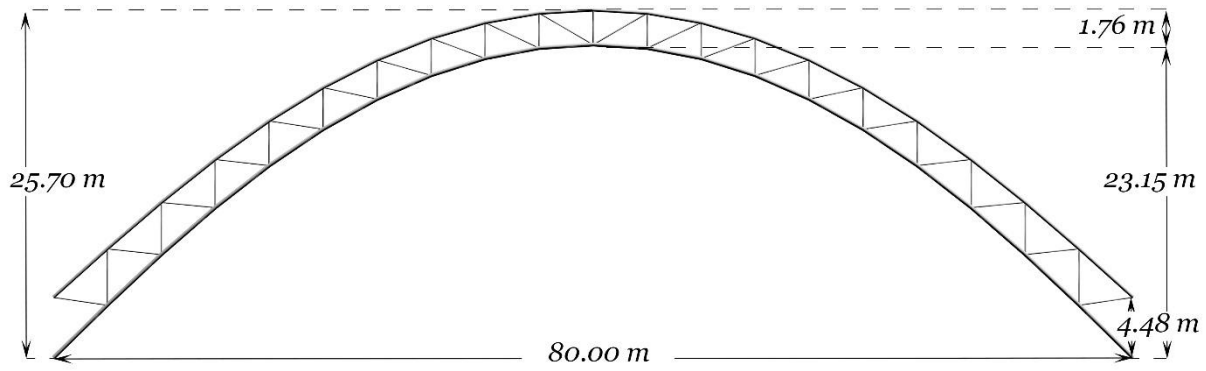

Figure 5. 56 Front view of the optimized truss arch with main dimensions (CASE 2 optimal solution)

The optimal values of topology and shape design variables are pointed out in *Table 5. 28,* thus showing that the arch is characterized by an arch span subdivision number (n_{int}) equal to 20. The truss arch under consideration resulted to be composed by 81 steel tubular elements and 42 pinned joints. Shape design variables in *Table 5. 28* determined the form of the optimal truss arch under consideration, by defining coordinates and weight factors of control points of upper and lower *thrid-degree Rational Bézier* arcs. On the other hand, the diameter, the minimum and maximum thicknesses for each element group are indicated in *Table 5. 29*.

Table 5. 28 Topology and shape optimization results for the CASE 2: optimal values of topology and shape design variables

Topology optimization results			
Design Variable (DV)	**Type of DV**	**Best value**	**Unit**
n_{int}	*topology*	20	$[adim.]$
Shape optimization results			
Design Variable (DV)	**Type of DV**	**Best value**	**Unit**
x_{P1l}	*shape*	34.8715	$[m]$
z_{P1l}	*shape*	38.3198	$[m]$
w_{P1l}	*shape*	0.5084	$[adim.]$
z_{P0u}	*shape*	4.4800	$[m]$
Δz	*shape*	1.2876	$[m]$

As in the previous case (discussed in *§5.3.4.1*) the lower chord elements required a greater diameter compared to other elements, because they are subjected to greater axial forces and bending moments (as shown in *Figure 5. 57*).

In particular, it was found that the lower chord was subjected to a compressive axial force varying from 715 kN to 1702 kN (see *Figure 5. 57(a)*) as well as to bending moments (whose diagram is illustrated in *Figure 5. 57(b)*) varying from 0.84 $kN.m$ to 1.97 $kN.m$.

Conversely, the upper chord supports a compressive axial force varying between 674 kN to 871 kN, as well as bending moments varying from 0.55 $kN.m$ to 1.02 $kN.m$. Moreover, diagonal and vertical members are subjected to tensile axial forces (varying from 31 kN to 175 kN in diagonal, and from 44 kN to 161 kN in vertical bars), whereas diagonal tubes also withstand bending moment actions varying from 0.16 $kN.m$ to 0.31 $kN.m$.

Table 5. 29 Size optimization results for the CASE 2: optimal diameters and thicknesses of circular hollow cross-sections

Size optimization results					
Element groups	**Type of DV**	**Diameter** d_i	**Min. thickness** t_i	**Max. thickness** t_i	**Unit**
Bottom chord	*size*	0.2985	0.0059	0.01	$[m]$
Top chord	*size*	0.2445	0.0054	0.0063	$[m]$
Diagonals	*size*	0.108	0.0036	0.0059	$[m]$
Verticals	*size*	0.108	0.0036	0.0059	$[m]$

The arch diagram represented in *Figure 5. 58* validates the feasibility of the optimal solution here analysed, by indicating the maximum "utilization ratio" ($\max_{LC} Util_i^{LC}$) characterizing each i^{th} –element for the envelope of all load combinations, which proved to be always less than 0.99 (as required by the constraint function, corresponding to Eq. (47)). That diagram also demonstrates that most of elements are characterized by a "Demand/Capacity ratio" larger than 0.7. Furthermore, a "total utilization ratio" ($Util_{tot}$) expressing an estimated overall percentage of the material exploitation of the whole structure was evaluated as a weighted average of "Demand/Capacity ratios" ($\max_{LC} Util_i^{LC}$) shown in *Figure 5. 58,* with respect to the weight of each member (Eq. (51)).

More specifically, a value of "total utilization ratio" ($Util_{tot}$) about 71.4 % has been achieved in the considered case, once again ensuring a satisfactory level of structural performance of the optimized steel truss arch.

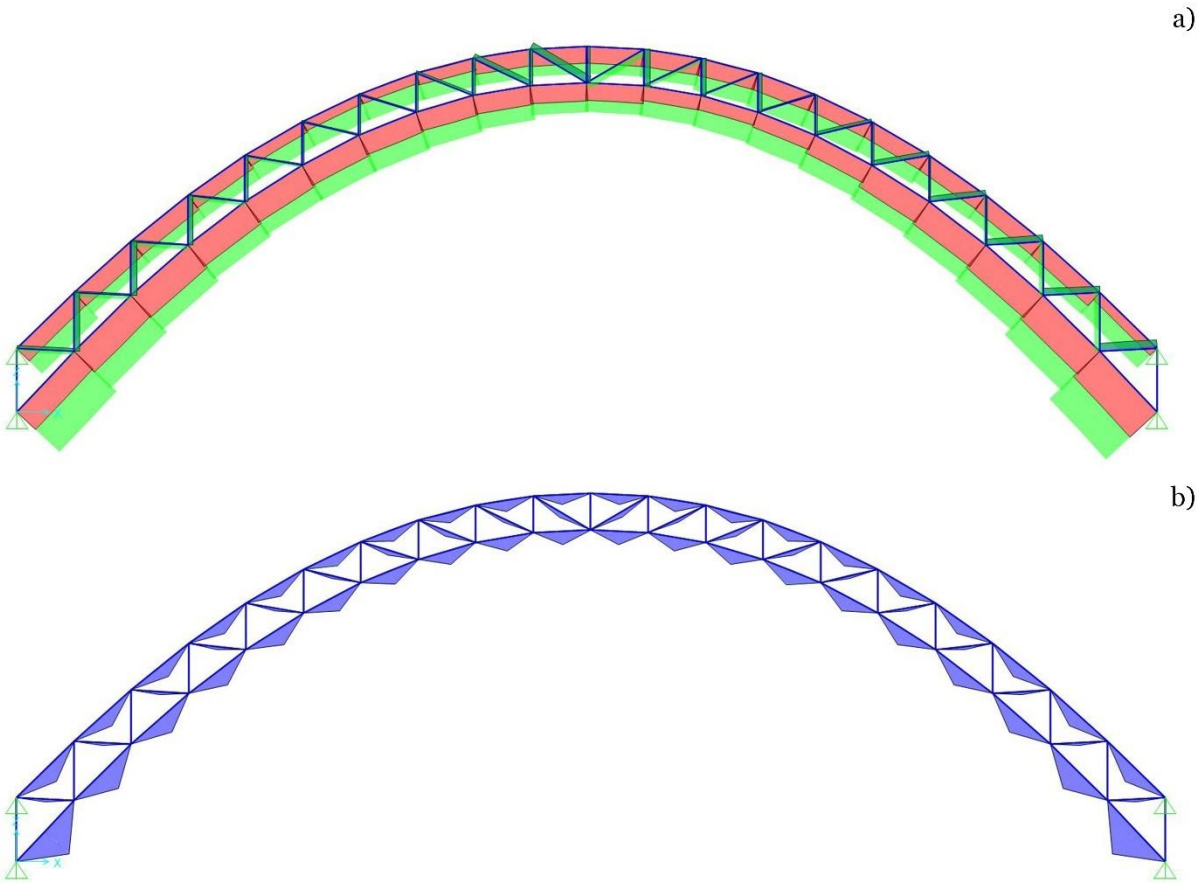

Figure 5. 57 *Finite Element Analysis (FEA) results for the CASE 2: (a) axial force diagram; (b) bending moment diagram*

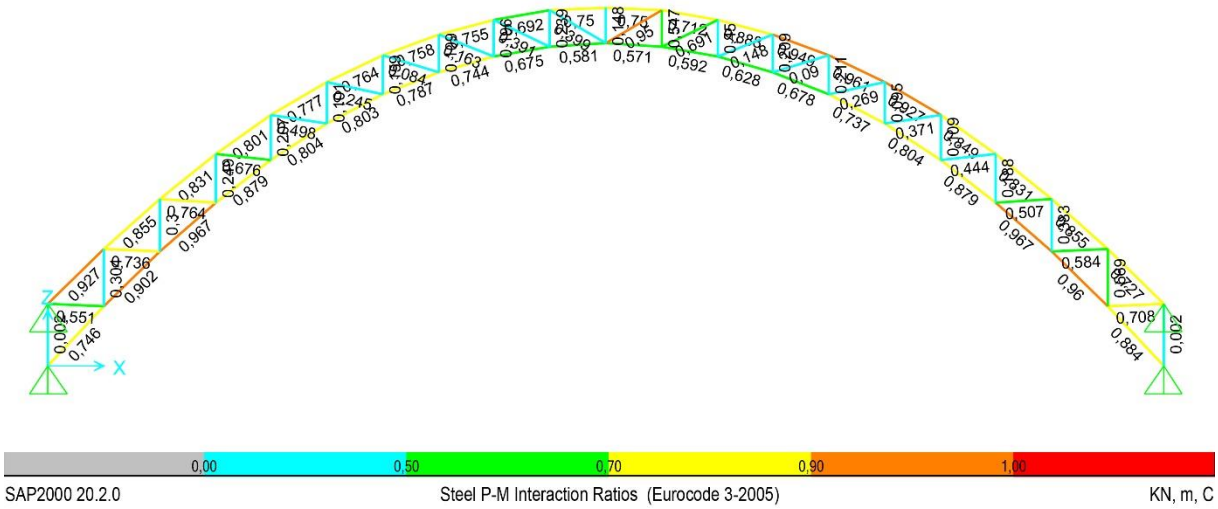

Figure 5. 58 *Finite Element Analysis (FEA) results for the CASE 2: Demand/Capacity ratio (also called "utilization ratio") diagram of the optimal solution for the envelope of all load cases*

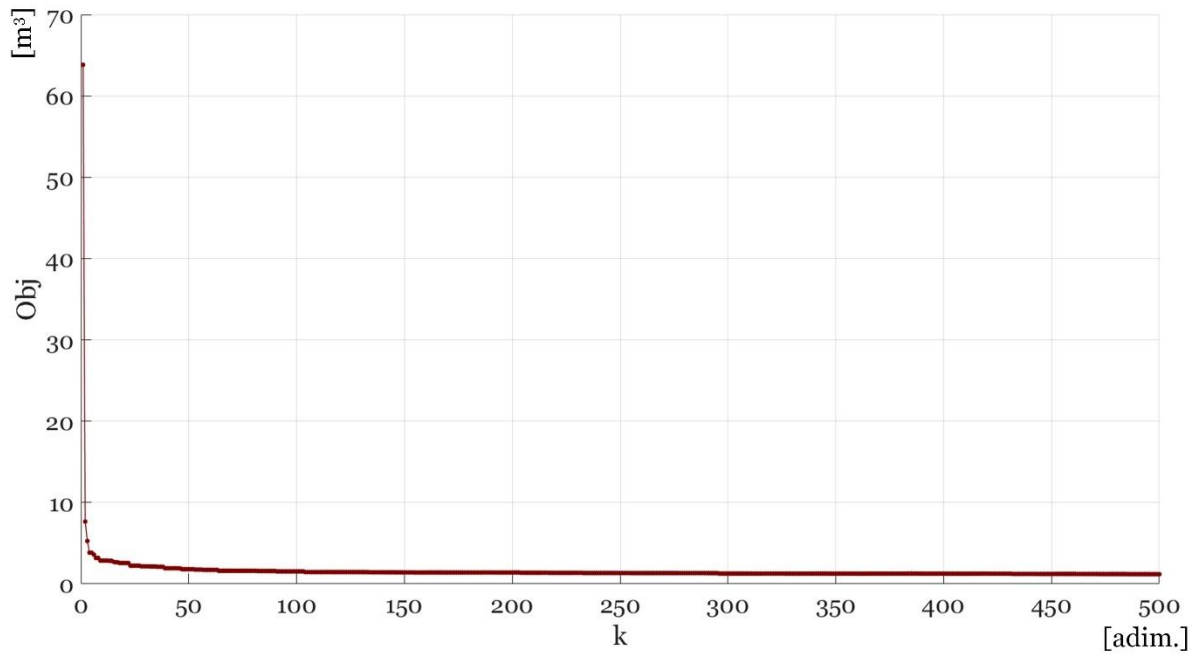

Figure 5. 59 *Convergence curve of the Objective (Obj) function (i.e. the volume of the arch) for all "generations" (for the CASE 2)*

The arch diagram represented in *Figure 5. 58* validates the feasibility of the optimal solution here analysed, by indicating the maximum "utilization ratio" ($\max_{LC} Util_i^{LC}$) characterizing each i^{th} –element for the envelope of all load combinations, which proved to be always less than 0.99 (as required by the constraint function, corresponding to Eq. (47)). That diagram also demonstrates that most of elements are characterized by a "Demand/Capacity ratio" larger than 0.7.

Furthermore, a "total utilization ratio" ($Util_{tot}$) expressing an estimated overall percentage of the material exploitation of the whole structure was evaluated as a weighted average of "Demand/Capacity ratios" ($\max_{LC} Util_i^{LC}$) shown in *Figure 5. 58,* with respect to the weight of each member (Eq. (51)). More specifically, a value of "total utilization ratio" ($Util_{tot}$) about 71.4 % has been achieved in the considered case, once again ensuring a satisfactory level of structural performance of the optimized steel truss arch.

On the other hand, *Figure 5. 59* shows the convergence curve of the "objective function" (i.e. the total volume of the structure) to be minimized, showing that the objective function tends to become almost flat from the 100^{th} generation, thus decreasing extremely slowly from this point.

The "zig-zag" trend of the "stagnation function" (in *Figure 5. 60(a)*) more clearly shows when any improvement in the objective function occurs or not. In this specific case, the "stagnation function" showed to have the greatest peaks from the 327^{th} to the 390^{th} generation, after which it continued to improve very slowly.

Figure 5. 60(b) shows the history of the "unfeasibility function" (ρ^k), which was introduced in section *§5.2.4.1* and defined by Eq. (52), as a ratio between "unfeasible individuals" (Unf^k) and all individuals (Pop^k) of a k^{th} –generation. It has been found that the optimization process produced and evaluated only feasible candidate solutions from the 30^{th} generation onwards (as shown in *Figure 5. 60(b)*).

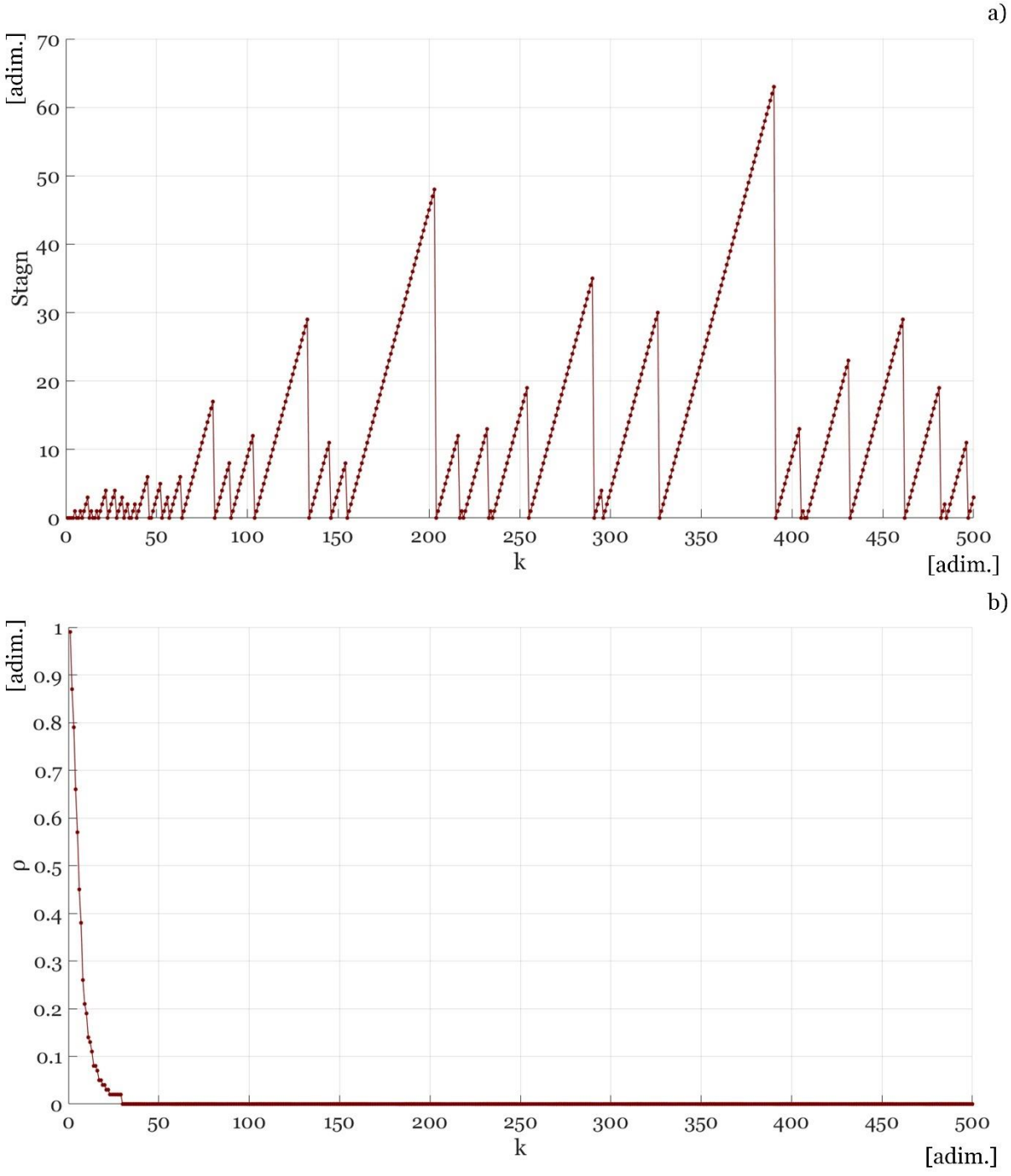

Figure 5. 60 *History of optimization functions (for the CASE 2): (a) stagnation function; (b) "unfeasibility function" (ρ)*

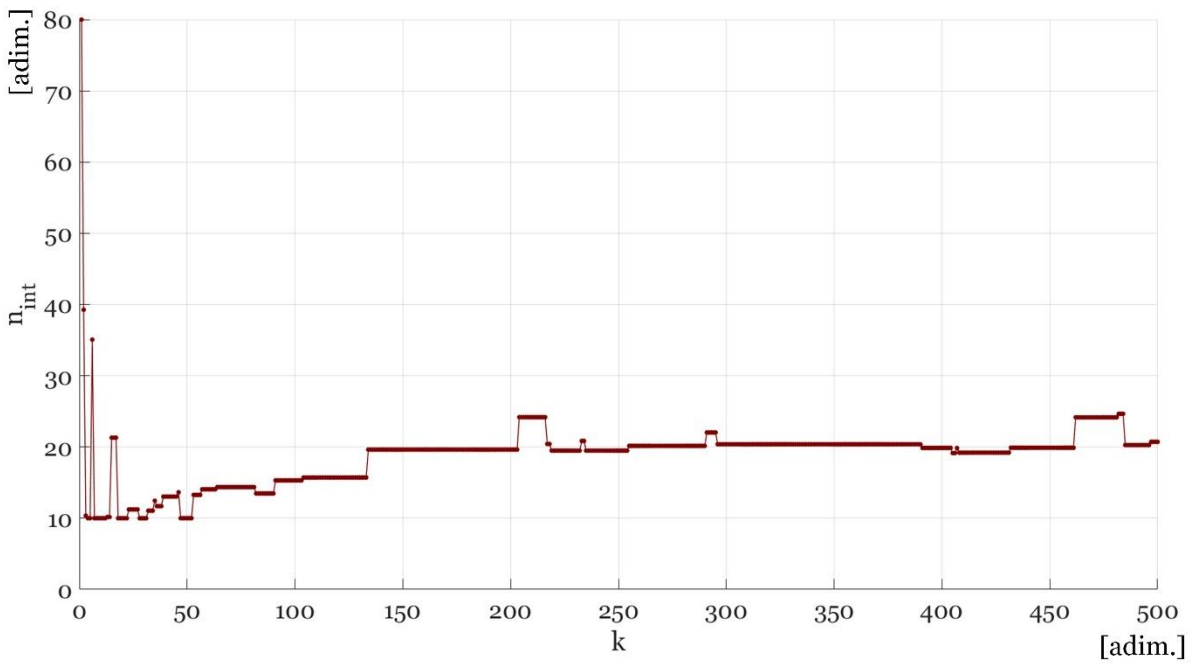

Figure 5. 61 Convergence curve of the topology design variable (n_{int}) for the CASE 2

The convergence curves of all design variables can further validate the reliability of results here discussed.

Among these, the topology design variable (n_{int}) has a great importance by a constructive point of view, since its value indirectly determines the number of elements and joints of the structure.

About that, *Figure 5. 61* shows the history of n_{int}. This parameter was defined as a continuous variable between 10 and 80 (to be later rounded to the nearest even integer). The convergence curve shows that since the first generations its best value only tends to oscillate between measures extremely close to the optimal one (to which 20 was the nearest even integer).

The convergence graphs of shape design variables (defining the shape of lower and upper arch chords parametrized by *third-degree Rational Bézier curves*) are presented in *Figure 5. 62* to prove the reliability of results, despite the large number and the variety of design variables. In the same way, a good convergence trend was also obtained for the size design variables determining the element group diameters (whose curves are shown in *Figure 5. 63*).

It can be easily noted that approximately after the first 150^{th} generations, the best values of all design variables tend to vary between rational numbers very close to the optimal ones finally obtained (summarized in *Table 5. 28* and in *Table 5. 29*). However, it is worth highlighting that convergence curves of design variables never become flat because the objective function never stops to improve even if extremely slowly.

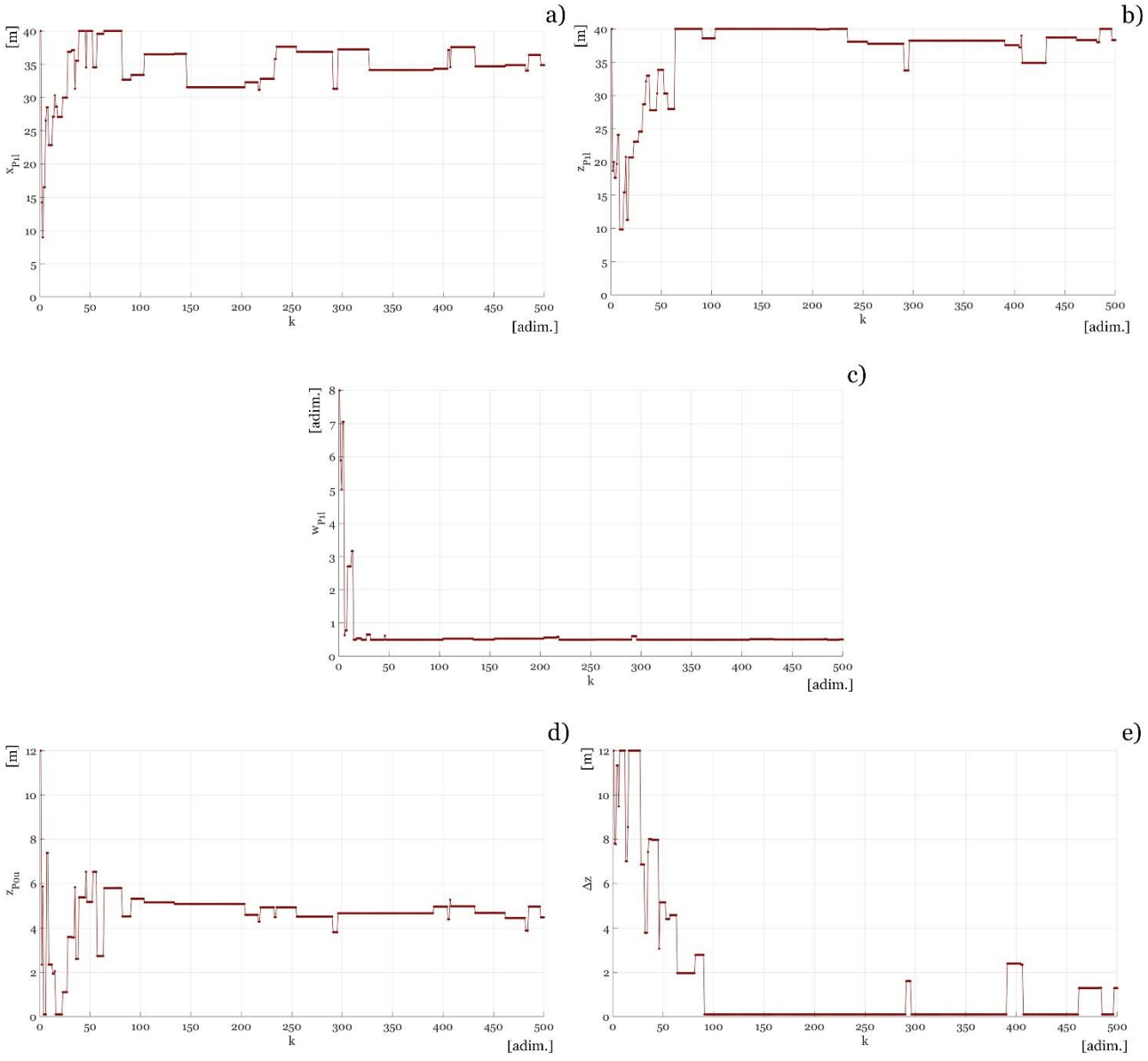

Figure 5. 62 Convergence curves of the shape design variables (variable parameters of third-degree rational Bézier curves) for the CASE 2: (a) x −coordinate of the second control point (x_{P1l}) of the bottom arched chord; (b) z −coordinate of the second control point (z_{P1l}) of the bottom arched chord; (c) weight factor of the second control point (w_{P1l}) of the bottom arched chord; (d) z −coordinate of the first control point (z_{P0u}) of the top arched chord;(e) the difference between the z −coordinates (in absolute value) of the top and bottom chord internal control points (Δz)

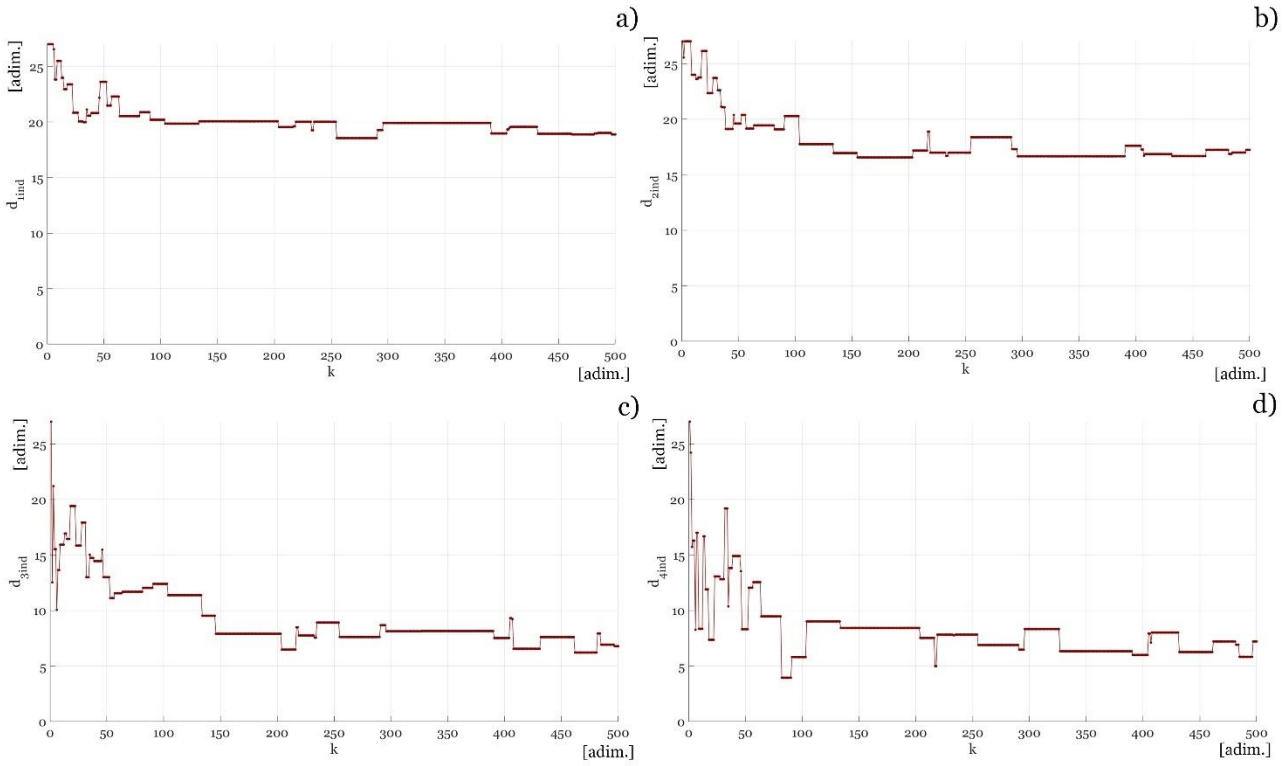

Figure 5. 63 Convergence curves of size design variables (i.e. indexes identifying the element group diameters in a list of commercial circular hollow cross-sections) for the CASE 2: (a) index identifying the bottom chord diameter; (b) index identifying the top chord diameter; (c) index identifying the diameter of diagonals; (d) index identifying the diameter of verticals

5.3.4.3 Case 3 optimal solution

In the present section, the solution of the optimization problem of a "hingeless" truss arch with a span of 120 meters, parametrically defined as shown in section *§5.3.1* and subjected to boundary conditions assumed in *§5.3.3*, is discussed. It was found an optimal truss arch with a minimum volume about 2.773 m^3, equivalent to a self-weight of 1.779 kN/m. All design variables, classified by type (topology, shape and size) with relative lower and upper bounds are indicated in *Table 5. 23*.

Figure 5. 64 shows the optimal shape of the truss arch under consideration with main dimensions, showing that it is characterized by a total height of 41.71 m and a rise of 38.02 m, as well as by a resulting "height-to-span ratio" and a "rise-to-span ratio" equal to 1/2.88 and 1/3.16, respectively. Moreover, it can be easily noted in *Figure 5. 64* that the arch depth at its crown (equal to 3.69 m) is still considerably smaller than its "base depth" (equal to 5.93 m).

The arch under consideration is therefore characterized by a "crown depth-to-span ratio" equal to 1/32.48, a "base depth-to-span ratio" corresponding to 1/20.22, as well as by a consequent "taper ratio" equal to 1/1.61, hence slightly larger than that one of the CASE 2 solution.

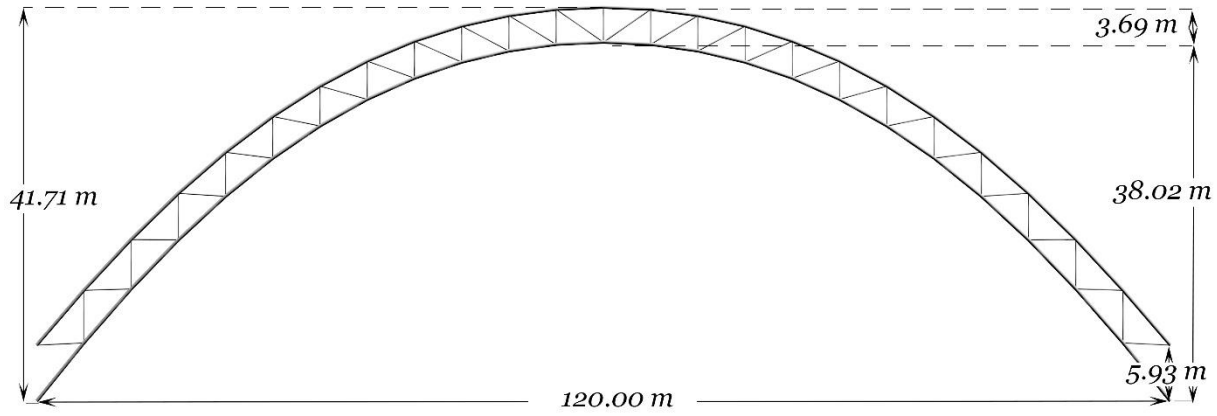

Figure 5. 64 *Front view of the optimized truss arch with main dimensions (CASE 3 optimal solution)*

The optimal values of topology and shape design variables are indicated in *Table 5. 30*, showing that the span of the considered arch resulted to be divided into 24 equal intervals ($n_{int} = 24$). The truss arch in *Figure 5. 64* is therefore composed by 97 elements and 50 pinned joints.

The values of shape design variables define the coordinates and weight factors of control points of upper and lower *thrid-degree Rational Bézier* arcs, thus determining the optimal shape of the considered truss arch.

Table 5. 30 *Topology and shape optimization results for the CASE 3: optimal values of topology and shape design variables*

Topology optimization results			
Design Variable (DV)	**Type of DV**	**Best value**	**Unit**
n_{int}	*topology*	24	$[adim.]$
Shape optimization results			
Design Variable (DV)	**Type of DV**	**Best value**	**Unit**
x_{P1l}	*shape*	33.8728	$[m]$
z_{P1l}	*shape*	43.2732	$[m]$
w_{P1l}	*shape*	2.4112	$[adim.]$
z_{P0u}	*shape*	5.9351	$[m]$
Δz	*shape*	3.3845	$[m]$

On the other hand, the diameter, the minimum and maximum thicknesses for each element group are indicated in *Table 5. 31*, showing that the lower chord elements required a slightly larger diameter compared to upper chord elements, because they are subjected to greater axial forces and bending moments (as shown in *Figure 5. 65*). For the same reason, diagonal and verticals

tubes required considerably smaller diameters and thicknesses compared to the elements composing the arched ribs.

Table 5. 31 Size optimization results for the CASE 3: optimal diameters and thicknesses of circular hollow cross-sections

Size optimization results					
Element groups	**Type of DV**	**Diameter d_i**	**Min. thickness t_i**	**Max. thickness t_i**	**Unit**
Bottom chord	*size*	0.368	0.0063	0.0125	$[m]$
Top chord	*size*	0.3556	0.0063	0.0088	$[m]$
Diagonals	*size*	0.1524	0.004	0.0071	$[m]$
Verticals	*size*	0.1143	0.0036	0.0063	$[m]$

Indeed, size optimization results are validated by the internal force diagrams shown in *Figure 5. 65*. In particular, the lower chord resulted to be subjected to a compressive axial force varying from 729 kN to 2267 kN (see *Figure 5. 65(a)*) as well as to bending moments (whose diagram is illustrated in *Figure 5. 65 (b)*) varying from 1.70 $kN.m$ to 5.22 $kN.m$.

Conversely, the upper chord showed to withstand compressive axial forces varying between 1010 kN to 1749 kN, as well as bending moments included between 1.70 $kN.m$ and 3.37 $kN.m$. Moreover, diagonal and vertical members bear tensile axial forces (varying from 58 kN to 263 kN in diagonal, and from 32 kN to 312 kN in vertical bars), whereas diagonal tubes also withstand bending moment actions varying from 0.42 $kN.m$ to 0.86 $kN.m$.

In *Figure 5. 66,* the maximum "utilization ratio" ($\max_{LC} Util_i^{LC}$) for the envelope of all load combinations (LC) is indicated for each i^{th} –element, showing to be always less than 0.99 (as required by the constraint function, expressed by Eq. (47)). That diagram thus demonstrates the feasibility of the obtained solution, and also that most of elements are characterized by a "Demand/Capacity ratio" larger than 0.7.

Furthermore, a weighted average of all "Demand/Capacity ratios" ($\max_{LC} Util_i^{LC}$) shown in *Figure 5. 66,* with respect to the weight of each i^{th} –member, has been evaluated as a "total utilization ratio" ($Util_{tot}$) to estimate an overall percentage of material exploitation of the whole structure (see Eq. (51)). A satisfactory level of structural performance has been therefore achieved since a value of "total utilization ratio" ($Util_{tot}$) about 70.0 % has been obtained.

The reliability of the obtained results can be proved by the convergence curves of the "objective function" and design variables that more characterized the optimized truss arch under consideration.

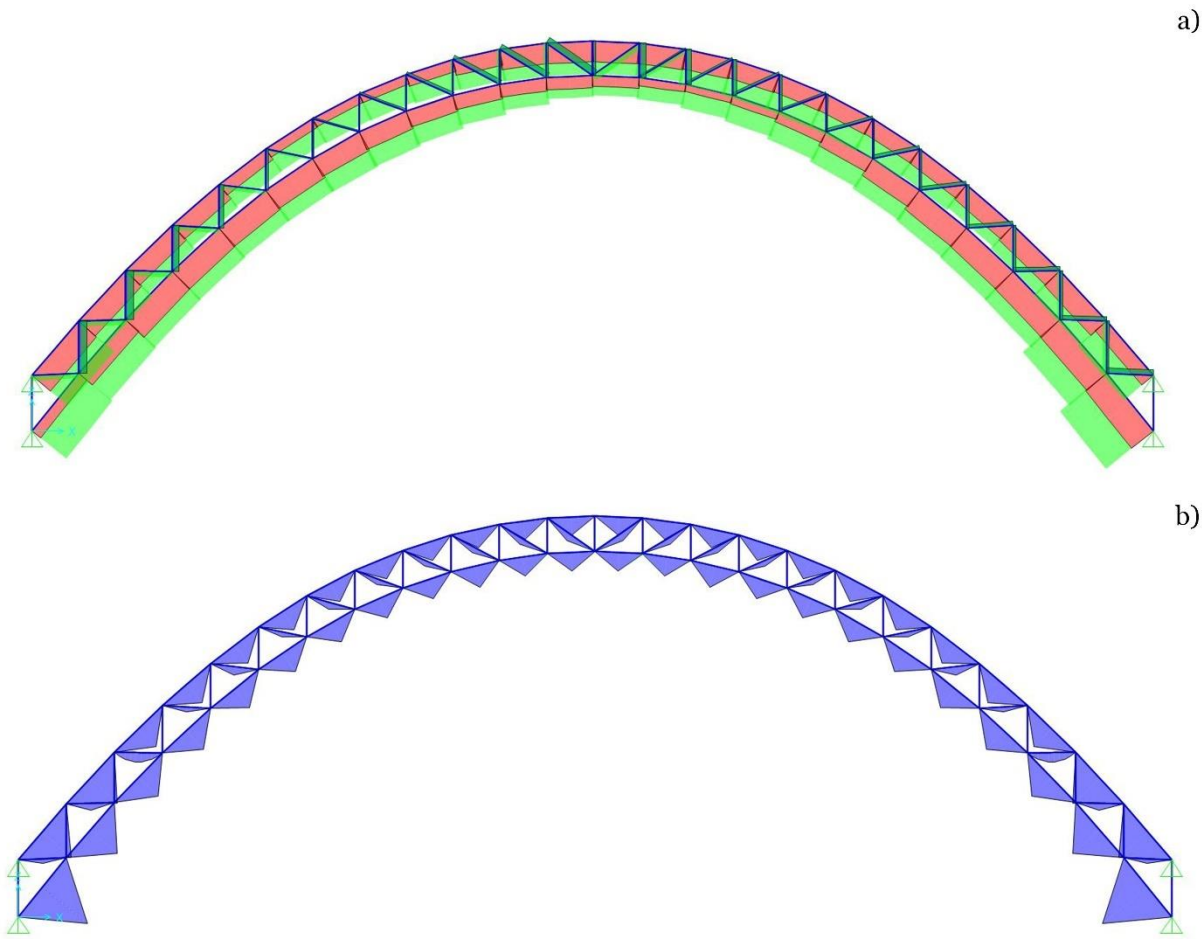

Figure 5. 65 Finite Element Analysis (FEA) results for the CASE 3: (a) axial force diagram; (b) bending moment diagram

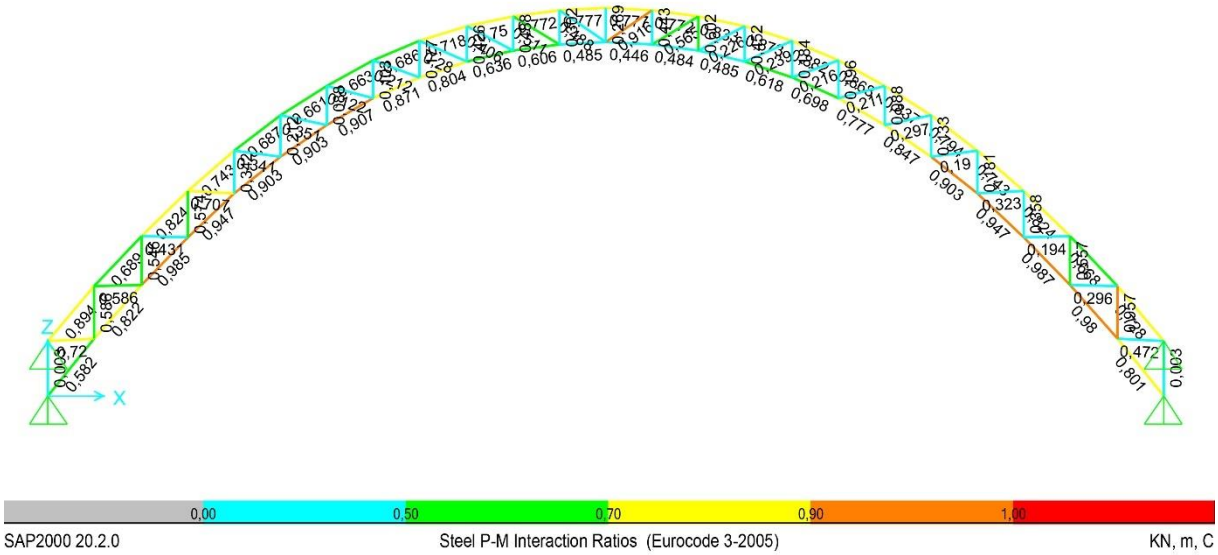

Figure 5. 66 Finite Element Analysis (FEA) results for the CASE 3: Demand/Capacity ratio (also called "utilization ratio") diagram of the optimal solution for the envelope of all load cases

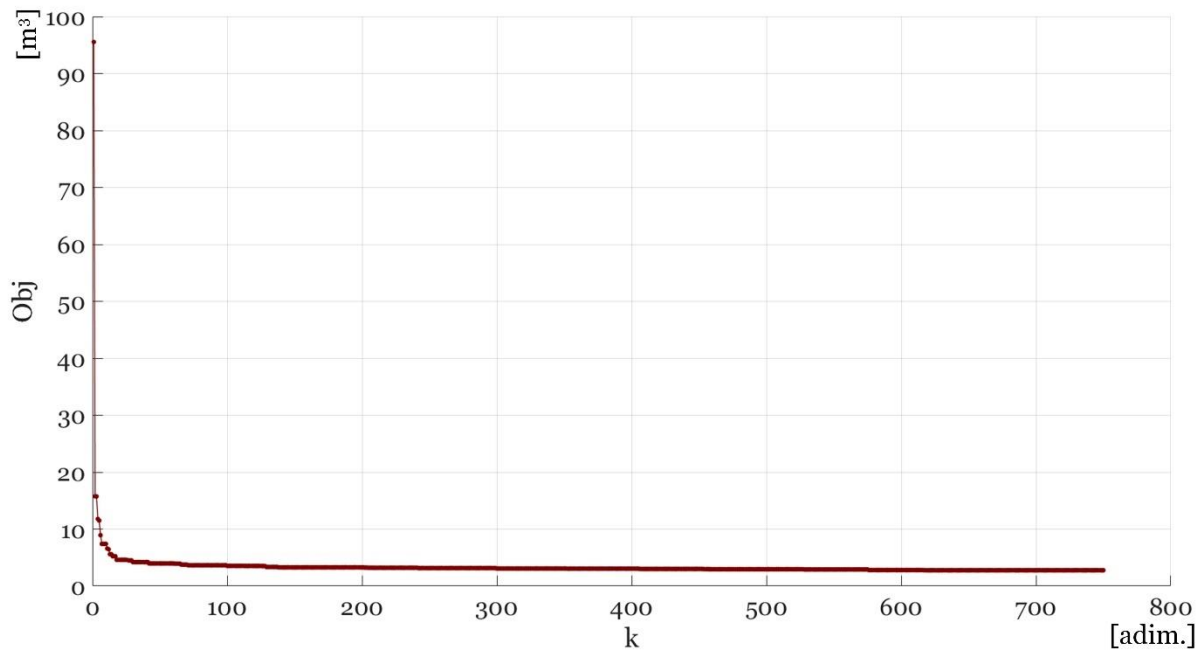

Figure 5. 67 *Convergence curve of the Objective (Obj) function (i.e. the volume of the arch) for all "generations" (for the CASE 3)*

In this regard, *Figure 5. 67* shows the convergence curve of the "objective function" (i.e. the total volume of the structure) to be minimized.

The curve in *Figure 5. 67,* which represents the best values of the "objective function" obtained at each generation of candidate solutions, seems becoming rapidly flat since it starts from an extremely high value, after which it first decreases very rapidly and then much slower. The "objective function" stops to significantly improve approximately from the 500^{th} generation.

The "zig-zag" trend of the "stagnation function" (in *Figure 5. 68(a)*) more clearly shows that from the 617^{th} generation onwards there is no longer any improvement in the "objective function".

On the other hand, *Figure 5. 68(b)* shows the history of the "unfeasibility function" (ρ^k), which produces values between 0 and 1, since it was defined as a ratio between "unfeasible individuals" (Unf^k) and all individuals (Pop^k) of a k^{th} –generation (see Eq. (52)). Despite the large dimensions of the optimization problem under consideration, the optimization process produced and evaluated only feasible candidate solutions from the 37^{th} generation onwards (as shown in *Figure 5. 68(b)*).

The convergence curves of all design variables can further validate the goodness of results here analysed.

Among these, the topology design variable (n_{int}) has a great importance by a constructive point of view, since its value indirectly determines the number of elements ($4n_{int} + 1$) and joints ($2n_{int} + 2$) of the structure. About that, *Figure 5. 69* shows the history of n_{int}. This parameter was defined as a continuous variable between 10 and 120 (to be later rounded to the nearest even integer). The convergence curve shows that from the 80^{th} generation, the value of n_{int} only varies between 24 and 26, until its optimal value closer to 24 was found.

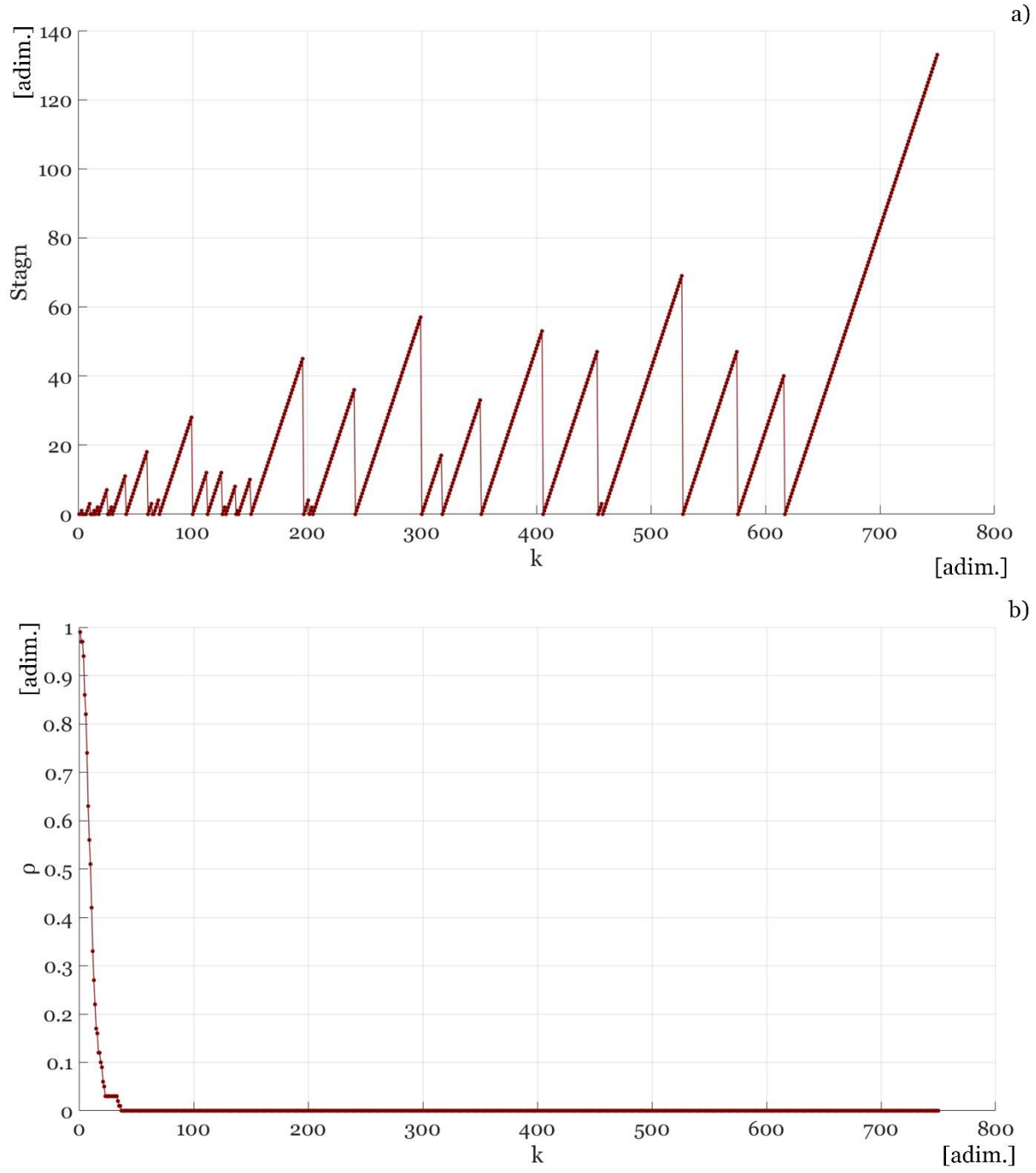

Figure 5. 68 History of optimization functions (for the CASE 3): (a) stagnation function; (b) "unfeasibility function" (ρ)

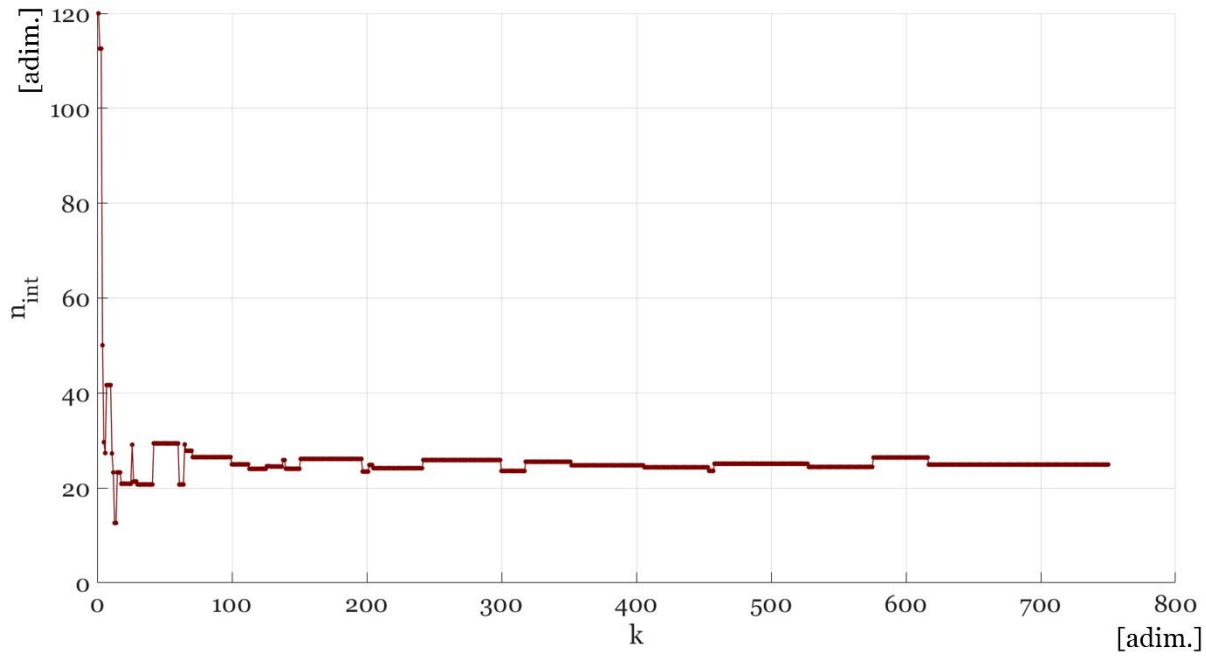

Figure 5. 69 Convergence curve of the topology design variable (n_{int}) for the CASE 3

The convergence diagrams of shape design variables (defining the shape of lower and upper arch chords parametrized by *third-degree Rational Bézier curves*) are presented in *Figure 5. 70* to prove the reliability of results, despite the large number and the variety of design variables.

For the same purpose, the convergence curves of size design variables determining the diameters characterizing each element group are represented in *Figure 5. 71*.

It is worth to remark that the optimal values of topology, shape and size design variables (summarized in *Table 5. 30* and in *Table 5. 31*) have been found at the 617^{th} generation, thus confirming what previously emerged from the history curve of the "stagnation function". This means that for more than 100 generations, the obtained final solution resulted to be the best one among all 100 candidate solutions of each generation.

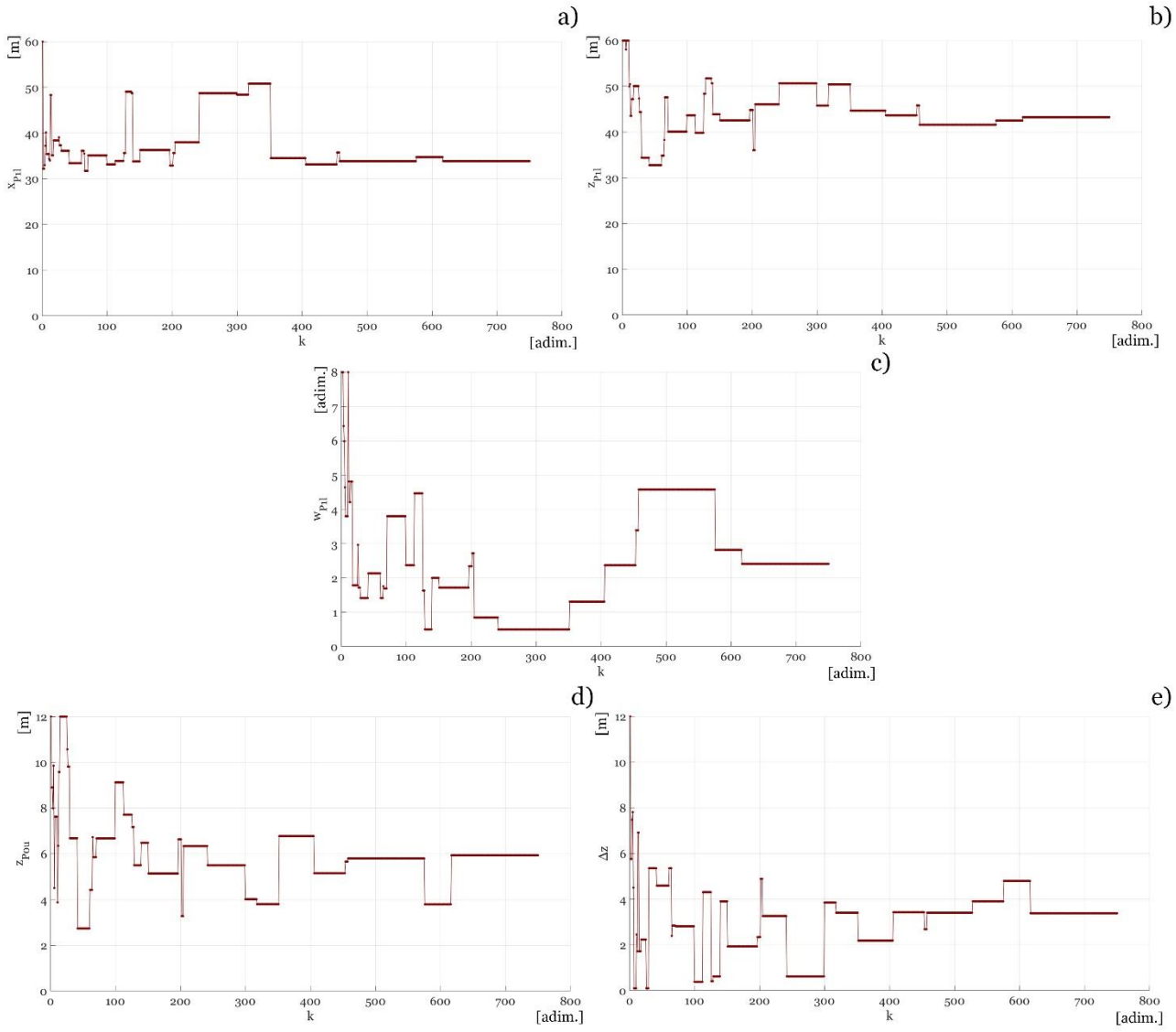

Figure 5. 70 Convergence curves of the shape design variables (variable parameters of third-degree rational Bézier curves) for the CASE 3: (a) x −coordinate of the second control point (x_{P1l}) of the bottom arched chord; (b) z −coordinate of the second control point (z_{P1l}) of the bottom arched chord; (c) weight factor of the second control point (w_{P1l}) of the bottom arched chord; (d) z −coordinate of the first control point (z_{P0u}) of the top arched chord;(e) the difference between the z −coordinates (in absolute value) of the top and bottom chord internal control points (Δz)

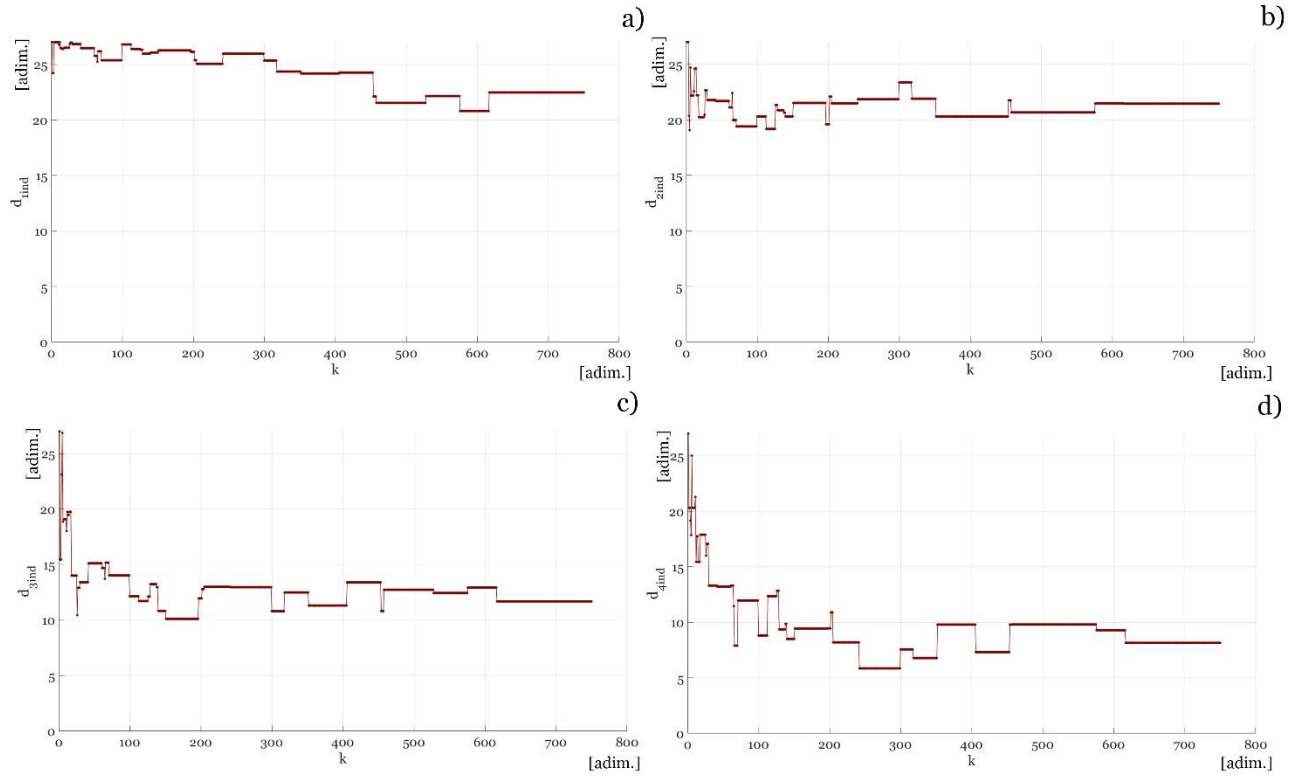

Figure 5. 71 Convergence curves of size design variables (i.e. indexes identifying the element group diameters in a list of commercial circular hollow cross-sections) for the CASE 3: (a) index identifying the bottom chord diameter; (b) index identifying the top chord diameter; (c) index identifying the diameter of diagonals; (d) index identifying the diameter of verticals

5.3.4.4 Case 4 optimal solution

As a last numerical case, the optimization problem of a "hingeless" truss arch with a span of 160 *m*, made of steel tubular elements, has been successfully solved under three vertical load combinations. As already stated in section *§5.3.2*, the problem was defined to minimize the total volume of the structure according with strength constraints, assuming a unique set of topology, shape and size design variables, indicated in *Table 5. 24* (with relative lower and upper limits). The present section aims to illustrate in detail the so-obtained solution.

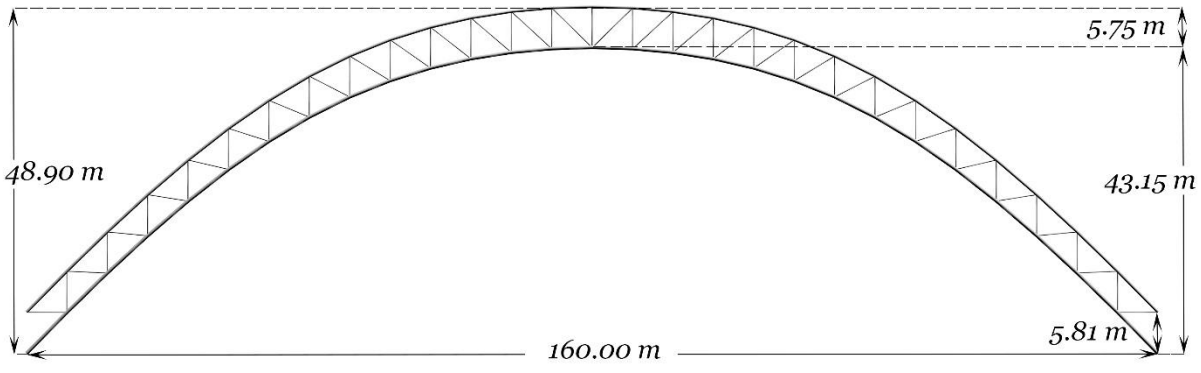

Figure 5. 72 Front view of the optimized truss arch with main dimensions (CASE 4 optimal solution)

Table 5. 32 *Topology and shape optimization results for the CASE 4: optimal values of topology and shape design variables*

Topology optimization results			
Design Variable (DV)	**Type of DV**	**Best value**	**Unit**
n_{int}	*topology*	28	$[adim.]$
Shape optimization results			
Design Variable (DV)	**Type of DV**	**Best value**	**Unit**
x_{P1l}	*shape*	45.3013	$[m]$
z_{P1l}	*shape*	46.7272	$[m]$
w_{P1l}	*shape*	4.0243	$[adim.]$
z_{P0u}	*shape*	5.8139	$[m]$
Δz	*shape*	5.7462	$[m]$

The optimal solution illustrated in *Figure 5. 72* has a volume of 4.839 m^3, and therefore a resulting self-weight of 2.328 kN/m. The arch is characterized by a total height of 48.904 m and a clear rise of 43.153 m, as well as by an almost constant depth, varying from 5.751 m to 5.814 m from its crown to its ends, determining a "taper ratio" almost equal to 1. The arch under consideration is therefore typified by a "height-to-span ratio" and a "rise-to-span ratio" of 1/3.27 and 1/3.71, respectively, as well as by a "crown depth-to-span ratio" and a "base depth-to-span ratio" almost the same and equal to 1/27.82 and 1/27.52, in that order. The flattened shape of the arch represented in *Figure 5. 72*, has been determined by the optimal values obtained for topology and shape design variables indicated in *Table 5. 33*.

Among this, a number of equal intervals into which the arch span is divided (n_{int}) equal to 28 was found, determining a total number of elements equal to 113 and 58 joints.

Table 5. 33 *Size optimization results for the CASE 4: optimal diameters and thicknesses of circular hollow cross-sections*

Size optimization results					
Element groups	**Type of DV**	**Diameter d_i**	**Min. thickness t_i**	**Max. thickness t_i**	**Unit**
Bottom chord	*size*	0.508	0.0071	0.0125	$[m]$
Top chord	*size*	0.4064	0.0063	0.008	$[m]$
Diagonals	*size*	0.1683	0.004	0.008	$[m]$
Verticals	*size*	0.1524	0.004	0.008	$[m]$

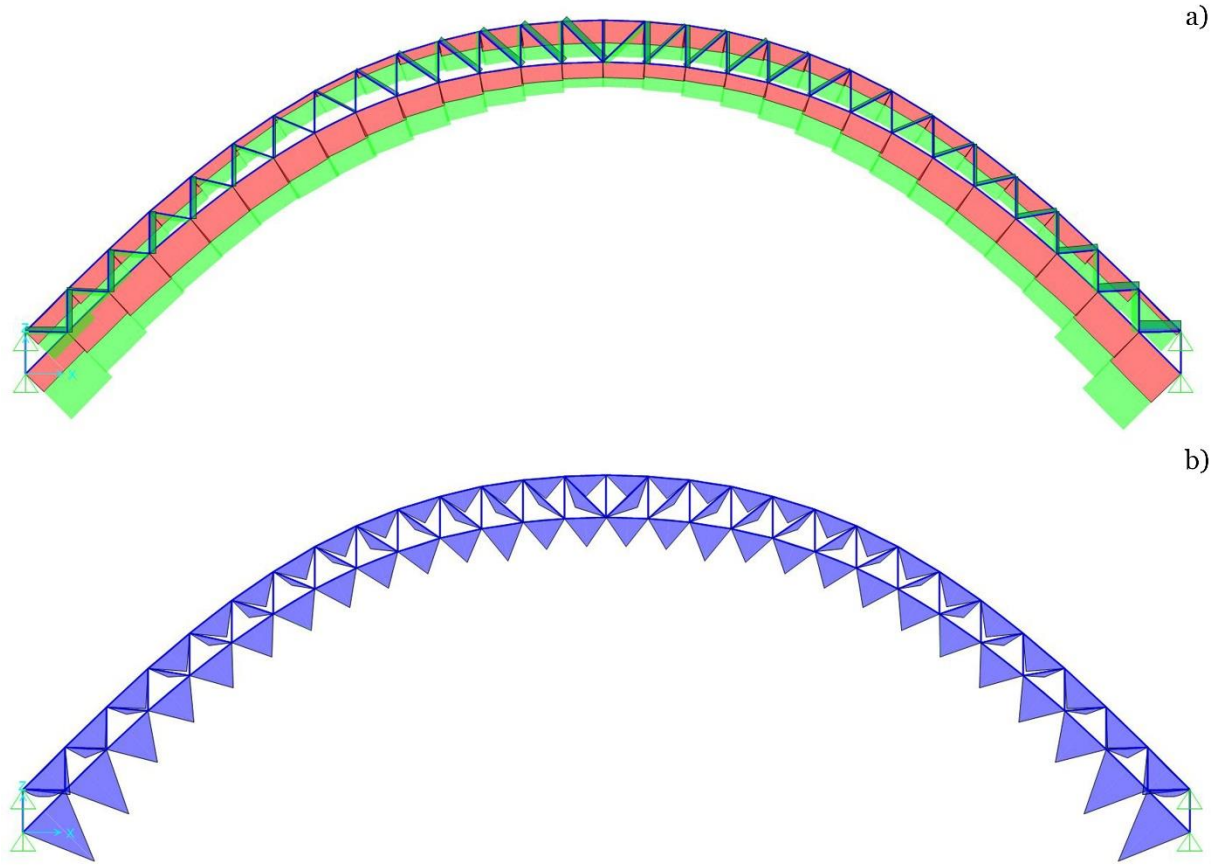

Figure 5. 73 Finite Element Analysis (FEA) results for the CASE 4: (a) axial force diagram; (b) bending moment diagram

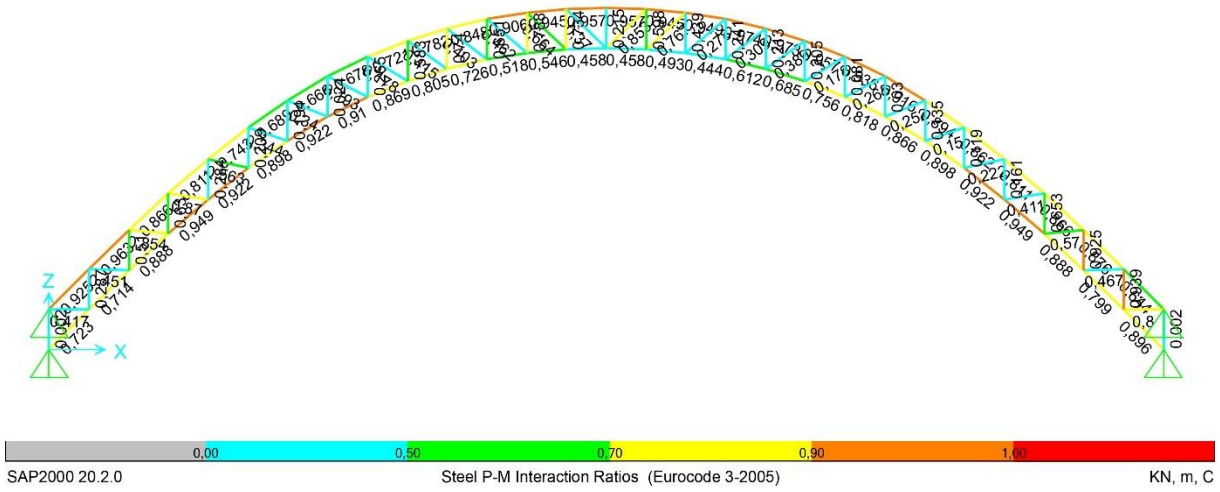

Figure 5. 74 Finite Element Analysis (FEA) results for the CASE 4: Demand/Capacity ratio (also called "utilization ratio") diagram of the optimal solution for the envelope of all load cases

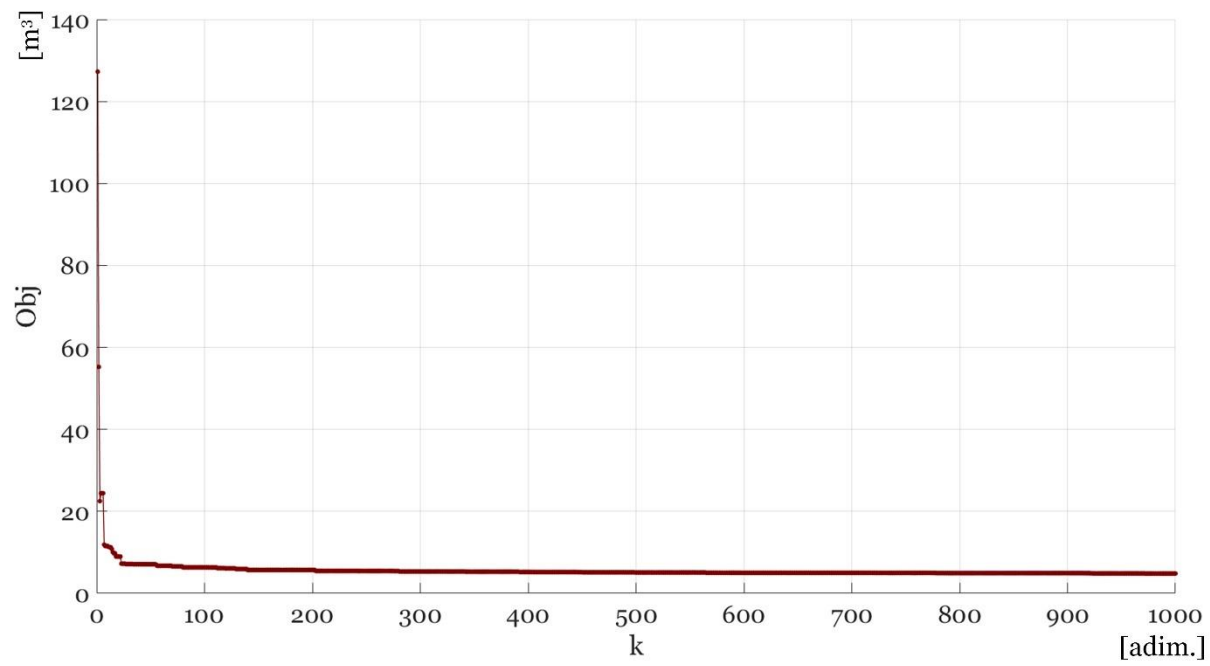

Figure 5. 75 *Convergence curve of the Objective (Obj) function (i.e. the volume of the arch) for all "generations" (for the CASE 4)*

As shown in *Table 5. 33,* the lower chord elements required a thickness varying from 0.0071 to 0.0125 m and greater diameter than other elements, in fact corresponding to the maximum diameter available in the list of commercial steel tubular cross-sections here adopted (see *Table 5. 5*), equal to 0.508 m. Significantly smaller diameters and thicknesses have been obtained for the other elements since they showed to be subjected to significantly smaller axial forces and bending moments (as shown in *Figure 5. 73)*.

In particular, the lower chord elements support an axial compressive force varying between 1200 kN and 3900 kN (see *Figure 5. 73(a))* and bending moments between 3.03 $kN.m$ and 8.02 $kN.m$ (see *Figure 5. 73(b))*, under the envelope of all assumed load combinations. On the other hand, the upper chord elements resulted to be subjected to a minimum and maximum compressive axial force of 1170 kN and 1950 kN, in that order; as well as to bending moment actions oscillating between 2.52 $kN.m$ and 4.45 $kN.m$.

As in the previous cases, diagonal elements showed to be mainly under tension (with a tensile axial force varying from 80 to 530 kN) and to also withstand bending moments oscillating between 0.60 $kN.m$ and 1.80 $kN.m$. Conversely, vertical elements resulted to be purely stretched (under a tensile axial force varying from 21 kN to 294 kN) since external loads have been applied as concentrated forces on lower joints).

The combined effect of axial forces and bending moments under the envelope of all assumed load cases (shown in *Figure 5. 47*) on the optimized truss arch under here analysed is more clearly represented by the arch diagram in *Figure 5. 74*.

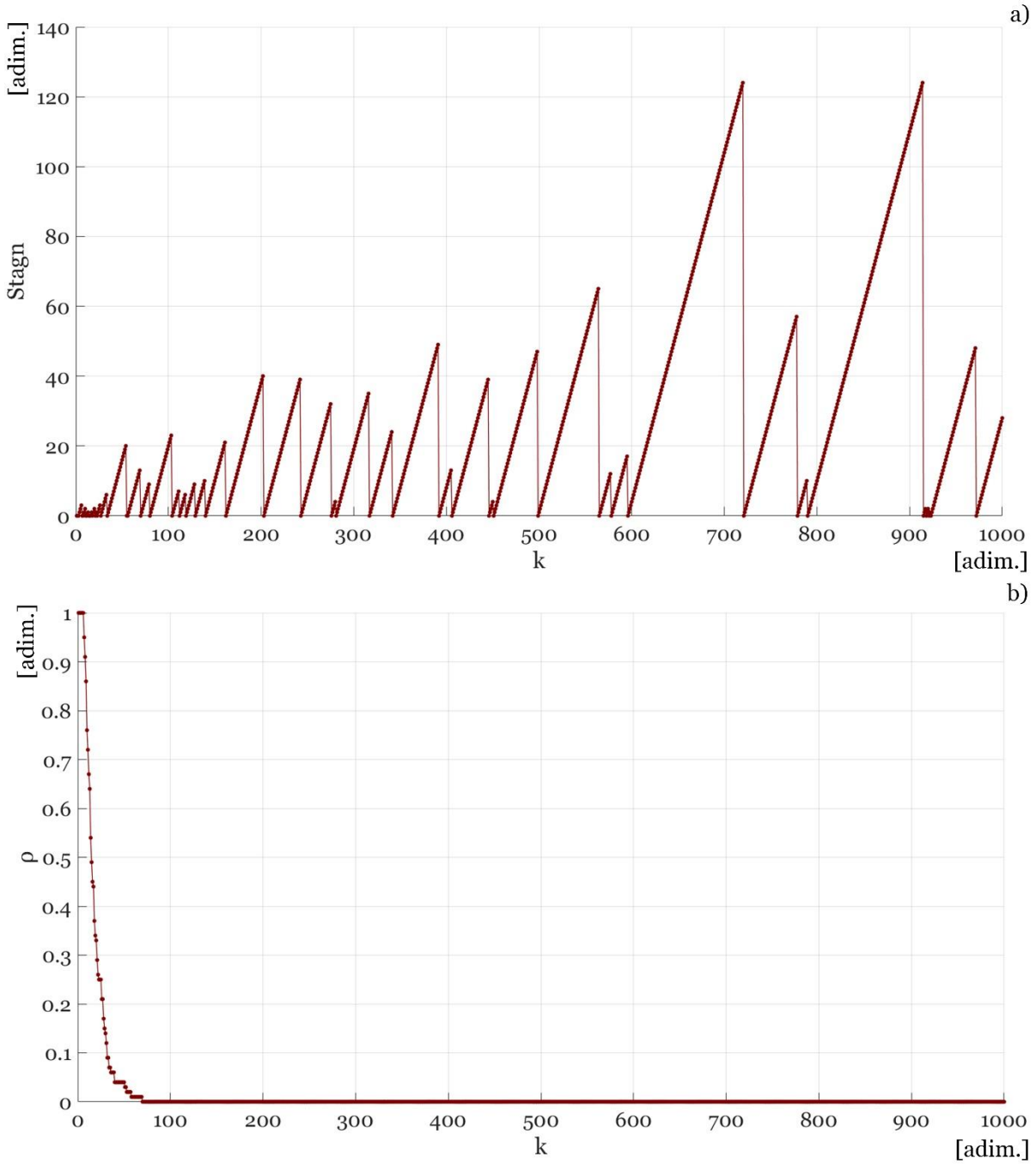

Figure 5. 76 *History of optimization functions (for the CASE 4): (a) stagnation function; (b) "unfeasibility function" (ρ)*

More specifically, the maximum "utilization ratio" ($\max_{LC} Util_i^{LC}$) for the envelope of all load combinations (LC) is pointed out in *Figure 5. 74* for each i^{th} –member, showing to be always less than 0.99 (as required by the constraint function, expressed by Eq. (47)), thus demonstrating the feasibility of the obtained solution.

Moreover, a "total utilization ratio" ($Util_{tot}$) was defined (by Eq. (51)) as a weighted average of all "Demand/Capacity ratios" ($\max_{LC} Util_i^{LC}$) shown in *Figure 5. 74,* with respect to the weight of each

i^{th} –member, to estimate an overall percentage of material exploitation of the whole structure. In this specific case, a percentage of material exploitation about 72.5 % has been reached.

Figure 5. 75 illustrates the convergence curve of the "objective function" that was minimized (i.e. the total volume of the truss arch), pointing out that it improves extremely slowly starting from the 450^{th} generation, until the optimal value has been achieved.

The history curve of the "stagnation function" (in *Figure 5. 76(a))* more precisely shows that the "objective function" stopped to improve longer from the 596^{th} to the 720^{th} generation, and also between the 790^{th} and the 914^{th} generation.

On the other hand, the trend of the "unfeasibility function" (expressed by Eq. (52)) proves that the optimization process generated and compared only feasible "individuals" (i.e. candidate solutions) starting from the 70^{th} onwards (see *Figure 5. 76(b)*).

In *Figure 5. 77* the convergence curve of the topology design variable (n_{int}) demonstrated that only best values close to the optimal one (that is 28) have been obtained since the 27^{th} generation until the end of the optimization process.

In accordance with what emerged so far, the convergence curves of shape design variables (represented in *Figure 5. 78*) prove that their corresponding optimal values have been approximately found around the 900^{th} generation. On the other hand, the history of size design variables in *Figure 5. 79* showed to be characterized by a better convergence, since from the first generations their value tends to oscillate around the optimal ones finally obtained.

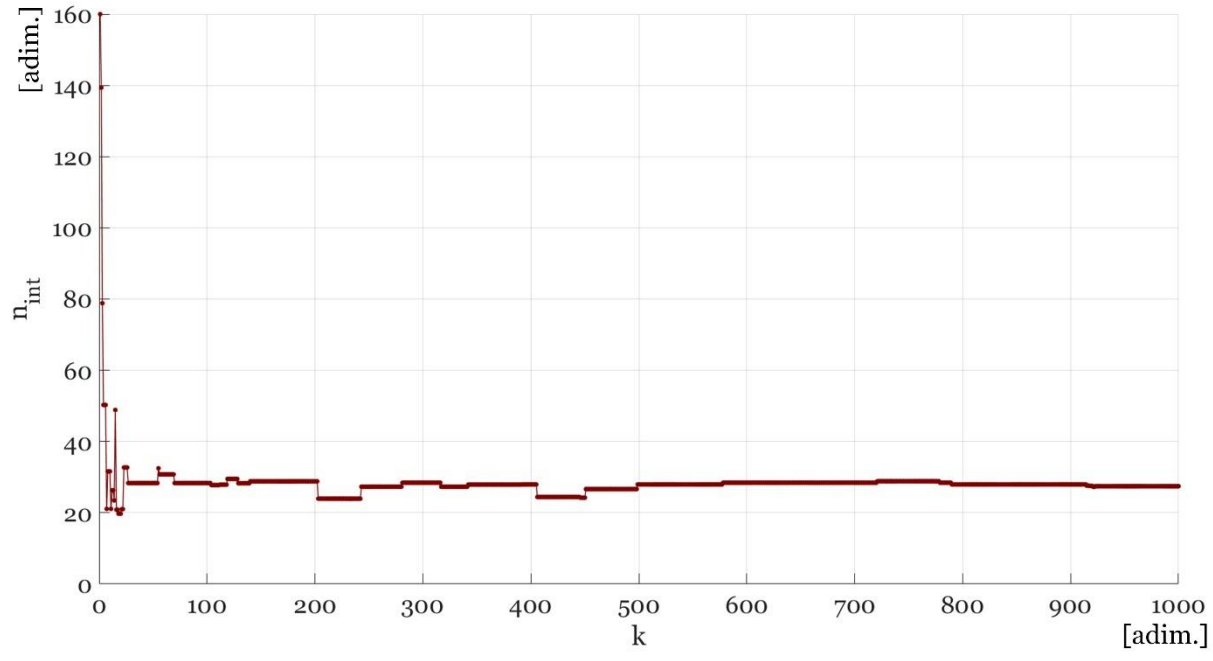

Figure 5. 77 Convergence curve of the topology design variable (n_{int}) for the CASE 4

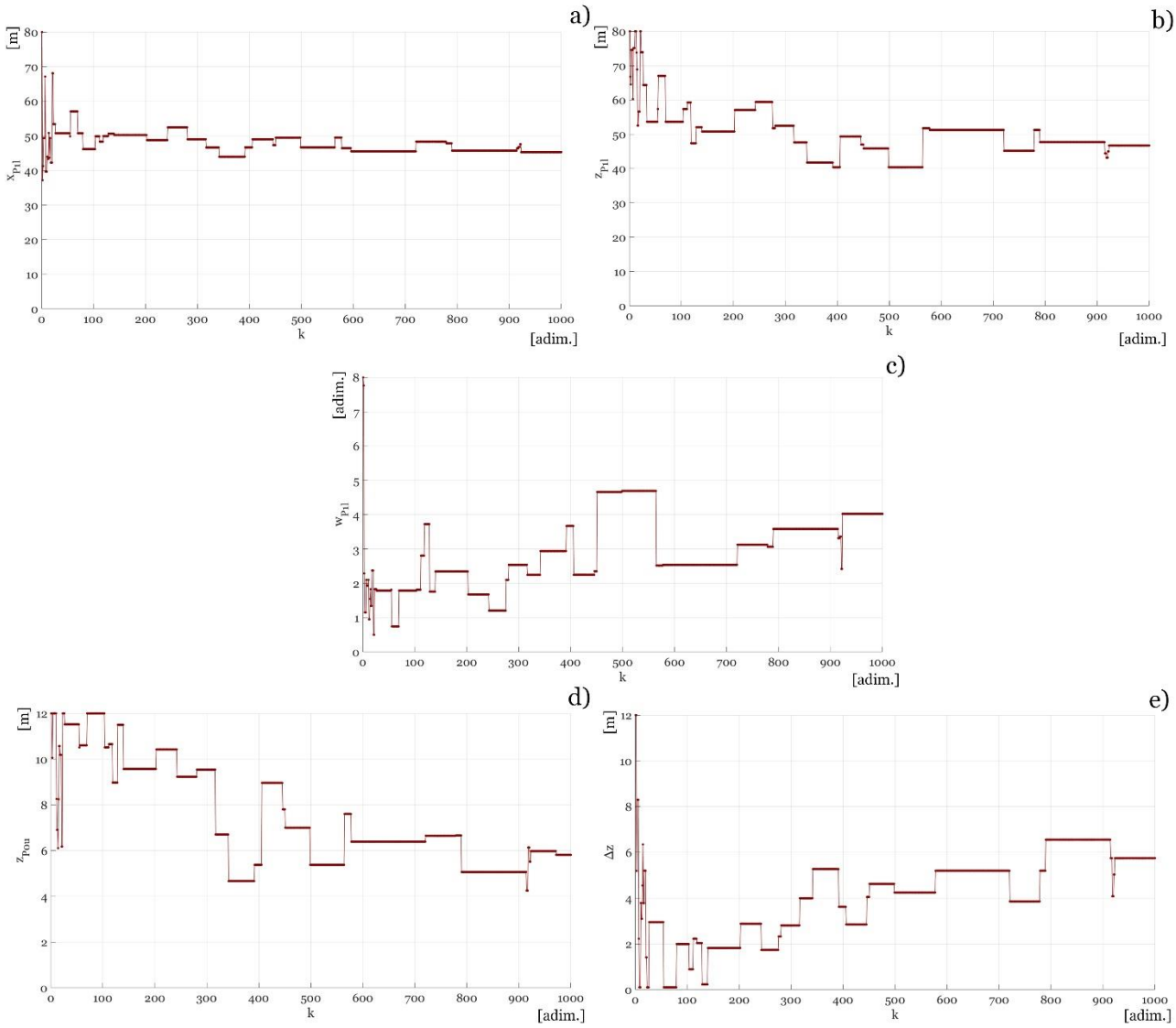

Figure 5. 78 Convergence curves of the shape design variables (variable parameters of third-degree rational Bézier curves) for the CASE 4: (a) x –coordinate of the second control point (x_{P1l}) of the bottom arched chord; (b) z –coordinate of the second control point (z_{P1l}) of the bottom arched chord; (c) weight factor of the second control point (w_{P1l}) of the bottom arched chord; (d) z –coordinate of the first control point (z_{P0u}) of the top arched chord;(e) the difference between the z –coordinates (in absolute value) of the top and bottom chord internal control points (Δz)

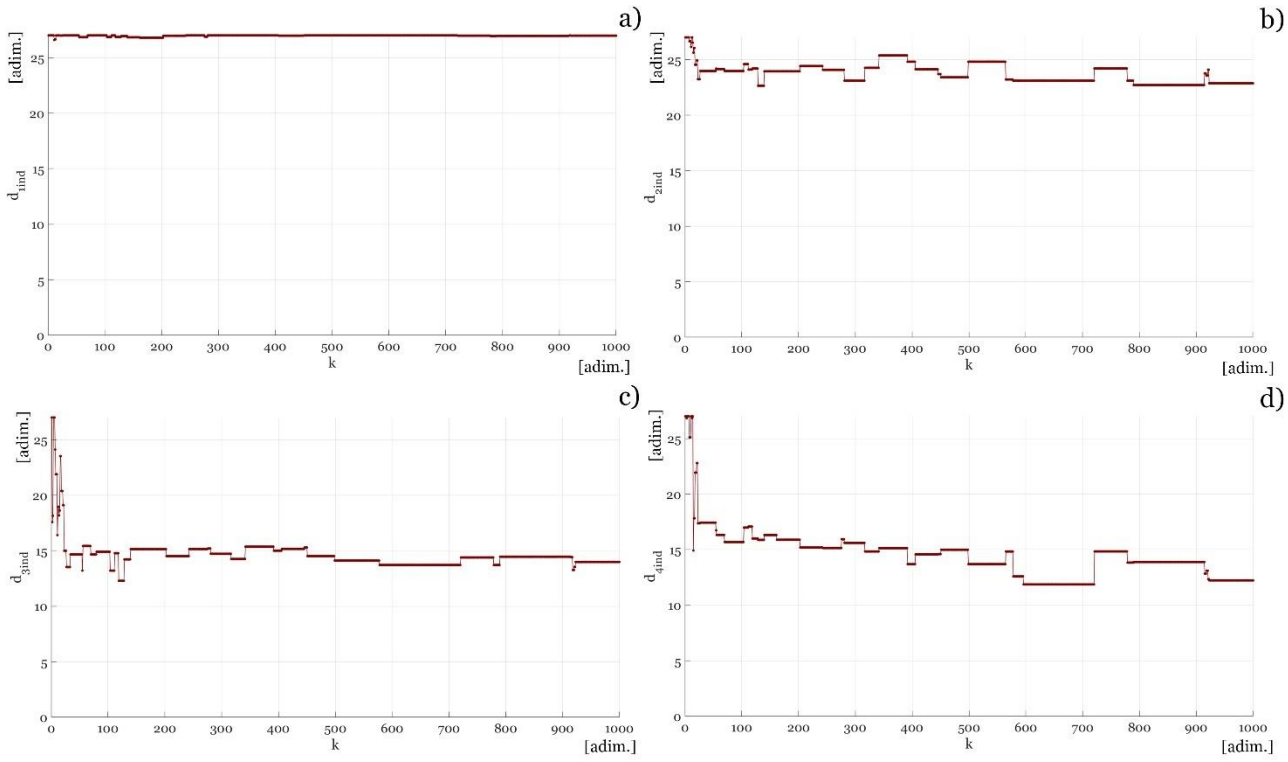

Figure 5. 79 Convergence curves of size design variables (i.e. indexes identifying the element group diameters in a list of commercial circular hollow cross-sections) for the CASE 4: (a) index identifying the bottom chord diameter; (b) index identifying the top chord diameter; (c) index identifying the diameter of diagonals; (d) index identifying the diameter of verticals

As for all previous cases, it can be stated that the trends of convergence curves (of the "objective function" and design variables) strongly validates the reliability of the obtained results, notwithstanding an extremely large set of design variables of different nature was assumed.

5.3.4.5 Comparison of optimal solutions

An analytical comparison of the optimal solution obtained for all different formulations (i.e. the CASES 1, 2, 3 and 4) of the optimization problem presented in section *§5.3* is here carried out, in order to deduce useful suggestion for an optimal design of steel truss arches.

A superimposition of optimal shapes of the presented solutions is represented in *Figure 5. 80* to more easily show how the optimal layout of the truss arch under consideration needs to change in increasing its span length. It can be immediately noted that, as the span grows, the arch becomes less tapered (i.e. its depth tends to become constant along its span) and slightly flattened at its top.

This observation is confirmed by the values of main geometrical parameters indicated below, in *Table 5. 34*. It is worth noting that the self-weight of the presented solutions increases almost linearly as the arch span grows (see *Figure 5. 81(b)*), but much slower compared to the self-weight of the two-hinged truss arches (see *Figure 5. 41(b)*) previously analysed.

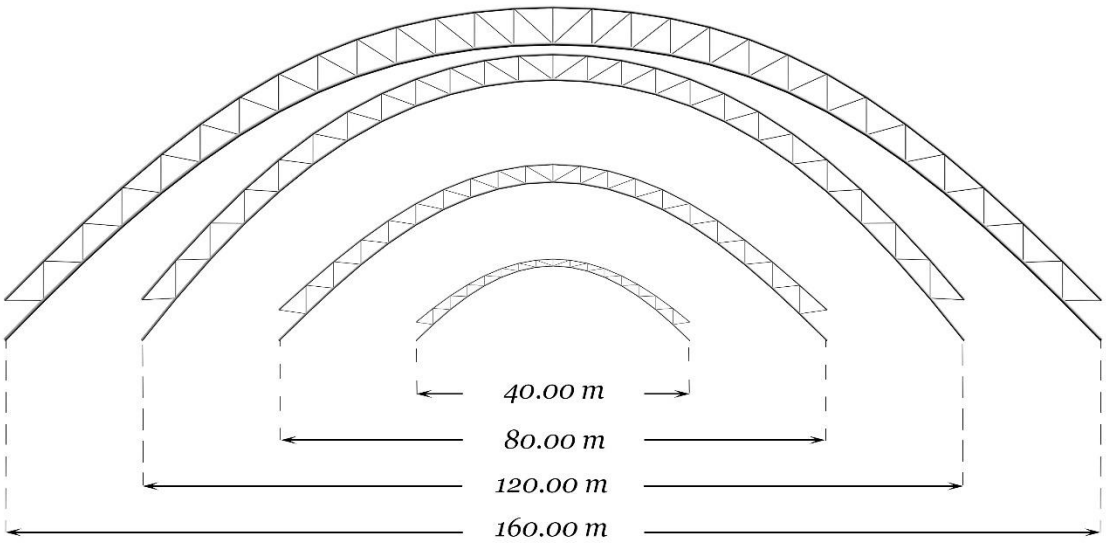

Figure 5. 80 Shape comparison of the optimal solutions for the CASES 1, 2, 3 and 4

Consequently, since variable loads were assumed to be constant and equal to 15.00 kN/m (as indicated in section *§5.3.3*), the "variable-to-permanent loads ratio" decreases as the arch self-weight increases (as shown in *Figure 5. 81(c)*), reaching a value of 1/1.75 for the hingeless truss arch 160 m long, that was conversely reached for the two-hinged truss arch with a span of 120 m (as previously shown in *Figure 5. 41(c)*).

As shown in *Table 5. 34,* the element number linearly varies from 65 to 113, as the arch span increases.

Table 5. 34 Comparison of main parameters characterizing the optimal solutions

CASE	Span length $[m]$	Min. volume $[m^3]$	Self-weight $[kN/m]$	Elem. number $[adim.]$	Height /span $[adim.]$	Rise/ span $[adim.]$	Crown-Depth/ span $[adim.]$	Base-Depth/ span $[adim.]$	Crown-Depth/ Base-Depth $[adim.]$
1	40	*0.293*	*0.563*	*65*	*1/3.36*	1/3.66	1/40.20	1/14.71	1/2.73
2	80	*1.194*	*1.149*	*81*	1/3.11	1/3.46	1/31.36	1/17.86	1/1.76
3	120	*2.773*	*1.779*	*97*	1/2.88	1/3.16	1/32.48	1/20.22	1/1.61
4	160	*4.839*	*2.328*	*113*	1/3.27	*1/3.71*	1/27.82	1/27.52	1/1.01

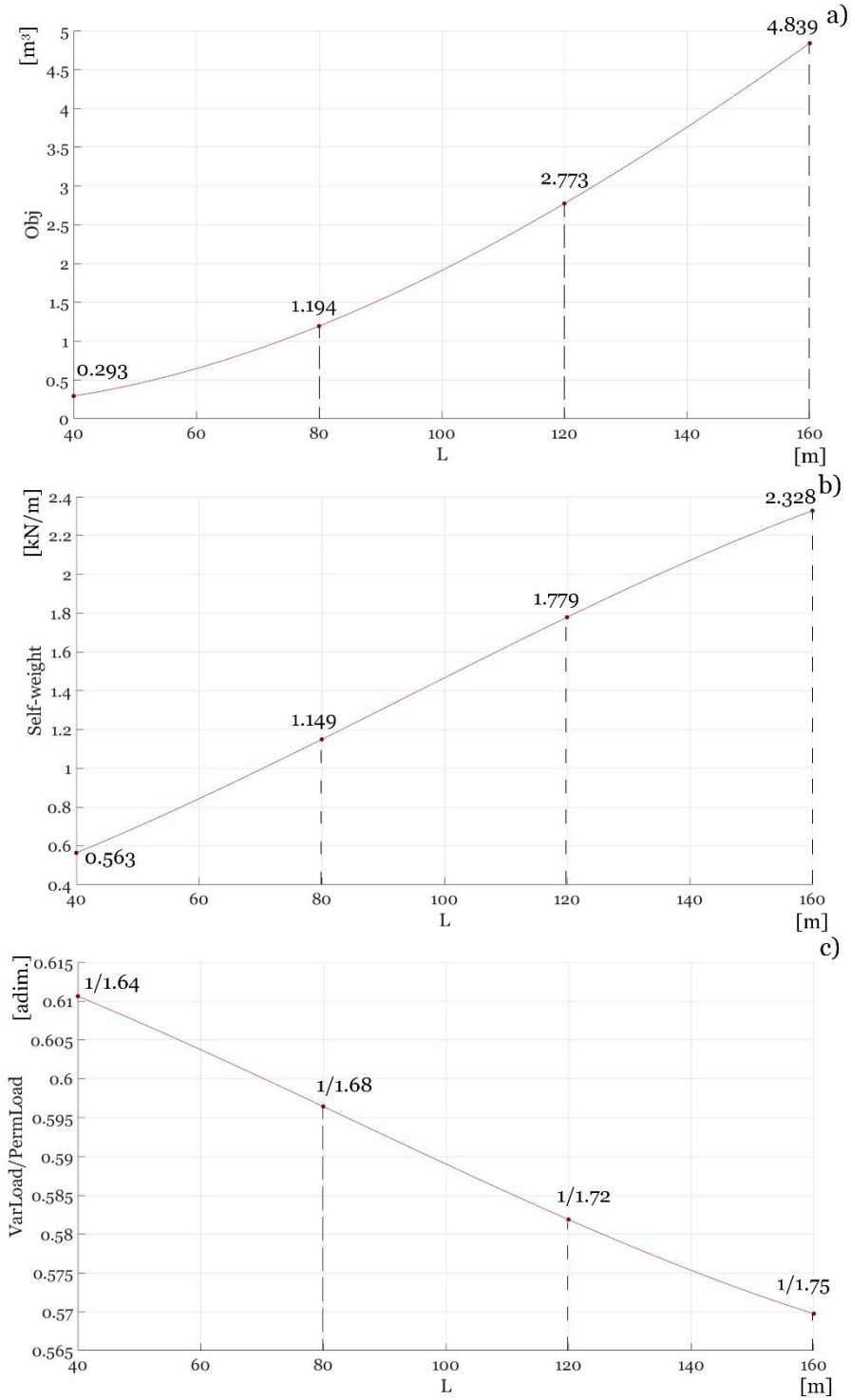

Figure 5. 81 *Comparison of the results of the optimal solutions: (a) best objective values; (b) arch self-weights per unit; (c) variable-to-permanent load ratios*

Table 5. 35 Comparison of optimal values of shape design variables

CASE	Span length $[m]$	x_{P1l} $[m]$	z_{P1l} $[m]$	w_{P1l} $[adim.]$	z_{P0u} $[m]$	Δz $[m]$	x_{P1l} /span $[adim.]$	z_{P1l} /span $[adim.]$
1	40	*16.758*	*16.585*	*0.643*	*2.719*	*0.100*	*1/2.38*	1/2.41
2	80	*34.871*	*38.320*	*0.508*	*4.480*	*1.287*	1/2.29	1/2.08
3	120	*33.873*	*43.273*	*2.411*	*5.935*	*3.384*	*1/3.54*	*1/2.77*
4	160	*45.301*	*46.727*	*4.024*	*5.814*	*5.46*	*1/3.53*	*1/3.42*

This is directly related to the optimal values of the topology design variable (n_{int}) pointed out in *Figure 5. 82,* which shows that they are perfectly collinear, i.e. lying on the same line of equation,

$$n_{int} = \frac{1}{10}L + 12 \tag{56}$$

which has been defined as a function of the arch span (L).

Therefore, since the element number (n_{frames}) of the structure in turn depends on n_{int} ($n_{frames} = 4n_{int} + 1$), a linear relationship correlating the optimal element number with the arch span, can be expressed by the following equation

$$n_{frames} = \frac{2}{5}L + 49 \tag{57}.$$

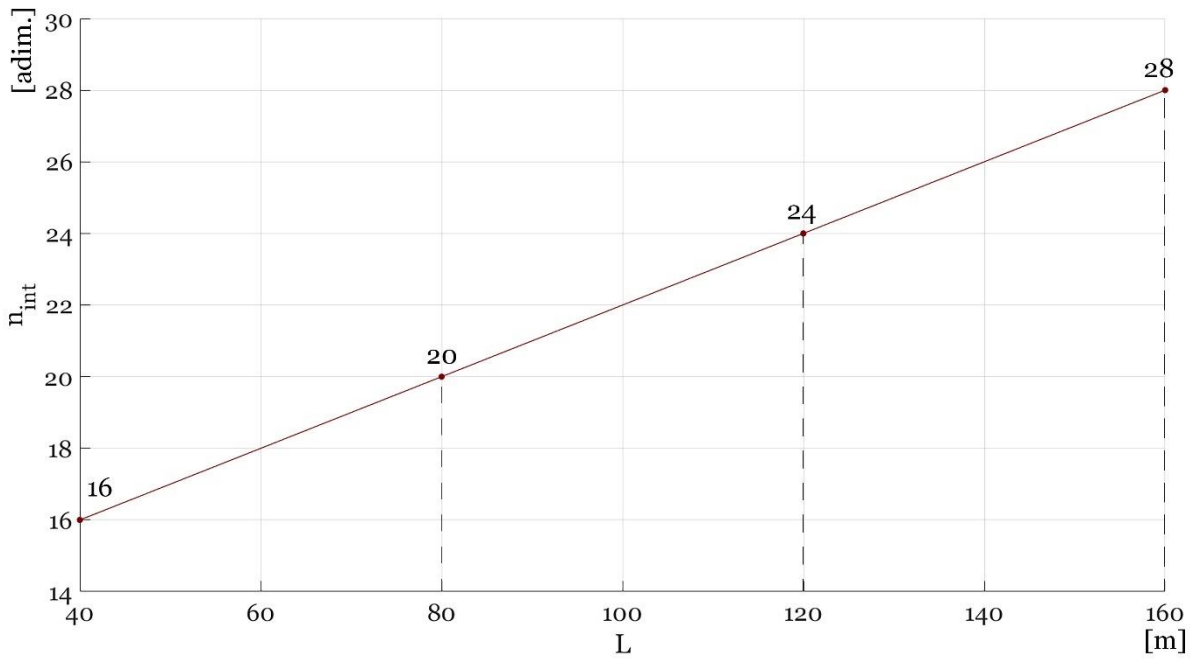

Figure 5. 82 Optimal values of the topology design variable (n_{int}), which defines the number of the truss arch element

In the same way, a linear equation expressing the optimal joint number (n_{nodes}) as a function of the arch span (L) can be easily deduced and written as follows,

$$n_{nodes} = \frac{1}{5}L + 26 \qquad (58).$$

Note that Eqs. (56-58) provides useful indications (and are valid only) for an optimal design of steel arched trusses of type Pratt, parametrically defined as described in section *§5.3.1* and subjected to the boundary conditions in *Figure 5. 47*.

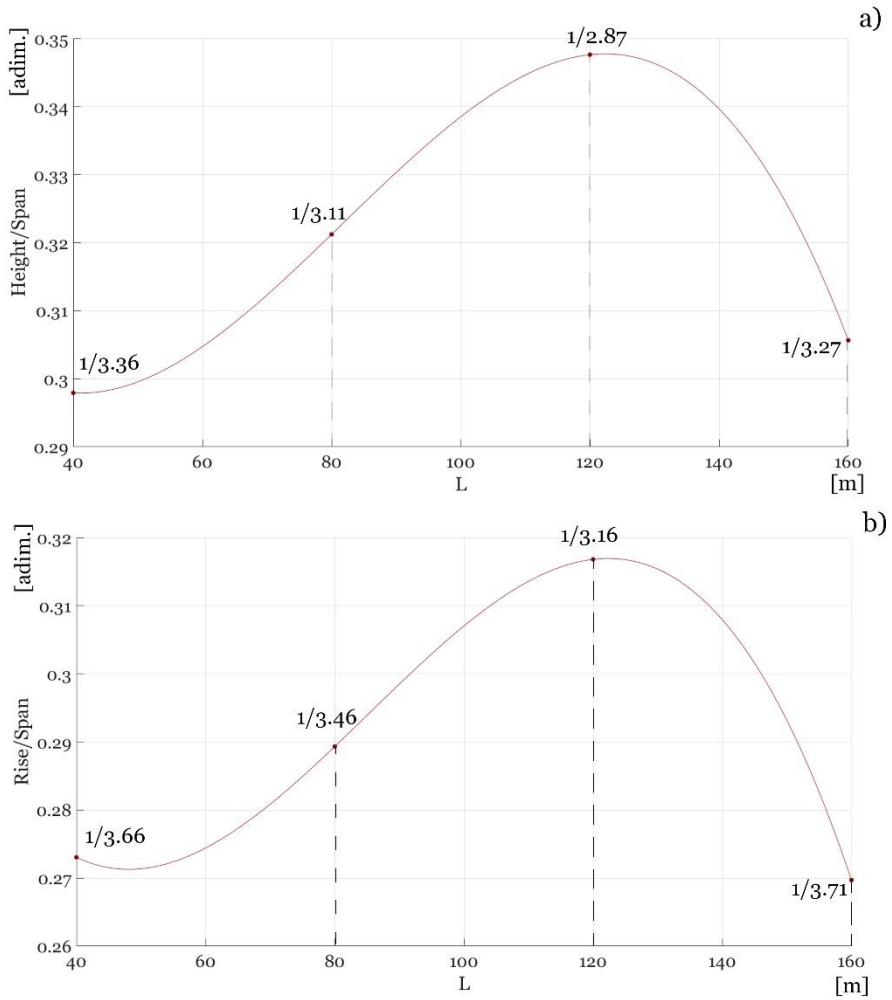

Figure 5. 83 *Comparison of the results of the optimal solutions: (a) height-to-span ratios; (b) rise-to-span ratios*

As already stated, the number of bars and joints of a truss structure has a great importance by a constructive point of view since the greater the number of joints, the higher the construction cost of the truss. As well-known, the "rise-to-span ratio" of an arch has also a great importance both from an architectural and structural point of view, since it strongly affects its aspect and its structural behaviour at the same time. Indeed, the smaller the rise of an arch, the greater the magnitude of horizontal thrusts that arise at its ends (as demonstrated by Eqs. (10) and (15) in *§2.1*).

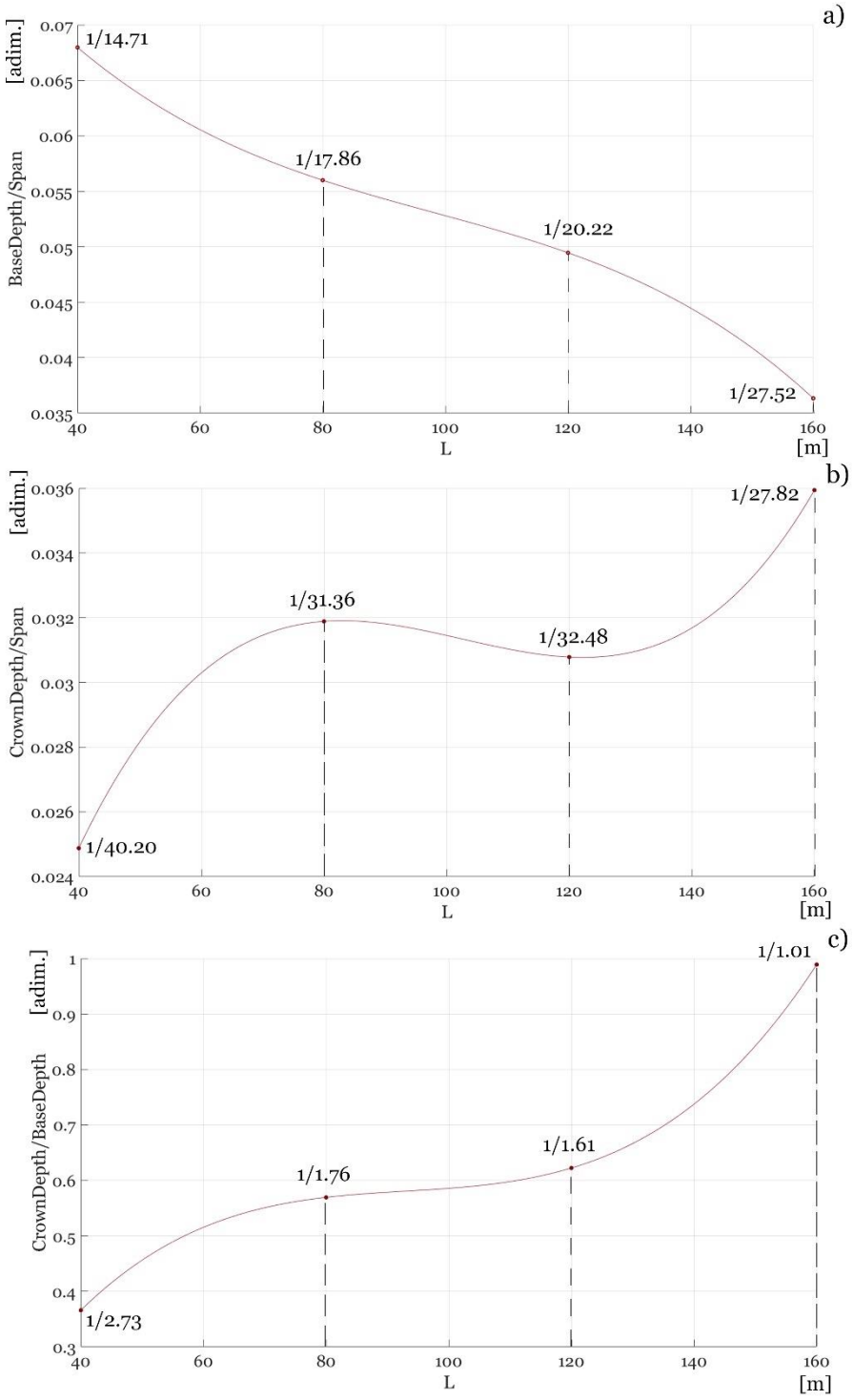

Figure 5. 84 Comparison of the results of the optimal solutions: (a) base depth-to-span ratios; (b) crown depth-to-span ratios; (c) taper ratios

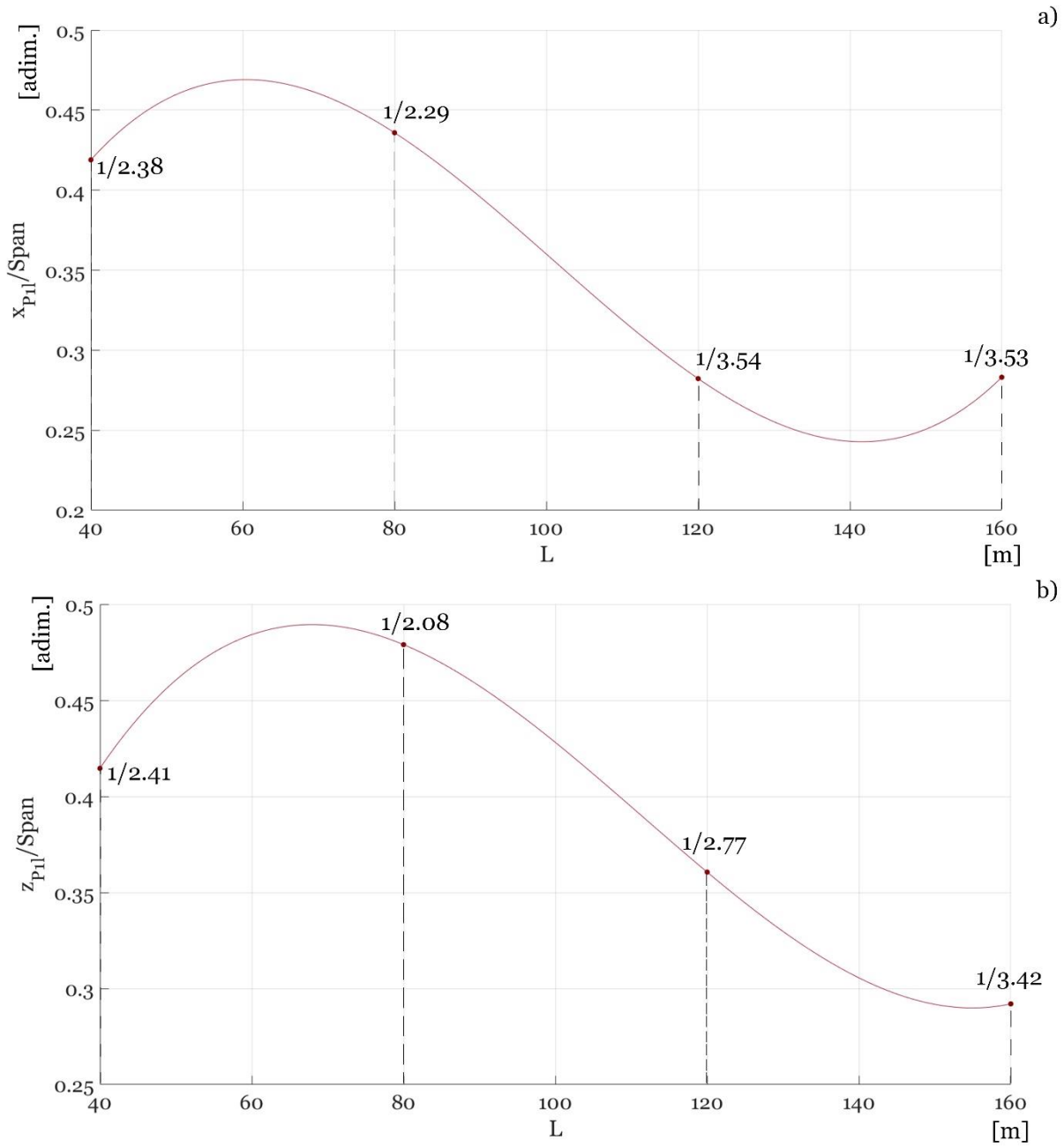

Figure 5. 85 *Comparison of the results of the optimal solutions: (a) x_{P1l}-to-span ratios; (b) z_{P1l}-to-span ratios*

However, as the arch height and rise increase, its visual impact deeply increases over the natural and anthropized landscape into which it is integrated.

In this regard, it can be immediately seen from the *Figure 5. 83(a)* that the arches under consideration are characterized by a "height-to-span ratio" growing from 1/3.36 to 1/2.87, as the arch span increases from 40.00 to 120.00 *m*, whereas decreasing to 1/3.27 when the arch span becomes equal to 160 *m*. Similarly, *Figure 5. 83(b)* shows that the "rise-to-span ratio" has a similar trend, increasing from 1/3.66 to 1/3.16 as the arch span grows from 40.00 to 120.00 *m*, and decreasing to 1/3.71 when the arch reaches a span of 160 *m*.

It is also worth noting that, unlike what previously emerged from the optimization results of two-hinged arches (discussed in section *§5.2.4*), in this case the values of the "height-to-span" and the "rise-to-span" ratios are quite close but they tend to more deviate from each other as the arch span increases, indeed corresponding to a growth of the "crown depth-to-span ratio" (from 1/40.20 to 1/27.82) of the arch (as shown in *Figure 5. 84(b)*). On the other hand, it can be seen from *Figure 5. 84(a)* the so-called "base depth-to-span ratio" (where the "base depth" indicates the arch depth at its ends) decreases (from 1/14.71 to 1/27.52) as the arch span increases.

Figure 5. 84(c) finally represents the trend of the aforementioned "taper ratio", which tends to decrease as the arch span growths, becoming almost equal to 1 when the arch reaches a span of 160 m (meaning that its depth tends to become constant).

All changes in the optimal shape of the arch as its span increases should be related to the progressive reduction of the effect of the asymmetric load combination of variable loads as the arch self-weight grows with its span.

Contrary to what came to light from the optimization results of two-hinged arches (in section *§5.2.4*), it can be observed from *Figure 5. 80* how the optimal shapes of the "hingeless" truss arches under consideration tend to flatten at the top as the arch span increases. This should be related to the optimal values of shape design variables (indicated in *Table 5. 35*) determining the coordinates and weight factors of control points defining in turn the shape of the lower and upper chord axis as *cubic Rational Bézier arcs*. In this regard, the resulting values of the "x_{P1l}-to-span" and "z_{P1l}-to-span" ratios are pointed out in *Figure 5. 85(a)* and *(b),* respectively, showing that the former assumed a value close to 1/2.3 for arches with spans of 40 and 80 m and around 1/3.5 for arches with spans of 120 and 160 m. It is worth to keep in mind that the smaller the "x_{P1l}-to-span ratio", more flattened the arch top becomes. Conversely, the "z_{P1l}-to-span ratio" showed to decrease (from 1/2.41 to 1/3.42) as the arch span grows, except for the arch 80 m long resulted to be characterized by a "z_{P1l}-to-span ratio" equal to 1/2.08. Note that the smaller the "z_{P1l}-to-span ratio", the lower the arch rise. However, the arch rise and height were also determined by the dimensionless value of the weight factors of internal control points here defined by the parameter w_{P1l}, which showed to increase from 0.508 to 4.02 as the arch span increases (as indicated in *Table 5. 35*).

It is worth remembering that the greater the value of the weight factor w_{P1l} (properly defined in section *§5.3.1.2*), the higher the arch. Moreover, since the total height of the arch also depends on the z −coordinates of internal control points defining the shape of the axis upper chord, evaluated by adding a variable quantity called Δz (included in the set of design variables in *§5.3.1.2)* to the z −coordinate of internal control points (z_{P1l}) defining the shape of the axis bottom chord.

Table 5. 35 shows that the value of Δz, which also determines the arch depth at its crown, increases (from 0.1 to 5.46 m) as the arch span grows, thus justifying the increasing trend of the "crown depth-to-span ratios" (shown in *Figure 5. 84(b)*).

Useful design recommendations for steel truss arches can be therefore deduced from results discussed so far and adopted, provided that boundary conditions similar to those ones here defined (see *§5.3.3*) were taken into account, paying particular attention to the ratio between variable and permanent loads in considering different load patterns.

In conclusion, *Figure 5. 86* shows that a "total utilization ratio" (introduced in section *§5.2.4.1* and defined by Eq. (26)) greater than 70% was obtained for all cases, reaching a peak of 72.5 % for the truss arch with a span of 160 meters. It can be therefore stated that the structural optimization process here proposed leaded to satisfactory results in terms of structural performances, since the "total utilization ratios" express the overall percentages of the material exploitation characterizing the optimized solutions.

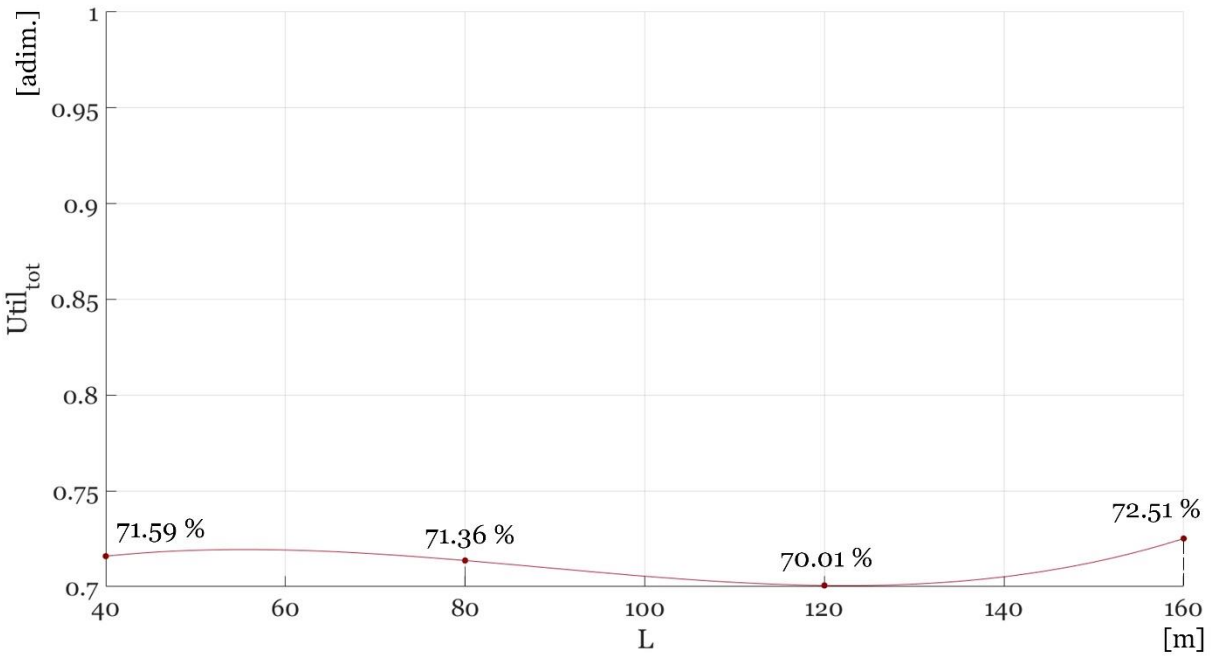

Figure 5. 86 *Resulting values of the "total utilization ratio" ($Util_{tot}$), evaluated through the Eq. (26), providing an overall percentage of the material exploitation*

Chapter 6

6. Parametric design and structural optimization of spatial arched trusses

In *§Chapter 5,* in-plane truss arches with different span lengths and structural boundary conditions have been optimized for multiple load cases (defined in sections *§5.2.3* and *§5.3.3*), only considering vertical loads (acting on the same plane as the arch), since in-plane arches are not suited to withstand out-of-plane loads.

The optimization strategy here developed and presented in section *§4.2* has been therefore adopted to simultaneously perform topology, shape and size optimization of a spatial arched truss (with lower and upper chords lying on different planes) under multiple load cases acting in different directions. The so-obtained results will be discussed in present *Chapter*.

6.1 Simultaneous topology, shape and size optimization of an arched truss under vertical and horizontal loads

The present section aims to provide a detailed description of the stepwise optimization process of a three-dimensional arched truss, with a span of 40 meters, subjected to vertical and horizontal load conditions. More specifically, an arched system composed by an upper arched chord lying on a horizontal plane and by a lower inclined arched chord, connected each other by a bracing system of type Pratt, was optimized by minimizing its total volume according with strength and serviceability constraints. Such an arched truss was for instance supposed to be suited to support the curved deck of a footbridge (Luigi Fenu, Congiu, and Briseghella 2016). The considered arched truss, made of steel tubular members (i.e. with circular hollow cross-sections), were optimally designed for three different vertical load patterns and a static seismic action, acting in parallel to the horizontal upper chord plane.

The so-obtained results will be illustrated and discussed in subsection *§6.1.4*.

6.1.1 Parametric design

As shown in the flowchart of the proposed optimization macro-algorithm illustrated in *Figure 4. 2,* a parametric formulation of the optimum design problem is indispensable to properly define

all design variables within a range of lower and upper bounds, as well as the objective and constraint functions as a function of the assumed design variables.

The higher the number of design variables to consider, the more crucial the role of this stage in the whole process becomes.

In this regard, the design problem of the three-dimensional arched truss here investigated depends on a large number of parameters, among which 93 have been assumed as design variables of different nature (1 topology, 7 shape and 85 size design variables).

6.1.1.1 Topology design variables

As in cases of in-plane truss arches treated in *§Chapter 5*, the topology optimization problem of the spatial arched truss under consideration has been formulated as a function of a variable number of bars and joints, thereby assuming, as a unique topology design variable of the problem, a parameter indicated as n_{int}, defining the number of equal "intervals" (dL), into which the arch span is subdivided (as expressed by Eq. (44) and indicated in *Figure 6. 2*).

The topology design variable n_{int} determines the node number and spacing (their x −coordinates), as well as the number of the truss bars. In particular, the curved truss under consideration is characterized by $2n_{int} + 2$ joints and $4n_{int} + 1$ members.

Furthermore, since a Pratt-type truss has been chosen as bracing system, n_{int} needs to be an even integer, as well as a discrete design variable. However, since the optimization method here adopted only allows the assumption of continuous variables, the value related to the parameter n_{int} is rounded to the nearest even integer during the optimization process.

6.1.1.2 Shape design variables: parameters defining Cubic Rational Bézier Curves

Analogously to what has been done in case of in-plane truss arches (see *Figure 6. 1(a)*), once again the axis shape of both the lower and the upper chords has been parametrized by *cubic Rational Bézier curves* with four control points (whose parametric equation can be expressed by Eq. (45)).

In particular, the upper chord was supposed to lie on a horizontal plane, whereas the lower rib was defined as an arch with a variable inclination in three-dimensional space (as shown in *Figure 6. 1(b)*).

Figure 6. 2 shows how the shapes of lower and upper chords depend on the positions of *Rational Bézier arcs* control points.

The spatial arched truss in *Figure 6. 2* was further assumed to be symmetrical with respect to a yz −plane with origin on the x −axis at the mid-span of the arched system.

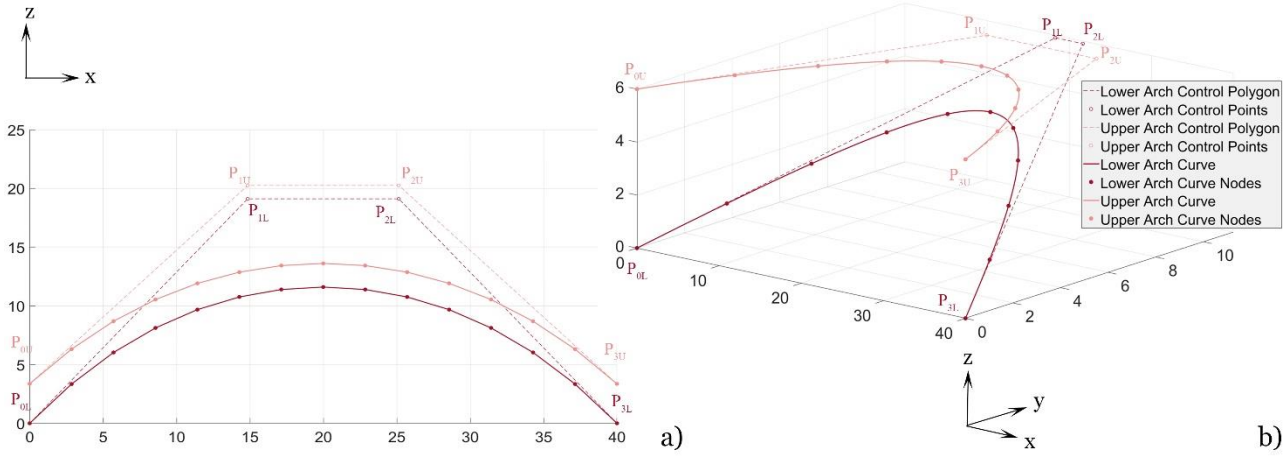

Figure 6. 1 Form-finding of planar (a) and spatial double-chord arches (b) through Cubic Rational Bézier Curves

On the basis of the aforementioned symmetry conditions, seven parameters typifying *cubic Rational Bézier curves* have been therefore assume as shape design variables; which are,

- x_{p1l}, x-coordinate of the second control point (P_{1l}) of the lower inclined chord. Note that the third control point (P_{2l}) of the bottom rib has been assumed as symmetric to P_{1l} (with respect to a yz −plane with origin on the x −axis at the mid-span of the arched system), by imposing $x_{P2l} = L - x_{P1l}$

- y_{p1l}, y-coordinate of the second control point (P_{1l}) of the lower inclined chord. For the imposed symmetry conditions, it was assumed that the third control point (P_{2l}) of the bottom rib has same y −coordinate ($y_{P2l} = y_{P1l}$)

- w_{1l}, non-negative weight factor of the second control point (P_{1l}) of the lower inclined chord, also corresponding to the weight factor of the third control point (P_{2l}) affecting the shape of the lower inclined chord

- Δz, absolute value of the difference between z-coordinates of the internal control points of upper and lower chords ($\Delta_z = |z_{p1u} - z_{p1l}| = |z_{p2u} - z_{p2l}|$), that defines the crown depth of the curved truss

- x_{p1u}, x-coordinate of the second control point (P_{1u}) of the upper chord. For the imposed symmetry conditions, the third control point (P_{2u}) of the top rib has been assumed as symmetric to P_{1u} (with respect to a yz −plane with origin on the x −axis at the mid-span of the arched system), by imposing $x_{P2u} = L - x_{P1u}$

- y_{p1u}, y-coordinate of the second control point (P_{1u}) of the upper chord. It was further assumed that the third control point (P_{2l}) of the horizontal rib has same y −coordinate ($y_{P2l} = y_{P1l}$)
- w_{1u}, weight factor of the second control point (P_{1u}) of the upper chord, whose value also define the non-negative weight factor of the third control point (P_{2u}) affecting the axis shape of the horizontal upper chord.

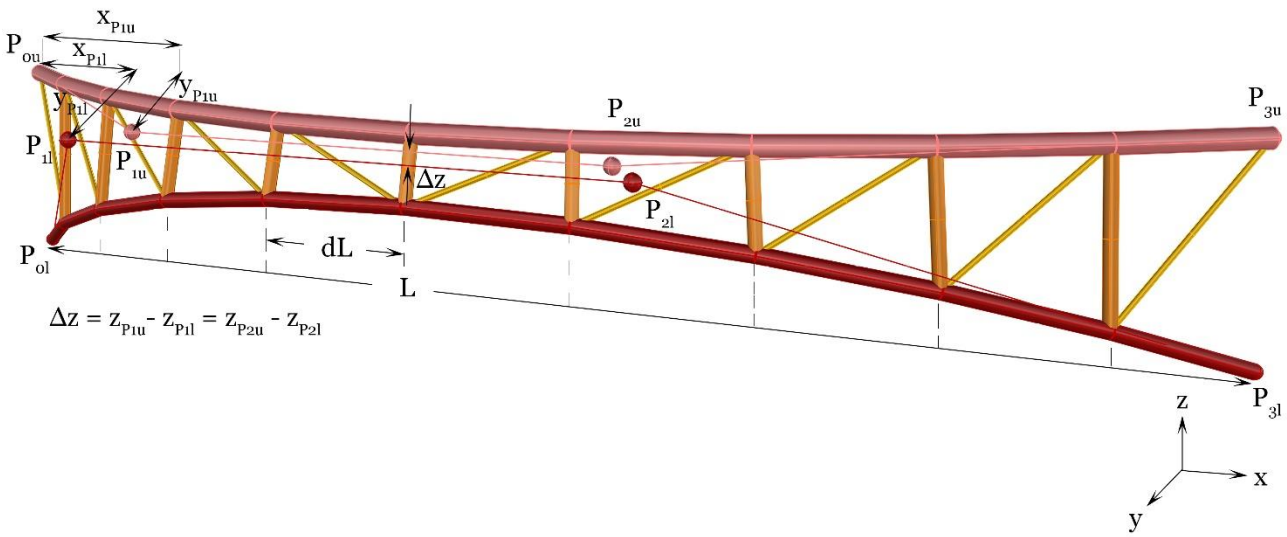

Figure 6. 2 *Parametric definition of the geometry as a function of shape design variables, by taking advantage of Cubic Rational Bézier Curves*

It is worth remarking that all coordinates of the first and last control points of both chords have been assumed as fixed, in order that the arched truss under consideration was characterized by a "base depth" (i.e. its height at its hinged ends) equal to 6.00 *m* and by a span of 40.00 *m*.

Furthermore, all shape design variables have been defined as continuous variables within proper ranges of lower and upper limits (indicated in *Table 6. 1*).

6.1.1.3 Size design variables

The size design variables define the dimensions of cross-sections of truss elements. Analogously to the case of in-plane truss arches (addressed in *§Chapter 5*) the arched truss under consideration is assumed to be composed by elements with circular hollow cross-sections, grouped as follow

- Bottom chord (lower chord) elements
- Top chord (upper chord) elements
- Diagonals
- Verticals.

Each group of elements is characterized by same diameter, thus assuming

- d_1 as diameter of bottom chord elements
- d_2 as diameter of top chord elements
- d_3 as diameter of diagonals
- d_4 as diameter of verticals.

On the other hand, a further symmetry condition imposed that couples of elements that are symmetrical with respect to a central vertical plane (i.e. placed in the mid-span and parallel to the reference yz −axis), must have same thickness. Therefore, four diameters and n different thicknesses t_i (with $i = 1, \dots n$ and $n = 81$) were assumed as size design variables, for each i_{th} −couple of symmetrical elements. Note that the allowable number of different thicknesses (n) depends on n_{int}^{u} (since it was assumed that $n = 2n_{int}^{u} + 1$), upper bound of the topological design variable n_{int}, here assumed equal to 40 (as indicated in *Table 6. 1)*. Therefore, the optimization problem under consideration showed to depend on 85 size design variables, given by 4 diameters and 81 thicknesses.

6.1.2 Problem formulation

Unlike the previous case of in-plane truss arches, a unique formulation of the optimization problem here discussed has been considered. As already stated, the problem has been defined as a function of 93 design variables, indicated in *Table 6. 1* with corresponding lower and upper bounds. Among these, the topology design variable (n_{int}), expressing the even integer of equal intervals into which the span is subdivided, was assumed to be variable between 10 (n_{int}^{l}) and 40 (n_{int}^{u}). The number of elements can therefore vary from $n_{el}^{MIN} = 4n_{int}^{l} + 1 = 41$ to $n_{el}^{MAX} = 4n_{int}^{u} + 1 = 161$, thus determining the required number of size design variables (defined in section *§6.1.1.3*).

It can be immediately seen from *Table 6. 1* that the upper bounds of coordinates x_{P1l}, y_{P1l} and y_{P1u} corresponds to the half span of the arch (thus equal to $\frac{L}{2} = 20.00\,m$), whereas the upper bound of x_{P1u} was limited to one third of the arched truss span (thus equal to $\frac{L}{3} = 13.33\,m$) in order to ensure that the horizontal upper chord had a smooth shape, since it was supposed to be properly design to support a curved deck of a footbridge (Luigi Fenu, Congiu, and Briseghella 2016). For the same purpose, the upper bounds of weight factors w_{P1l} and w_{P1u} have been limited to 1.

Size design variables were defined as indexes (as indicated in *Table 6. 1)*, which allow to take the values of diameters and thicknesses from a table of commercial circular hollow cross-sections (see *Table 6. 2*).

Table 6. 1 Lower and upper bounds of design variables

Design Variable (DV)	Type of DV	Lower bound	Upper bound	Unit
n_{int}	*topology*	10	40	$[adim.]$
x_{P1l}	*shape*	0.1	20.0	$[m]$
y_{P1l}	*shape*	10.0	20.0	$[m]$
w_{P1l}	*shape*	0.5	1	$[adim.]$
Δz	*shape*	0.1	5.0	$[m]$
x_{P1u}	*shape*	0.1	13.3	$[m]$
y_{P1u}	*shape*	10.0	20.0	$[m]$
w_{P1u}	*shape*	0.5	1	$[adim.]$
$index_{d1}$	*size*	1	38	$[adim.]$
$index_{d2}$	*size*	1	38	$[adim.]$
$index_{d3}$	*size*	1	38	$[adim.]$
$index_{d4}$	*size*	1	38	$[adim.]$
$index_{t(i)}$ *	*size*	2	18	$[adim.]$

* with $i = 1, \dots n$ (n was defined in the section *§6.1.1.3* by the Eq. (21))

It is worth noting that, since the spatial arched truss under consideration showed to be much more flexible than in-plane truss arches analysed in *§Chapter 5*, a list of circular hollow cross-sections with larger diameters ($0.1016\ m \leq d_j \leq 0.925\ m$, with $j = 1, \dots 4$) was here adopted. Size design variables should be assumed as discrete. However, since the optimization method here proposed (in *§4.2*) can only generate continuous values among lower and upper bounds, discrete size design variables were obtained by rounding the corresponding continuous values to the nearest integers during the optimization process.

As in previous numerical examples, the total volume of the structure was assumed as objective function to be minimized (and calculated by Eqs. (38) and (39)).

Moreover, strength constraints have been imposed to keep the stress values under allowable limits. More specifically, the inequality constraint function generalized by Eq. (47), imposes that the maximum value of the afore-mentioned "Utilization ratio" (also called "Demand/Capacity ratio", since it corresponds to the ratio between real and allowable stresses acting in a section) among all truss members be less than (or equal to) 0.99 for all considered load cases (feasibility condition).

Table 6. 2 Commercial circular hollow cross-sections

d [m]	t [m]	t [m]	t [m]	t [m]	t [m]	t [m]	t [m]	t [m]	t [m]	t [m]	t [m]	t [m]	t [m]	t [m]	t [m]	t [m]	t [m]	t [m]
0.1016	0.0036	0.004	0.0045	0.005	0.0054	0.0056	0.0059											
0.108	0.0036	0.004	0.0045	0.005	0.0054	0.0056	0.0059											
0.1143	0.0036	0.004	0.0045	0.005	0.0054	0.0056	0.0059	0.0063										
0.127		0.004	0.0045	0.005	0.0054	0.0056	0.0059	0.0063	0.0071									
0.133		0.004	0.0045	0.005	0.0054	0.0056	0.0059	0.0063	0.0071	0.008								
0.1397		0.004	0.0045	0.005	0.0054	0.0056	0.0059	0.0063	0.0071	0.008								
0.1524		0.004	0.0045	0.005	0.0054	0.0056	0.0059	0.0063	0.0071	0.008								
0.159		0.004	0.0045	0.005	0.0054	0.0056	0.0059	0.0063	0.0071	0.008								
0.1683		0.004	0.0045	0.005	0.0054	0.0056	0.0059	0.0063	0.0071	0.008								
0.1937			0.0045	0.005	0.0054	0.0056	0.0059	0.0063	0.0071	0.008								
0.2191				0.005	0.0054	0.0056	0.0059	0.0063	0.0071	0.008	0.0088							
0.2445					0.0054	0.0056	0.0059	0.0063	0.0071	0.008	0.0088	0.01						
0.273						0.0056	0.0059	0.0063	0.0071	0.008	0.0088	0.01	0.011	0.0125				
0.2985							0.0059	0.0063	0.0071	0.008	0.0088	0.01	0.011	0.0125				
0.3239							0.0059	0.0063	0.0071	0.008	0.0088	0.01	0.011	0.0125				
0.3556								0.0063	0.0071	0.008	0.0088	0.01	0.011	0.0125	0.0142			
0.368								0.0063	0.0071	0.008	0.0088	0.01	0.011	0.0125	0.0142			
0.4064								0.0063	0.0071	0.008	0.0088	0.01	0.011	0.0125	0.0142	0.016		
0.419									0.0071	0.008	0.0088	0.01	0.011	0.0125	0.0142	0.016		
0.4572									0.0071	0.008	0.0088	0.01	0.011	0.0125	0.0142	0.016	0.0175	
0.47									0.0071	0.008	0.0088	0.01	0.011	0.0125	0.0142	0.016	0.0175	
0.508									0.0071	0.008	0.0088	0.01	0.011	0.0125	0.0142	0.016	0.0175	0.02
0.521									0.0071	0.008	0.0088	0.01	0.011	0.0125	0.0142	0.016	0.0175	0.02
0.5588									0.0071	0.008	0.0088	0.01	0.011	0.0125	0.0142	0.016	0.0175	0.02
0.572									0.0071	0.008	0.0088	0.01	0.011	0.0125	0.0142	0.016	0.0175	0.02
0.6096									0.0071	0.008	0.0088	0.01	0.011	0.0125	0.0142	0.016	0.0175	0.02
0.622									0.0071	0.008	0.0088	0.01	0.011	0.0125	0.0142	0.016	0.0175	0.02
0.6604										0.008	0.0088	0.01	0.011	0.0125	0.0142	0.016	0.0175	0.02
0.673										0.008	0.0088	0.01	0.011	0.0125	0.0142	0.016	0.0175	0.02
0.7112										0.008	0.0088	0.01	0.011	0.0125	0.0142	0.016	0.0175	0.02
0.724										0.008	0.0088	0.01	0.011	0.0125	0.0142	0.016	0.0175	0.02
0.762											0.0088	0.01	0.011	0.0125	0.0142	0.016	0.0175	0.02
0.775											0.0088	0.01	0.011	0.0125	0.0142	0.016	0.0175	0.02
0.8128											0.0088	0.01	0.011	0.0125	0.0142	0.016	0.0175	0.02
0.825											0.0088	0.01	0.011	0.0125	0.0142	0.016	0.0175	0.02
0.8636											0.0088	0.01	0.011	0.0125	0.0142	0.016	0.0175	0.02
0.9144												0.01	0.011	0.0125	0.0142	0.016	0.0175	0.02
0.925												0.01	0.011	0.0125	0.0142	0.016	0.0175	0.02

The critical "Utilization ratio" of bars subjected to compression axial forces was calculated by evaluating (by Eqs. (40) and (41) in section *§4.2.3*) the combined effect of compression axial forces and bending moments by also considering flexural and lateral-torsional buckling of cross-sections. On the other hand, the "utilization ratio" of members subjected to tensile axial forces is evaluated by checking the combined effect of axial forces and bending moments by means of the Eq. (42) introduced in section *§4.2.3*.

However, since the arched truss under consideration showed to be considerably more flexible compared with planar truss arches analysed in the previous *Chapter*, serviceability constraints have been additionally defined.

It was therefore imposed that the absolute values of the maximum displacements in the $x-$ ($\max_i(U_1)_i^{LC}$) and $y-$directions ($\max_i(U_2)_i^{LC}$) among all $i^{th}-$nodes for each load case (LC) be limited as follows,

$$\left|\max_i(U_1)_i^{LC}\right| \leq H/300 \tag{59}$$

$$\left|\max_i(U_2)_i^{LC}\right| \leq H/300 \tag{60}$$

where H indicates the height of the considered arched truss (i.e. the truss depth at its ends), assumed to be equal to 6.00 m.

Furthermore, it was assumed that the absolute value of the maximum displacements in the $z-$direction ($\max_i(U_3)_i^{LC}$) among all $i^{th}-$nodes for each load case (LC) be limited as follows,

$$\left|\max_i(U_3)_i^{LC}\right| \leq L/500 \tag{61}$$

where L represents the span length of the arched truss, here assumed equal to 40.00 m.

As shown in *Figure 4. 2*, the total weight of the structure, as well as the "Demand/Capacity ratios" of each section and nodes displacements in all directions are obtained by performing *Finite Element Analysis (FEA)* through *SAP2000,* to evaluate the "objective" and "constraint functions" for each candidate solution of the optimization problem.

6.1.3 Boundary conditions

The two chords of the arched truss under consideration are hinged at their ends. The four hinges are therefore aligned two by two in the vertical direction, at each truss side. Since the considered spatial truss is composed by the same parametric number of bars and pinned joints as the in-plane "hingeless" truss arches investigated in section *§5.3,* it can be easily proved (by demonstrating that $2n_{nodes} < n_{frames} + gdv_{ext}$, where gdv_{ext} is equal to 8 in case of four hinges) that the spatial arched truss in *Figure 6. 2* is equally redundant (i.e. statically indeterminate).

As previously mentioned, vertical and horizontal multiple load cases have been applied, since the structural behaviour of structures is strongly affected by the loading to which they are subjected. Three different load combinations of external vertical loads (orthogonal to the $xy-$plane on which the horizontal arch lies) have been considered (see *Figure 6. 3*):

- LOAD CASE 1: Non-structural Dead Loads (24.00 kN/m) + Live Loads (15.00 kN/m) applied along the total length of the arch
- LOAD CASE 2: Non-structural Dead Loads (24.00 kN/m) applied along the total length of the arch

- LOAD CASE 3: Non-Structural Dead Loads (24.00 kN/m) applied along the total length of the arch + Live Loads (15.00 kN/m) applied along the right half of the arch.

It is worth to remark that external loads have been applied as concentrated forces on nodes (of the upper chord), equivalent to non-structural Dead Loads (24.00 kN/m) and Live Loads (15.00 kN/m), uniformly distributed along the arch span.

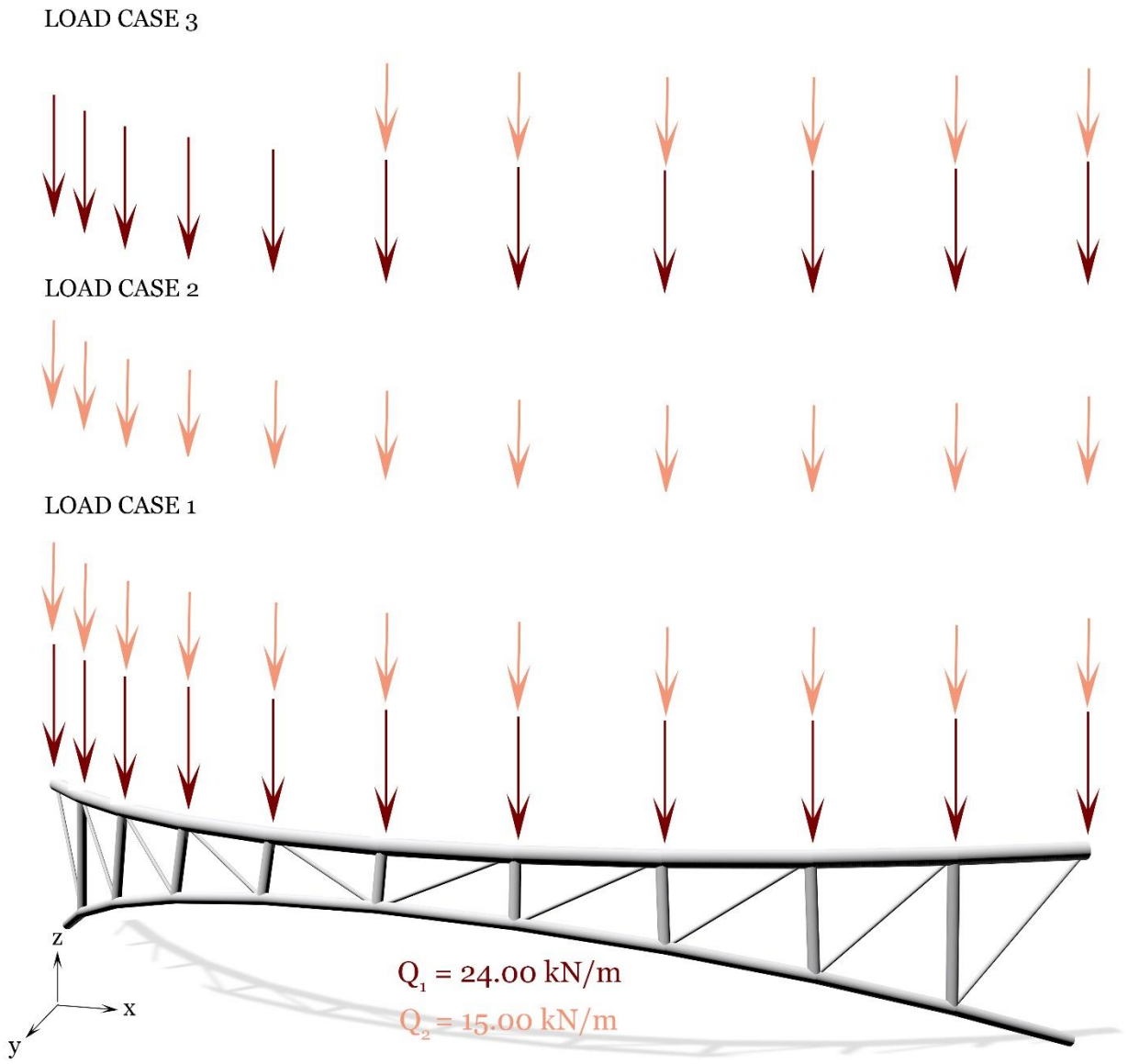

Figure 6. 3 Vertical load cases

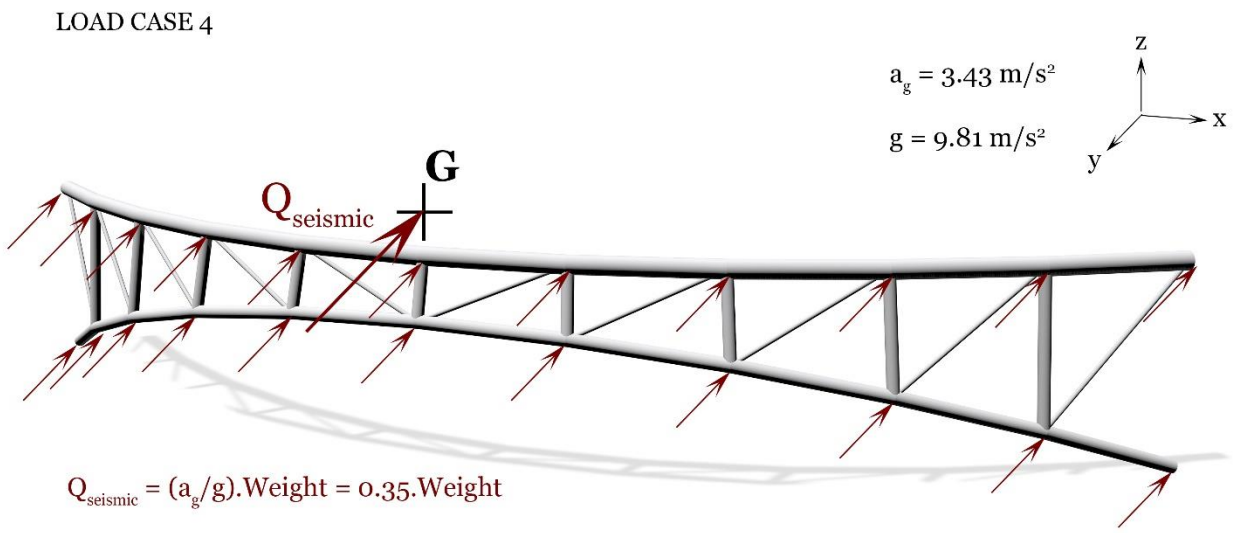

Figure 6. 4 Horizontal load case (static seismic action)

In addition, a fourth horizontal load case (LOAD CASE 4) has been defined, simulating a static seismic action (see *Figure 6. 4*), given by multiplying the weight of the structure (for each candidate solution) by a normalized seismic acceleration equal to 0.35 (corresponding to an actual acceleration equal to $a_g = 0.35 \cdot g = 3.343\ m/s^2$, where g is the gravity acceleration), acting in the horizontal direction orthogonally to the truss span (i.e. in the y −direction). Unlike the other load cases, it can be seen from *Figure 6. 4* that the static seismic load has been applied as concentrated forces on all nodes of the considered arched truss.

6.1.4 Results

The optimum design problem of the spatial arched truss parametrically defined in section *§6.1.1,* subjected to three different combinations of vertical loadings and to a horizontal static seismic action (as shown in section *§6.1.3*), has been solved, by the optimization hybrid algorithm previously presented in section *§4.2*, producing significant results both in terms of structural performance and architectural value.

Since the optimization problem has been formulated as a function of 93 design variables, the *Differential Evolution Algorithm* (described in detail in section *§4.2.2*) included in the proposed macro-algorithm, was performed assuming a "population" of 100 "individuals" and a maximum number of "generations" equal to 300 (stop criterion of the optimization routine).

Figure 6. 5 shows the shape of the optimal solution obtained for a given span of 40.00 *m* of the arched chords and a fixed depth of 6.00 *m* at the truss ends (also called "base depth"). The upper chord showed to be characterized by a total length of 43.516 *m* and a "horizontal rise" equal to 7.571 *m* (see *Figure 6. 5(a)*), leading to a resulting "rise-to-span ratio" corresponding to 1/5.28. On the other hand, *Figure 6. 5(b)* also shows that the lower chord turned out to be characterized

by a total length of 44.521 m and inclination about 27.5° over the horizon, as well as by an "inclined rise" of 9.022 m and a resulting "inclined rise-to-span ratio" about 1/4.43. Furthermore, the projection of the inclined arched chord on a horizontal plane showed to be characterized by a "projected rise" of 8.000 m, thus corresponding to a "projected rise-to-span ratio" of 1/5.

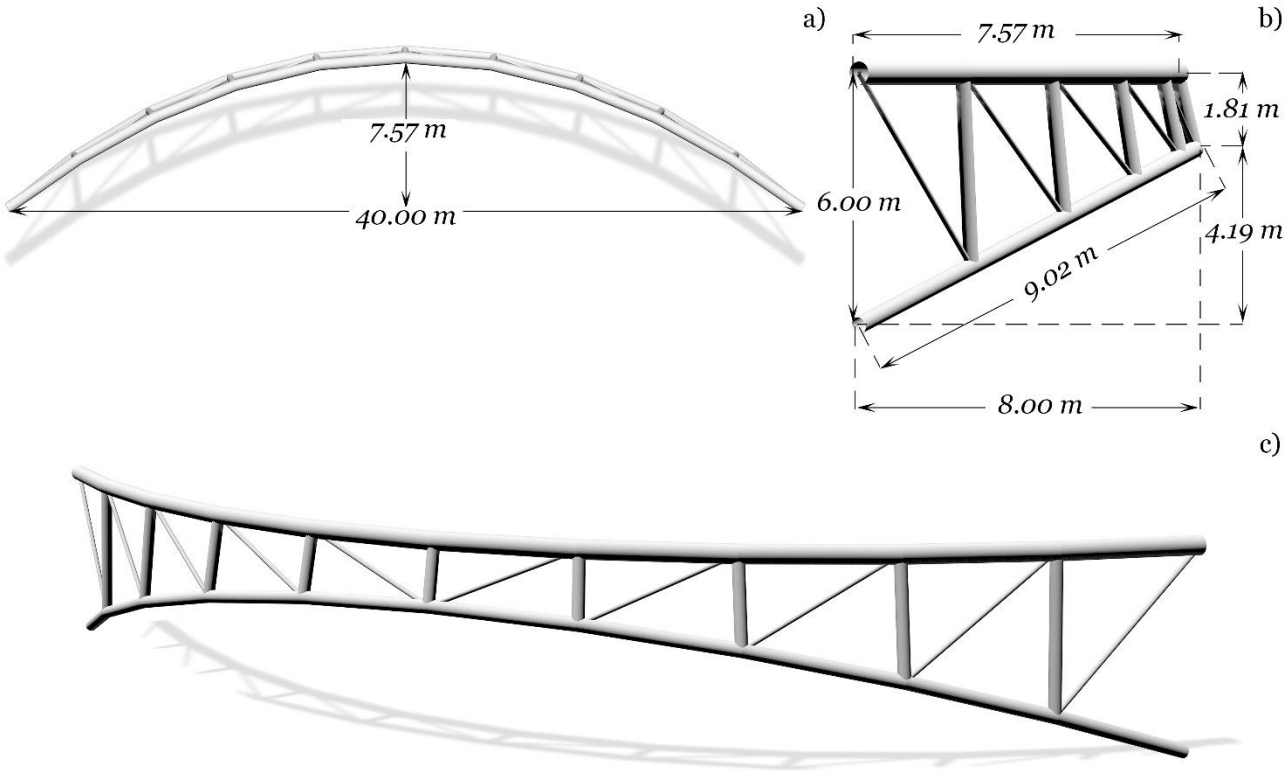

Figure 6. 5 *Spatial arched truss optimal shape with main dimensions: (a) top view; (b) lateral view; (c) perspective view*

The spatial curved is further typified by a "crown depth" of 1.81 m, approximately corresponding to 1/22 of the arch span (which is its resulting "crown depth-to span ratio"), leading to a "taper ratio" (defined as a ratio of the arch "crown depth" over its "base depth") about 1/3.32.

The shape of the optimal solution in *Figure 6. 5* was determined by the obtained values of shape design variables (indicated in *Table 6. 3*), defining the coordinates and corresponding weight factors of control points of the upper and lower *Rational Bézier arcs*.

It can be easily seen from *Table 6. 3* that the value of the x –coordinates of the internal control points ($x_{P1u} = x_{P2u}$) defining the shape of the horizontal arched chord correspond to 1/3.00 of the arch span, whereas the value determining the x –coordinates of the internal control points ($x_{P1l} = x_{P2l}$) defining the shape of the inclined arched chord corresponds to 1/2.18 of the arch span.

Table 6. 3 *Topology and shape optimization results: optimal values of topology and shape design variables*

Topology optimization results			
Design Variable (DV)	**Type of DV**	**Best value**	**Unit**
n_{int}	*topology*	10	$[adim.]$
Shape optimization results			
Design Variable (DV)	**Type of DV**	**Best value**	**Unit**
x_{P1l}	*shape*	18.3298	$[m]$
y_{P1l}	*shape*	11.2507	$[m]$
w_{P1l}	*shape*	0.8168	$[adim.]$
Δz	*shape*	0.100	$[m]$
x_{P1u}	*shape*	13.3191	$[m]$
y_{P1u}	*shape*	10.0941	$[m]$
w_{P1u}	*shape*	1.00	$[adim.]$

Table 6. 4 *Size optimization results: optimal diameters and thicknesses of circular hollow cross-sections*

Size optimization results					
Element groups	**Type of DV**	**Diameter d_i**	**Min. thickness t_i**	**Max. thickness t_i**	**Unit**
Bottom chord	*size*	0.4064	0.0063	0.0063	$[m]$
Top chord	*size*	0.5588	0.0071	0.0071	$[m]$
Diagonals	*size*	0.133	0.004	0.008	$[m]$
Verticals	*size*	0.3556	0.0063	0.0142	$[m]$

Furthermore, a value about 1/3.96 of the arch span was obtained for the y −coordinates of the internal control points ($y_{P1u} = y_{P2u}$) affecting the shape of the horizontal arched chord, whereas a slightly larger value, equal to 1/3.55 of the arch span, was obtained for the y −coordinates of the internal control points ($y_{P1l} = y_{P2l}$) determining the shape of the inclined arched chord, 0.40 m more protruding (in the y −direction) with respect to the horizontal upper chord (see *Figure 6. 5(b)*).

The size optimization results are summarized in *Table 6. 4*, showing that, as expected, the tubular elements of the horizontal upper chord required a significantly larger diameter compared with other elements. Furthermore, both the upper and lower chords elements needed a constant thickness (equal to 0.0071 m and 0.0063 m, respectively). It is worth noting that, unlike the case

of in-plane truss arches analysed in *§Chapter 5*, in this case vertical elements required large diameter and thicknesses.

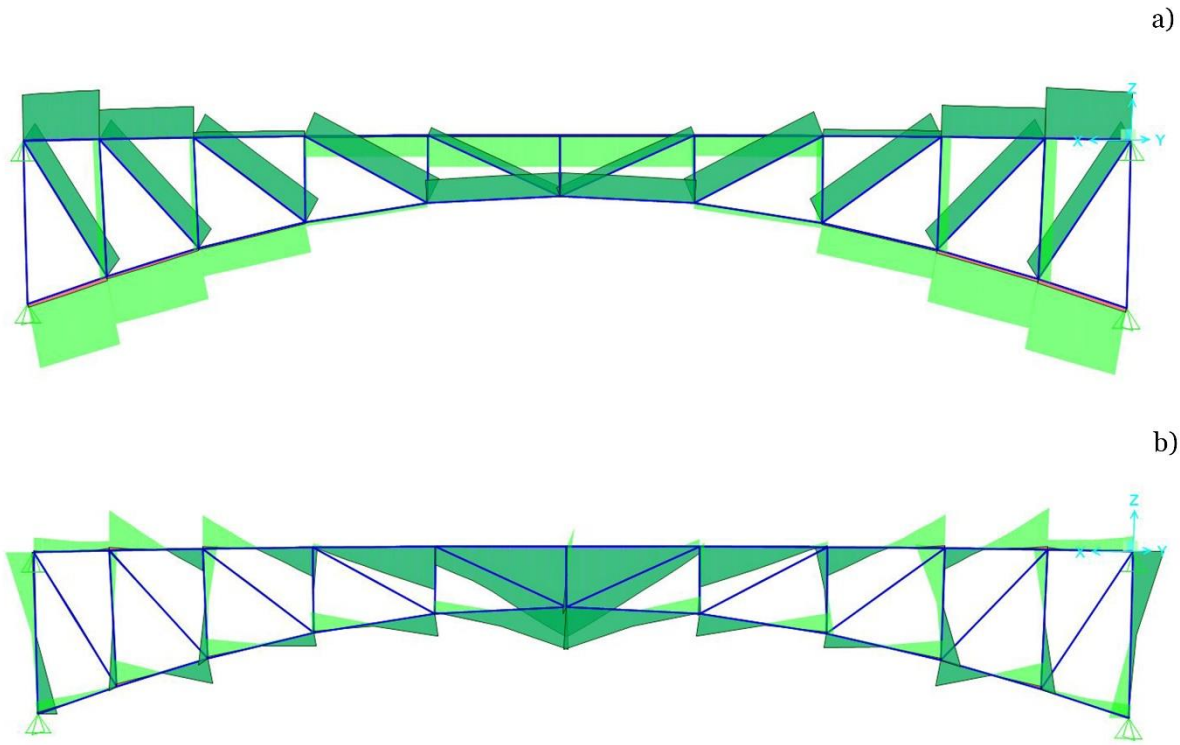

Figure 6. 6 *Finite Element Analysis (FEA) results: (a) axial force diagram; (b) bending moment diagram*

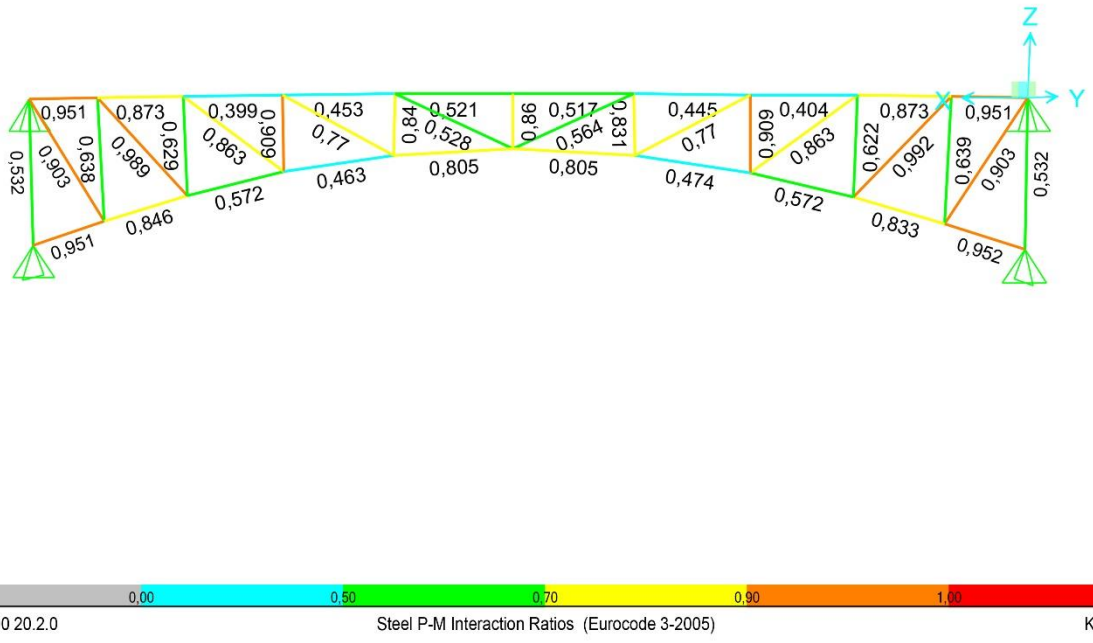

Figure 6. 7 *Finite Element Analysis (FEA) results: Demand/Capacity ratio (also called "utilization ratio") diagram of the optimal solution for the envelope of all load cases*

The size optimization results are validated by the axial force and bending moment diagrams evaluated for the envelope of all considered load combinations (see *Figure 6. 6*). More specifically, it has been found that the six more external elements of the upper chord are subjected to a tensile axial force, varying from 95 to 978 kN, whereas its four internal members are subjected to a compressive axial force between 28 and 552 kN. Conversely, the eight more external tubes composing the lower inclined chord turned out to be subjected to a compressive axial force varying from 75 to 1415 kN, while its two internal bars bear a tensile axial force of 402 kN (see the axial force diagram in *Figure 6. 6(a)*). As a matter of fact, the upper chords elements required a greater cross-section although they are subjected to smaller tensile and compressive axial forces compared with the lower chord members. However, the steel tubes composing the upper horizontal rib supports considerably greater bending moments, varying between 23 $kN.m$ and 120 $kN.m$.

Indeed, the lower chord bars showed to withstand bending moment actions smaller than 54 $kN.m$ (as shown in *Figure 6. 6(b)).*

Unlike what emerged from results of structural optimization of in-plane truss arches, the diagonal elements are here subjected to only tensile axial forces, varying from 141 to 500 kN. On the other hand, vertical elements withstands a compressive axial force included between 7 and 482 kN, as well as bending moments smaller than 50 $kN.m$.

Analogously to what has been done for in-plane truss arches, the stress level in the structure to be optimized was kept within an allowable range of values, imposing that the maximum "utilization ratio" (i.e. the "demand/capacity ratio" evaluated by Eqs. (40-42)) of all truss members, for all applied load cases, was less or equal to 0.99 (see Eq. (47) assumed as strength constraint function). Eqs. (40-42) check the combined effect of axial forces and bending moments by also considering flexural and lateral-torsional buckling of cross-sections subjected to combined axial compressive and bending stresses. In this regard, *Figure 6. 7* shows a diagram of the optimal arched truss here analysed, indicating the maximum i^{th} −element "utilization ratio" ($\max_{LC} Util_i^{LC}$), for the envelope of all considered load combinations, thus proving the feasibility of the considered solution regarding the strength constraints. However, also all serviceability constraints were satisfied.

Furthermore, a weighted average of Demand/Capacity ratios ($\max_{LC} Util_i^{LC}$) shown in *Figure 6. 7,* with respect to the weight of each member was evaluated by Eq. (51), to obtain a "total utilization ratio" ($Util_{tot}$) expressing an overall percentage of the material exploitation of the whole structure. A satisfactory percentage of material exploitation, about 69.6 % has been therefore obtained as a guarantee of a high level of structural performance of the spatial arched truss under consideration.

The quality of the optimization results here discussed is proved by the convergence curve of the minimized "objective function" (i.e. the total volume of the structure) shown in *Figure 6. 8*. A minimum volume of 1.388 m^3 was obtained since the 196^{th} generation. This is further confirmed by the history curve of the "stagnation function", which grows continuously from the 196^{th} generation onwards, as shown in *Figure 6. 9(a)*.

Figure 6. 9(b) shows the history of the "unfeasibility function" (ρ^k), which was introduced in section *§5.2.4.1* and defined by Eq. (52), as a ratio between "unfeasible individuals" (Unf^k) and all individuals (Pop^k) of a k^{th} –generation. In this specific case, it has been found that ρ becomes and remains zero from the 22^{th} generation onwards, meaning that the optimization process produced and evaluated only feasible candidate solutions from this point on (as shown in *Figure 6. 9(b)*).

The quality of the obtained results is also proved by the trend of convergence curves of design variables that most typified the final optimal solution.

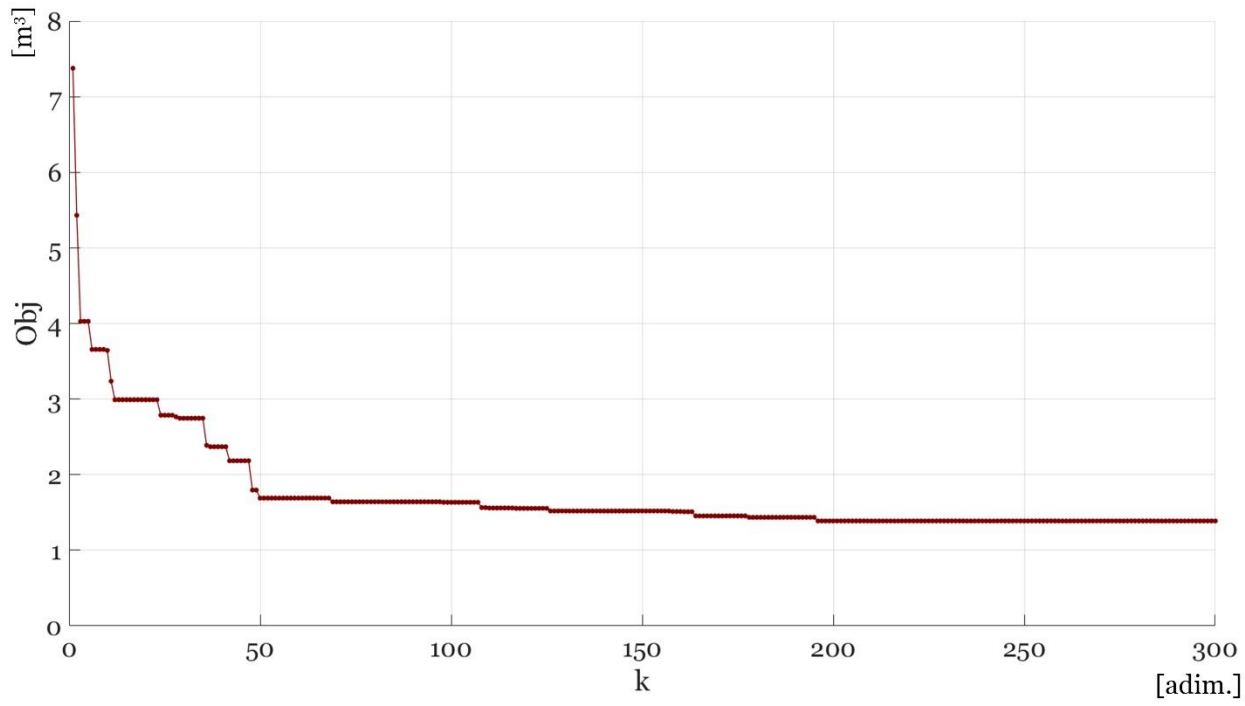

Figure 6. 8 *Convergence curve of the Objective (Obj) function (i.e. the volume of the arch) for all "generations"*

Among all design variables, the topology parameter n_{int} has a great importance by a constructive and structural point of view, since its value indirectly determined the number of elements and joints composing the structure. As shown in *Figure 6. 10,* the final optimal value equal to 10 (for which the arched truss under consideration resulted to be composed by 41 tubular members, connected by 22 pinned joints) was achieved since the third generation.

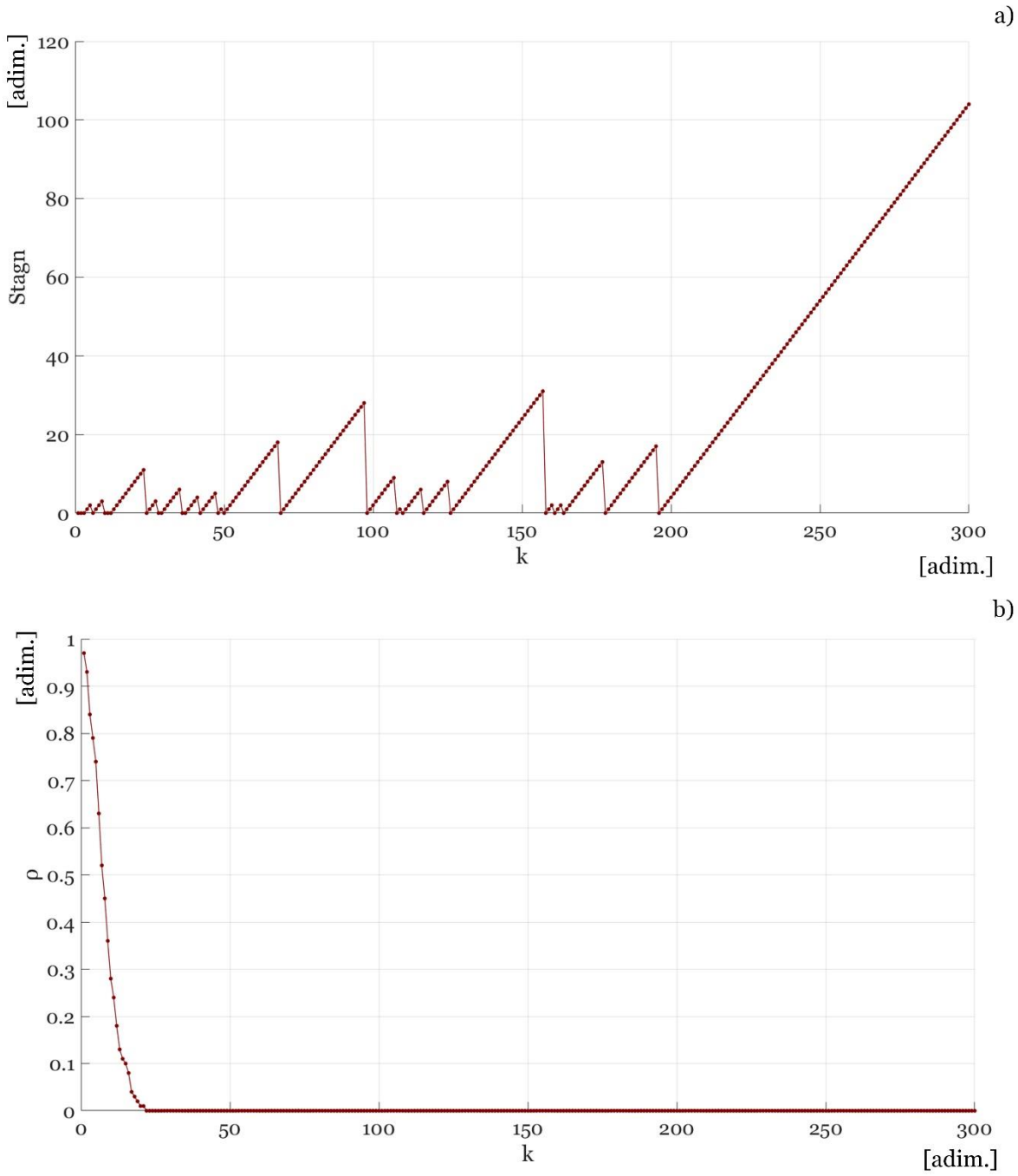

Figure 6. 9 *History of optimization functions: (a) stagnation function; (b) "unfeasibility function" (called "ρ-function"*

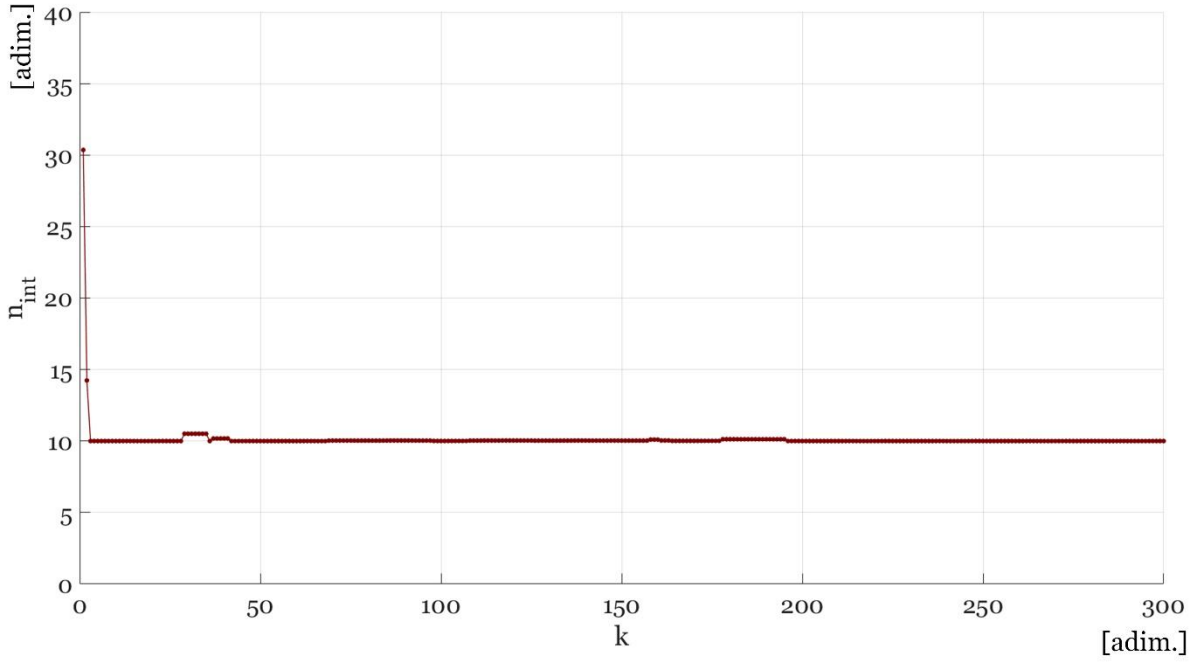

Figure 6. 10 Convergence curve of the topology design variable (n_{int})

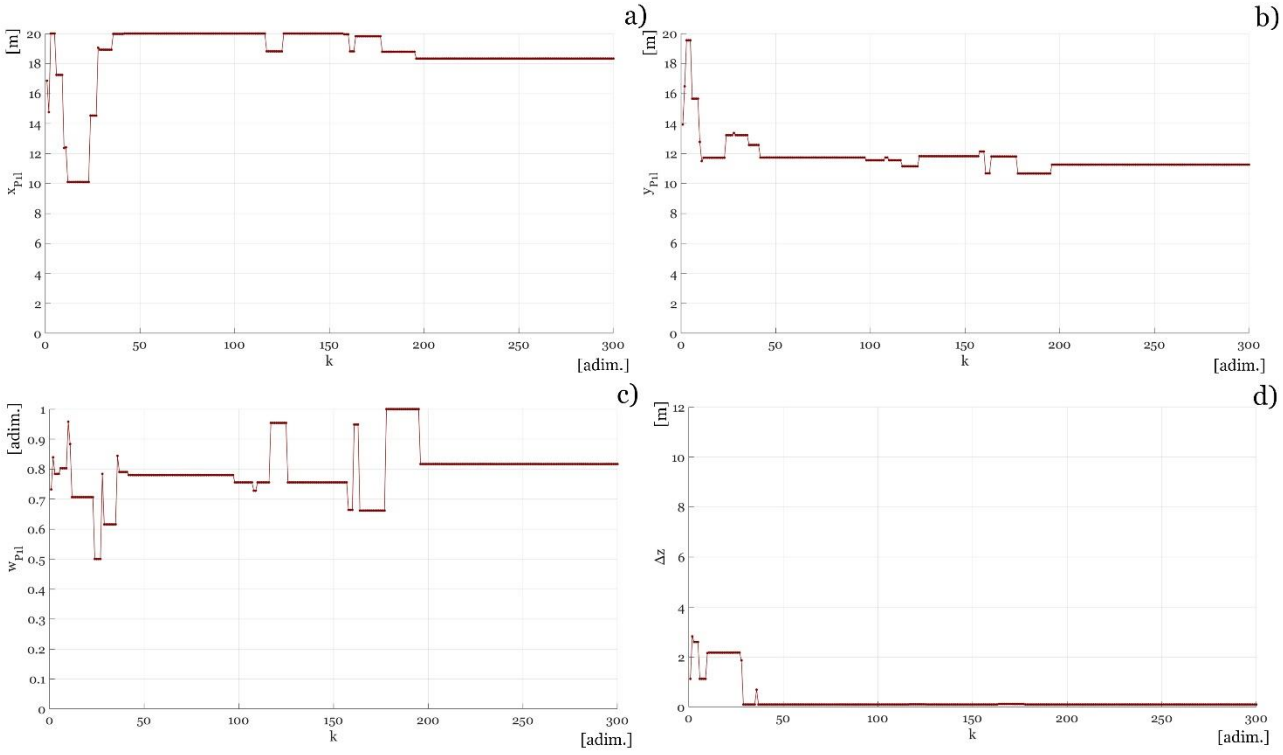

Figure 6. 11 Convergence curves of the shape design variables (variable parameters of third-degree rational Bézier curves): (a) x –coordinate of the second control point (x_{P1l}) of the bottom arched chord; (b) y –coordinate of the second control point (y_{P1l}) of the bottom arched chord; (c) weight factor of the second control point (w_{P1l}) of the bottom arched chord;(d) the difference between the z –coordinates (in absolute value) of the top and bottom chord internal control points (Δz)

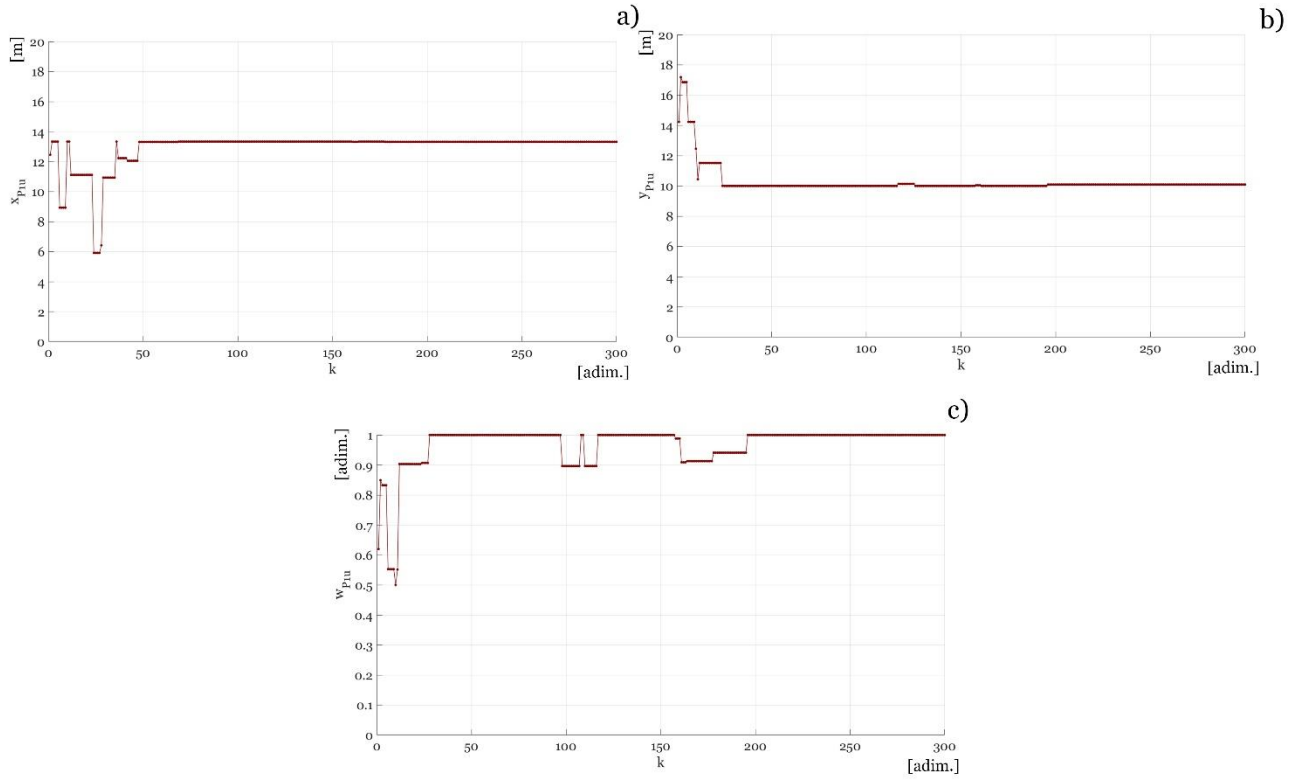

Figure 6. 12 Convergence curves of the shape design variables (variable parameters of third-degree rational Bézier curves): (a) x −coordinate of the second control point (x_{P1u}) of the top arched chord; (b) y −coordinate of the second control point (y_{P1u}) of the top arched chord; (c) weight factor of the second control point (w_{P1u}) of the top arched chord

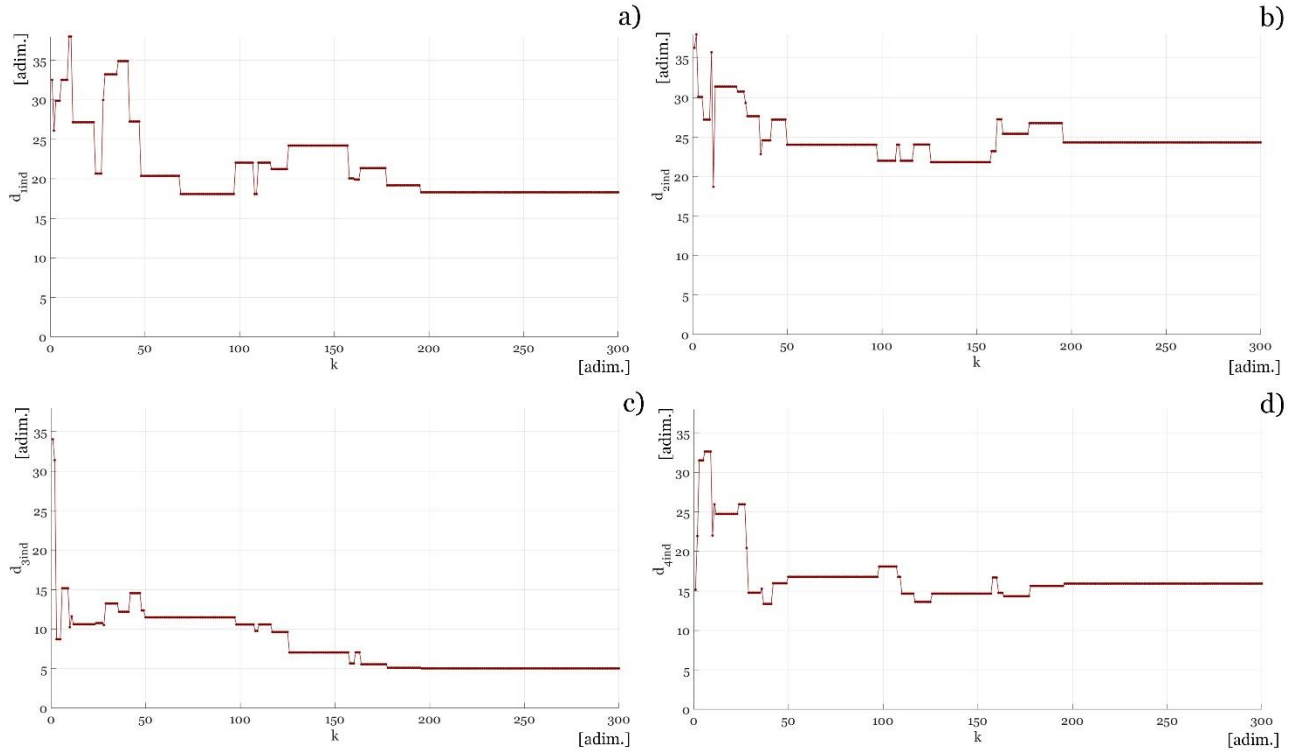

Figure 6. 13 Convergence curves of size design variables (i.e. indexes identifying the element group diameters in a list of commercial circular hollow cross-sections): (a) index identifying the bottom chord diameter; (b) index identifying the top chord diameter; (c) index identifying the diameter of diagonals; (d) index identifying the diameter of verticals

The good convergence level of the history curves of shape design variables is demonstrated by *Figure 6. 11* and *Figure 6. 12*. More specifically, the optimal values of design variables determining the shape of the lower inclined chord (which are x_{P1l}, y_{P1l} and w_{P1l}) have been achieved at the 196^{th} generation (as shown in *Figure 6. 11(a-c))* except for Δz, whose optimal value was reach since the 30^{th} generation (see *Figure 6. 11(d))*. On the other hand, the final values of design variables determining the shape of the upper horizontal chord have been achieved before the 50^{th} generation, except for the value of the weight factor w_{P1u} that has been finally found since the 196^{th} generation (see *Figure 6. 12*).

Since the number of size design variables here assumed is extremely large (as shown in section *§6.1.1*), only the convergence curves of design variables determining the diameters of four element groups have been presented in *Figure 6. 13*, showing that their optimal values have been reached since the 196^{th} generation, further confirming the quality of the obtained results notwithstanding the large number of design variables here assumed and their different nature (topology, shape and size).

Part IV

Conclusions

Chapter 7

7. Conclusions and future developments

7.1 Conclusions

The present dissertation has addressed the problem of optimizing planar and spatial arched trusses (made by steel tubular elements) under multiple load cases.

For this purpose, a hybrid optimization routine integrating a parametric definition of the design problem (i.e. its geometry, boundary conditions, as well as objective and constraint functions, as a function of properly selected design variables), a metaheuristic optimization algorithm and a code for Finite Element Analysis (FEA) has been developed through a MATLAB program (in detail described in section *§4.2*). In particular, structural analysis was required to be performed by the *FEM* software *SAP2000* to evaluate the objective and constraints functions of the considered optimization problem. However, the *FEM* model for structural analysis is entirely defined and updated (for each design variable vector) in the *MATLAB* environment, by using the so-called *Open Application Programming Interface (OAPI)* functions, in order to minimize the total computational time of the whole process.

The proposed method allowed to simultaneously optimize planar and spatial steel arched trusses considering a unique set of a large number of design variables, notwithstanding their different nature (topology, shape and size, as well as continuous and discrete variables have been considered).

At an early stage, the results obtained from the optimization of planar truss arches subjected to single and multiple load cases were compared. In doing so, it has been demonstrated that structural optimization of in-plane truss arches with two chords subjected to a single load case leads to optimal solutions in which upper and lower chords tend to coincide with each other and with the “funicular curve” (i.e. the “line of thrust”) for that given load.

This first demonstrative application of the structural optimization strategy proposed in this thesis thus proved that truss arches are not suitable to be optimized considering a single load pattern only. At the same time, this consideration also allows to state that single-rib arches would not be appropriate to be optimized for multiple load conditions.

In light of the above, simultaneous topology, shape and size optimization of steel truss arches with two arched chords linked each other through a bracing system (with variable Pratt-type pattern) has been formulated for multiple load cases and different structural boundary conditions (as illustrated in *§Chapter 5*).

The problem of the optimum design of two-hinged and hingeless in-plane truss arches was addressed considering four different formulations, each one characterized by a different span (40, 80, 120 and 160 $meters$) and different numbers of size design variables (which were assumed to be proportional to the allowable range of the element number for each span length). The variable number of the arch elements was defined as a function of the chosen topology design variable n_{int}, indicating the even integer of equal intervals into which the arch span was subdivided.

It is worth highlighting that the shape design variables have been chosen among the parameters defining the cubic parametric form of *Rational Bézier Curves* with four control points. *Third-degree Rational Bézier Curves* have been chosen to optimize the shape of the arch chords because they can represent a wide family of curves (also including conic curves), depending on a small number of parameters, thus allowing to assume a limited number of shape design variables.

Furthermore, the elements of arched trusses under consideration were characterized by circular hollow cross-sections, whose diameters and thicknesses were assumed as discrete size design variables, since their values were taken from a list of commercial steel tubes.

In so doing, in-plane truss arches with different span lengths and structural boundary conditions have been successfully optimized for multiple load cases, only considering vertical loads (acting in the same plane as the arch), since in-plane arches are not suited to withstand out-of-plane loads.

The obtained optimal results have been presented and investigated in this dissertation, thus deducing useful suggestions for the design of steel arched trusses.

For instance, in cases of two-hinged arches, it was found that:

- The optimal number of the arch span subdivision (n_{int}) resulted to be constant and equal to 12 for the arches with spans of 40, 80 and 120 meters, whereas it resulted to be equal to 22 for the truss arch with a span of 160 meters
- All optimal shapes resulted to be characterized by a “rise-to-span ratio” included between 1/6.1 and 1/6.9 for truss arches with spans of 40, 80 and 120 meters, whereas a value 1/4.8 has been obtained for the two-hinged truss arch with a span of 160 meters. Note that as the arch span increases, its optimal shape becomes less and less lowered (i.e. looking less flattened at its crown), finding an almost parabolic optimal shape for the arch with a span of 120 meters

- All optimal shapes are characterized by a "crown depth-to-span ratio" between 1/9.1 and 1/9.6 for truss arches with spans of 40, 80 and 120 meters, whereas a value about 1/12.15 has been obtained for the two-hinged truss arch with a span of 160 meters. It is worth noting that as the arch span increases, its "crown depth" is significantly reduced
- The optimal solutions are characterized by an overall percentage of the material exploitation (also called "total utilization ratio") always bigger than 70 % (i.e. between 71.5 % and 79.2 %).

On the other hand, considerably different results have been obtained for the truss arches connected to the soil by means of two double hinges (vertically aligned), thus comparable to hingeless truss arches. In cases of "hingeless" truss arches with spans of 40, 80, 120 and 160 meters, it was found that:

- The optimal number of the arch span subdivisions (n_{int}), which indirectly determines the optimal element number of the arch, resulted to be linearly dependent on the arch span as follows, $n_{int} = \frac{1}{10}.L + 12$ (where L indicates the arch span)
- The optimal shapes of arches with span from 40 to 120 meters are characterized by a "rise-to-span ratio" increasing from 1/3.7 to 1/3.2, whereas the optimal truss arch 160 meters long showed to have a "rise-to-span ratio" once again equal to 1/3.7. Note that their shapes are therefore significantly less lowered than optimal two-hinged arches
- The optimal "hingeless" truss arches under consideration are also characterized by significantly smaller "crown-depth-to-span ratios", varying between 1/28 and 1/40, compared with values between 1/9 and 1/12 obtained for the two-hinged solutions
- Evaluating a "taper ratio" as a ratio of "crown" and "base" depths, it was found that this value varies between 1/2.7 and 1. This means that as the arch span increases, the distance between two arch chords tends to become constant.
- Analogously to what emerged for two-hinged truss arches, the optimal solutions of the considered "hingeless" arches were also characterized by an overall percentage of the material exploitation (also called "total utilization ratio") always greater than 70 % and included between 70.1 % and 72.5 %.

All illustrated results should be correlated to the strong increase in the self-weight of the arch, as its span increases. As a matter of fact, as the arch span increases, the more its self-weight increases with respect to variable loads, thus strongly reducing the influence of the asymmetrical load condition. It is important to remark that the self-weight of two-hinged arches increased much more rapidly as the arch span increased, compared with "hingeless" truss arches.

At a later stage (in *§Chapter 6*), a spatial arched truss with two arched chords lying on different planes has been optimally designed for multiple loadings acting in different directions. In

particular, a steel truss with a lower arched chord variably inclined in the 3D-space and a horizontal upper arched chord linked each other through a bracing system (of type Pratt), has been optimally designed under three combinations of vertical loadings and a horizontal seismic action (obtained by multiplying the weight of the structure by a normalized acceleration equal to 0.35) parallel to the upper chord plane.

The spatial arched truss under consideration, with a given horizontal span of 40 meters and a fixed depth at its ends of 6 meters, was optimally designed, according to strength and serviceability constraints, as well as assigning larger cross-sections to the truss elements, due to its lower stiffness. However, significant results were obtained both in terms of structural performance and architectural value. In particular, the optimal slender shape of the considered arched truss showed to be characterized by a "horizontal rise-to-span ratio" of the upper arched chord equal to 1/5.28, an "inclined rise-to-span ratio" of the lower arched chord equal to 1/4.43 and by an extremely small "crown-depth" approximately corresponding to a 1/22 of the arch span. Furthermore, a high level of structural performance is ensured by an overall percentage of material exploitation (i.e. expressed by the aforementioned "total utilization ratio") equal to 69.7 %, although also serviceability constraints have been imposed requiring greater cross-sections compared with in plane truss arches analysed in *§Chapter 5*.

It is worth noting that it was unfortunately not possible to optimize spatial arched trusses with larger spans because of the high deformability of the structure. However, the obtained arched truss with a given span of 40 meters, optimized for multiple load cases also considering a static seismic action, would be suitable to support the curved deck of a footbridge, similarly to what has been done by Fenu et al. (Luigi Fenu, Congiu, and Briseghella 2016).

In conclusion, analysing the obtained results, useful suggestions for steel truss arch design can be deduced and adopted as general guidelines.

7.2 Future works

As demonstrated by the results discussed in §Chapters 5 and 6, the optimization macro-algorithm here proposed, implemented by a MATLAB program containing a parametric definition of the optimization problem and geometry, a metaheuristic optimization algorithm and a code for Finite Element Analysis (FEA), showed to be effective and robust in handling and solving optimization problems characterized by large numbers of design variables of different nature, minimizing the assumed objective function in accordance with several constraint functions.

The present research was focused on the structural optimization of in-plane and spatial steel arched trusses with span from 40 to 160 meters, subjected to different load cases.

Since truss arches are mainly used in steel and CFST (Concrete Filled Steel Tubes) arch bridges, especially when the arch span exceeds 200 meters, the present research should be extended to the structural optimization of planar steel truss arches with span larger than 160 meters, also overcoming 200 meters of span. However, long span truss arches are commonly designed for road or railway bridges, whereas the load patterns here assumed are comparable to dead and live loads considered in footbridges design. Therefore, in extending the present research to truss arches with long spans (longer than 200 meters), different combinations of more various load patterns should be considered.

A further innovative aspect of the proposed approach was the assumption of the parametric cubic equation of *Rational Bézier curves* as shape function, to parametrize the shape of the arched chords as a function of a limited number of design variables. More specifically, *third-degree Rational Bézier curves* have been adopted to represent an extremely wide family of curves (also including conic curves) assuming a small number of shape design variables. It would be therefore interesting to extend, in the future, the application of the optimization macro-algorithm here proposed (*§4.2*) to the optimization problem of vaults and shells, continuous and discrete (e.g. the "grid-shells"), synclastic and anticlastic, by parametrizing them by means of high-degree functions of *Rational Bézier Surfaces* (whose shape needs to be defined by a set of control points and corresponding weight factors) to considerably limit the number of necessary shape design variables.

Appendix A

Rational Bézier Curves

Bézier curves are parametric curves very used in vector graphics to model smooth curves that can be scaled indefinitely but are also in animation applications (Gerald Farin 1988; Farin, Hoschek, and Kim 2002; Piegl and Tiller 1997). Quadratic and cubic *Bézier curves* are most common because higher degree curves are more computationally expensive to evaluate. The higher the degree of the Bézier function, the weaker the relationship between the Bézier curve and its control polygon (polyline obtained by linking the control points) becomes.

Composite quadratic and cubic *Bézier* (series of *Bézier curves* joined end to end) functions are generally very used to model curved shape but standard Bézier curves can't exactly represent arcs of conic sections, except parabolic arcs.

Conversely, parametric *Rational Bézier curves* can exactly represent conic sections and are widely used in CAD (Computer Aided Design)/CAGD (Computer Aided Geometric Design) fields to model freeform curves because they can be easily deformed by changing the control point coordinates or by varying its corresponding non-negative weight factors (whose values define the attraction level that the control polygon exerts on the curve).

The mathematical basis for *Bézier* curves is the *Bernstein polynomials* (known since 1912).

The $n + 1$ *Bernstein basis polynomials* of degree n are defined as

$$B_{i,n}(\boldsymbol{u}) = \binom{n}{i}\boldsymbol{u}^i(1-\boldsymbol{u})^{n-i} \tag{A.1}$$

where $i = 0, \dots, n$ and $0 \leq \mathbf{u} \leq 1$, whereas the quantity $\binom{n}{i}$ is a binomial coefficient that is given by,

$$\binom{n}{i} = \frac{n!}{i!(n-i)!} \tag{A.2}.$$

The standard parametric expression of a n-degree *Bézier Curve* is defined as follows

$$C(\boldsymbol{u}) = \sum_{i=0}^{n} B_{i,n}(\boldsymbol{u})P_i \tag{A.3}$$

where which P_i are the $n + 1$ *control points*.

The coordinates of each point of the curve are obtained as a sum of *blending functions* multiplied by the control point coordinates. Both *Rational* and *Non-Rational Bézier Curves* pass through

the first and the last control points and are tangent at those points respectively to the first and the last control polygon (obtained as interpolation of control points) segments.

Standard *Bézier Curves* can't exactly represent conic sections, except for parabolic arcs that can be represented by polynomial curves. Conversely, *second-degree Rational Bézier Curves* (with three control points and corresponding weight factors) can exactly represent conic sections. When the weight factors are all the same, a *Rational Bézier Curve* becomes equivalent to a *Standard (non-rational) Bézier curve* (for instance, a second-degree *Rational Bézier* function with all weights equal to 1 represents a parabolic arc).

The general parametric expression of a *Rational Bézier* n^{th} *−degree Curve* can be written as follows,

$$C(\mathbf{u}) = \sum_{i=0}^{n} R_{i,n}(\mathbf{u}) P_i \tag{A.4}$$

In which the quantity $R_{i,n}(\mathbf{u})$, being called as *blending function*, is a n^{th} −degree rational function in **u** with the following parametric expression,

$$R_{i,n}(\mathbf{u}) = \frac{B_{n,i}(\mathbf{u}) w_i}{\sum_{j=0}^{n} B_{n,j}(\mathbf{u}) w_j} \tag{A.5}.$$

The parametric form of a *second-degree Rational Bézier function* (which can exactly represent conic sections) can be expressed as follow,

$$C(\mathbf{u}) = \frac{\left(P_0.w_0.(1-\mathbf{u})^2 + P_1.w_1.2\mathbf{u}.(1-\mathbf{u}) + P_2.w_2.\mathbf{u}^2\right)}{\left(w_0.(1-\mathbf{u})^2 + w_1.2\mathbf{u}.(1-\mathbf{u}) + w_2.\mathbf{u}^2\right)} \tag{A.6}$$

where P_0, P_1 and P_2 are the *control points*, w_0, w_1 and w_2 are the corresponding *weight factors* and **u** is the parameter included in the interval [0,1].

The value of the *weight factor* w_1 (of the internal *control point* P_1) can be considered as a *shape coefficient* since,

- When $w_1 < 1$ the Rational Quadratic Bézier function represents an *elliptical* arc;
- When $w_1 = 1$ the Rational Quadratic Bézier function represents a *parabolic* arc;
- When $w_1 > 1$ the Rational Quadratic Bézier function represents a *hyperbolic* arc

as shown in *Figure A. 1*.

On the other hand, *third-degree Rational Bézier functions* represent a wider family of curves, also including *conic sections*.

The parametric form of a *cubic Rational Bézier curve,* here adopted as shape function in parametrizing the shape of the considered arches, can be expressed by the following equation,

$$C(\mathbf{u}) = \frac{(P_0.w_0.(1-\mathbf{u})^3+P_1.w_1.3\mathbf{u}.(1-\mathbf{u})^2+P_2^2.w_2.3\mathbf{u}^2.(1-\mathbf{u})+P_3.w_3.\mathbf{u}^3)}{(w_0.(1-\mathbf{u})^3+w_1 3\mathbf{u}.(1-\mathbf{u})^2+w_2.3\mathbf{u}^2.(1-\mathbf{u}).w_2+w_3.\mathbf{u}^3)} \quad (A.7)$$

depending on the coordinates of four *control points* P_0, P_1, P_2 and P_3, on the corresponding *weight factors* (w_0, w_1, w_2 and w_3) and on the parameter **u.**

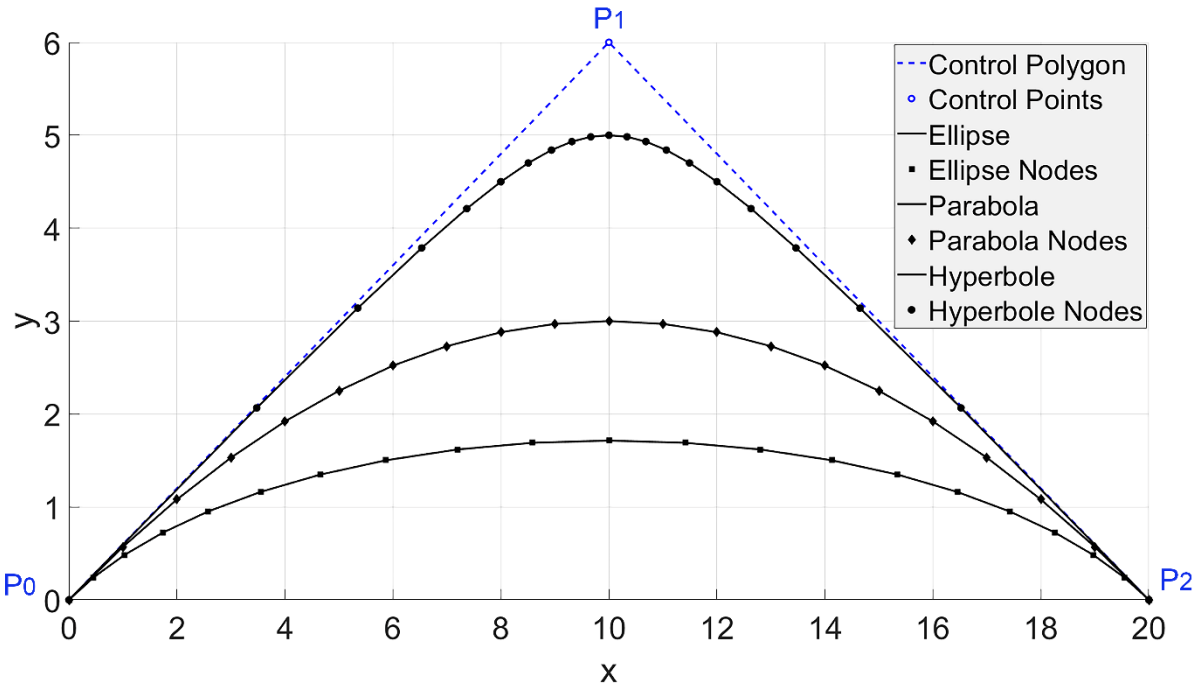

Figure A. 1 Quadratic Rational Bézier curves representing the conic sections

Rational Bézier curves can be further considered as a special case of *NURBS (Non-Uniform Rational B-Splines)* curves and they then satisfy all the peculiar properties of these curves.

A *NURBS Curve* is a piecewise composed by *Rational Bézier* curve segments and it interpolates the first P_0 and the last P_n *control points* (*endpoints interpolation property*). A *NURBS* Curve (as well as a *Rational Bézier* Curve) is entirely contained in the hull of the convex polygon obtained as interpolation of the *control points*, since the *weights* are non-negative factors. A *Bézier curve* of any degree n can be converted in a *Bézier curve* of degree $n + 1$ with same shape, by multiplying each component of $B_{i,n}(\mathbf{u})P_i$ by $(1 - \mathbf{u})\mathbf{u}$.

Furthermore, a point in a *Bézier curve*, can be evaluated by means of the *De Casteljau's Algorithm*, a recursive algorithm that exploit an important property of *Bézier Curves*: any *Bézier Curve* can be split into multiple parts to trace out the curve as straight lines. Computers use the *De Casteljau's Algorithm* to draw a *Bézier Curve*.

The *De Casteljau's Algorithm* takes the control points and finds the midpoints along each line, then joins these midpoints. After that, it takes the midpoints along the newly drawn lines and

finds the midpoints again, then draws a line connecting these. By doing this until we are down to only one point, we can approximate the Bézier curve (Šír and Jüttler 2015).

References

Adriaenssens, Sigrid, Philippe Block, Diederik Veenendaal, and Chris Williams. 2014. *Shell Structures for Architecture*. Edited by Sigrid Adriaenssens, Philippe Block, Diederik Veenendaal, and Chris Williams. New York: Taylor & Francis - Routledge. https://doi.org/10.4324/9781315849270.

Afshar, MH, and A Faramarzi. 2010. "Size Optimization of Truss Structures by Cellular Automata." *Computer Systems Science and Engineering* 3 (1): 1–9.

Ashlock, Daniel. 2006. *Evolutionary Computation for Modeling and Optimization*. Edited by Daniel Ashlock. *Springer*. New York: Springer Science+Business Media, Inc.

Askarzadeh, Alireza, and Esmat Rashedi. 2017. "Harmony Search Algorithm." In *Recent Developments in Intelligent Nature-Inspired Computing*, 1–36. Hershey: IGI Global. https://doi.org/10.4018/978-1-5225-2322-2.ch001.

Bäck, Thomas. 1996. *Evolutionary Algorithms in Theory and Practice : Evolution Strategies, Evolutionary Programming, Genetic Algorithms*. New York: Oxford University Press.

Bendsøe, M P, and O Sigmund. 2003. *Topology Optimization. Theory, Methods and Applications*. Berlin: Springer Berlin Heidelberg.

Bendsøe, Martin Philip, and Noboru Kikuchi. 1988. "Generating Optimal Topologies in Structural Design Using a Homogenization Method." *Computer Methods in Applied Mechanics and Engineering* 71 (2): 197–224. https://doi.org/10.1016/0045-7825(88)90086-2.

Block, Philippe. 2009. "Thrust Network Analysis : Exploring Three-Dimensional Equilibrium." Massachusetts Institute of Technology.

Block, Philippe, Matt DeJong, and John Ochsendorf. 2006. "As Hangs the Flexible Line: Equilibrium of Masonry Arches." *Nexus Network Journal* 8 (2): 13–24. https://doi.org/10.1007/s00004-006-0015-9.

Block, Philippe, and John Ochsendorf. 2007. "Thrust Network Analysis: A New Methodology for Three-Dimensional Equilibrium." *Journal of the International Association for Shell and Spatial Structures* 48 (155): 167–73.

Cavazzuti, Marco. 2013. "Deterministic Optimization." In *Optimization Methods*, 77–102. Berlin,

Heidelberg: Springer Berlin Heidelberg. https://doi.org/10.1007/978-3-642-31187-1_4.Chen, Wai-Fah, and Lian Duan. 2014. *Bridge Engineering Handbook Second Edition - Superstructure Design*. Edited by Wai-Fah Chen and Lian Duan. *Civ. Eng. (N.Y.)*. Second. Vol. 73. Boca Raton: CRC Press Taylor & Francis Group.

Cheng, Jin. 2010. "Optimum Design of Steel Truss Arch Bridges Using a Hybrid Genetic Algorithm." *Journal of Constructional Steel Research* 66: 1011–17.

Cheng, Jin, and Hui Jin. 2017. "Reliability-Based Optimization of Steel Truss Arch Bridges." *International Journal of Steel Structures* 17 (4): 1415–25. https://doi.org/10.1007/s13296-017-1212-y.

Clune, Rory. 2013. "Algorithm Selection in Structural Optimization." Massachusetts Institute of Technology.

Colaianni, Vito Giorgio. 1967. *Le Volte Leccesi*. Bari: Dedalo libri.

Conte, Carla, Carlo Rainieri, Maria Antonietta Aiello, and Giovanni Fabbrocino. 2011. "On-Site Assessment of Masonry Vaults: Dynamic Tests and Numerical Analysis." *GEOFIZIKA* 28 (1): 127–43.

Fallacara, Giuseppe. 2012. "The Lecce Vault: History, Construction Techniques, and New Design Perspectives." *Nuts & Bolts of Culture, Technology and Society Construction History, Vol. 3. Paris* 3: 99–106.

Farin, Gerald E., Josef. Hoschek, and Myung-Soo. Kim. 2002. *Handbook of Computer Aided Geometric Design*. Elsevier.

Feng, Yue. 2014. "An Optimization Index to Identify the Optimal Solution of Bridges." University of Trento, University IUAV of Venezia. https://doi.org/10.1080/00325481.1971.11697712.

Fenu, L, B Briseghella, and E Congiu. 2016. "Thrust Network Analysis (TNA) in Designing Curved Shell Supported Bridges : Italian Concrete Days L'analisi TNA (Thrust Network Analysis) Nel Progetto Di Ponti in Curva a Guscio : Giornate Aicap 2016 Congresso CTE." In *Italian Concrete Days Giornate Aicap 2016 Congresso CTE*. Roma.

Fenu, Luigi, Bruno Briseghella, and Eleonora Congiu. 2016. "Curved Footbridges Supported by a Shell Obtained as an Envelope of Thrust-Lines." In *ARCH'16 - 8th International Conference on Arch Bridges . Wroclaw*, 921–32. Wroclaw (Poland).

Fenu, Luigi, Bruno Briseghella, and Tobia Zordan. 2015. "Curved Shell-Supported Footbridges." *IABSE Symposium Report* 105 (43): 1–8. https://doi.org/10.2749/222137815818357430.

Fenu, Luigi, Eleonora Congiu, and Bruno Briseghella. 2016. "Curved Deck Arch Bridges

Supported by an Inclined Arch." In *19th IABSE Congress*, 273–80. Stockholm.

Fenu, Luigi, Eleonora Congiu, Bruno Briseghella, and Giuseppe Carlo Marano. 2017. "Ponte in Curva Sorretto Da Gusci Anticlastici Speculari in Cemento Armato Progettati Con l'uso Del Metodo TNA (Thrust Network Analysis)." *Structural* 209.

Fenu, Luigi, Eleonora Congiu, Davide Lavorato, Bruno Briseghella, and Giuseppe Carlo Marano. 2019. "Curved Footbridges Supported by a Shell Obtained through Thrust Network Analysis." *Journal of Traffic and Transportation Engineering (English Edition)* 6 (1): 65–75. https://doi.org/10.1016/J.JTTE.2018.10.007.

Gerald Farin. 1988. *Curves and Surfaces for Computer Aided Geometric Design. A Pratical Guide*. Edited by Academic Press. 4th ed. San Diego, USA.

Haftka, Raphael T., and Zafer. Gürdal. 1992. *Elements of Structural Optimization*. Kluwer Academic Publishers.

Heyman, Jacques. 1998. *Structural Analysis : A Historical Approach*. Cambridge University Press.

Huang, X., and Y. M. Xie. 2010. "Evolutionary Topology Optimization of Continuum Structures with an Additional Displacement Constraint." *Structural and Multidisciplinary Optimization* 40 (1–6): 409–16. https://doi.org/10.1007/s00158-009-0382-4.

Karnovsky, Igor A., and Olga Lebed. 2010. *Advanced Methods of Structural Analysis*. *Advanced Methods of Structural Analysis*. https://doi.org/10.1007/978-1-4419-1047_9.

Kennedy, James, and Russel Eberhart. 1995. "Particle Swarm Optimization." In *IEEE International Conference on Neural Networks*, IV:1942–48.

Khaoula Msaaf. 2017. "Multi-Objective Optimization of Arch Bridges." MIT - Department of Civil and Environmental Engineering.

Kilian, Axel, and John Ochsendorf. 2005. "Particle Spring Systems for Structural Form Finding." *Journal of the International Association for Shell and Spatial Structures* 46 (147): 77–84.

Kirckpatrick, S., C. D. Gelatt, and M. P. Vecchi. 1983. "Optimization by Simulated Annealing." *Science* 220 (4598): 671–80. https://doi.org/10.1126/science.220.4598.671.

Leontovich, Valerian. 1959. *Frames and Arches. Condensed Solutions for Structural Analysis*. Edited by Valerian Leontovich. New York (U.S.): McGraw-Hill Book Company, Inc.

Luenberger, David G. 1969. *Optimization by Vector Space Methods*. Edited by Ronald A. Howard. *John Wiley & Sons, Inc.* New York: John Wiley & Sons, Inc. https://doi.org/10.1049/sqj.1970.0088.

Makert, Rodrigo, and Gilfranco Alves. 2016. “Between Designer and Design: Parametric Design and Prototyping Considerations on Gaudí’s Sagrada Familia.” *Periodica Polytechnica Architecture* 47 (2): 89–93. https://doi.org/10.3311/ppar.10335.

Makiabadi, M H, A Baghlani, H Rahnema, and M A Hadianfard. 2013. “Optimal Design of Truss Bridges Using Teaching-Learning-Based Optimization Algorithm.” *International Journal of Optimization in Civil Engineering* 3 (3): 499–510.

Marano, Giuseppe Carlo, Francesco Trentadue, Rita Greco, Ivo Vanzi, and Bruno Briseghella. 2018. “Volume/Thrust Optimal Shape Criteria for Arches under Static Vertical Loads.” *Journal of Traffic and Transportation Engineering (English Edition)* 5 (6): 503–9. https://doi.org/https://doi.org/10.1016/j.jtte.2018.10.005.

Marano, Giuseppe Carlo, Francesco Trentadue, and Floriana Petrone. 2014. “Optimal Arch Shape Solution under Static Vertical Loads.” *Acta Mechanica* 225 (3): 679–86. https://doi.org/10.1007/s00707-013-0985-0.

Melan, Josef. 1915. *Plain and Reinforced Concrete Arches*. Wiley.

Michell, A.G.M. 1904. “The Limits of Economy of Material in Frame-Structures.” *The London, Edinburgh, and Dublin Philosophical Magazine and Journal of Science* 8 (47): 589–97. https://doi.org/10.1080/14786440409463229.

Michiels, Tim. 2018. “Form Finding of Arches and Shell Structures Subjected to Seismic Loading.” Princeton University. https://doi.org/10.13140/RG.2.2.18163.22562.

Michiels, Tim, and Sigrid Adriaenssens. 2018. “Form-Finding Algorithm for Masonry Arches Subjected to in-Plane Earthquake Loading.” *Computers and Structures* 195 (2018): 85–98. https://doi.org/10.1016/j.compstruc.2017.10.001.

Momo, T. Sun. 2017. “Nervi’s Design and Construction Methods for Two Thin-Shell Structures: The Leverone Field House and Thompson Arena.” Massachusetts Institute of Technology.

Monmarché, Nicolas., Frederic. Guinand, and Patrick. Siarry. 2010. *Artificial Ants : From Collective Intelligence to Real-Life Optimization and Beyond*. London: ISTE Ltd.

Monti, Giorgio, Giuseppe Quaranta, and Giuseppe Carlo Marano. 2010. “Genetic-Algorithm-Based Strategies for Dynamic Identification of Nonlinear Systems with Noise-Corrupted Response.” *Journal of Computing in Civil Engineering* 24 (2): 173–87. https://doi.org/10.1061/(ASCE)CP.1943-5487.0000024.

Mou, Tingmin, Bikun Fan, Bo Tian, and Qiyu Tao. 2015. “Scheme Design of a 530m CFST Arch Bridge--the First Yangtze River Bridge in Hejiang , Sichuan , China.” In *6th International*

Conference on Arch Bridges.

Mushthofa, Malik, Akhmad Aminullah, and Muslikh. 2019. "Cross Section and Geometry Optimization of Steel Truss Arch Bridges Based on Internal Forces." In *International Conference on Sustainable Civil Engineering Structures and Construction Materials (SCESCM 2018)*. Vol. 258. https://doi.org/10.1051/matecconf/201925802002.

Nocedal, Jorge, and Stephen J Wright. 1999. *Numerical Optimization*. Edited by Peter Glynn and Stephen M Robinson. New York: Springer-Verlag New York, Inc.

Paul, Anu K, Phani Charan, Rohini G Nair, and Rachel Skd. 2015. "Application of Topology Optimisation to the Design of an Arch Bridge." *International Journal of Engineering Trends and Technology* 28 (8): 426–31.

Pezeshk, S., C. V. Camp, and D. Chen. 2000. "Design of Nonlinear Framed Structures Using Genetic Optimization." *Journal of Structural Engineering (ASCE)* 126 (3): 382–88.

Piegl, Les., and Wayne. Tiller. 1997. *The NURBS Book*. Springer Berlin Heidelberg.

Poli, Riccardo. 2008. "Analysis of the Publications on the Applications of Particle Swarm Optimisation." *Journal of Artificial Evolution and Applications* 2008 (2): 1–10. https://doi.org/10.1155/2008/685175.

Pouraminian, Majid, and Mohsen Ghaemian. 2015. "Shape Optimization of Concrete Open Spandrel Arch Bridges." *Gradjevinar* 67 (12): 1177–85. https://doi.org/10.14256/JCE.1223.2015.

Pouraminian, Majid, and Somayyeh Pourbakhshian. 2019. "Multi-Criteria Shape Optimization of Open-Spandrel Concrete Arch Bridges: Pareto Front Development and Decision-Making." *World Journal of Engineering* 16 (5): 670–80. https://doi.org/10.1108/WJE-04-2019-0104.

Prager, W., and G.I.N. Rozvany. 1977. "Optimization of Structural Geometry." *Dynamical Systems*, January, 265–93. https://doi.org/10.1016/B978-0-12-083750-2.50023-0.

Querin, Osvaldo Maximo, Mariano Victoria, and Pascual Martí. 2010. "Topology Optimization of Truss-like Continua with Different Material Properties in Tension and Compression." *Structural and Multidisciplinary Optimization* 42 (1): 25–32. https://doi.org/10.1007/s00158-009-0473-2.

Rozvany, G. I. N., M. Zhou, and W. Gollub. 1993. "Layout Optimization by COC Methods: Analytical Solutions." In *Optimization of Large Structural Systems*, 77–102. Dordrecht: Springer Netherlands. https://doi.org/10.1007/978-94-010-9577-8_3.

Sadhwani, Lavina H. 2000. “Design Optimization of Parabolic Arches Subject to Non-Uniform Loads.” Massachusetts Institute of Technology.

Sang, Hong-Yan, Pei-Yong Duan, and Jun-Qing Li. 2018. “An Effective Invasive Weed Optimization Algorithm for Scheduling Semiconductor Final Testing Problem.” *Swarm and Evolutionary Computation* 38 (February 2018): 42–53. https://doi.org/https://doi.org/10.1016/j.swevo.2017.05.007.

Schek, H.-J. 1974. “The Force Density Method for Form Finding and Computation of General Networks.” *Computer Methods in Applied Mechanics and Engineering* 3 (1): 115–34. https://doi.org/10.1016/0045-7825(74)90045-0.

Serra, M. 1994. “Optimal Arch: Approximate Analytical Numerical Solutions.” *Computers & Structures* 52 (6): 1213–20.

Shen, Yadong, Jianhu Feng, Xiaohan Cheng, Xuntao Wang, and Changhao Zhang. 2018. “A Form Finding Method for Arch Bridges Using Parametric Level Set Method.” *Advances in Civil Engineering* 2018. https://doi.org/10.1155/2018/2198696.

Stam, Jos. 2009. “Nucleus: Towards a Unified Dynamics Solver for Computer Graphics.” *Proceedings - 2009 11th IEEE International Conference on Computer-Aided Design and Computer Graphics, CAD/Graphics 2009*, no. SEPTEMBER 2009: 1–11. https://doi.org/10.1109/CADCG.2009.5246818.

Storn, Rainer, and Kenneth Price. 1995. “Differential Evolution - A Simple and Efficient Adaptive Scheme for Global Optimization over Continuous Spaces.” *Journal of Global Optimization* 23 (1). https://doi.org/10.1023/A:1008202821328.

———. 1997. “Differential Evolution – A Simple and Efficient Heuristic for Global Optimization over Continuous Spaces.” *Journal of Global Optimization* 11 (4): 341–59. https://doi.org/10.1023/A:1008202821328.

Tadjbakhsh, I. G. 1981. “Stability and Optimum Design of Arch-Type Structures.” *International Journal of Solids and Structures* 17 (6): 565–74. https://doi.org/10.1016/0020-7683(81)90019-6.

Tedeschi, Arturo, Fulvio Wirz, and Stefano Andreani. 2014. *AAD, Algorithms-Aided Design : Parametric Strategies Using Grasshopper*. 1st ed. Brienza, Italy: Le Penseur Publisher.

Tejani, Ghanshyam G., Vimal J. Savsani, Vivek K. Patel, and Poonam V. Savsani. 2018. “Size, Shape, and Topology Optimization of Planar and Space Trusses Using Mutation-Based Improved Metaheuristics.” *Journal of Computational Design and Engineering* 5 (2): 198–214. https://doi.org/10.1016/j.jcde.2017.10.001.

Tejani, Ghanshyam G, Vimal Savsani, and Sujin Bureerat. 2018. *Truss Topology Optimization : A Review*. Edited by Ghanshyam G Tejani, Vimal Savsani, and Sujin Bureerat. Beau Bassin: Scholar's press.

Timoshenko, Stephen, and James M. Gere. 2009. *Theory of Elastic Stability*. Dover Publications.

Timoshenko, Stephen, and Donovan Harold Young. 1965. *Theory of Structures*. McGraw-Hill.

Tomás, Antonio, and Pascual Martí. 2010. "Shape and Size Optimisation of Concrete Shells." *Engineering Structures* 32 (6): 1650–58. https://doi.org/10.1016/j.engstruct.2010.02.013.

Trentadue, Francesco, Giuseppe Carlo Marano, Ivo Vanzi, and Bruno Briseghella. 2018. "Optimal Arches Shape for Single-Point-Supported Deck Bridges." *Acta Mechanica* 229 (January): 2291–97. https://doi.org/10.1007/s00707-017-2084-0.

"Types of Optimization Problems | NEOS." n.d. Accessed August 31, 2019. https://neos-guide.org/optimization-tree.

Vanderplaats, G. N., and S. H. Han. 1990. "Arch Shape Optimization Using Force Approximation Methods." *Structural Optimization* 2 (4): 193–201. https://doi.org/10.1007/BF01748223.

Vanderplaats, Garret N. 1984. *Numerical Optimization Techniques for Engineering Design : With Applications*. New York: McGraw-Hill.

Vatulia, Glib L., Sophia D. Komagorova, Olena V. Opanasenko, and Oleksii V. Lobiak. 2020. *Optimal Design of a Three-Hinged Arch with Given Topology Under Constant Load*. *Lecture Notes in Civil Engineering*. Vol. 47. Springer International Publishing. https://doi.org/10.1007/978-3-030-27011-7_64.

Veenendaal, D., and P. Block. 2012. "An Overview and Comparison of Structural Form Finding Methods for General Networks." *International Journal of Solids and Structures* 49 (26): 3741–53. https://doi.org/10.1016/j.ijsolstr.2012.08.008.

Wang, D., W. H. Zhang, and J. S. Jiang. 2002. "Combined Shape and Sizing Optimization of Truss Structures." *Computational Mechanics* 29 (4–5): 307–12. https://doi.org/10.1007/s00466-002-0343-x.

Woodbury, Robert Francis. 2010. *Elements of Parametric Design*. Routledge.

Yang, Xin-She. 2014. *Nature-Inspired Optimization Algorithms*. London: Elsevier.

Zheng, Jielian, and Jianjun Wang. 2018. "Concrete-Filled Steel Tube Arch Bridges in China." *Engineering* 4 (1): 143–55. https://doi.org/10.1016/j.eng.2017.12.003.

Relevant publications by author

Fenu, L, B Briseghella, and E Congiu. 2016. “Thrust Network Analysis (TNA) in Designing Curved Shell Supported Bridges : Italian Concrete Days L’analisi TNA (Thrust Network Analysis) Nel Progetto Di Ponti in Curva a Guscio : Giornate Aicap 2016 Congresso CTE.” In *Italian Concrete Days Giornate Aicap 2016 Congresso CTE*. Roma.

Fenu, Luigi, Bruno Briseghella, and Eleonora Congiu. 2016. “Curved Footbridges Supported by a Shell Obtained as an Envelope of Thrust-Lines.” In *ARCH’16 - 8th International Conference on Arch Bridges . Wroclaw*, 921–32. Wroclaw (Poland).

Fenu, Luigi, Eleonora Congiu, and Bruno Briseghella. 2016. “Curved Deck Arch Bridges Supported by an Inclined Arch.” In *19th IABSE Congress*, 21–23. Stockholm.

Fenu, Luigi, Eleonora Congiu, Bruno Briseghella, and Giuseppe Carlo Marano. 2017. “Ponte in Curva Sorretto Da Gusci Anticlastici Speculari in Cemento Armato Progettati Con l’uso Del Metodo TNA (Thrust Network Analysis).” *Structural* 209.

Fenu, Luigi, Eleonora Congiu, Davide Lavorato, Bruno Briseghella, and Giuseppe Carlo Marano. 2019. “Curved Footbridges Supported by a Shell Obtained through Thrust Network Analysis.” *Journal of Traffic and Transportation Engineering (English Edition)* 6 (1): 65–75. https://doi.org/10.1016/J.JTTE.2018.10.007.

Fenu, Luigi, Giuseppe C. Marano, Eleonora Congiu, and Bruno Briseghella. 2019. “Optimum Design of an Arched Truss under Vertical and Horizontal Multi-Load Cases.” In *IASS Annual Symposium 2019 - Structural Membranes 2019*. Barcelona.

———. 2019b. “Steel Truss-Type Arches Optimization under Multi-Load Cases.” In *2019 IABSE Congress New York City*. New York.